THE UNIVERSITY OF TULSA
THE GRADUATE SCHOOL

PERFORMANCE OF HORIZONTAL WELLS

by
Erdal Ozkan

A dissertation submitted in partial fulfillment of
the requirements for the degree of Doctor of Philosphy
in the Discipline of Petroleum Engineering
The Graduate School
The University of Tulsa
1988

THE UNIVERSITY OF TULSA

THE GRADUATE SCHOOL

PERFORMANCE OF HORIZONTAL WELLS

A DISSERTATION

APPROVED FOR THE DISCIPLINE OF

PETROLEUM ENGINEERING

By Dissertation Committee

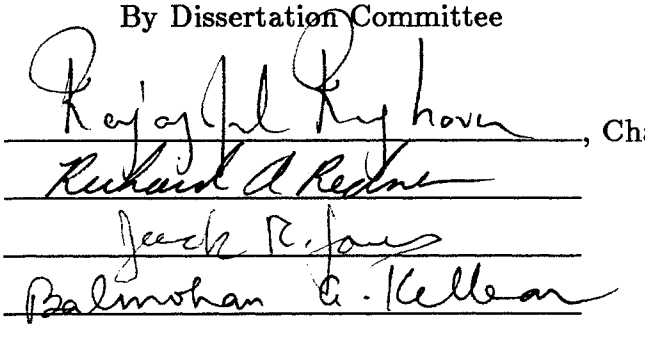

, Chairperson

ABSTRACT

Ozkan, Erdal (Doctor of Philosophy in Petroleum Engineering)
Performance of Horizontal Wells (290 pp. – Chapter V)
Directed by Dr. Rajagopal Raghavan

(307 WORDS)

This dissertation examines the performance of horizontal wells. The performance of horizontal wells are compared to that of vertically fractured wells and vertical wells. The performance comparisons are expressed in terms of pseudoskin factors and effective wellbore radii when the top and the bottom boundaries of the reservoir are impermeable. Applications of the pressure normalized by the derivative procedure to analyze horizontal well and vertically fractured well responses are presented. This procedure eliminates some of the nonuniqueness problems usually encountered in type curve matching the pressure data. It also provides a means to determine the correct semilog straight line on a semilog plot of pressure data.

Performance of horizontal wells under bottom water drive conditions is also discussed. Comparison of the basic phenomena underlying the bottom water drive and the edge water drive mechanisms is presented. Influence of reservoir boundaries on the well response is investigated. Charts are presented whereby vertical and horizontal well performances under bottom water drive conditions can be compared. Results presented here can also be used to determine breakthrough times, water free oil recovery, and well spacing.

A new procedure that combines the Laplace transformation and the source function approach is presented to develop solutions to the transient flow problem in porous media. An extensive library of solutions for most well-reservoir

systems of interest is provided. These solutions can be used to obtain pressure distributions in homogeneous and naturally fractured reservoirs. The solutions presented are in terms of the Laplace transform variable; they can be used to incorporate the influence of wellbore storage and skin and to obtain the rate responses under constant pressure production condition.

Computational issues involved in the numerical evaluation of the Laplace domain solutions presented here are also addressed. Applications of some of the solutions are considered to demonstrate the utility of the procedures developed in this work.

ACKNOWLEDGEMENTS

I wish to express my sincere gratitute to Dr. Rajagopal Raghavan, my graduate advisor, for his assistance and guidance throughout the course of this study. I would also like to thank Dr. Richard A. Redner, Dr. Jack R. Jones, and Dr. Balmoham G. Kelkar, members of the dissertation committee, for their critisims and suggestions. Special thanks to Dr. Sada D. Joshi for the valuable discussions and suggestions he provided during the investigation of horizontal well performances.

Financial assistance provided by the Ministry of Education of Turkey is gratefully acknowledged. I also thank the University of Tulsa for providing the computing facilities.

The manuscript was typed in part by Ms. Becky Salas and the figures were drafted by Ms. Laura Passiglia. Their contribution is also gratefully appreciated.

I am especially grateful for the moral support of my family and my wife. Their support provided the incentive to complete this work.

TABLE OF CONTENTS

List of Tables

List of Figures

CHAPTER I

INTRODUCTION

A review of production performance over the past few years conclusively establishes the advantage of horizontal wells and drainholes[1,2]. Like vertically fractured wells, horizontal well completions are intended to provide a larger surface area for fluid withdrawal and thus improve well productivity. It has been suggested that this mode of completion should be effective in *(i)* reservoirs that are thin or reservoirs with high vertical permeability, *(ii)* reservoirs wherein gas and/or water coning problems preclude the efficient operation of vertical wells, and *(iii)* reservoirs that are naturally fractured. The primary purpose of this work is to present information on the productivity of horizontal wells and enable the engineer to decide whether horizontal wells are more advantageous than vertical well completions. We examine two situations of interest: both top and bottom boundaries closed and bottom boundary at a constant pressure. Results for the case where bottom boundary is at a constant pressure may be used to examine bottom water or gas cap drive.

During the course of the investigation of the performance of horizontal wells, we used the Green's functions and the method of sources and sinks approach introduced to the petroleum literature by Gringarten and Ramey[3]. Although this approach is extremely powerful in solving two and three dimensional unsteady flow problems as in the case of horizontal wells, we encountered difficulties in extending our results to more complicated yet practical problems such as incorporating the influence of storage and skin effects and variable rate production. These problems could be readily solved if the Laplace transform of the solutions provided by Gringarten and Ramey were available. Even in this case, an important problem, production from

naturally fractured reservoirs, would still be solved by other means since the source functions developed by Gringarten and Ramey only consider flow in homogeneous porous media. Our attempt to overcome the limitations of the approach suggested by Gringarten and Ramey led us to the result that many problems one encounters in obtaining the Laplace transforms of pressure distributions in reservoirs (homogeneous or naturally fractured) can be resolved if one examines the appropriate point source solutions. The result of our attempt is a new source function approach to obtain solutions to a broad range of problems of unsteady single phase flow in porous media. Thus, in Chapter II, point source solutions are derived in the Laplace transform domain and an extensive library of solutions is documented to obtain pressure distributions and well responses for a wide variety of wellbore configurations: partially penetrating vertical wells, horizontal wells, fractured wells (complete or partial penetration). The top and bottom boundaries are assumed to be sealed or at a pressure equal to the initial reservoir pressure. Wells may be located in infinite or bounded systems (rectangular or circular reservoirs). For rectangular drainage areas several combinations of closed and/or constant pressure outer boundary conditions are considered. For circular systems the outer boundary may be closed or at a constant pressure. Solutions given here may be used to examine homogeneous or naturally fractured reservoirs. Although some solutions presented in Chapter II do not directly pertain to horizontal well performance, considering the importance of these solutions, we believe that complete documentation of these solutions is wothwhile.

The central new result to follow from Chapter II is that our source function approach permits the analyst to obtain solutions for a wide variety of complex problems useful in well test analysis. Computational considerations in obtaining well responses and pressure distributions for several problems discussed in the literature are also noted in Chapter II. In addition, new asymptotic expressions for pressure distributions in closed drainage volumes that are applicable during the boundary-dominated flow period are derived. Interestingly, these expressions are much simpler than the expressions available in the literature and can be used to derive shape

factors for a variety of completion conditions (vertical wells, horizontal wells, and vertically fractured wells). Application of constant rate solutions to more complex conditions, such as wellbore storage and constant pressure production are presented.

As mentioned above, the development of the new source function approach presented in Chapter II of this work is subsequent to the development of the results pertaining to the performance of horizontal wells presented in Chapters III and IV. Therefore, Chapters III and IV use the source function approach suggested by Gringarten and Ramey to obtain the basic solutions.

The major objective of Chapter III is to present detailed information on horizontal well productivity and to provide new physical insight of the variables that govern horizontal well performance. To be a viable method of completion for primary recovery, horizontal well productivity must be comparable to the productivity of vertically fractured wells. Therefore, in Chapter III, we compare horizontal well performance to that of vertically fractured wells. Performance comparison with unstimulated vertical wells is also presented.

The analysis of pressure data in horizontal wells may prove to be an exceedingly difficult problem. First, three dimensional aspects of the problem must be considered. Second, if horizontal well lengths are long, then conventional semilog techniques may not be applicable. Thus, in this work new applications of the derivative procedure examined by Chow[4] are discussed. Although, the method of Chow is probably the oldest derivative method, this method was not well-known in the petroleum industry until recently. It was applied to horizontal wells and also vertically fractured wells in Ref. 5. Three other recent references[6,7,8] have also discussed the applications of this method. Chow's procedure should eliminate some of the nonuniqueness problems often encountered in the analysis of data by type curve matching. The method can also be extremely useful in identifying semilog straight lines. New analysis procedures are discussed in Chapter III.

Chapter IV examines the influence of bottom water drive on horizontal well productivity. Methods to determine circumstances under which this completion mode would be appropriate are discussed. The distinct flow characteristics of bot-

tom water drive reservoirs are noted. Basic phenomena underlying bottom water drive and edge water drive mechanisms are examined and differences between the two systems are documented. Well productivity is examined in terms of displacement efficiencies. Charts are presented whereby vertical well and horizontal well performances can be compared. Results given in Chapter IV can also be used to determine breakthrough times, water free oil recovery, and well spacing.

CHAPTER II

SOME NEW SOLUTIONS TO SOLVE PROBLEMS IN WELL TEST ANALYSIS

The importance of the transient flow of a slightly compressible fluid is well-known and many techniques are available for solving the problem of the transient flow of slightly compressible fluids in porous media. These include transform techniques such as Laplace and Fourier transforms, Green's functions and the method of sources and sinks. In 1973, Gringarten and Ramey[3] considerably expanded our ability to solve problems of transient flow by exploring the use of source functions and the Newman product method. Their work provides an extensive library of solutions. Although this work is extremely useful, it is difficult to extend their solutions to other situations of interest. For example, the utility of these solutions could be enhanced tremendously if wellbore storage effects could be readily incorporated. This objective can be achieved if the Laplace transforms of the solutions provided by Gringarten and Ramey are available. More importantly, the transformed solutions could also be used for history matching purposes through the use of the Stehfest algorithm[9] and it becomes easier to consider variable rate conditions; for example, constant pressure production. If we consider a specific example, the pressure drop at the wellbore for an infinite-conductivity or uniform-flux vertical fracture is given by[10]

$$p_D(x_D, y_D = 0, t_D) = \frac{\sqrt{\pi}}{4} \int_0^{t_D} \left[\mathrm{erf} \frac{(1 - x_D)}{2\sqrt{\tau}} + \mathrm{erf} \frac{(1 + x_D)}{2\sqrt{\tau}} \right] \frac{d\tau}{\sqrt{\tau}}. \qquad (2.1)$$

Obtaining the Laplace transform of the right hand side of Eq. 2.1 is not straightforward (for example, see Ref. 11). One of the objectives of this chapter is to

obtain the Laplace transform of the right hand side of Eq. 2.1 and then incorporate the existence of storage and skin effects (see Refs. 12 and 13). The procedure we present here is much more general and can be used for more complex problems such as vertically fractured wells in naturally fractured reservoirs (see Refs. 14 and 15). In addition, we extend these solutions to other well systems; for example, horizontal wells.

In §§2.1 – 2.3, we present a procedure that combines the Laplace transformation technique and the source function approach to develop solutions to the transient flow problem in porous media. In order to obtain expressions corresponding to Eq. 2.1 in terms of the Laplace transform variable, our work indicates that it is convenient to first obtain the pressure distribution due to the continuous point source and then incorporate the outer boundary conditions by the method of images. The wellbore conditions (vertical fractures, horizontal wells, partially penetrating wells) can be subsequently incorporated by the appropriate integration of the source functions. These solutions can then be used in the manner suggested by van Everdingen and Hurst[16] to incorporate the existence of wellbore storage and skin effects or variable rate production.

Obtaining solutions in terms of the transform variable represents only the first step in computing well responses. Computational aspects must also be addressed. As is well known, the solutions for the well responses in many cases require the computation of integrals involving the modified Bessel function of zero order, $K_0(x)$, for small values of its argument. Such computations can be exceedingly difficult[15,17]. In other cases, such as the horizontal well problem in an infinite reservoir, components of the solution converge extremely slowly (convergence is not obtained even after several thousand terms in the series are computed). For bounded reservoir systems, some solutions we present (partially penetrating vertical wells, horizontal wells) require the computation of "double infinite Fourier series". Researchers have reported difficulties in the computation of solutions that involve double infinite series. These issues are addressed in §§2.5 and 2.6 and methods to overcome these difficulties are presented. In §2.6, we examine the following problems of interest:

1. A vertically fractured well in an infinite reservoir that is naturally fractured and produced at a constant rate. This problem examines the computation of integrals involving the modified Bessel function of zero order, $K_0(x)$, for small values of its argument. Problems involved in such computations are discussed in Refs. 15 and 17.
2. Computation of horizontal well responses in homogeneous or naturally fractured reservoirs. The primary issue we deal with involves recasting series which behave as if they are divergent series over certain time ranges into series that converge rapidly.
3. Computation of dimensionless pressure distributions for fractured wells in bounded systems (circles and rectangles). Consideration of this problem provides us an opportunity to discuss procedures to compute responses for *all* times. Thus "patching" of infinite reservoir and bounded reservoir solutions is avoided.
4. Some of the solutions presented in §§2.1 – 2.3 involve the computation of double infinite Fourier series and these computations can be exceedingly difficult. These computational problems are addressed by examining horizontal well performance in a closed rectangular drainage region. This discussion should also enable the reader to obtain solutions for other boundary conditions.

Obtaining solutions in terms of the Laplace variable has other advantages. It is possible to obtain approximate solutions for long and short times rather easily if solutions are available in terms of the Laplace variable. In §2.7, we derive asymptotic approximations for some of the problems noted above and use the long time asymptotic expansions to compute shape factors for wells producing in bounded systems. These shape factors can be used to compute inflow relationships for a wide variety of conditions.

As mentioned earlier, the principal advantage of the solutions given in §§2.1 – 2.3, is that they permit us to solve more complex problems, particularly variable rate problems. In §2.8, we demonstrate this aspect by considering two variable rate problems of interest for vertically fractured and horizontal wells: *(i)* the influence

of wellbore storage and skin and *(ii)* constant pressure production.

In summary, our objectives in this chapter are: *(i)* to present a suite of solutions similar to that considered in Ref. 3 in terms of the Laplace transform variable *(ii)* to document procedures to overcome some of the practical problems in computing well responses for constant rate production, and *(iii)* to present applications of some of the solutions developed here in order to demonstrate the utility of these solutions. The solutions we present are applicable to the naturally fractured reservoir idealization of Warren and Root[18] or Kazemi[19] and deSwaan-O[20]. Solutions in infinite and bounded reservoirs are considered. For rectangular drainage areas, the well may be located at any point within the reservoir with any combination of outer boundary conditions (closed or constant pressure). Solutions for circular reservoirs are also presented.

2.1 Point Source Solution in Laplace Space

We consider the problem of production from an infinite, naturally fractured reservoir. We assume that the behavior of a naturally fractured reservoir (or double porosity medium[21]) can be represented by the model suggested by Warren and Root[18]. This representation assumes that the reservoir system consists of two separate media - the matrix system and the fracture system. The matrix system is assumed to be a medium of high storativity and low permeability. It is also assumed that production is only by virtue of the fracture system; that is, the wellbore has no direct connection with the matrix system.

The equation governing the flow of a slightly compressible fluid in the fracture system is obtained by using the law of conservation of mass and Darcy's law and is given by

$$\nabla \cdot \left(\frac{\tilde{k}_f}{\mu} \nabla \Delta p_f \right) = (V \phi c_t)_f \frac{\partial \Delta p_f}{\partial t} + q^*. \tag{2.1.1}$$

Here the subscript f is used to denote the fracture system, Δp_f is the pressure drop from the initial pressure which is assumed uniform throughout the system, μ is viscosity of the fluid, $(V \phi c_t)_f$ is the storativity of the fracture system, and q^* is the

volumetric flow rate from the matrix system to the fracture system. $\tilde{k}_f$ in Eq. 2.1.1 represents the permeability tensor for the fracture system with nonzero elements only on the diagonal (that is, we assume that the principal axes of permeability coincide with the coordinate axes of Eq. 2.1.1).

Ignoring flow within the matrix system, the equivalent form of Eq. 2.1.1 for the matrix system is given by

$$q^* = (V\phi c_t)_m \frac{\partial \Delta p_m}{\partial t}. \tag{2.1.2}$$

In Eq. 2.1.2, the subscript m refers to the matrix system.

Flow from the matrix system to the fracture system is proportional to the difference between the pressures of the two systems. If we assume pseudosteady flow from the matrix system to the fracture system (Warren and Root idealization[18]), then we can also write

$$q^* = -\alpha \frac{k_m}{\mu}(\Delta p_m - \Delta p_f), \tag{2.1.3}$$

where α is the interporosity shape factor[18] and k_m is the permeability of the matrix system.

Combining Eqs. 2.1.1, 2.1.2, and 2.1.3, the following equations are obtained.

$$\nabla.(\tilde{k}_f \nabla \Delta p_f) = (V\phi c_t)_f \mu \frac{\partial \Delta p_f}{\partial t} + (V\phi c_t)_m \mu \frac{\partial \Delta p_m}{\partial t}, \tag{2.1.4}$$

$$\alpha k_m (\Delta p_m - \Delta p_f) = -(V\phi c_t)_m \mu \frac{\partial \Delta p_m}{\partial t}. \tag{2.1.5}$$

If we define a dimensionless distance x_{Dj} by

$$x_{Dj} = \frac{x_j}{L}\sqrt{\frac{k_f}{k_{fj}}}, \tag{2.1.6}$$

then the dimensionless operator $bigtriangledown^2_D$ is defined by

$$\nabla^2_D = \sum_{j=1}^{3} \frac{\partial^2}{\partial x^2_{Dj}}. \tag{2.1.7}$$

In Eq. 2.1.6, L is some reference length in the system, k_{fj} is the principal permeability of the fracture system in j direction, and k_f is an arbitrary constant that may be chosen to be the permeability of an equivalent isotropic system ($k = \sqrt[3]{\prod_{j=1}^{3} k_{fj}}$). Defining also the dimensionless time, t_D, by

$$t_D = \frac{\eta t}{L^2}, \tag{2.1.8}$$

where

$$\eta = \frac{k_f}{[(V\phi c_t)_f + (V\phi c_t)_m]\mu}, \tag{2.1.9}$$

and the dimensionless storativity, w, and the dimensionless transfer coefficient, λ, respectively by

$$w = \frac{(V\phi c_t)_f}{(V\phi c_t)_f + (V\phi c_t)_m}, \tag{2.1.10}$$

and

$$\lambda = \alpha \frac{k_m}{k_f} L^2, \tag{2.1.11}$$

Eqs. 2.1.4 and 2.1.5 can be written as

$$\nabla_D^2(\Delta p_f) = w\frac{\partial \Delta p_f}{\partial t_D} + (1-w)\frac{\partial \Delta p_m}{\partial t_D}, \tag{2.1.12}$$

$$\lambda(\Delta p_m - \Delta p_f) = -(1-w)\frac{\partial \Delta p_m}{\partial t_D}. \tag{2.1.13}$$

We will assume that the fluid flow in the reservoir results from an instantaneous pressure drop created at $t = 0$ at the origin of the coordinate system. In our terminology, a point at which an instantaneous pressure drop is created due to instantaneous removal of fluids from this point is called an instantaneous point source. Since we consider an infinite reservoir with only one point source located at the origin, Δp should only depend on the radial coordinate r_D, where

$$r_D = \sqrt{\sum_{j=1}^{3} x_{Dj}^2} = \sqrt{x_D^2 + y_D^2 + z_D^2}. \tag{2.1.14}$$

Therefore, using the appropriate spherical form of the operator ∇_D^2, we can write Eq. 2.1.12 as

$$\frac{1}{r_D^2}\frac{\partial}{\partial r_D}\left(r_D^2\frac{\partial \Delta p_f}{\partial r_D}\right) = w\frac{\partial \Delta p_f}{\partial t_D} + (1-w)\frac{\partial \Delta p_m}{\partial t_D}. \tag{2.1.15}$$

We assume that at $t = 0$, a finite volume of fluid, $\widetilde{q}$, is removed from the reservoir at the source location instantaneously. We must require that the cumulative flux through the surface of a small sphere about the source must equal the volume of fluid removed from the source, $\widetilde{q}$:

$$\int_0^t \left[\lim_{\epsilon \to 0+} \frac{4\pi k_f}{\mu} L\left(r_D^2\frac{\partial \Delta p_f}{\partial r_D}\right)_{r_D=\epsilon}\right] dt = \widetilde{q} \tag{2.1.16}$$

It should be realized that although the removal of fluids from the source occurs instantaneously, resulting flow in the system and therefore the flux through the surface of the spherical region about the source is a continuous action in time. In other words, if we let q represent the withdrawal rate resulting from the distribution of the instantaneous fluid removal $\widetilde{q}$ over the time period between 0 and t, then mass balance for the system requires that the cumulative production from the system at time t be equal to the amount of fluid instantaneously withdrawn from the source:

$$\widetilde{q} = \int_0^t q(t)dt \tag{2.1.17}$$

Using the property of the symbolic $\delta(t)$ function

$$\int_a^b \delta(t)dt = \left\{\begin{matrix} 1 & \text{if } [a,b] \text{ contains the origin} \\ 0 & \text{otherwise} \end{matrix}\right\} \tag{2.1.18}$$

we can replace $q(t)$ in Eq. 2.1.17 by $\widetilde{q}\delta(t)$ and hence write Eq. 2.1.16 in terms of instantaneous fluid removal as

$$\lim_{\epsilon \to 0+} \frac{4\pi k_f}{\mu} L\left(r_D^2\frac{\partial \Delta p_f}{\partial r_D}\right)_{r_D=\epsilon} = -\widetilde{q}\delta(t). \tag{2.1.19}$$

If we now take the Laplace transform of Eqs. 2.1.15 and 2.1.13 with respect to t_D, we obtain respectively

$$\frac{1}{r_D^2}\frac{d}{dr_D}\left(r_D^2\frac{d\overline{\Delta p_f}}{dr_D}\right) = ws\overline{\Delta p_f} + (1-w)s\overline{\Delta p_m} \tag{2.1.20}$$

and

$$\overline{\Delta p_m} = \frac{\lambda}{\lambda + (1-w)s}\overline{\Delta p_f} \tag{2.1.21}$$

where $\overline{\Delta p}$ denotes the Laplace transform of Δp and s is the Laplace transform variable. Substituting the right hand side of Eq. 2.1.21 into 2.1.20 for $\overline{\Delta p_m}$, we can write

$$\frac{1}{r_D^2}\frac{d}{dr_D}\left(r_D^2\frac{d\overline{\Delta p_f}}{dr_D}\right) - sf(s)\overline{\Delta p_f} = 0, \tag{2.1.22}$$

where we define

$$f(s) = \frac{sw(1-w)+\lambda}{s(1-w)+\lambda}. \tag{2.1.23}$$

Also noting that

$$\int_0^\infty \exp(-st_D)\delta(t)dt_D = \frac{\eta}{L^2}\int_0^\infty \exp(-s\frac{\eta}{L^2}t)\delta(t)dt = \frac{\eta}{L^2}, \tag{2.1.24}$$

we can obtain the Laplace transform of Eq. 2.1.19 as

$$\lim_{\epsilon \to 0}\frac{4\pi k_f}{\mu}L\left(r_D^2\frac{d\overline{\Delta p_f}}{dr_D}\right)_{r_D=\epsilon} = -\frac{k_f\tilde{q}}{[(V\phi c_t)_f + (V\phi c_t)_m]\mu L^2}. \tag{2.1.25}$$

We define the strength of the source by $\tilde{q}/[(V\phi c_t)_f + (V\phi c_t)]$ and, for simplicity, we assume that the strength of the source is unity. Then setting

$$\frac{\tilde{q}}{(V\phi c_t)_f + (V\phi c_t)_m} = 1, \tag{2.1.26}$$

we can write Eq. 2.1.25 as

$$\lim_{\epsilon \to 0} 4\pi L^3\left(r_D^2\frac{d\overline{\Delta p_f}}{dr_D}\right)_{r_D=\epsilon} = -1 \tag{2.1.27}$$

If we now substitute

$$g = r_D\overline{\Delta p_f} \tag{2.1.28}$$

into Eq. 2.1.22, we obtain

$$\frac{d^2g}{dr_D^2} - sf(s)g = 0. \tag{2.1.29}$$

The general solution of Eq. 2.1.29 is given by

$$g = A\exp\left[-\sqrt{sf(s)}r_D\right] + B\exp\left[\sqrt{sf(s)}r_D\right]. \tag{2.1.30}$$

Therefore, from Eqs. 2.1.28 and 2.1.30, we have

$$\overline{\Delta p_f} = A\frac{\exp\left[-\sqrt{sf(s)}r_D\right]}{r_D} + B\frac{\exp\left[\sqrt{sf(s)}r_D\right]}{r_D} \tag{2.1.31}$$

By the requirement that $\overline{\Delta p_f}$ vanish at infinity, we must have $B = 0$ in Eq. 2.1.31. From the condition given by Eq. 2.1.27, we find

$$A = \frac{1}{4\pi L^3}. \tag{2.1.32}$$

Then $\overline{\Delta p_f}$ is given by

$$\overline{\Delta p_f} = \frac{\exp\left[-\sqrt{sf(s)}r_D\right]}{4\pi L^3 r_D}. \tag{2.1.33}$$

$\overline{\Delta p_f}$ given by Eq. 2.1.33 is the Laplace space solution of the pressure distribution due to a unit strength instantaneous point source located at the origin. The pressure distribution due to a point source at some arbitrary location x_{wD}, y_{wD}, z_{wD} is obtained from Eq. 2.1.33 by translation. If we use the notation

$$R_D = \sqrt{(x_D - x_{wD})^2 + (y_D - y_{wD})^2 + (z_D - z_{wD})^2}, \tag{2.1.34}$$

then the pressure distribution due to a unit strength *instantaneous* point source is given by

$$\overline{\Delta p_f} = \frac{\exp\left[-\sqrt{sf(s)}R_D\right]}{4\pi L^3 R_D}. \tag{2.1.35}$$

If the strength of the source is different from unity, then Eq. 2.1.35 becomes

$$\overline{\Delta p_f} = \frac{\tilde{q}}{(V\phi c_t)_f + (V\phi c_t)_m}\left\{\frac{\exp[-\sqrt{sf(s)}R_D]}{4\pi L^3 R_D}\right\}. \tag{2.1.36}$$

Although the instantaneous point source solution is useful to develop solutions for the analysis of slug test problems (see for example Ref. 22), in general well testing applications we assume that the pressure distribution in the reservoir is a result of the continuous withdrawal of fluid at a rate $\tilde{q}(t)$ from time 0 to t. The *continuous* point source solution can be obtained by applying the principle of superposition to the instantaneous sources distributed over the time interval from 0 to t. If we define

$$\overline{S} = \frac{\exp\left[-\sqrt{sf(s)}R_D\right]}{4\pi L^3 R_D}, \tag{2.1.37}$$

then the real inversion of Eq. 2.1.36 yields

$$\Delta p_f = \frac{\tilde{q} S(t_D)}{(V\phi c_t)_f + (V\phi c_t)_m}. \tag{2.1.38}$$

If we consider continuous withdrawal of fluid from the point source located at x_{wD}, y_{wD}, z_{wD}, then by the principle of superposition, we can write

$$\Delta p_f = \frac{1}{(V\phi c_t)_f + (V\phi c_t)_m} \int_0^t \tilde{q}(\tau) S(t_D - \tau) d\tau = \frac{L^2 \mu}{k_f} \int_0^{t_D} \tilde{q}(\tau_D) S(t_D - \tau_D) d\tau_D. \tag{2.1.39}$$

The Laplace transform of Eq. 2.1.39 gives

$$\overline{\Delta p} = \frac{\bar{\tilde{q}} \mu}{4\pi k L} \frac{\exp\left[-\sqrt{u}\sqrt{(x_D - x_{wD})^2 + (y_D - y_{wD})^2 + (z_D - z_{wD})^2}\right]}{\sqrt{(x_D - x_{wD})^2 + (y_D - y_{wD})^2 + (z_D - z_{wD})^2}}, \tag{2.1.40}$$

where we have dropped the subscript f (since we only solve for the pressure drop in the fracture system) and defined

$$u = sf(s). \tag{2.1.41}$$

Eq. 2.1.40 is the Laplace space solution for the pressure distribution due to a *continuous* point source located at x_{wD}, y_{wD}, z_{wD}. If we set $f(s)$ to be unity and modify the definition of t_D, then Eq. 2.1.40 also represents the pressure distribution in a homogeneous reservoir. In fact, with these modifications, Eq. 2.1.40 is the Laplace transform of Lord Kelvin's point source solution[23]. Eq. 2.1.40 may also be extended to the naturally fractured reservoir model suggested by Kazemi[19] and deSwaan-O[20] by replacing the function $f(s)$ given by Eq. 2.1.23 by

$$f(s) = 1 + \sqrt{\frac{\lambda' w'}{3s}} \tanh\left(\sqrt{\frac{3w's}{\lambda'}}\right). \tag{2.1.42}$$

The definitions of λ' and w' are given by[24]

$$w' = \frac{(\phi c_t h)_m}{(\phi c_t h)_f} \tag{2.1.43}$$

and

$$\lambda' = \frac{12L^2}{h_m^2} \frac{(kh)_m}{(kh)_f}. \tag{2.1.44}$$

In Eqs. 2.1.43 and 2.1.44, h_m and h_f are the thickness of the individual matrix and fracture elements, respectively. The definition of the dimensionless time for this model is given by[24]

$$t_D = \frac{k_f t}{(\phi c_t)_f \mu L^2}. \tag{2.1.45}$$

Thus far, we have used the classical mathematical formulation of the problem under consideration. In fact, this formulation is equivalent to finding the Green's function of the problem and Eq. 2.1.35 represents the Laplace transform of the Green's function for our problem. The Green's function approach has been used to solve the same problem considered here by Refs. 25 and 26. The procedure used in this work is considerably simpler than the Green's function procedure taken by Refs. 25 and 26, and its systematic application enables us to generate closed form solutions in Laplace space for a variety of well (source) types in naturally fractured reservoirs.

If we define

$$G\left(x_D - x_{wD}, y_D - y_{wD}, z_D - z_{wD}\right) = \frac{\overline{\Delta p}}{\bar{\tilde{q}}}, \tag{2.1.46}$$

then by the application of the principle of superposition, pressure distribution corresponding to the withdrawal of fluid from a line, a surface, or a volume, S, is obtained by

$$\overline{\Delta p} = \int_S \bar{\tilde{q}}\left(x_{wD}, y_{wD}, z_{wD}\right) G\left(x_D - x_{wD}, y_D - y_{wD}, z_D - z_{wD}\right) dS, \tag{2.1.47}$$

where dS denotes the differential element of the line, surface, or volume. Unless specified otherwise, in the following development of the results, we will assume that the source distribution in time and over the path of integration in Eq. 2.1.47 is uniform and therefore we will use Eq. 2.1.47 in the following form:

$$\overline{\Delta p} = \frac{\tilde{q}}{s} \int_S G\left(x_D - x_{wD}, y_D - y_{wD}, z_D - z_{wD}\right) dS. \tag{2.1.48}$$

Fundamentally, Eq. 2.1.48 will represent the pressure distribution for a uniform-flux well producing at a constant rate. Pressure distributions due to production from

an infinite-conductivity well can be closely approximated by using the uniform-flux well solution. The procedure to obtain infinite-conductivity source solutions by using the solutions for uniform-flux sources has been extensively discussed in the literature (see for example Refs. 3 and 10) and will not be discussed here. In the following sections of this chapter, we will use Eq. 2.1.40 with $\bar{\tilde{q}}$ replaced with $\tilde{q}/s$. We will also establish the convention that $\tilde{q}$ represents the constant withdrawal rate from a continuous point source and q represents the constant withdrawal rate from a line, point, or volumetric source. The relation between the constant production rate from the continuous point source, $\tilde{q}$, and the constant production rate from the uniform-flux line, surface, or volumetric source, q, will be given by $\tilde{q} = q/S$, where S is the length, area, or the volume of the source.

2.2 Solutions Useful in Well Test Analysis

We will first consider solutions for wells in reservoirs that extend to infinity laterally. We examine a wide variety of wellbore conditions (partially penetrating vertical wells, partially penetrating vertical fractures, and horizontal wells). We then extend these solutions to wells located at the center of circular reservoirs. Finally, we obtain solutions for wells located in rectangular drainage regions and consider several combinations of boundary conditions.

I. Solutions for Laterally Infinite Reservoirs In the previous section, we obtained the point source solution in an infinite reservoir. Since the actual reservoirs have a finite thickness, here we will derive the point source solution in a laterally infinite reservoir of thickness h. The bounding planes at $z = 0$ and h may be both impermeable, or both at constant pressure equal to the initial pressure, or the plane at $z = 0$ may be assumed to be impermeable while the plane at $z = h$ is at constant pressure equal to the initial pressure.

We will first consider the case where the boundaries at $z = 0$ and h are both impermeable. The point source solution in such a system can be obtained by ap-

plying the method of images to the point source solution given by Eq. 2.1.40. This procedure yields

$$\overline{\Delta p} = \frac{\tilde{q}\mu}{4\pi kLs} \sum_{n=-\infty}^{+\infty} \left\{ \frac{\exp\left[-\sqrt{u}\sqrt{r_D^2 + (z_D - z_{wD} - 2nh_D)^2}\right]}{\sqrt{r_D^2 + (z_D - z_{wD} - 2nh_D)^2}} + \frac{\exp\left[-\sqrt{u}\sqrt{r_D^2 + (z_D + z_{wD} - 2nh_D)^2}\right]}{\sqrt{r_D^2 + (z_D + z_{wD} - 2nh_D)^2}} \right\}. \tag{2.2.1}$$

In Eq. 2.2.1, we defined

$$r_D^2 = (x_D - x_{wD})^2 + (y_D - y_{wD})^2, \tag{2.2.2}$$

and

$$h_D = \frac{h}{L}\sqrt{\frac{k}{k_z}}. \tag{2.2.3}$$

Eq. 2.2.1 can be cast into a more suitable form for computational purposes by using a formula derived from Poisson's summation formula given by[23]

$$\sum_{n=-\infty}^{+\infty} \exp\left[-\frac{(\xi - 2n\xi_e)^2}{4\tau}\right] = \frac{\sqrt{\pi\tau}}{\xi_e}\left[1 + 2\sum_{n=1}^{+\infty} \exp\left(-\frac{n^2\pi^2\tau}{\xi_e^2}\right)\cos n\pi\frac{\xi}{\xi_e}\right]. \tag{2.2.4}$$

Multiplying both sides of Eq. 2.2.4 by $\exp[-a^2/(4\tau)]/\sqrt{\pi\tau^3}$ and then taking the Laplace transform of the resulting expression with respect to τ, the following summation formula is obtained:

$$\sum_{n=-\infty}^{+\infty} \frac{\exp\left[-\sqrt{\nu}\sqrt{a^2 + (\xi - 2n\xi_e)^2}\right]}{\sqrt{a^2 + (\xi - 2n\xi_e)^2}} = \frac{1}{\xi_e}\left[K_0\left(a\sqrt{\nu}\right) + 2\sum_{n=1}^{\infty} K_0\left(a\sqrt{\nu + \frac{n^2\pi^2}{\xi_e^2}}\right)\cos n\pi\frac{\xi}{\xi_e}\right]. \tag{2.2.5}$$

If we use the summation formula given by Eq. 2.2.5, then the pressure distribution for a continuous point source located at x_{wD}, y_{wD}, z_{wD} in a laterally infinite reservoir bounded by two impermeable planes at $z = 0$ and h given by Eq. 2.2.1 can be written as

$$\overline{\Delta p} = \frac{\tilde{q}\mu}{2\pi kLh_D s}\left[K_0\left(r_D\sqrt{u}\right) + 2\sum_{n=1}^{\infty} K_0\left(r_D\sqrt{u + \frac{n^2\pi^2}{h_D^2}}\right)\cos n\pi\frac{z_D}{h_D}\cos n\pi\frac{z_{wD}}{h_D}\right]. \tag{2.2.6}$$

Similarly, if the horizontal boundaries at $z = 0$ and h are at constant pressure, then the continuous point source solution corresponding to this case is given by

$$\overline{\Delta p} = \frac{\tilde{q}\mu}{4\pi kLs} \sum_{n=-\infty}^{+\infty} \left\{ \frac{\exp\left[-\sqrt{u}\sqrt{r_D^2 + (z_D - z_{wD} - 2nh_D)^2}\right]}{\sqrt{r_D^2 + (z_D - z_{wD} - 2nh_D)^2}} - \frac{\exp\left[-\sqrt{u}\sqrt{r_D^2 + (z_D + z_{wD} - 2nh_D)^2}\right]}{\sqrt{r_D^2 + (z_D + z_{wD} - 2nh_D)^2}} \right\}, \tag{2.2.7}$$

which, by means of Eq. 2.2.5, can be transformed to

$$\overline{\Delta p} = \frac{\tilde{q}\mu}{\pi kLh_D s} \left[\sum_{n=1}^{\infty} K_0 \left(r_D \sqrt{u + \frac{n^2\pi^2}{h_D^2}} \right) \sin n\pi \frac{z_D}{h_D} \sin n\pi \frac{z_{wD}}{h_D} \right]. \tag{2.2.8}$$

Finally, if the boundary at $z = 0$ is impermeable while the boundary at $z = h$ is at constant pressure, then the solution for a continuous point source is given by the following expression:

$$\overline{\Delta p} = \frac{\tilde{q}\mu}{4\pi kLs} \sum_{n=-\infty}^{+\infty} (-1)^n \left\{ \frac{\exp\left[-\sqrt{u}\sqrt{r_D^2 + (z_D - z_{wD} - 2nh_D)^2}\right]}{\sqrt{r_D^2 + (z_D - z_{wD} - 2nh_D)^2}} + \frac{\exp\left[-\sqrt{u}\sqrt{r_D^2 + (z_D + z_{wD} - 2nh_D)^2}\right]}{\sqrt{r_D^2 + (z_D + z_{wD} - 2nh_D)^2}} \right\}. \tag{2.2.9}$$

If we note that

$$\sum_{k=-\infty}^{+\infty} (-1)^k \exp\left[-\frac{a\,(x_D - 2kx_{eD})^2}{4\xi}\right] =$$

$$\sum_{k=-\infty}^{+\infty} \left\{ 2\exp\left[-\frac{a\,(x_D - 2k2x_{eD})^2}{4\xi}\right] - \exp\left[-\frac{a\,(x_D - 2kx_{eD})^2}{4\xi}\right] \right\}, \tag{2.2.10}$$

then with the aid of the summation formula given by Eq. 2.2.5, we can recast Eq. 2.2.9 in the following form:

$$\overline{\Delta p} = \frac{\tilde{q}\mu}{\pi kLh_D s} \left\{ \sum_{n=1}^{\infty} K_0 \left[r_D \sqrt{u + \frac{(2n-1)^2\pi^2}{4h_D^2}} \right] \cos(2n-1)\frac{\pi}{2}\frac{z_D}{h_D} \cos(2n-1)\frac{\pi}{2}\frac{z_{wD}}{h_D} \right\}. \tag{2.2.11}$$

Eqs. 2.2.6, 2.2.8, and 2.2.11 can now be used with Eqs. 2.1.46 and 2.1.48 to generate solutions for a variety of well-reservoir systems. For example, if the boundaries at $z = 0$ and h are impermeable, then the solution for a vertical line source well of length h_w can be obtained by integrating the right hand side of Eq. 2.2.6 from $z_w - h_w/2$ to $z_w + h_w/2$ with respect to z'_w. This solution corresponds to a partially penetrating vertical well with the penetrated interval equal to h_w. If $h_w = h$, then this procedure yields the solution for a fully penetrating vertical line source well. Similarly, the solution for a horizontal line source well of length L_h results from the integration of the right hand side of Eq. 2.2.6 from $x_w - L_h/2$ to $x_w + L_h/2$ with respect to x'_w. Solution for a plane vertical fracture of height h_w and length $2L_{x_f}$ is obtained by integrating Eq. 2.2.6 once from $z_w - h_w/2$ to $z_w + h_w/2$ with respect to z'_w and then from $x_w - L_h/2$ to $x_w + L_h/2$ with respect to x'_w. Again, as in the line source well case, using $h_w = h$ the solution for a fully penetrating fracture is obtained. All such solutions can now be obtained directly in terms of the Laplace variable. To our knowledge, this approach for obtaining solutions in terms of the Laplace variable is new.

Solutions for a variety of well types in laterally infinite reservoirs are presented in Table 1 of Appendix A. For each type of well, the relations between the production rate from the well, q, and the production rate from the point source, $\tilde{q}$, are also noted. In case of partially penetrating vertical wells and fractures, h_w is used to denote the length of the open interval in the vertical plane. The horizontal length of a vertical fracture is denoted by $2L_{x_f}$ and the length of a horizontal line source well is denoted by L_h. Solutions presented in Table $1 - A$ correspond to the case where the boundaries at $z = 0$ and h are impermeable. Table $1 - B$ presents the solutions for the case where the boundaries at $z = 0$ are at constant pressure and Table $1 - C$ presents the solutions for the case where the boundary at $z = 0$ is impermeable and the boundary at $z = h$ is at constant pressure. Note that using $u = s$ $[f(s) = 1]$ in the solutions given in Table 1 of Appendix A, we obtain the solutions for homogeneous reservoirs. In this case the Laplace inversion of the solutions presented in Table 1 of Appendix A can be easily found in standard tables

of Laplace transforms (see for example the one given by Ref. 27). For convenience, Table $1-A$ which pertains to solutions for a system with top and bottom boundaries sealed is reproduced in Table 2.2.1.

Some of the solutions presented in Table 1 of Appendix A can be found in the literature; however, the procedure used here to obtain these solutions is considerably simpler than the ones used in the literature. The solution for a fully penetrating vertical well given in Table $1-A$ is a standard result and is presented for completeness. The fully penetrating vertical fracture solution presented in Table $1-A$ has been reported by Ref. 15. Another solution which is different in form but identical to that given in Table $1-A$ for fully penetrating vertical fractures in homogeneous reservoirs has recently been reported in Ref. 28. A real time solution for partially penetrating vertical wells has been obtained in Ref. 25 by using the Green's functions and the Newman's product solution procedure. The Laplace transform of the partially penetrating vertical well solution (the case corresponding to $u = s$ in Table $1-A$) has been obtained directly from the real time domain solution by Kuchuk and Kirwan[29]. To the best of our knowledge, other solutions in Table 1 of Appendix A have not been reported in the literature and the procedure used here to obtain the solutions is new. Solutions for horizontal wells in homogeneous reservoirs presented in Tables $1-A$ and $1-C$ are used for evaluating pseudoskin factors in Chapter III and studying well productivity under bottom water drive in Chapter IV. Note that our procedure not only yields the wellbore responses but also yields the pressure distribution.

Numerical evaluation of the integrals appearing in some of the solutions presented in Table 1 of Appendix A will pose difficulties as $y_D \rightarrow y_{wD}$ (see for example Ref. 15). In §2.5, we present alternative forms of these integrals to be used in numerical computations. To our knowledge, these alternative forms are not discussed in the literature. The results are extremely important in that they render the approach presented extremely attractive for computational purposes. Not having these alternative forms has been one of the main obstacles in obtaining solutions even when the Laplace transform solution is available.

TABLE 2.2.1
SOLUTIONS FOR WELLS IN INFINITE RESERVOIRS
IMPERMEABLE BOUNDARIES AT $z_D = 0$ AND $z_D = h_D$

WELL TYPE	PRESSURE DISTRIBUTION IN LAPLACE SPACE, $\overline{\Delta p}$
POINT SOURCE $q = \tilde{q}$	$\frac{\tilde{q}\mu}{2\pi k L h_D s}\left[K_0\left(r_D\sqrt{u}\right) + 2\sum_{n=1}^{\infty} K_0\left(r_D\sqrt{u+\frac{n^2\pi^2}{h_D^2}}\right) \cos n\pi\frac{z}{h}\cos n\pi\frac{z_w}{h}\right]$
FULLY PENETRATING VERTICAL WELL $q = \tilde{q}h$	$\frac{\tilde{q}\mu h}{2\pi k L h_D s} K_0\left(r_D\sqrt{u}\right)$
PARTIALLY PENETRATING VERTICAL WELL $q = \tilde{q}h_w$	$\frac{\tilde{q}\mu h_w}{2\pi k L h_D s} K_0\left(r_D\sqrt{u}\right) + \frac{2\tilde{q}\mu h}{\pi^2 k L h_D s}\sum_{n=1}^{\infty}\left[\frac{1}{n} K_0\left(r_D\sqrt{u+\frac{n^2\pi^2}{h_D^2}}\right) \sin n\pi\frac{h_w}{2h}\cos n\pi\frac{z_w}{h}\cos n\pi\frac{z}{h}\right]$
FULLY PENETRATING VERTICAL FRACTURE $q = 2\tilde{q}hL_{x_f}$	$\frac{\tilde{q}\mu h}{2\pi k h_D s}\int_{-L_{x_f}/L}^{+L_{x_f}/L} K_0\left[\sqrt{u}\sqrt{(x_D - x_{wD} - \alpha\sqrt{k/k_x})^2 + (y_D - y_{wD})^2}\right] d\alpha$
PARTIALLY PENETRATING VERTICAL FRACTURE $q = 2\tilde{q}h_w L_{x_f}$	$\frac{\tilde{q}\mu h_w}{2\pi k h_D s}\int_{-L_{x_f}/L}^{+L_{x_f}/L} K_0\left[\sqrt{u}\sqrt{(x_D - x_{wD} - \alpha\sqrt{k/k_x})^2 + (y_D - y_{wD})^2}\right] d\alpha + \frac{2\tilde{q}\mu h}{\pi^2 k h_D s}\sum_{n=1}^{\infty}\frac{1}{n}\sin n\pi\frac{h_w}{2h}\cos n\pi\frac{z_w}{h}\cos n\pi\frac{z}{h}$ $\int_{-L_{x_f}/L}^{+L_{x_f}/L} K_0\left[\sqrt{u+\frac{n^2\pi^2}{h_D^2}}\sqrt{(x_D - x_{wD} - \alpha\sqrt{k/k_x})^2 + (y_D - y_{wD})^2}\right] d\alpha$
HORIZONTAL WELL $q = \tilde{q}L_h$	$\frac{\tilde{q}\mu}{2\pi k h_D s}\left\{\int_{-L_h/(2L)}^{+L_h/(2L)} K_0\left[\sqrt{u}\sqrt{(x_D - x_{wD} - \alpha\sqrt{k/k_x})^2 + (y_D - y_{wD})^2}\right] d\alpha + 2\sum_{n=1}^{\infty}\cos n\pi\frac{z}{h}\cos n\pi\frac{z_w}{h}\right.$ $\left.\int_{-L_h/(2L)}^{+L_h/(2L)} K_0\left[\sqrt{u+\frac{n^2\pi^2}{h_D^2}}\sqrt{(x_D - x_{wD} - \alpha\sqrt{k/k_x})^2 + (y_D - y_{wD})^2}\right] d\alpha\right\}$

II. Solutions for Bounded Reservoirs - Cylindrical Coordinates As in the case of laterally infinite reservoirs considered above, we first generate the solution for a point source well. The equation that describes the flow in cylindrical coordinate system is given in Laplace space by

$$\frac{1}{r_D}\frac{\partial}{\partial r_D}\left(r_D\frac{\partial\overline{\Delta p}}{\partial r_D}\right)+\frac{\partial^2\overline{\Delta p}}{\partial z_D^2}-u\overline{\Delta p}=0, \tag{2.2.12}$$

where $r_D=\sqrt{x_D^2+y_D^2}$ and x_D, y_D, and z_D are defined by Eq. 2.1.6. The solution of Eq. 2.2.12 is required to satisfy the following flux condition at the source location $(r_D\to 0+, z_D=z_{wD}+)$:

$$\lim_{\epsilon_D\to 0}\left(\lim_{r_D\to 0}\frac{2\pi kL}{\mu\epsilon_D}\int_{z_{wD}-\epsilon_D/2}^{z_{wD}+\epsilon_D/2} r_D\frac{\partial\overline{\Delta p}}{\partial r_D}dz_{wD}\right)=-\frac{\widetilde{q}}{s}. \tag{2.2.13}$$

The structure of Eq. 2.2.13 deserves comment. In writing Eq. 2.2.13, we visualize a point source as a line source of length ϵ as the length of the source vanishes. Before proceeding to the limit as $\epsilon_D\to 0$, the left hand side of Eq. 2.2.13 yields the average value of flux along the line source. Therefore, as the length of the line source vanishes ($\epsilon_D\to 0$), the left hand side of Eq. 2.2.13 represents the flux around a point source located at $r_D=0$ and $z_D=z_{wD}$. (It should be realized that if Eq. 2.2.13 is to represent the flux condition for a point source, the order of the limits as $r_D\to 0$ and as $\epsilon\to 0$ must be interchangable; proof of this, however, is outside the scope of our discussion). Note also that the right hand side of Eq. 2.2.13 assumes continuous withdrawal of fluid at a constant rate $\widetilde{q}$. If we wish to consider an instantaneous point source, then the right hand side of Eq. 2.2.13 is written by a similar procedure as discussed in §2.1 (see Eq. 2.1.25) and the appropriate equation is given by

$$\lim_{\epsilon_D\to 0}\left(\lim_{r_D\to 0}\frac{2\pi kL}{\mu\epsilon_D}\int_{z_{wD}-\epsilon_D/2}^{z_{wD}+\epsilon_D/2} r_D\frac{\partial\overline{\Delta p}}{\partial r_D}dz_{wD}\right)=-\frac{k_f\widetilde{q}}{[(V\phi c_t)_f+(V\phi c_t)_m]\mu L^2}. \tag{2.2.14}$$

We will assume that the reservoir is bounded by a cylindrical surface located at $r_D=r_{eD}$ (it should be realized that a cylindrical reservoir in transformed coordinate, r_D, would correspond to a cylindrical reservoir in real coordinate, r, only if

$k_x = k_y$). The bounding surface at $r_D = r_{eD}$ will be assumed either impermeable or at a constant pressure equal to the initial pressure. The bounding planes at $z_D = 0$ and h_D may be both impermeable, at constant pressure, or the plane at $z_D = 0$ may be impermeable while the plane at $z_D = h_D$ is at constant pressure.

We seek a solution of Eq. 2.2.12 in the following form:

$$\overline{\Delta p} = P + R. \tag{2.2.15}$$

In Eq. 2.2.15, P is a solution of Eq. 2.2.12 satisfying the condition given by Eq. 2.2.13 and the boundary conditions at $z_D = 0$ and h_D. It should be clear that P can be chosen as one of the solutions given by Eqs. 2.2.6, 2.2.8, or 2.2.11, depending on the boundary conditions at $z_D = 0$ and h_D (if one considers an instantaneous point source, then the equivalent forms of Eqs. 2.2.6, 2.2.8, or 2.2.11 for an instantaneous point source should be used). R in Eq. 2.2.15 is also a solution of Eq. 2.2.12 satisfying the boundary conditions at $z_D = 0$ and h_D and chosen such that $P + R$ satisfies the boundary condition at $r_D = r_{eD}$ and the flux condition given by Eq. 2.2.13 (since we have already required that P satisfy the flux condition, this means that the contribution of R to the flux as $r_D \to 0$ should vanish). A similar procedure is used by Muskat[30] to generate solutions for vertical line source wells in cylindrical reservoirs under steady flow assumption.

Let us first consider the case where the boundary conditions at $z_D = 0$ and h_D and at $r_D = r_{eD}$ are given, respectively, by

$$\frac{\partial \overline{\Delta p}}{\partial z_D}|_{z_D=0,h_D} = 0, \tag{2.2.16}$$

and

$$\frac{\partial \overline{\Delta p}}{\partial r_D}|_{r_D=r_{eD}} = 0. \tag{2.2.17}$$

In accordance with the boundary condition given by Eq. 2.2.16, we choose P as the solution given by the right hand side of Eq. 2.2.6. It can be shown that one of the solutions of Eq. 2.2.12 satisfying the condition given by Eq. 2.2.16 and not contributing to the flux as $r_D \to 0$ is the following expression:

$$R = AI_0(r_D\sqrt{u}) + \sum_{n=1}^{\infty} B_n\, I_0\left(r_D\sqrt{u + \frac{n^2\pi^2}{h_D^2}}\right)\cos n\pi\frac{z}{h}\cos n\pi\frac{z_w}{h} \tag{2.2.18}$$

If the coefficients A and B_n in Eq. 2.2.18 are chosen as

$$A = \frac{\tilde{q}\mu}{2\pi k L h_D s} \frac{K_1(r_{eD}\sqrt{u})}{I_1(r_{eD}\sqrt{u})}, \tag{2.2.19}$$

and

$$B_n = \frac{\tilde{q}\mu}{\pi k L h_D s} \frac{K_1\left(r_{eD}\sqrt{u+\frac{n^2\pi^2}{h_D^2}}\right)}{I_1\left(r_{eD}\sqrt{u+\frac{n^2\pi^2}{h_D^2}}\right)}, \tag{2.2.20}$$

then $P + R$ satisfies the boundary condition at $r_D = r_{eD}$ given by Eq. 2.2.17 and therefore the continuous point source solution for the system considered can be written from Eq. 2.2.15 as

$$\begin{aligned}\overline{\Delta p} = \frac{\tilde{q}\mu}{2\pi k L h_D s}\Bigg\{ & K_0\left(r_D\sqrt{u}\right) + \frac{I_0(r_D\sqrt{u})K_1(r_{eD}\sqrt{u})}{I_1(r_{eD}\sqrt{u})} \\ & + 2\sum_{n=1}^{\infty} \cos n\pi\frac{z}{h}\cos n\pi\frac{z_w}{h} \\ & \left[K_0\left(r_D\sqrt{u+\frac{n^2\pi^2}{h_D^2}}\right) + \frac{I_0\left(r_D\sqrt{u+\frac{n^2\pi^2}{h_D^2}}\right)K_1\left(r_{eD}\sqrt{u+\frac{n^2\pi^2}{h_D^2}}\right)}{I_1\left(r_{eD}\sqrt{u+\frac{n^2\pi^2}{h_D^2}}\right)}\right]\Bigg\}.\end{aligned} \tag{2.2.21}$$

If, in the above system, we replace the boundary condition given by Eq. 2.2.17 by

$$\overline{\Delta p}|_{r_D=r_{eD}} = 0, \tag{2.2.22}$$

then the function P would still be given by the right hand side of Eq. 2.2.6 but the function R would have to be chosen as

$$\begin{aligned}R = -\frac{\tilde{q}\mu}{2\pi k L h_D s}\Bigg\{ & \frac{I_0\left(r_D\sqrt{u}\right)K_0\left(r_{eD}\sqrt{u}\right)}{I_0\left(r_{eD}\sqrt{u}\right)} \\ & + 2\sum_{n=1}^{\infty}\cos n\pi\frac{z}{h}\cos n\pi\frac{z_w}{h}\left[\frac{I_0\left(r_D\sqrt{u+\frac{n^2\pi^2}{h_D^2}}\right)K_0\left(r_{eD}\sqrt{u+\frac{n^2\pi^2}{h_D^2}}\right)}{I_0\left(r_{eD}\sqrt{u+\frac{n^2\pi^2}{h_D^2}}\right)}\right]\Bigg\}.\end{aligned} \tag{2.2.23}$$

Therefore, the solution satisfying the boundary condition given by Eq. 2.2.22 would

be

$$\overline{\Delta p} = \frac{\tilde{q}\mu}{2\pi k L h_D s}\left\{K_0\left(r_D\sqrt{u}\right) - \frac{I_0\left(r_D\sqrt{u}\right)K_0\left(r_{eD}\sqrt{u}\right)}{I_0\left(r_{eD}\sqrt{u}\right)}\right.$$
$$+ 2\sum_{n=1}^{\infty}\cos n\pi\frac{z}{h}\cos n\pi\frac{z_w}{h}$$
$$\left.\left[K_0\left(r_D\sqrt{u+\frac{n^2\pi^2}{h_D^2}}\right) - \frac{I_0\left(r_D\sqrt{u+\frac{n^2\pi^2}{h_D^2}}\right)K_0\left(r_{eD}\sqrt{u+\frac{n^2\pi^2}{h_D^2}}\right)}{I_0\left(r_{eD}\sqrt{u+\frac{n^2\pi^2}{h_D^2}}\right)}\right]\right\}. \tag{2.2.24}$$

In general, after choosing the P function as one of the solutions given by Eqs. 2.2.6, 2.2.8, or 2.2.11, appropriate for the boundary conditions at $z_D = 0$ and h_D, the R function can be obtained by replacing the $K_0\left(r_D\sqrt{a}\right)$ terms in the P function by $I_0\left(r_D\sqrt{a}\right)K_1\left(r_{eD}\sqrt{a}\right) / I_1\left(r_{eD}\sqrt{a}\right)$ if the boundary condition at $r_D = r_{eD}$ is given by Eq. 2.2.17 and by $-I_0\left(r_D\sqrt{a}\right)K_0\left(r_{eD}\sqrt{a}\right) / I_0\left(r_{eD}\sqrt{a}\right)$ if the boundary condition at $r_D = r_{eD}$ is given by Eq. 2.2.22.

Continuous point source solutions for different combinations of boundary conditions at $z_D = 0$ and h_D are given in Table $2 - A$ of Appendix A. Solutions for line, surface, and volumetric sources can now be obtained by replacing $\overline{\Delta p}$ in Eq. 2.1.46 (note that we assume $\bar{\tilde{q}} = \tilde{q}/s$) with the point source solutions derived in this section and then using Eq. 2.1.48. Obtaining the solutions for line source wells and vertically fractured wells by using Eq. 2.1.48 follows the same lines as that explained in §2.2 II and will not be repeated here. Solutions for line source wells and vertically fractured wells obtained from the point source solutions given in Table $2 - A$ of Appendix A by using Eq. 2.1.48 are given in Tables $2 - B$ – $2 - E$ of Appendix A. All the solutions given in Table 2 of Appendix A assume that the flux distribution on the surface of the source and also in time is uniform. The relation between the production rate from the appropriate source, q, and the production rate from a point source, $\tilde{q}$, is also noted in Table 2 for each source type considered. We use h_w to denote the length of the open interval of the pay in case of limited entry wells, L_{x_f} to denote the half-length of a vertical fracture, and L_h to denote the length of horizontal line source wells. To the best of our knowledge,

all solutions, except the solutions for vertical line source wells, given in Table 2 of Appendix A are new. The solution for a partially penetrating vertical well in a double porosity medium is presented in Ref. 31 for finite wellbore radius, r_w.

Finally some care should be taken in applying solutions in Table 2 of Appendix A. If $k_x = k_y$, then the solutions given here correspond to a well located in a circular reservoir. If $k_x \neq k_y$ then the solutions given here will be applicable for wells at the center of reservoirs with elliptical outer boundaries.

III. Solutions for Bounded Reservoirs - Rectangular Reservoirs In this section, we derive the solutions for point source wells in rectangular reservoirs. Again we consider three combinations of boundary conditions for the top and the bottom of the reservoir. We consider all possible combinations of impermeable and constant pressure conditions along the bounding surfaces of the rectangular drainage region.

When the reservoir boundaries consist of planar surfaces, the method of images can be used to obtain the solutions in bounded systems by using the solution in an infinite system. It should be realized that two or three dimensional bounded system solutions cannot be obtained by using the appropriate one dimensional system solution as in Ref. 3 since Newman's product method is not applicable in Laplace domain[23]. Therefore, for each combination of boundary conditions, solutions must be obtained separately. This, of course, requires deriving more basic solutions (namely, point source solutions) than those required in real time domain (see Ref. 3); however, once the point source solutions are obtained for all combinations of boundary conditions, solutions for different source geometries can be simply obtained by using Eq. 2.1.48 (only integration of trigonometric functions is required). Note that, for homogeneous reservoirs, one may obtain the desired solution in real time domain by using the source functions given in Ref. 3 and then take the Laplace transform of the resulting solution. In this case, however, the procedure of taking the Laplace transform and evaluating some of the known series should be performed for every source-reservoir system considered (for example, see

Ref. 32).

Although obtaining the point source solutions in rectangular reservoirs by using the method of images is fairly easy, recasting the resulting expressions in a more managable form for computational purposes is not straightforward. Evaluation of triple infinite Fourier series in x, y and z directions is required; however, the triple infinite summations can be readily reduced by the procedure outlined in Appendix B. For two dimensional problems, these triple summations reduce to the computation of single summations, and for three dimensional problems, a double infinite series must be computed.

In order to briefly demonstrate the procedure used to generate the solutions given in this section, we consider an example case wherein all reservoir boundaries are impermeable. For convenience, we define

$$S_{i,j,l} = \frac{\exp\left[-\sqrt{u}\sqrt{(\tilde{x}_{Di} - 2kx_{eD})^2 + (\tilde{y}_{Dj} - 2my_{eD})^2 + (\tilde{z}_{Dl} - 2nh_D)^2}\right]}{\sqrt{(\tilde{x}_{Di} - 2kx_{eD})^2 + (\tilde{y}_{Dj} - 2my_{eD})^2 + (\tilde{z}_{Dl} - 2nh_D)^2}} \tag{2.2.25}$$

for i, j, $l = 1$ or 2, where

$$\tilde{x}_{D1} = x_D - x_{wD}, \tag{2.2.26}$$

$$\tilde{x}_{D2} = x_D + x_{wD}, \tag{2.2.27}$$

$$\tilde{y}_{D1} = y_D - y_{wD}, \tag{2.2.28}$$

$$\tilde{y}_{D2} = y_D + y_{wD}, \tag{2.2.29}$$

$$\tilde{z}_{D1} = z_D - z_{wD}, \tag{2.2.30}$$

and

$$\tilde{z}_{D2} = z_D + z_{wD}, \tag{2.2.31}$$

Physically, $S_{i,j,l}$ represents the contribution of each individual well in an infinite array of wells used to generate the influence of boundaries to the pressure distribution in the reservoir. By using Eqs. 2.1.40 and 2.2.25 and the method of images,

the point source solution in a reservoir as described above can be written as

$$\overline{\Delta p} = \frac{\tilde{q}\mu}{4\pi kLs} \sum_{k=-\infty}^{+\infty} \sum_{m=-\infty}^{+\infty} \sum_{n=-\infty}^{+\infty} (S_{1,1,1} + S_{2,1,1} + S_{1,2,1} + S_{2,2,1} + S_{1,1,2} + S_{2,1,2} + S_{1,2,2} + S_{2,2,2}). \tag{2.2.32}$$

(Note that in writing Eq. 2.2.32, we have assumed a uniform continuous source in time.) Using the triple summation formula given by Eq. $B-6$ in Appendix B for each triple summation in Eq. 2.2.32 and simplifying, we obtain the first solution given in Table $3-A$ of Appendix A:

$$\overline{\Delta p} = \frac{\tilde{q}\mu}{2kLx_{eD}s} \left\{ \frac{ch\sqrt{u}\,(y_{eD} - |y_D - y_{wD}|) + ch\sqrt{u}[y_{eD} - (y_D + y_{wD})]}{\sqrt{u}\,sh\sqrt{u}\,y_{eD}} \right.$$

$$+2\sum_{k=1}^{\infty} \cos k\pi \frac{x_D}{x_{eD}} \cos k\pi \frac{x_{wD}}{x_{eD}}$$

$$\frac{ch\sqrt{u+a}\,(y_{eD} - |y_D - y_{wD}|) + ch\sqrt{u+a}[y_{eD} - (y_D + y_{wD})]}{\sqrt{u+a}sh\sqrt{u+a}y_{eD}}$$

$$+2\sum_{n=1}^{\infty} \cos n\pi \frac{z_D}{h_D} \cos n\pi \frac{z_{wD}}{h_D}$$

$$\left[\frac{ch\sqrt{u+b}\,(y_{eD} - |y_D - y_{wD}|) + ch\sqrt{u+b}[y_{eD} - (y_D + y_{wD})]}{\sqrt{u+b}sh\sqrt{u+b}y_{eD}} \right.$$

$$+2\sum_{k=1}^{\infty} \cos k\pi \frac{x_D}{x_{eD}} \cos k\pi \frac{x_{wD}}{x_{eD}}$$

$$\left. \left. \frac{ch\sqrt{u+c}\,(y_{eD} - |y_D - y_{wD}|) + ch\sqrt{u+c}[y_{eD} - (y_D + y_{wD})]}{\sqrt{u+c}sh\sqrt{u+c}y_{eD}} \right] \right\}, \tag{2.2.33}$$

where $a = k^2\pi^2/x_{eD}^2$, $b = n^2\pi^2/h_D^2$, and $c = n^2\pi^2/h_D^2 + k^2\pi^2/x_{eD}^2$. $ch(x)$ and $sh(x)$ are used to denote the hyperbolic cosine and hyperbolic sine functions, respectively.

The procedure outlined above can be used to obtain the point source solutions for different combinations of boundary conditions. Triple summation formulas to be used in deriving appropriate solutions are given in Appendix B and the resulting point source solutions are tabulated in Table 3 of Appendix A. For convenience, we grouped these solutions in three sections. Solutions given in Table $3-A$ of Appendix

A are for rectangular reservoirs with impermeable top and bottom boundaries. In Table $3-B$ of Appendix A, the top and the bottom boundaries of the reservoir are assumed to be at constant pressure. Solutions given in Table $3-C$ of Appendix A assume that the reservoir boundary at the top ($z_D = 0$) is impermeable while the boundary at the bottom ($z_D = h_D$) is at constant pressure. The symbols $ch(x)$ and $sh(x)$ used in these tables denote hyperbolic cosine and hyperbolic sine functions, respectively. Shown to the left of each solution is the areal view of the reservoir corresponding to the respective solution. In these figures, unbroken lines denote the impermeable boundaries and dashed lines denote the constant pressure boundaries. The appropriate combinations of $S_{i,j,l}$ to be used in Eq. 2.2.32 are also noted. The point source is assumed to be located at some arbitrary point x_{wD}, y_{wD}, z_{wD} and its action is assumed to be continuous and uniform in time. (Although the list is extensive, for coding purposes, no particular difficulties are involved since many of the components of the solutions are identical.)

Point source solutions presented in Table 3 of Appendix A have not been reported in the literature. Utilizing the point source solutions given in Table 3 of Appendix A, solutions for a large variety of well-reservoir systems can be obtained by a simple integration with respect to x_w and/or z_w. Due to the large number of possible solutions and the simplicity of the required operations, solutions for different source geometries will not be presented in detail. The procedure to obtain the solutions for different source geometries is demonstrated on some example cases in §2.3.

2.3 Some Solutions for Rectangular Systems

To demonstrate the utility of the solutions presented in §2.2 III, here we derive three solutions of interest: a fully penetrating vertical well, a fully penetrating vertical fracture, and a horizontal well in a closed rectangular reservoir. The top and the bottom boundaries of the reservoir are assumed to be impermeable. We will assume that the flux distribution on the surface of the well is uniform. For generality,

we will express the solutions in terms of the dimensionless pressure defined by

$$\overline{p}_D = \frac{2\pi kh}{q\mu}\overline{\Delta p}. \tag{2.3.1}$$

We will define the dimensionless time, t_D, as in Eq. 2.1.8 with $L = r_w$, L_{x_f}, and $L_h/2$ for vertical well, vertically fractured well, and horizontal well, respectively. For discussion, we will also assume that the reservoir is isotropic; that is, $k = k_x = k_y = k_z$.

<u>I. Fully Penetrating Vertical Well</u> As required by Eq. 2.1.48, the solution for this problem is obtained by integrating the solution given in Eq. 2.2.33 with respect to z'_w over the interval 0 to h. (Note that only the integral of $\cos \alpha z_w$ needs to be determined.) The appropriate result is

$$\begin{aligned}\overline{\Delta p} = \frac{\tilde{q}\mu h}{2kLx_{eD}h_D s}\Bigg[&\frac{ch\sqrt{u}(y_{eD} - |y_D - y_{wD}|) + ch\sqrt{u}[y_{eD} - (y_D + y_{wD})]}{\sqrt{u}sh\sqrt{u}y_{eD}} \\ &+ 2\sum_{k=1}^{\infty}\cos k\pi\frac{x_D}{x_{eD}}\cos k\pi\frac{x_{wD}}{x_{eD}} \\ &\frac{ch\sqrt{u+\frac{k^2\pi^2}{x_{eD}^2}}(y_{eD} - |y_D - y_{wD}|) + ch\sqrt{u+\frac{k^2\pi^2}{x_{eD}^2}}[y_{eD} - (y_D + y_{wD})]}{\sqrt{u+\frac{k^2\pi^2}{x_{eD}^2}}\ sh\ \sqrt{u+\frac{k^2\pi^2}{x_{eD}^2}}y_{eD}}\Bigg].\end{aligned} \tag{2.3.2}$$

If we use the definition of $\overline{p}_D$ given by Eq. 2.3.1 (with $q = \tilde{q}h$), then we can write Eq. 2.3.2 as

$$\begin{aligned}\overline{p}_D(x_D, y_D) = \frac{\pi}{x_{eD}s}\Bigg[&\frac{ch\sqrt{u}\,(y_{eD} - |y_D - y_{wD}|) + ch\sqrt{u}[y_{eD} - (y_D + y_{wD})]}{\sqrt{u}\ sh\ \sqrt{u}y_{eD}} \\ &+ 2\sum_{k=1}^{\infty}\cos k\pi\frac{x_D}{x_{eD}}\cos k\pi\frac{x_{wD}}{x_{eD}} \\ &\frac{ch\sqrt{u+\frac{k^2\pi^2}{x_{eD}^2}}(y_{eD} - |y_D - y_{wD}|) + ch\sqrt{u+\frac{k^2\pi^2}{x_{eD}^2}}[y_{eD} - (y_D + y_{wD})]}{\sqrt{u+\frac{k^2\pi^2}{x_{eD}^2}}sh\sqrt{u+\frac{k^2\pi^2}{x_{eD}^2}}y_{eD}}\Bigg].\end{aligned} \tag{2.3.3}$$

Here s represents the Laplace transform variable with respect to dimensionless time based on the wellbore radius, r_w.

II. Fully Penetrating Vertically Fractured Well The solution for this problem is obtained by integrating the solution given in Eq. 2.2.33 with respect to z'_w over the interval 0 to h and then with respect x'_w over the interval $x_w - L_{x_f}$ to $x_w + L_{x_f}$. (Note that only integrals of $\cos \alpha z_w$ and $\cos \alpha x_w$ need to be determined.) Using the definition of the dimensionless pressure given by Eq. 2.3.1 (with $q = 2\tilde{q}hL_{x_f}$), the result is the following expression:

$$\bar{p}_D(x_D, y_D) = \frac{\pi}{x_{eD}s}\left[\frac{ch\sqrt{u}\,(y_{eD} - |y_D - y_{wD}|) + ch\sqrt{u}[y_{eD} - (y_D + y_{wD})]}{\sqrt{u}\;sh\;\sqrt{u}y_{eD}}\right.$$
$$+ \frac{2x_{eD}}{\pi}\sum_{k=1}^{\infty}\frac{1}{k}\sin\; k\pi\frac{1}{x_{eD}}\cos\; k\pi\frac{x_{wD}}{x_{eD}}\cos\; k\pi\frac{x_D}{x_{eD}}$$
$$\left.\frac{ch\sqrt{u + \frac{k^2\pi^2}{x_{eD}^2}}(y_{eD} - |y_D - y_{wD}|) + ch\sqrt{u + \frac{k^2\pi^2}{x_{eD}^2}}[y_{eD} - (y_D + y_{wD})]}{\sqrt{u + \frac{k^2\pi^2}{x_{eD}^2}}sh\sqrt{u + \frac{k^2\pi^2}{x_{eD}^2}}y_{eD}}\right]. \tag{2.3.4}$$

Here s represents the Laplace transform variable with respect to dimensionless time based on fracture half-length, L_{x_f}.

Recently, Fraim and Lee[32] used the solution presented by Gringarten *et al.*[10] (Eq. 29 of Ref. 10) and derived an expression for the Laplace transform of the dimensionless wellbore pressure for a vertical fracture located at the center of a closed, square drainage region ($x_{wD} = x_{eD}/2$, $y_{wD} = y_{eD}/2$, $x_{eD} = y_{eD}$). Their expression can be obtained from Eq. 2.3.4 to be

$$\bar{p}_{wD} = \frac{\pi}{\tilde{s}}\frac{coth\,\sqrt{\frac{\tilde{u}}{4}}}{\sqrt{\tilde{u}}}$$
$$+ \frac{x_{eD}}{\tilde{s}}\sum_{k=1}^{\infty}\frac{1}{k}\sin 2k\pi\frac{1}{x_{eD}}\cos 2k\pi\frac{x_D}{x_{eD}}\frac{coth\sqrt{\frac{\tilde{u}}{4} + k^2\pi^2}}{\sqrt{\tilde{u} + 4k^2\pi^2}}. \tag{2.3.5}$$

In Eq. 2.3.5, $\tilde{s}$ denotes the Laplace transform variable with respect to t_{DA} where

$$t_{DA} = \frac{t_D}{x_{eD}^2}, \tag{2.3.6}$$

and $\tilde{u} = \tilde{s}f(\tilde{s})$. To account for the change in time scale, we used the Laplace transformation property

$$c\overline{F}(cs) = \mathcal{L}\{F(t/c)\}, \tag{2.3.7}$$

wher $\mathcal{L}$ denotes the Laplace transform operator. Using $f(\tilde{s}) = 1$, we recognize that Eq. 2.3.5 is the solution given by Ref. 32 for homogeneous reservoirs.

III. Horizontal Well The solution for this case is obtained by integrating the point source solution given by Eq. 2.2.33 from $x_w - L_h/2$ to $x_w + L_h/2$ with respect to x'_w. The appropriate expression for the dimensionless pressure drop is given by

$$\overline{p}_D = \overline{p}_{Df} + \overline{F}_1, \tag{2.3.8}$$

where $\overline{p}_D$ is defined by Eq. 2.3.1 (with $q = \tilde{q}L_h$), $\overline{p}_{Df}$ is the fracture solution given by the right hand side of Eq. 2.3.4, and $\overline{F}_1$ is defined by

$$\begin{aligned}
\overline{F}_1 &= \frac{2\pi}{x_{eD}s}\sum_{n=1}^{\infty}\cos n\pi z_D \cos n\pi z_{wD} \\
&\frac{ch\sqrt{u+a}\,(y_{eD} - |y_D - y_{wD}|) + ch\sqrt{u+a}[y_{eD} - (y_D + y_{wD})]}{\sqrt{u+a}\;sh\sqrt{u+a}\,y_{eD}} \\
&+ \frac{4}{s}\sum_{n=1}^{\infty}\cos n\pi z_D \cos n\pi z_{wD}\sum_{k=1}^{\infty}\frac{1}{k}\sin k\pi\frac{1}{x_{eD}}\cos k\pi\frac{x_{wD}}{x_{eD}}\cos k\pi\frac{x_D}{x_{eD}} \\
&\frac{ch\sqrt{u+b}\,(y_{eD} - |y_D - y_{wD}|) + ch\sqrt{u+b}[y_{eD} - (y_D + y_{wD})]}{\sqrt{u+b}\;sh\sqrt{u+b}\,y_{eD}}.
\end{aligned} \tag{2.3.9}$$

Here $a = n^2\pi^2 L_D^2$ and $b = n^2\pi^2 L_D^2 + k^2\pi^2/x_{eD}^2$. In Eqs. 2.3.8 and 2.3.9, s is the Laplace transform variable with respect to dimensionless time, t_D, based on the horizontal well half length, $L_h/2$ and z_D and L_D are defined, respectively, by

$$z_D = z/h \tag{2.3.10}$$

and

$$L_D = \frac{L}{2h} = \frac{1}{h_D}. \tag{2.3.11}$$

As mentioned earlier, obtaining the solution for the pressure distribution, is only the first step toward the computation of well responses. Examining the solutions derived in this section, it is reasonable for one to be concerned about the computational difficulties involved. These aspects are addressed in §§2.5 and 2.6.

2.4 Anisotropic Reservoirs

Solutions presented in §§2.1 and 2.2 consider that the reservoir may be anisotropic in the three principal directions, x, y, z; that is, k_x, k_y, k_z, are the permeabilities in x, y, and z directions, respectively, and k represents the permeability of an equivalent isotropic system. In the solutions presented in §§2.1 and 2.2, k is defined by

$$k = \sqrt[3]{k_x k_y k_z}. \tag{2.4.1}$$

In many instances, it is convenient to define the permeability in the horizontal plane (x - y) by

$$k_h = \sqrt{k_x k_y}, \tag{2.4.2}$$

and replace k in the definitions of dimensionless variables by k_h. The procedure to accomplish this objective is as follows: Let t_D denote the dimensionless time based on k given by Eq. 2.4.1 and $\tilde{t}_D$ denote the dimensionless time based on k_h given by Eq. 2.4.2. Then we have the follwing relation:

$$\tilde{t}_D = \frac{k_h}{k} t_D. \tag{2.4.3}$$

Eq. 2.4.3 indicates that solutions based on the dimensionless time $\tilde{t}_D$ can be obtained from solutions based on the dimensionless time t_D by simply replacing t_D by $(k/k_h)\tilde{t}_D$ in real time domain. Since in our solutions we apply the Laplace transformation to dimensionless time, t_D, this operation can be accomplished through the use of the following property of the Laplace transforms:

$$c\overline{F}(cs) = \mathcal{L}\{F(t/c)\}. \tag{2.4.4}$$

Therefore, if we wish to obtain solutions defined in terms of dimensionless variables based on k_h (or for $k_x = k_y$), then the property of the Laplace transformation given by Eq. 2.4.4 should be applied to the solutions presented in §§2.1 and 2.2. As an example, let us consider the case of a horizontal well in an infinite reservoir. Assuming that the well center is at the origin ($x_{wD} = y_{wD} = 0$) and using $L = L_h/2$

where L_h is the length of the well, the horizontal well solution given in Table $1-A$ of Appendix A can be written as:

$$\begin{aligned}
&\overline{\Delta p}(x_D, y_D, z_D, z_{wD}, h_D, s) = \frac{\tilde{q}\mu}{2\pi k h_D s} \\
&\left\{ \int_{-1}^{+1} K_0 \left[\sqrt{sf(s)} \sqrt{\left(x_D - \alpha\sqrt{k/k_x}\right)^2 + y_D^2} \right] d\alpha \right. \\
&+ \sum_{n=1}^{\infty} \cos n\pi z_D \cos n\pi z_{wD} \\
&\left. \int_{-1}^{+1} K_0 \left[\sqrt{sf(s) + \frac{n^2\pi^2}{h_D^2}} \sqrt{\left(x_D - \alpha\sqrt{k/k_x}\right)^2 + y_D^2} \right] d\alpha \right\}.
\end{aligned} \tag{2.4.5}$$

In Eq. 2.4.5, s denotes the Laplace transform variable with respect to dimensionless time, t_D, based on k and x_D, y_D, z_D, and h_D are defined by

$$x_D = \frac{2x}{L_h}\sqrt{\frac{k}{k_x}}, \tag{2.4.6}$$

$$y_D = \frac{2y}{L_h}\sqrt{\frac{k}{k_y}}, \tag{2.4.7}$$

$$z_D = \frac{z}{h}, \tag{2.4.8}$$

and

$$h_D = \frac{2h}{L_h}\sqrt{\frac{k}{k_z}}. \tag{2.4.9}$$

If we define the following dimensionless variables based on k_h

$$\tilde{x}_D = \sqrt{\frac{k_h}{k}} x_D, \tag{2.4.10}$$

$$\tilde{y}_D = \sqrt{\frac{k_h}{k}} y_D, \tag{2.4.11}$$

$$\tilde{h}_D = \sqrt{\frac{k_h}{k}} h_D, \tag{2.4.12}$$

and also note that

$$h_D = \frac{2h}{L_h}\sqrt{\frac{k}{k_z}} = \frac{2h}{L_h}\frac{\sqrt{k_x k_y}\sqrt{k}}{k^{3/2}} = \frac{2h}{L_h}\frac{k_h}{k}, \tag{2.4.13}$$

then we can rearrange Eq. 2.4.5 to write the following solution expressed in terms of the dimensionless variables given by Eqs. 2.4.10 – 2.4.12:

$$\begin{aligned}
&\widetilde{\overline{\Delta p}}(\tilde{x}_D, \tilde{y}_D, z_D, z_{wD}, \tilde{h}_D, s) = \frac{\tilde{q}\mu\,(k/k_h)}{2\pi\,(2h/L_h)\,k_h\,(k/k_h)\,s} \\
&\left\{\int_{-1}^{+1} K_0\left[\sqrt{\frac{k}{k_h}s\tilde{f}\left(\frac{k}{k_h}s\right)}\sqrt{\left(\tilde{x}_D - \alpha\sqrt{k_h/k_x}\right)^2 + \tilde{y}_D^2}\right] d\alpha\right. \\
&+ \sum_{n=1}^{\infty} \cos n\pi z_D \cos n\pi z_{wD} \\
&\left.\int_{-1}^{+1} K_0\left[\sqrt{\frac{k}{k_h}s\tilde{f}\left(\frac{k}{k_h}s\right) + \frac{n^2\pi^2}{\tilde{h}_D^2}}\sqrt{\left(\tilde{x}_D - \alpha\sqrt{k_h/k_x}\right)^2 + \tilde{y}_D^2}\right] d\alpha\right\},
\end{aligned} \tag{2.4.14}$$

where

$$\tilde{f}\left(\frac{k}{k_h}s\right) = \frac{(k/k_h)\,sw\,(1-w) + \tilde{\lambda}}{(k/k_h)\,s\,(1-w) + \tilde{\lambda}} \tag{2.4.15}$$

and

$$\tilde{\lambda} = \frac{k}{k_h}\lambda. \tag{2.4.16}$$

Comparing Eqs. 2.4.5 and 2.4.14, it can be shown that

$$\widetilde{\overline{\Delta p}} = \frac{kh_D}{(2h/L_h)\,k_h}\left[\frac{k}{k_h}\overline{\Delta p}\left(\frac{k}{k_h}s\right)\right] = \frac{kh_D}{(2h/L_h)\,k_h}\mathcal{L}\{\Delta p\,(\tilde{t}_D)\}, \tag{2.4.17}$$

where the last equality follows from the relation given by Eq. 2.4.4 and $\tilde{t}_D$ is defined by Eq. 2.4.3. Then, if we define $\tilde{s}$ as the Laplace transform variable with respect to $\tilde{t}_D$, we can write the following relation:

$$\widetilde{\overline{\Delta p}} = \frac{kh_D}{(2h/L_h)\,k_h}\overline{\Delta p}\,(\tilde{s})\,. \tag{2.4.18}$$

Using the relation given by Eq. 2.4.18 and Eq. 2.4.5, the horizontal well solution expressed in terms of the dimensionless variables based on k_h can be written as

$$\begin{aligned}
&\widetilde{\overline{\Delta p}}(\tilde{x}_D, \tilde{y}_D, z_D, z_{wD}, \tilde{h}_D, \tilde{s}) = \frac{\tilde{q}\mu}{2\pi\,(2h/L_h)\,k_h\tilde{s}} \\
&\left\{\int_{-1}^{+1} K_0\left[\sqrt{\tilde{s}\tilde{f}\,(\tilde{s})}\sqrt{\left(\tilde{x}_D - \alpha\sqrt{k_h/k_x}\right)^2 + \tilde{y}_D^2}\right] d\alpha\right. \\
&+ \sum_{n=1}^{\infty} \cos n\pi z_D \cos n\pi z_{wD} \\
&\left.\int_{-1}^{+1} K_0\left[\sqrt{\tilde{s}\tilde{f}\,(\tilde{s}) + \frac{n^2\pi^2}{\tilde{h}_D^2}}\sqrt{\left(\tilde{x}_D - \alpha\sqrt{k_h/k_x}\right)^2 + \tilde{y}_D^2}\right] d\alpha\right\}.
\end{aligned} \tag{2.4.19}$$

The procedure outlined above can be applied to all solutions presented in §§2.1 and 2.2 to take into account the anisotropy of the formation in different forms.

2.5 Computational Remarks

In the preceding sections, we have developed solutions for a wide variety of well-reservoir systems that are of interest in well testing. As already mentioned, in some cases, the direct result of the analytical derivations may not provide a form of the solution which is convenient for computational purposes. In fact, it is for this reason that some of the Laplace domain solutions which were available in the literature previously (for example, the solution for a vertically fractured well in an infinite reservoir[15]) did not find wide utility. One of the major contributions of this section is to provide the means to compute the solutions presented in the preceding sections. In §2.6, we consider representative examples to demonstrate the procedure to recast the solutions in forms that are convenient for computational purposes. Here we consider some common components of the solutions that cause computational problems and develop alternate forms that should be used in computations. Specifically, in this section, we discuss the evaluation of integrals of the form $\int_{-a}^{+a} K_0[f(x-\alpha)]d\alpha$ and some of the slowly converging series for small values of time (large value of the Laplace variable). The use of the alternate forms of these integrals and series is demonstrated in §2.6.

I. Evaluation of the Integral $\int_{-a}^{+a} K_0\left[b\sqrt{(x_D-\alpha\sqrt{k/k_x})^2}\right]d\alpha$

The Bessel function $K_0(z)$ is real and positive when $z>0$. If $|x_D| \le a\sqrt{k/k_x}$, we can write

$$\int_{-a}^{+a} K_0\left[b\sqrt{(x_D-\alpha\sqrt{k/k_x})^2}\right]d\alpha =$$

$$\int_{-a}^{x_D\sqrt{k_z/k}} K_0\left[b(x_D-\alpha\sqrt{k/k_x})\right]d\alpha + \int_{x_D\sqrt{k_z/k}}^{+a} K_0\left[b(\alpha\sqrt{k/k_x}-x_D)\right]d\alpha$$

$$= \frac{1}{b\sqrt{k/k_x}}\left[\int_0^{b(a\sqrt{k/k_x}+x_D)} K_0(u)du + \int_0^{b(a\sqrt{k/k_x}-x_D)} K_0(u)du\right]. \qquad (2.5.1)$$

Similarly, if $|x_D| \geq a\sqrt{k/k_x}$, we can write

$$\int_{-a}^{+a} K_0\left[b\sqrt{(x_D - \alpha\sqrt{k/k_x})^2}\right] d\alpha = \frac{1}{b\sqrt{k/k_x}}\left[\int_0^{b(|x_D|+a\sqrt{k/k_x})} K_0(u)du - \int_0^{b(|x_D|-a\sqrt{k/k_x})} K_0(u)du\right]. \tag{2.5.2}$$

If $|x_D| = a\sqrt{k/k_x}$, then from Eqs. 2.5.1 and 2.5.2, we have

$$\int_{-a}^{+a} K_0\left[b\sqrt{(x_D - \alpha\sqrt{k/k_x})^2}\right] d\alpha = \frac{1}{b\sqrt{k/k_x}} \int_0^{2ab\sqrt{k/k_x}} K_0(u)du. \tag{2.5.3}$$

The following series expansion for $\int_0^x K_0(u)du$ given by Ref. 27 can be used to compute the right hand side of Eqs. 2.5.1 - 2.5.3:

$$\int_0^x K_0(u)du = -(\ln\frac{x}{2} + \gamma)x\sum_{k=0}^{\infty}\frac{(x/2)^{2k}}{(k!)^2(2k+1)} + x\sum_{k=0}^{\infty}\frac{(x/2)^{2k}}{(k!)^2(2k+1)^2} + x\sum_{k=1}^{\infty}\frac{(x/2)^{2k}}{(k!)^2(2k+1)}\sum_{n=1}^{k}\frac{1}{n}, \tag{2.5.4}$$

where γ is Euler's constant ($\gamma = 0.5772...$). Note that the number of terms used for the convergence of the infinite series on the right hand side of Eq. 2.5.4 increases as x becomes large. As $x \to \infty$, however, the following relation is known[27]:

$$\int_0^{\infty} K_0(u)du = \frac{\pi}{2} \tag{2.5.5}.$$

We have found that, for $x \geq 20$, the right hand side of Eq. 2.5.4 approaches $\pi/2$ for all practical purposes. For $x < 20$, the series on the right hand side of Eq. 2.5.4 converge fast.

An alternate form of the integral $\int_0^x K_0(u)du$ can be written by using Eq. 2.5.5 as follows:

$$\int_0^x K_0(u)du = \frac{\pi}{2} - Ki_1(x), \tag{2.5.6}$$

where

$$Ki_1(x) = \int_x^{\infty} K_0(u)du. \tag{2.5.7}$$

Values of $Ki_1(x)$ can be obtained from the table given by Ref. 27 (Table 11.1 of Ref. 27) or by numerical integration. By using Table 11.1 of Ref. 27, we can also show that $Ki_1(x)$ can be neglected compared to $\pi/2$, for example, within 1% when $x \geq 3.6$ and therefore, $\int_0^x K_0(u)du \approx \pi/2$ within 1% for $x \geq 3.6$.

II. Computation of the Series

$$\sum_{n=1}^{\infty} \frac{\cos n\pi z \cos n\pi z_w}{\sqrt{u + \frac{n^2\pi^2}{h_D^2} + a^2}} \exp\left[-\sqrt{u + \frac{n^2\pi^2}{h_D^2} + a^2 y_D}\right]$$

at Large Values of u for $y_D > 0$

We can write

$$\sum_{n=1}^{\infty} \frac{\cos n\pi z \cos n\pi z_w}{\sqrt{u + \frac{n^2\pi^2}{h_D^2} + a^2}} \exp\left[-\sqrt{u + \frac{n^2\pi^2}{h_D^2} + a^2 y_D}\right] =$$

$$0.5\left[\sum_{n=1}^{\infty} \frac{\cos n\pi(z - z_w)}{\sqrt{u + \frac{n^2\pi^2}{h_D^2} + a^2}} + \sum_{n=1}^{\infty} \frac{\cos n\pi(z + z_w)}{\sqrt{u + \frac{n^2\pi^2}{h_D^2} + a^2}}\right] \exp\left[-\sqrt{u + \frac{n^2\pi^2}{h_D^2} + a^2 y_D}\right]. \tag{2.5.8}$$

If we let u denote the Laplace transform variable with respect to τ, then we can show that

$$\sum_{n=1}^{\infty} \frac{\cos n\pi x}{\sqrt{u + \frac{n^2\pi^2}{h_D^2} + a^2}} \exp\left[-\sqrt{u + \frac{n^2\pi^2}{h_D^2} + a^2 y_D}\right] = \mathcal{L}\{F\}, \tag{2.5.9}$$

where $\mathcal{L}$ denotes the Laplace transform operator and F is given by

$$F = \frac{1}{\sqrt{\pi\tau}} \exp\left(-\frac{y_D^2}{4\tau}\right) \exp\left(-a^2\tau\right) \sum_{n=1}^{\infty} \cos n\pi x \exp\left(-\frac{n^2\pi^2}{h_D^2}\tau\right). \tag{2.5.10}$$

Using Poisson's summation formula given by Eq. 2.2.4 in §2.2, the right hand side of Eq. 2.5.10 can be written as

$$F = \frac{h_D \exp\left(-a^2\tau\right)}{2\pi\tau} \sum_{n=-\infty}^{+\infty} \exp\left[-\frac{(x - 2n)^2 h_D^2 + y_D^2}{4\tau}\right] - \frac{\exp\left(-\frac{y_D^2}{4\tau}\right) \exp\left(-a^2\tau\right)}{2\sqrt{\pi\tau}}. \tag{2.5.11}$$

Taking the Laplace transform of Eq. 2.5.11, we obtain

$$\mathcal{L}\{F\} = \frac{h_D}{\pi} \sum_{n=-\infty}^{+\infty} K_0 \left[\sqrt{(x-2n)^2 h_D^2 + y_D^2} \sqrt{u+a^2} \right] - \frac{\exp\left(-\sqrt{u+a^2} y_D\right)}{2\sqrt{u+a^2}}. \tag{2.5.12}$$

Substituting the right hand side of Eq. 2.5.12 into Eq. 2.5.9 for $\mathcal{L}\{F\}$, we write the following relation

$$\sum_{n=1}^{\infty} \frac{\cos n\pi x}{\sqrt{u + \frac{n^2\pi^2}{h_D^2} + a^2}} \exp\left[-\sqrt{u + \frac{n^2\pi^2}{h_D^2} + a^2} y_D \right] =$$

$$\frac{h_D}{\pi} \sum_{n=-\infty}^{+\infty} K_0 \left[\sqrt{(x-2n)^2 h_D^2 + y_D^2} \sqrt{u+a^2} \right] - \frac{\exp\left(-\sqrt{u+a^2} y_D\right)}{2\sqrt{u+a^2}}. \tag{2.5.13}$$

Using the relation given by Eq. 2.5.13 in Eq. 2.5.8, we finally obtain

$$\sum_{n=1}^{\infty} \frac{\cos n\pi z \cos n\pi z_w}{\sqrt{u + \frac{n^2\pi^2}{h_D^2} + a^2}} \exp\left[-\sqrt{u + \frac{n^2\pi^2}{h_D^2} + a^2} y_D \right] =$$

$$\frac{h_D}{2\pi} \sum_{n=-\infty}^{+\infty} \left\{ K_0 \left[\sqrt{(z - z_w - 2n)^2 h_D^2 + y_D^2} \sqrt{u+a^2} \right] \right.$$

$$\left. + K_0 \left[\sqrt{(z + z_w - 2n)^2 h_D^2 + y_D^2} \sqrt{u+a^2} \right] \right\} - \frac{\exp\left(-\sqrt{u+a^2} y_D\right)}{2\sqrt{u+a^2}}. \tag{2.5.14}$$

Note that if u is large, $u + n^2\pi^2/h_D^2 + a^2 \approx u$ until $n^2\pi^2/h_D^2 + a^2$ becomes comparable to u. Therefore, at large values of u, the partial sum of the series in the left hand side of Eq. 2.5.14 will be changing even though several thousand terms are considered. The series on the right hand side of Eq. 2.5.14, on the other hand, converges rapidly since $K_0(x)$ approaches zero rapidly as x becomes large.

III. Computation of the Series

$$\sum_{n=1}^{\infty} \frac{\sin n\pi z \sin n\pi z_w}{\sqrt{u + \frac{n^2\pi^2}{h_D^2} + a^2}} \exp\left[-\sqrt{u + \frac{n^2\pi^2}{h_D^2} + a^2} y_D \right]$$

at Large Values of u for $y_D > 0$

We can write

$$\sum_{n=1}^{\infty} \frac{\sin n\pi z \sin n\pi z_w}{\sqrt{u + \frac{n^2\pi^2}{h_D^2} + a^2}} \exp\left[-\sqrt{u + \frac{n^2\pi^2}{h_D^2} + a^2}\, y_D\right] =$$

$$0.5\left[\sum_{n=1}^{\infty} \frac{\cos n\pi\,(z - z_w)}{\sqrt{u + \frac{n^2\pi^2}{h_D^2} + a^2}} - \sum_{n=1}^{\infty} \frac{\cos n\pi\,(z + z_w)}{\sqrt{u + \frac{n^2\pi^2}{h_D^2} + a^2}}\right] \exp\left[-\sqrt{u + \frac{n^2\pi^2}{h_D^2} + a^2}\, y_D\right]. \tag{2.5.15}$$

Using Eq. 2.5.13, we obtain the following relation

$$\sum_{n=1}^{\infty} \frac{\sin n\pi z \sin n\pi z_w}{\sqrt{u + \frac{n^2\pi^2}{h_D^2} + a^2}} \exp\left[-\sqrt{u + \frac{n^2\pi^2}{h_D^2} + a^2}\, y_D\right] =$$

$$\frac{h_D}{2\pi} \sum_{n=-\infty}^{+\infty} \left\{ K_0\left[\sqrt{(z - z_w - 2n)^2 h_D^2 + y_D^2}\sqrt{u + a^2}\right] \right.$$

$$\left. - K_0\left[\sqrt{(z + z_w - 2n)^2 h_D^2 + y_D^2}\sqrt{u + a^2}\right]\right\}. \tag{2.5.16}$$

IV. Computation of the Series

$$\sum_{n=1}^{\infty} \frac{\cos(2n-1)\frac{\pi}{2} z \cos(2n-1)\frac{\pi}{2} z_w}{\sqrt{u + \frac{(2n-2)^2\pi^2}{4h_D^2} + a^2}} \exp\left[-\sqrt{u + \frac{(2n-1)^2\pi^2}{4h_D^2} + a^2}\, y_D\right]$$

at Large Values of u for $y_D > 0$

We can write

$$\sum_{n=1}^{\infty} \frac{\cos\,(2n-1)\,\frac{\pi}{2} z \cos\,(2n-1)\,\frac{\pi}{2} z_w}{\sqrt{u + \frac{(2n-1)^2\pi^2}{4h_D^2} + a^2}} \exp\left[-\sqrt{u + \frac{(2n-1)^2\pi^2}{4h_D^2} + a^2}\, y_D\right] =$$

$$0.5\left[\sum_{n=1}^{\infty} \frac{\cos\,(2n-1)\,\frac{\pi}{2}\,(z - z_w)}{\sqrt{u + \frac{(2n-1)^2\pi^2}{4h_D^2} + a^2}} + \sum_{n=1}^{\infty} \frac{\cos\,(2n-1)\,\frac{\pi}{2}\,(z + z_w)}{\sqrt{u + \frac{n^2\pi^2}{h_D^2} + a^2}}\right]$$

$$\exp\left[-\sqrt{u + \frac{(2n-1)^2\pi^2}{4h_D^2} + a^2}\, y_D\right]. \tag{2.5.17}$$

By similar arguments as explained above, we can show the following relation:

$$\sum_{n=1}^{\infty} \frac{\cos(2n-1)\frac{\pi}{2}x}{\sqrt{u+\frac{(2n-1)^2\pi^2}{4h_D^2}+a^2}} \exp\left[-\sqrt{u+\frac{(2n-1)^2\pi^2}{4h_D^2}+a^2}\,y_D\right] =$$

$$\frac{h_D}{2\pi}\sum_{n=-\infty}^{+\infty}(-1)^n K_0\left[\sqrt{(x-2n)^2 h_D^2+y_D^2}\sqrt{u+a^2}\right]. \qquad (2.5.18)$$

Using Eq. 2.5.18 and Eq. 2.5.17, we obtain

$$\sum_{n=1}^{\infty} \frac{\cos(2n-1)\frac{\pi}{2}z\cos(2n-1)\frac{\pi}{2}z_w}{\sqrt{u+\frac{(2n-1)^2\pi^2}{4h_D^2}+a^2}} \exp\left[-\sqrt{u+\frac{(2n-1)^2\pi^2}{4h_D^2}+a^2}\,y_D\right] =$$

$$\frac{h_D}{4\pi}\sum_{n=-\infty}^{+\infty}(-1)^n\left\{K_0\left[\sqrt{(z-z_w-2n)^2 h_D^2+y_D^2}\sqrt{u+a^2}\right]\right.$$

$$\left.+K_0\left[\sqrt{(z+z_w-2n)^2 h_D^2+y_D^2}\sqrt{u+a^2}\right]\right\}. \qquad (2.5.19)$$

2.6 Computational Considerations

As mentioned before, even if solutions in terms of the Laplace transform variable, s, are available, computations can be exceedingly difficult. First, difficulties in computing integrals of the form $\int_{-a}^{+a} K_0\left[f\left(u-\alpha\right)\right]d\alpha$ for small values of $f\left(u-\alpha\right)$ must be overcome. Second, in some cases, components of the solution converge extremely slowly – in fact, in some cases, for certain time ranges the series behave as if they are divergent series. Third, computation of double infinite Fourier series can also pose problems. Thus, even though some of the solutions given in Tables 1-3 of Appendix A are available in the literature, these solutions have not found wide utility. The developments given in §2.5 overcome most of the computational problems and we believe represent an important contribution to the literature. In this section, we examine some example solutions to briefly discuss computational issues one will frequently encounter. Solutions presented in this section are expressed in terms of the dimensionless pressure defined by Eq. 2.3.1 in §2.3. In all computations presented in this and the following sections, we used the Laplace inversion

algorithm suggested by Stehfest[9]. We have found that the Stehfest algorithm can be successfully used to numerically invert the solutions presented in this chapter.

At this point, a remark on the use of the Stehfest algorithm appears to be appropriate. The accuracy of the results obtained by using the numerical inversion algorithm suggested by Stehfest is governed by a parameter denoted by N. Briefly, the parameter N determines the number of terms to be considered in the computation of the series used to approximate the Laplace inversion of the subject function (see Ref. 9 for details). Theoretically, the accuracy of the numerical inversion should improve as the value of N increases. In practice, however, as N becomes too large, the result suffers from rounding errors. Stehfest suggests that the optimum value of N is approximately proportional to the number of digits used in computations. The optimum value for N, however, should still be determined by examining the variation of the results by the changes in the values of N. In our experience, as a starting guess, N can be chosen as 8 for the inversion of infinite acting system solutions and as 16 for the inversion of bounded system solutions. In many cases however, variations do occur in the optimum value of N by the variations of the behavior of the subject function from one time interval to the other. In dealing with such functions, it is often useful to develop a procedure to test the sensitivity of the results to the variations in the value of N (note however that insensitivity to the value of N does not guarantee the correct numerical inversion; the result should also be checked by other means). In obtaining the results presented in this chapter, we used an algorithm to determine the maximum value of N in the range from 6 to 18 for which the minimum variation occured from the results computed by using the next lower value of N.

<u>I. Vertically Fractured Well, Infinite Reservoir</u> For this well system, the solution given in Table 1-A of Appendix A yields the following expression for the Laplace transform of the dimensionless pressure, $\overline{p}_D$:

$$\overline{p}_D = \frac{1}{2s}\int_{-1}^{+1} K_0\left[\sqrt{u}\sqrt{(x_D-\alpha)^2+y_D^2}\right] d\alpha. \qquad (2.6.1)$$

Here we have assumed an isotropic reservoir ($k = k_x = k_y = k_z$) with the well center at the origin ($x_{wD} = y_{wD} = 0$) and used $L = L_{x_f}$. Eq. 2.6.1 was also obtained in Ref. 15 by superimposing line sources. Although it can be shown analytically that the integral in the right hand side of Eq. 2.6.1 is bounded for all values of the argument $K_0[f(\alpha)]$, computational problems may arise if y_D in Eq. 2.6.1 is small. More specifically, if we wish to compute the wellbore pressure or the pressure on the fracture surface ($y_D = 0$), then the argument of the integral in the right hand side of Eq. 2.6.1 becomes unbounded as $\alpha \rightarrow x_D$. The numerical problems involved in the evaluation of the integral in Eq. 2.6.1 are documented in Ref. 15. Houze *et al.*[15] outline an approximate procedure to compute the integral. They recommend that the fracture length be divided into N equal segments and the integrand be computed at each of these segments. The integral in Eq. 2.6.1 is then approximated by the average value of N solutions. To obtain accurate results, particularly at early times, as many as 100 segments are needed. They also note that segments must be chosen to ensure that the center of any of the segments is not close to the pressure measurement point ($x_D = 0$ for the uniform-flux idealization and $x_D = 0.732$ for the infinite-conductivity idealization[10]); otherwise results will be erroneous. Numerical problems, however, can be eliminated completely by using Eqs. 2.5.1 - 2.5.3 given in §2.5. Using Eq. 2.5.1, for example, the dimensionless pressure on the surface of the fracture ($|x_D| \leq 1$ and $y_D = 0$) can be written from Eq. 2.6.1 as follows:

$$\overline{p}_D\left(|x_D| \leq 1, y_D = 0\right) = \frac{1}{2s\sqrt{u}}\left[\int_0^{\sqrt{u}(1-x_D)} K_0\left(z\right) dz + \int_0^{\sqrt{u}(1+x_D)} K_0\left(z\right) dz\right]. \tag{2.6.2}$$

The integrals on the right hand side of Eq. 2.6.2 approach values between 0 as $|x_D| \rightarrow 1$ and $\pi/2$ as $s \rightarrow \infty$ since[27] $\int_0^\infty K_0(u)du = \pi/2$. Any difficulties encountered in computing these integrals for large or small values of s can be eliminated through the use of the relations given by Eqs. 2.5.4 and 2.5.5. Solutions discussed below were obtained by this procedure.

As a first step, we computed well responses for the homogeneous reservoir case by using $u = s$ in Eq. 2.6.2. Values of the wellbore pressure, p_{wD}, obtained from Eq.

2.6.2 are identical to that given in Table 1 of Ref. 10 for both infinite-conductivity ($x_D = 0.732$) and uniform-flux ($x_D = 0$) idealizations. For the fractured reservoir case, we obtained good agreement with the solutions of Yeh *et al.*[33] and Davison[34].

For completeness, we note that the Laplace transform of the pressure response on the surface of the fracture ($|x_D| \leq 1$ and $y_D = 0$) is also reported by Kuchuk[28]. His solution is given by the following expression:

$$\begin{aligned}\overline{p}_D =& \frac{\pi(1-x_D)}{4s} \\ & \left\{ K_1\left[(1-x_D)\sqrt{s}\right] L_0\left[(1-x_D)\sqrt{s}\right] + K_0\left[(1-x_D)\sqrt{s}\right] L_1\left[(1-x_D)\sqrt{s}\right] \right\} \\ & + \frac{\pi(1+x_D)}{4s} \\ & \left\{ K_1\left[(1+x_D)\sqrt{s}\right] L_0\left[(1+x_D)\sqrt{s}\right] + K_0\left[(1+x_D)\sqrt{s}\right] L_1\left[(1+x_D)\sqrt{s}\right] \right\} \\ & + \frac{(1-x_D)}{2s} K_0\left[(1-x_D)\sqrt{s}\right] + \frac{(1+x_D)}{2s} K_0\left[(1+x_D)\sqrt{s}\right]. \end{aligned} \tag{2.6.3}$$

Here $K_0(x)$ and $K_1(x)$ are modified Bessel functions and $L_0(x)$ and $L_1(x)$ are modified Struve functions. Ref. 28 suggests that the infinite-conductivity fracture responses be computed from Eq. 2.6.3 at $x_D = 0.74009714$ instead of $x_D = 0.732$ as suggested by Ref. 10, and presents the form of Eq. 2.6.3 for the infinite-conductivity case. Eq. 2.6.3 can be obtained from Eq. 2.6.2 by the relation[35]

$$\begin{aligned}\int_0^x K_0(z)dz &= \frac{\pi x}{2}\left[K_0(x)L_{-1}(x) + K_1(x)L_0(x)\right] \\ &= \frac{\pi x}{2}\left[K_0(x)L_1(x) + K_1(x)L_0(x)\right] + xK_0(x). \end{aligned} \tag{2.6.4}$$

We believe that, computationally, it is advantageous to use Eq. 2.6.2 instead of Eq. 2.6.3. Furthermore, with the development given in §2.5 I, Eqs. 2.6.1 and 2.6.2 provide the pressure distribution at all points in the reservoir.

Fig. 2.6.1 presents a typical set of infinite-conductivity vertical fracture responses in naturally fractured reservoirs. We computed the infinite-conductivity responses from Eq. 2.6.2 (which is valid for uniform-flux fractures) at $x_D = 0.732$ as

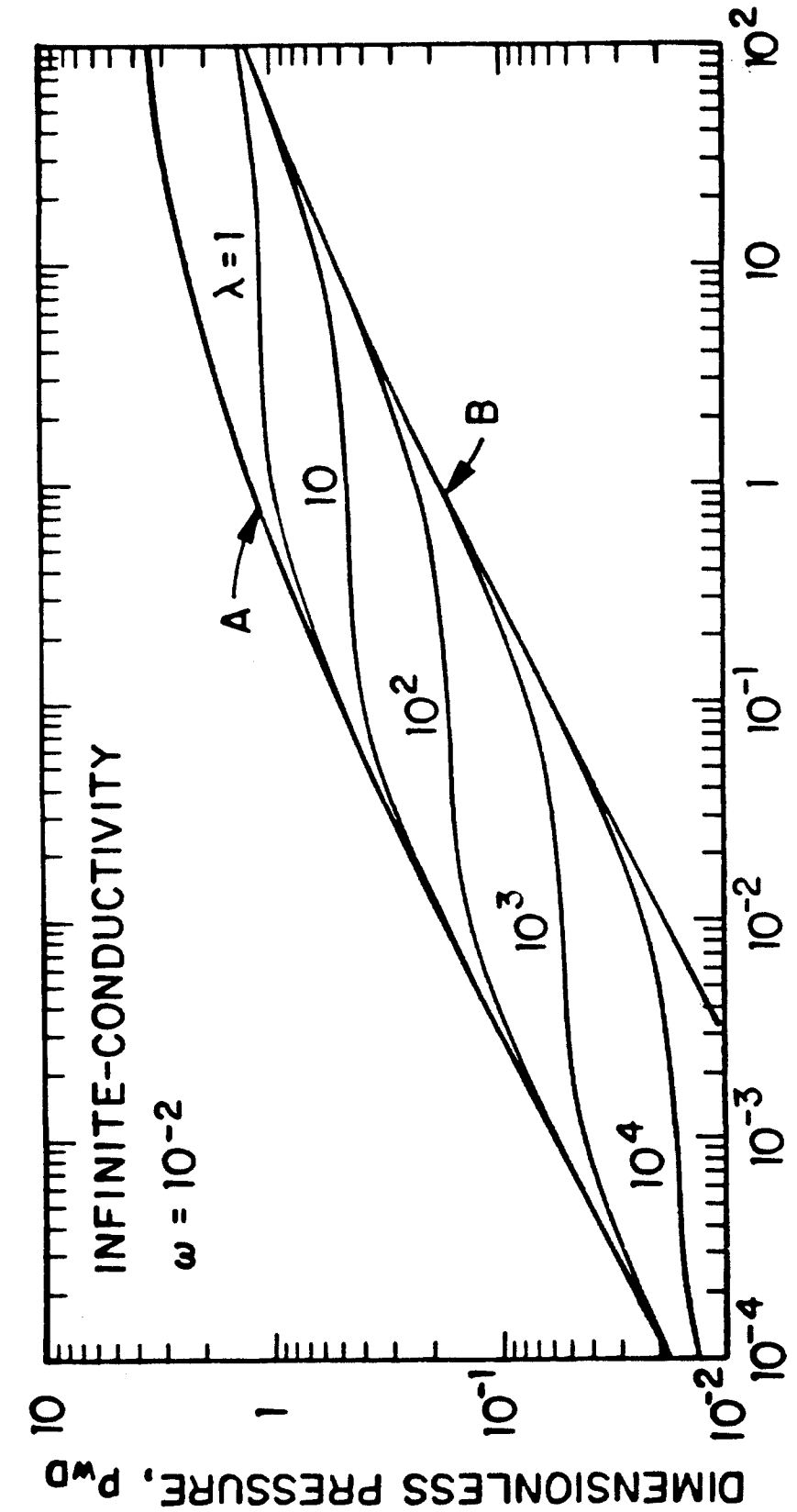

Fig. 2.6.1 - Typical Responses of Vertically Fractured Wells in Fractured Reservoirs.

suggested by Ref. 10. In Fig. 2.6.1, the dimensionless storativity, $w = 10^{-2}$ and the dimensionless transfer coefficient, λ, is the variable of interest. The top curve (Curve A) represents the homogeneous reservoir solution ($w = 1$, $\lambda = 0$). The bottom curve (Curve B) also represents a homogeneous reservoir solution with ϕc_t product equal to the total system porosity-compressibility product, $(V\phi c_t)_f + (V\phi c_t)_m$, ($w = 10^{-2}$, $\lambda \to \infty$). Characteristics typical of vertically fractured wells in naturally fractured reservoirs are clearly evident. As expected, a log-log plot of p_{wD} vs. t_D/w (where t_D is based on fracture half-length; that is $L = L_{x_f}$ in Eq. 2.1.8) yields a half slope line at early times manifesting the existence of the early linear flow period. The responses possess a transition period during which they deviate from the homogeneous reservoir solution (Curve A) and approach the solution corresponding to $\lambda = \infty$ (Curve B). This transition period is characterized by approximately constant values of p_{wD} and is typical of responses predicted by the Warren and Root[18] model. At late times, all the responses show the characteristics of pseudoradial flow period (during this flow period $dp_{wD}/d\ln t_D = 0.5$). As the characteristics of these solutions are well documented in Refs. 33 and 34, we will not discuss this aspect here.

<u>II. Horizontal Well, Infinite Reservoir</u> Problems involved in computing well responses for horizontal wells can also be readily resolved by the methods outlined in §2.5. If we consider an isotropic reservoir ($k = k_x = k_y = k_z$) with the well located at (0, 0, z_{wD}), then the solution given in Table $1 - A$ of Appendix A for this case (with $L = L_h/2$) can be written as

$$\begin{aligned}\bar{p}_D = {} & \frac{1}{2s}\int_{-1}^{+1} K_0\left[\sqrt{u}\sqrt{(x_D-\alpha)^2+y_D^2}\right]d\alpha \\ & + \frac{1}{s}\sum_{n=1}^{\infty}\cos n\pi z_D \cos n\pi z_{wD} \\ & \int_{-1}^{+1} K_0\left[\sqrt{u+n^2\pi^2 L_D^2}\sqrt{(x_D-\alpha)^2+y_D^2}\right]d\alpha.\end{aligned} \tag{2.6.5}$$

In Eq. 2.6.5, z_D and L_D are defined respectively by

$$z_D = \frac{z}{h} \tag{2.6.6}$$

and

$$L_D = \frac{1}{h_D} = \frac{L}{2h}. \tag{2.6.7}$$

To the best of our knowledge, the solution given by Eq. 2.6.5 has not been reported until now. As in the case of vertically fractured well solution presented above, the computation of the wellbore responses by the right hand side of Eq. 2.6.5 can be a formidable problem. Note that the solution given by Eq. 2.6.5 assumes a line source well ($r_w \to 0$). In Chapter III, it is shown that wellbore pressures can be computed by assuming $y_D = 0$ and $z_D = z_{wD} + r_{wD}$, where $r_{wD} = (r_w/h)$. Therefore, in order to compute the pressure responses along the well ($|x_D| \leq 1, y_D = 0$ and $z_D = z_{wD} + r_{wD}$), Eq. 2.6.5 should be recast in the following form by using Eq. 2.5.1 of §2.5:

$$\overline{p}_D\left(|x_D| \leq 1, y_D = 0, z_D = z_{wD} + r_{wD}\right) = \frac{1}{2s\sqrt{u}}\left[\int_0^{\sqrt{u}(1-x_D)} K_0(z)\,dz + \int_0^{\sqrt{u}(1+x_D)} K_0(z)\,dz\right] + \overline{F}(x_D, z_D, z_{wD}, L_D), \tag{2.6.8}$$

where

$$\overline{F}(x_D, z_D, z_{wD}, L_D) = \frac{1}{s}\sum_{n=1}^{\infty} \frac{\cos n\pi z_D \cos n\pi z_{wD}}{\sqrt{u + n^2\pi^2 L_D^2}} \left[\int_0^{\sqrt{u+n^2\pi^2L_D^2}(1-x_D)} K_0(z)dz + \int_0^{\sqrt{u+n^2\pi^2L_D^2}(1+x_D)} K_0(z)dz\right]. \tag{2.6.9}$$

Note that $\overline{F}$ is the difference between the pressure drop for a horizontal well and that for a vertically fractured well (see Eq. 2.6.2). That is, $\overline{F}$ is the pseudoskin function for a horizontal well (this aspect will be discussed in detail in Chapter III). The integrals involving $K_0(x)$ can be computed along the lines already discussed. One major obstacle still remains. Although it appears innocuous, the series appearing in the right hand side of Eq. 2.6.9 converges extremely slowly for large values of

s (small times). This difficulty, however, can be eliminated as follows. Using the relation[27]

$$\int_0^x K_0(u)du = \frac{\pi}{2} - Ki_1(x), \tag{2.6.10}$$

where $Ki_1(x) = \int_x^\infty K_0(u)du$, we rewrite Eq. 2.6.9 as

$$\overline{F} = \overline{F}_1(z_D, z_{wD}, L_D) - \frac{1}{s}\sum_{n=1}^{\infty} \frac{\cos n\pi z_D \cos n\pi z_{wD}}{\sqrt{u + n^2\pi^2 L_D^2}} \left\{ Ki_1\left[\sqrt{u + n^2\pi^2 L_D^2}\,(1 - x_D)\right] + Ki_1\left[\sqrt{u + n^2\pi^2 L_D^2}\,(1 + x_D)\right]\right\}. \tag{2.6.11}$$

In Eq. 2.6.11, $\overline{F}_1$ is given by

$$\overline{F}_1(z_D, z_{wD}) = \frac{\pi}{s}\sum_{n=1}^{\infty} \frac{\cos n\pi z_D \cos n\pi z_{wD}}{\sqrt{u + n^2\pi^2 L_D^2}}. \tag{2.6.12}$$

Computation of $Ki_1,(x)$ is straightforward (see remarks given in §2.5 following Eq. 2.5.7). Since $K_0(x)$ approaches 0 at large values of x, $Ki_1(x) = \int_x^\infty K_0(u)du$ approaches zero at large values of x. Therefore, the series on the right hand side of Eq. 2.6.11 converges rapidly for large values of s. Convergence problems associated with the series on the right hand side of Eq. 2.6.12 for large values of s are eliminated as follows: First note that

$$\sum_{n=1}^{\infty} \frac{\cos n\pi z}{\sqrt{u + n^2\pi^2 L_D^2}} = \mathcal{L}\{G\}, \tag{2.6.13}$$

where G is given by

$$G = \frac{1}{\sqrt{\pi\tau}}\sum_{n=1}^{\infty} \cos n\pi z \exp\left(-n^2\pi^2 L_D^2 \tau\right) \tag{2.6.14}$$

and $\mathcal{L}$ denotes the Laplace transform operator with respect to τ with u being the Laplace transform variable. Using Poisson's summation formula[23] given by

$$\sum_{n=-\infty}^{+\infty} \exp\left[-\frac{(\xi - 2n\xi_e)}{4\tau}\right] = \frac{\sqrt{\pi\tau}}{\xi_e}\left[1 + 2\sum_{n=1}^{\infty} \exp\left(-\frac{n^2\pi^2}{\xi_e^2}\tau\right)\cos n\pi\frac{\xi}{\xi_e}\right], \tag{2.6.15}$$

we can show that (details are given in §2.5)

$$\sum_{n=1}^{\infty} \frac{\cos n\pi z}{\sqrt{u + n^2\pi^2 L_D^2}} = \frac{1}{\pi L_D}\sum_{n=-\infty}^{+\infty} K_0\left(\frac{|z - 2n|}{L_D}\sqrt{u}\right) - \frac{1}{2\sqrt{u}}. \tag{2.6.16}$$

Thus Eq. 2.6.12 may be writen as (see Eq. 2.5.14)

$$\overline{F}_1(z_D, z_{wD}, L_D) = \frac{1}{2L_D s}\sum_{n=-\infty}^{+\infty}\left[K_0\left(\frac{|z_D - z_{wD} - 2n|\sqrt{u}}{L_D}\right) + K_0\left(\frac{|z_D + z_{wD} - 2n|\sqrt{u}}{L_D}\right)\right] - \frac{\pi}{2s\sqrt{u}}. \tag{2.6.17}$$

Computations indicate that the right hand side of Eq. 2.6.17 converges rapidly. Eq. 2.6.17 is extremely important to compute the wellbore pressures of horizontal wells. The series on the right hand side of Eq. 2.6.12 is convergent; yet, if s is large (u is large), then $\sqrt{u + n^2\pi^2 L_D^2} \approx \sqrt{u}$ until $n^2\pi^2 L_D^2$ becomes comparable to u and the series on the right hand side of Eq. 2.6.12 behaves like the divergent series $\sum_{n=1}^{\infty} \cos n\pi z_D \cos n\pi z_{wD}$. Therefore, at large values of s, the partial sum of the series given by the right hand side of Eq. 2.6.12 will be changing significantly even after considering *several thousand* terms. On the other hand, unless s is extremely small (very late times), the series on the right hand side of Eq. 2.6.17 converges very rapidly since $K_0(x)$ approaches zero rapidly as x becomes large. Therefore, for large values of s, Eq. 2.6.8 can be written in the following form:

$$\begin{aligned}
&\overline{p}_D(|x_D| \le 1, y_D = 0, z_D = z_{wD} + r_{wD}) = \\
&\frac{1}{2s\sqrt{u}}\left[\int_0^{\sqrt{u}(1-x_D)} K_o(z)\,dz + \int_0^{\sqrt{u}(1+x_D)} K_o(z)\,dz\right] \\
&+ \frac{1}{2L_D s}\sum_{n=-\infty}^{+\infty}\left[K_0\left(\frac{|z_D - z_{wD} - 2n|\sqrt{u}}{L_D}\right) + K_0\left(\frac{|z_D + z_{wD} - 2n|\sqrt{u}}{L_D}\right)\right] \\
&- \frac{\pi}{2s\sqrt{u}} - \frac{1}{s}\sum_{n=1}^{\infty}\frac{\cos n\pi z_D \cos n\pi z_{wD}}{\sqrt{u + n^2\pi^2 L_D^2}} \\
&\left\{Ki_1\left[\sqrt{u + n^2\pi^2 L_D^2}\,(1 - x_D)\right] + Ki_1\left[\sqrt{u + n^2\pi^2 L_D^2}\,(1 + x_D)\right]\right\}.
\end{aligned} \tag{2.6.18}$$

We tested the solutions given by Eqs. 2.6.8 and 2.6.18 for homogenous reservoirs ($u = s$). We found excellent agreement between the values computed from Eqs. 2.6.8 and 2.6.18 by using Stehfest algorithm[9] and our results computed from the real time solution reported in Ref. 5 and Chapter III.

We now consider horizontal well responses in naturally fractured reservoirs. Figs. 2.6.2 and 2.6.3 present typical horizontal well responses in naturally fractured reservoirs for the case where the dimensionless storativity, $w = 10^{-2}$. The variable of interest is the transfer coefficient, λ. The responses shown in Fig. 2.6.2 correspond to the case where $L_D = 5$ and the responses shown in Fig. 2.6.3 correspond to the case where $L_D = 100$ (L_D is the dimensionless horizontal well half-length defined by Eq. 2.6.7). In both figures, the well is assumed to be located midway between the top and the bottom boundaries of the reservoir ($z_{wD} = 0.5$) and the dimensionless wellbore radius, $r_{wD} = 2 \times 10^{-3}$. As in Ref. 5 and Chapter III, we assumed that the infinite-conductivity responses can be computed from the uniform-flux solutions (Eqs. 2.6.8 and 2.6.18) at $x_D = 0.732$.

The responses shown in Figs. 2.6.2 and 2.6.3 display characteristics typical of horizontal wells and naturally fractured reservoirs. Curves A and B in Figs. 2.6.2 and 2.6.3 represent the responses in homogeneous reservoirs corresponding respectively to $w = 1$, $\lambda = 0$ and $w = 10^{-2}$, ∞ respectively. At early times, the responses follow the homogeneous reservoir solution corresponding to $\lambda = 0$ (Curve A) and display the characteristics of radial flow in the vertical plane typical of horizontal wells (see Ref. 5 and Chapter III). During this time period, for all practical purposes, the influence of the matrix system is negligible (the responses are independent of λ) and the responses are governed by the porosity-compressibility product of the fracture system, $(V\phi c_t)_f$. The time at which the solutions deviate from the $\lambda = 0$ solution (Curve A) depends on the magnitude of λ; the larger the magnitude of λ, the earlier the deviation time. Following a transitional period characterized by approximately constant values of p_{wD}, typical of the Warren and Root[18] model, the responses in naturally fractured reservoirs ultimately merge with the homogeneous reservoir response solution with system porosity-compressibilty product equal to $(V\phi c_t)_f + (V\phi c_t)_m$ (Curve B). The late time responses shown in Figs. 2.6.2 and 2.6.3 display the pseudoradial flow behavior in the horizontal plane during which the logarithmic derivative of the pressure responses, $dp_{wD}/d\ln(t_D/w)$, attain the constant value of 0.5 (see Ref. 5 and Chapter III). As mentioned earlier,

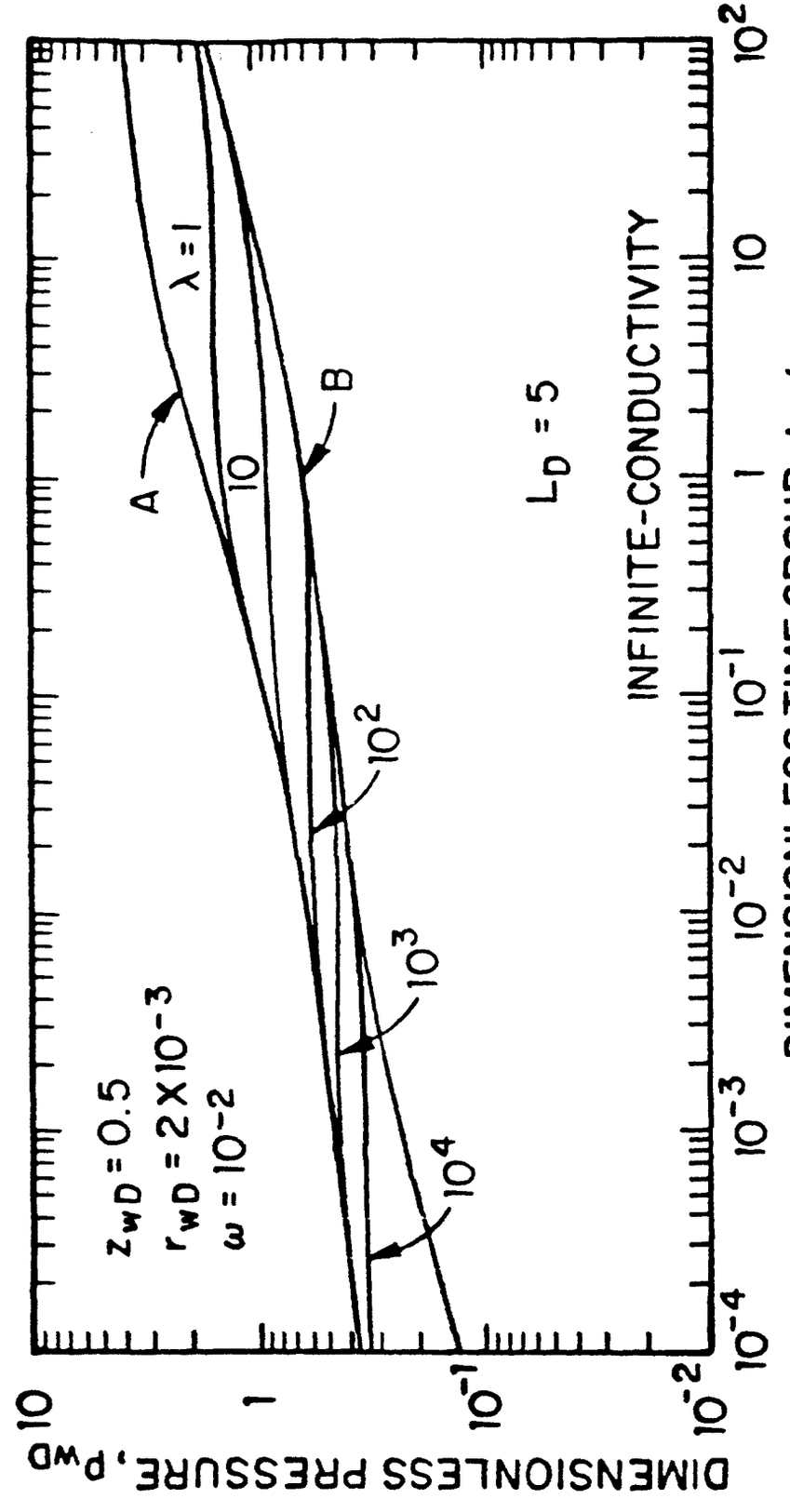

Fig. 2.6.2 - Typical Responses of Horizontal Wells in Fractured Reservoirs ($L_D = 5$).

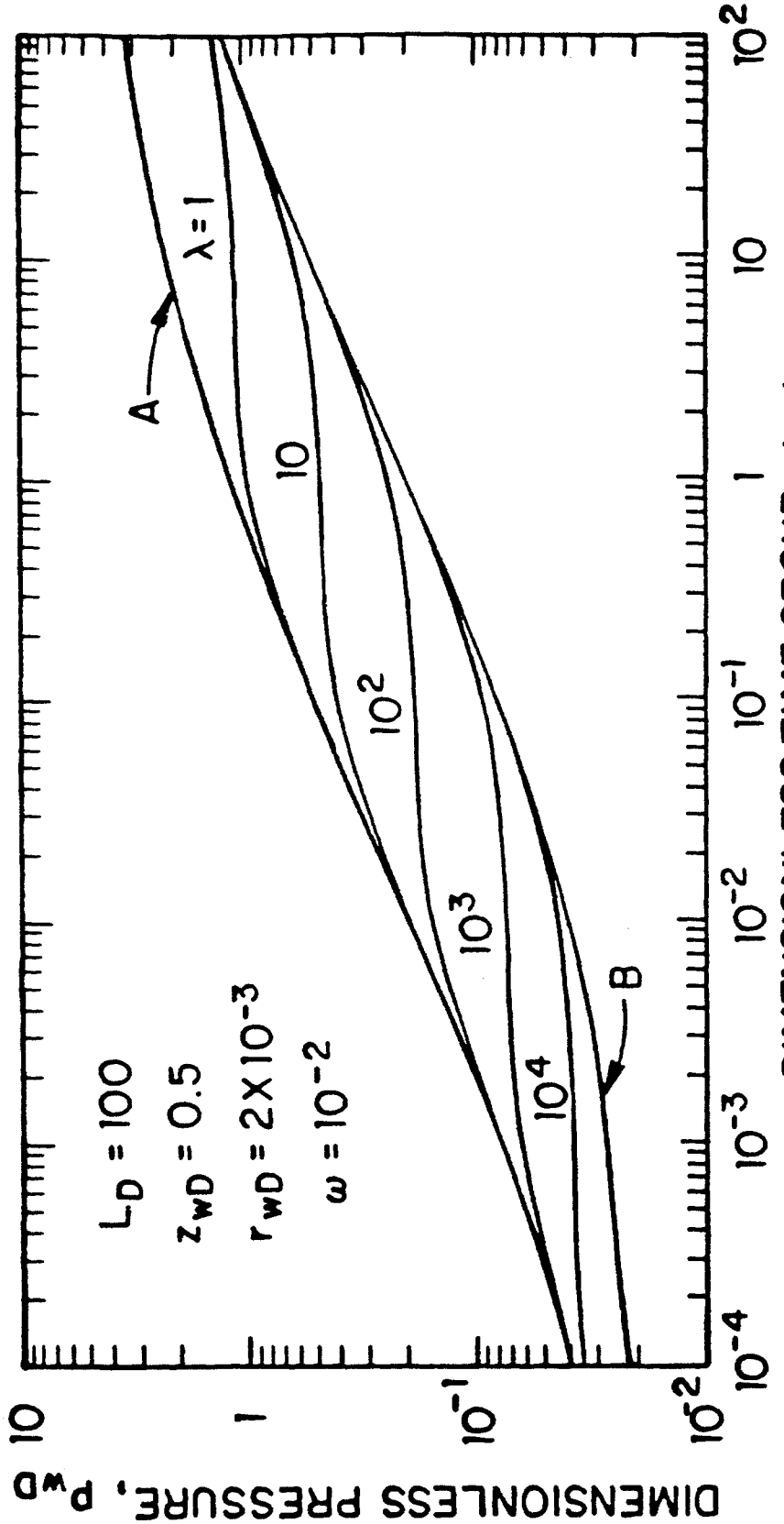

Fig. 2.6.3 - Typical Responses of Horizontal Wells in Fractured Reservoirs ($L_D = 100$).

detailed discussion of the responses is outside the scope of this section. Our objective in displaying Figs. 2.6.2 and 2.6.3 is to merely highlight the utility of our solution procedure.

The two examples considered above have been chosen to not only demonstrate the advantages of the solutions presented in this chapter but also to discuss and solve some of the problems encountered by us[5] and the others[15]. These two examples also clearly demonstrate the fact that recasting the analytical solutions involving infinite series and singular functions in a form suitable for numerical evaluations is as equally important as obtaining the solution itself. Our approach for computing the vertically fractured well solution given by Eq. 2.6.2 provides definite advantages over that given by Eq. 2.6.1 since it eliminates the need for the approximate integration procedure suggested by Ref. 15. Similarly, the form of the horizontal well solution given by Eq. 2.6.18 is essential for efficient and accurate numerical evaluation of the well response particularly for large values of s (small times).

If note is made of the computational remarks in §2.5, then one can numerically compute pressure responses from all solutions given in Table 1 of Appendix A.

III. Vertically Fractured Wells, Bounded Reservoirs In general, the main problem that must be overcome is that the bounded reservoir solutions will not converge rapidly during the transient period. To solve this problem, bounded reservoir solutions must be first written in the form:

$$\overline{\Delta p} = \overline{\Delta p}_{inf} + \overline{\Delta p}_b, \tag{2.6.19}$$

where $\overline{\Delta p}_{inf}$ is the solution given in Table 1 of Appendix A for the appropriate well in an infinite reservoir and $\overline{\Delta p}_b$ represents the terms due to the bounded nature of the reservoir. Solutions for the infinite reservoir case can be computed along the lines given above. Second, the expression for $\overline{\Delta p}_b$ should be such that it converges rapidly for small times. Here we consider two examples for fractured wells in bounded reservoirs.

Let us consider the case of a fully penetrating vertical fracture in a closed, cylin-

drical, isotropic ($k = k_x = k_y = k_z$) reservoir. The pressure drop along the surface of the fracture ($|x_D| \leq 1, y_D = 0$) can be written from Table $2 - B$ of Appendix A (with $L = L_{x_f}$) as

$$\overline{p}_D = \frac{1}{2s} \int_{-1}^{+1} \left[K_0 \left(\tilde{r}_D \sqrt{u} \right) + \frac{I_0 \left(\tilde{r}_D \sqrt{u} \right) K_1 \left(r_{eD} \sqrt{u} \right)}{I_1 \left(r_{eD} \sqrt{u} \right)} \right] d\alpha. \tag{2.6.20}$$

In Eq. 2.6.20, r_{eD} is the dimensionless drainage radius and $\tilde{r}_D$ is given by

$$\tilde{r}_D = \sqrt{(x_D - \alpha)^2 + y_D^2}. \tag{2.6.21}$$

Eq. 2.6.20 can be also written in the following form:

$$\overline{p}_D = \overline{p}_{D\ inf} + \frac{K_1 \left(r_{eD} \sqrt{u} \right)}{2s I_1 \left(r_{eD} \sqrt{u} \right)} \int_{-1}^{+1} I_0 \left[\sqrt{u} \sqrt{(x_D - \alpha)^2} \right] d\alpha, \tag{2.6.22}$$

where $\overline{p}_{D\ inf}$ is given by Eq. 2.6.1. Note that at large values of u (early times), the ratio of Bessel functions, $K_1 \left(r_{eD} \sqrt{u} \right) / I_1 \left(r_{eD} \sqrt{u} \right)$, approaches zero and the second term on the right hand side of Eq. 2.6.22 does not contribute to the solution. Also as $u \rightarrow 0$ (late times) and/or $\alpha \rightarrow x_D$, $I_0 \left[\sqrt{u} \sqrt{(x_D - \alpha)^2} \right]$ remains bounded and therefore the integral on the right hand side of Eq. 2.6.22 can be numerically evaluated. We have found, however, that the accuracy of numerical evaluations can be further improved by computing the integral in Eq. 2.6.22 in the following form:

$$\int_{-1}^{+1} I_0 \left[\sqrt{u} \sqrt{(x_D - \alpha)^2} \right] d\alpha = \int_0^1 I_0 \left(\sqrt{u} |x_D - \alpha| \right) d\alpha + \int_0^1 I_0 \left(\sqrt{u} |x_D + \alpha| \right) d\alpha. \tag{2.6.23}$$

Similar remarks apply for the computation of the other solutions in Table 2 of Appendix A.

We now consider a fully penetrating vertically fractured well in a closed, isotropic ($k = k_x = k_y = k_z$) reservoir with a rectangular drainage region. Solution for the pressure distribution for this case has been obtained in §2.3 and is given by

the following expression:

$$\bar{p}_D(x_D,y_D)=\frac{\pi}{x_{eD}s}\left[\frac{ch\,\sqrt{u}\,(y_{eD}-|y_D-y_{wD}|)+ch\,\sqrt{u}[y_{eD}-(y_D+y_{wD})]}{\sqrt{u}\;sh\;\sqrt{u}y_{eD}}\right.$$
$$+\frac{2x_{eD}}{\pi}\sum_{k=1}^{\infty}\frac{1}{k}\sin\;k\pi\frac{1}{x_{eD}}\cos\;k\pi\frac{x_{wD}}{x_{eD}}\cos\;k\pi\frac{x_D}{x_{eD}}$$
$$\left.\frac{ch\sqrt{u+\frac{k^2\pi^2}{x_{eD}^2}}(y_{eD}-|y_D-y_{wD}|)+ch\sqrt{u+\frac{k^2\pi^2}{x_{eD}^2}}[y_{eD}-(y_D+y_{wD})]}{\sqrt{u+\frac{k^2\pi^2}{x_{eD}^2}}sh\sqrt{u+\frac{k^2\pi^2}{x_{eD}^2}}y_{eD}}\right]. \tag{2.6.24}$$

The coordinate system for Eq. 2.6.24 is chosen to be at the bottom left hand corner of the reservoir. The location of the well is determined by x_{wD} and y_{wD} and the length of the sides of the rectangular drainage region is defined by x_{eD} and y_{eD}. $ch(x)$ and $sh(x)$ denote the hyperbolic cosine and hyperbolic sine functions respectively.

Note that the ratios of hyperbolic functions on the right hand side of Eq. 2.6.24 may cause computational problems when their arguments approach zero or infinity. The ratios of hyperbolic functions in Eq. 2.6.24, however, can be written in the following form:

$$\frac{ch\sqrt{a}\,(y_{eD}-\tilde{y}_D)}{sh\sqrt{a}y_{eD}}=\frac{\exp\left(-\sqrt{a}\tilde{y}_D\right)+\exp\left[-\sqrt{a}\,(2y_{eD}-\tilde{y}_D)\right]}{1-\exp\left(-2\sqrt{a}y_{eD}\right)}. \tag{2.6.25}$$

The computation of the right hand side of Eq. 2.6.25 can still be difficult if $\sqrt{a}y_{eD}$ becomes very small since the denominator of this expression approaches zero. If we use, however, the relation given by the following expression[36]

$$\left[1-\exp\left(-2\sqrt{a}y_{eD}\right)\right]^{-1}=1+\sum_{m=1}^{\infty}\exp\left(-2m\sqrt{a}y_{eD}\right), \tag{2.6.26}$$

then Eq. 2.6.25 can also be written as

$$\frac{ch\sqrt{a}\,(y_{eD}-\tilde{y}_D)}{sh\sqrt{a}y_{eD}}=\left\{\exp\left(-\sqrt{a}\tilde{y}_D\right)+\exp\left[-\sqrt{a}\,(2y_{eD}-\tilde{y}_D)\right]\right\}$$
$$\left[1+\sum_{m=1}^{\infty}\exp\left(-2m\sqrt{a}y_{eD}\right)\right]. \tag{2.6.27}$$

The right hand side of Eq. 2.6.27 can be used to compute the ratio of the hyperbolic functions for both small and large arguments.

If the relations given by Eqs. 2.6.25 – 2.6.27 are used to compute the ratio of hyperbolic functions, $ch(\alpha)/sh(\beta)$, at large values of the arguments of the hyperbolic functions, the pressure distribution can be computed using Eq. 2.6.24 for times $t_{DA} \geq 10^{-2}$, where t_{DA} is the dimensionless time based on the drainage area and is given by

$$t_{DA} = t_D/A_D, \tag{2.6.28}$$

where $A_D = A/L^2 = x_e y_e/L_{x_f}^2$.

For smaller values of time, we write Eq. 2.6.24 in the following form:

$$\overline{p}_D = \overline{p}_{D\ inf} + \overline{p}_{Db}, \tag{2.6.29}$$

where $\overline{p}_{D\ inf}$ is the solution for a fractured well in an infinite reservoir given by Eq. 2.6.1 and $\overline{p}_{Db}$ represents the contribution of reservoir boundaries. The expression for $\overline{p}_{Db}$ is obtained as follows: Using Eq. 2.6.27, we can recast Eq. 2.6.24 in the following form:

$$\overline{p}_D = \overline{p}_{D1} + \overline{p}_{Db1} + \overline{p}_{Db2}, \tag{2.6.30}$$

where

$$\overline{p}_{D1} = \frac{2}{s}\sum_{k=1}^{\infty}\frac{1}{k}\sin k\pi\frac{1}{x_{eD}}\cos k\pi\frac{x_D}{x_{eD}}\cos k\pi\frac{x_{wD}}{x_{eD}}\frac{\exp\left(-\sqrt{u+a}|y_D - y_{wD}|\right)}{\sqrt{u+a}}, \tag{2.6.31}$$

$$\begin{aligned}\overline{p}_{Db1} =& \frac{\pi}{x_{eD}s\sqrt{u}}\Big\{\exp\left[-\sqrt{u}\,(y_D + y_{wD})\right] + \exp\left[-\sqrt{u}\,[2y_{eD} - (y_D + y_{wD})]\right] \\ &+ \exp\left(-\sqrt{u}|y_D - y_{wD}|\right) + \exp\left[-\sqrt{u}\,(2y_{eD} - |y_D - y_{wD}|)\right]\Big\} \\ &\left[1 + \sum_{m=1}^{\infty}\exp\left(-2m\sqrt{u}y_{eD}\right)\right],\end{aligned} \tag{2.6.32}$$

and

$$\overline{p}_{Db2} = \frac{2}{s}\sum_{k=1}^{\infty}\frac{1}{k}\frac{\sin k\pi\frac{1}{x_{eD}}\cos k\pi\frac{x_D}{x_{eD}}\cos k\pi\frac{x_{wD}}{x_{eD}}}{\sqrt{u+a}}$$

$$\left\{\left\{\exp\left[-\sqrt{u+a}\,(y_D+y_{wD})\right]+\exp\left[-\sqrt{u+a}\,[2y_{eD}-(y_D+y_{wD})]\right]\right.\right.$$

$$\left.\left.+\exp\left[-\sqrt{u+a}\,(2y_{eD}-|y_D-y_{wD}|)\right]\right\}\left[1+\sum_{m=1}^{\infty}\exp\left(-2m\sqrt{u+a}y_{eD}\right)\right]\right.$$

$$\left.+\exp\left(-\sqrt{u+a}|y_D-y_{wD}|\right)\sum_{m=1}^{\infty}\exp\left(-2m\sqrt{u+a}y_{eD}\right)\right\}. \qquad (2.6.33)$$

In Eqs. 2.6.31 and 2.6.33, $a = k^2\pi^2/x_{eD}^2$. We note that $\overline{p}_{D1}$ given by Eq. 2.6.31 can be written as

$$\overline{p}_{D1} = \frac{\pi}{x_{eD}s}\sum_{k=1}^{\infty}\int_{x_{wD}-1}^{x_{wD}+1}\frac{\cos k\pi\frac{x'_{wD}}{x_{eD}}\cos k\pi\frac{x_D}{x_{eD}}}{\sqrt{u+a}}\exp\left(-\sqrt{u+a}|y_D-y_{wD}|\right)dx'_{wD} \qquad (2.6.34)$$

Using Eq. 2.5.14 given in §2.5 and making the change of variable $\alpha = x_{wD} - x'_{wD}$, we can write Eq. 2.6.34 in the following form:

$$\overline{p}_{D1} = \frac{1}{2s}\int_{-1}^{+1}\sum_{k=-\infty}^{+\infty}\left\{K_0\left[\sqrt{(x_D-x_{wD}-2kx_{eD}-\alpha)^2+(y_D-y_{wD})^2}\sqrt{u}\right]\right.$$

$$\left.+K_0\left[\sqrt{(x_D+x_{wD}-2kx_{eD}-\alpha)^2+(y_D-y_{wD})^2}\sqrt{u}\right]\right\}d\alpha$$

$$-\frac{\pi\exp\left(-\sqrt{u}|y_D-y_{wD}|\right)}{x_{eD}s\sqrt{u}} \qquad (2.6.35)$$

Note that Eq. 2.6.35 can be written as

$$\overline{p}_{D1} = \overline{p}_{D\ inf} + \overline{p}_{Db3}, \qquad (2.6.36)$$

where $\overline{p}_{D\ inf}$ is the vertical fracture solution in an infinite reservoir given by

$$\overline{p}_{D\ inf} = \frac{1}{2s}\int_{-1}^{+1}K_0\left[\sqrt{(x_D-x_{wD}-\alpha)^2+(y_D-y_{wD})^2}\sqrt{u}\right]d\alpha, \qquad (2.6.37)$$

and $\bar{p}_{Db3}$ is given by

$$\bar{p}_{Db3} = \frac{1}{2s}\int_{-1}^{+1} K_0\left[\sqrt{(x_D + x_{wD} - \alpha)^2 + (y_D - y_{wD})^2}\sqrt{u}\right] d\alpha$$

$$+\frac{1}{2s}\sum_{k=1}^{\infty}\int_{-1}^{+1}\left\{K_0\left[\sqrt{(x_D - x_{wD} - 2kx_{eD} - \alpha)^2 + (y_D - y_{wD})^2}\sqrt{u}\right]\right.$$

$$+K_0\left[\sqrt{(x_D + x_{wD} - 2kx_{eD} - \alpha)^2 + (y_D - y_{wD})^2}\sqrt{u}\right]$$

$$+K_0\left[\sqrt{(x_D - x_{wD} + 2kx_{eD} - \alpha)^2 + (y_D - y_{wD})^2}\sqrt{u}\right]$$

$$\left.+K_0\left[\sqrt{(x_D + x_{wD} + 2kx_{eD} - \alpha)^2 + (y_D - y_{wD})^2}\sqrt{u}\right]\right\} d\alpha$$

$$-\frac{\pi \exp\left(-\sqrt{u}|y_D - y_{wD}|\right)}{x_{eD}s\sqrt{u}} \tag{2.6.38}$$

Therefore, the pressure distribution due to production from a vertically fractured well in a closed rectangular reservoir is given by

$$\bar{p}_D = \bar{p}_{D\ inf} + \bar{p}_{Db}, \tag{2.6.39}$$

where $\bar{p}_{D\ inf}$ is given by Eq. 2.6.37 and $\bar{p}_{Db}$ is given by

$$\bar{p}_{Db} = \bar{p}_{Db1} + \bar{p}_{Db2} + \bar{p}_{Db3}. \tag{2.6.40}$$

In Eq. 2.6.40, $\bar{p}_{Db1}$, $\bar{p}_{Db2}$, and $\bar{p}_{Db3}$ are given respectively by Eqs. 2.6.32, 2.6.33 and 2.6.38. Integrals appearing in Eq. 2.6.38 can be computed along the lines suggested in §2.5 for $y_D = y_{wD}$. For example, for $|x_D - x_{wD}| \leq 1$, $y_D = y_{wD}$ (along the fracture surface), using the relations given by Eqs. 2.5.1 and 2.5.2 in §2.5, Eq.

2.6.38 can be written as

$$\bar{p}_{Db3} = \frac{1}{2s\sqrt{u}}\left\{\int_0^{\sqrt{u}(x_D+x_{wD}+1)} K_0(z)\,dz - \int_0^{\sqrt{u}(x_D+x_{wD}-1)} K_0(z)\,dz \right.$$
$$+ \sum_{k=1}^{\infty}\left[\int_0^{\sqrt{u}(2kx_{eD}-x_D+x_{wD}+1)} K_0(z)\,dz - \int_0^{\sqrt{u}(2kx_{eD}-x_D+x_{wD}-1)} K_0(z)\,dz\right.$$
$$+ \int_0^{\sqrt{u}(2kx_{eD}+x_D-x_{wD}+1)} K_0(z)\,dz - \int_0^{\sqrt{u}(2kx_{eD}+x_D-x_{wD}-1)} K_0(z)\,dz$$
$$+ \int_0^{\sqrt{u}(2kx_{eD}-x_D-x_{wD}+1)} K_0(z)\,dz - \int_0^{\sqrt{u}(2kx_{eD}-x_D-x_{wD}-1)} K_0(z)\,dz$$
$$\left.\left. + \int_0^{\sqrt{u}(2kx_{eD}+x_D+x_{wD}+1)} K_0(z)\,dz - \int_0^{\sqrt{u}(2kx_{eD}+x_D+x_{wD}-1)} K_0(z)\,dz\right]\right\}$$
$$- \frac{\pi}{x_{eD}s\sqrt{u}}. \tag{2.6.41}$$

Expressing the solution in this form has two distinct advantages. First, convergence problems for small times are eliminated; second the need to "patch" the infinite reservoir solutions and the bounded reservoir solutions is eliminated since Eqs. 2.6.29 and 2.6.40 can also be used for the transient period.

Table 2.6.1 presents the dimensionless pressure, p_{wD}, for a uniform-flux vertical fracture located at the center of a closed homogeneous reservoir as a function of dimensionless time, t_{DA} (Eq. 2.6.28). In Table 2.6.1, A_D is the dimensionless drainage area $\left(A_D = A/L_{x_f}^2\right)$ and can be considered to be the measure of fracture penetration in the lateral direction. Four values of A_D are considered; A_D = 4, 16, 100, and 400. Dimensionless pressures presented in Cols. 1, 3, 5, and 7 are for vertical fractures in cylindrical reservoirs $\left(A_D = \pi r_{eD}^2\right)$ computed from Eq. 2.6.22 and the dimensionless responses presented in Cols. 2, 4, 6, and 8 are for vertical fractures located at the center of square drainage regions $\left(x_{eD} = y_{eD};\ A_D = x_{eD}^2\right)$ computed from Eqs. 2.6.24 and 2.6.29. Dimensionless pressures presented in Table 2.6.1 for square drainage regions are in excellent agreement with those given by Ref. 10. As expected, at early times excellent agreement is obtained between the dimensionless pressures for cylindrical and square drainage regions. At late times, dimensionless pressures for cylindrical drainage regions are slightly lower than those

TABLE 2.6.1
UNIFORM-FLUX VERTICAL FRACTURE IN A BOUNDED RESERVOIR

t_{DA}	$A_D = 4$		$A_D = 16$		$A_D = 100$		$A_D = 400$	
	p_{wD} CIRCLE	p_{wD} SQUARE	p_{wD} CIRCLE	p_{wD} SQUARE	p_{wD} CIRCLE	p_{wD} SQUARE	p_{wD} CIRCLE	p_{wD} SQUARE
1.0×10^{-4}	0.0354	0.0354	0.0709	0.0709	0.1773	0.1773	0.3545	0.3545
1.5×10^{-4}	0.0434	0.0434	0.0868	0.0868	0.2171	0.2171	0.4340	0.4340
2.0×10^{-4}	0.0501	0.0501	0.1003	0.1003	0.2507	0.2507	0.5007	0.5007
3.0×10^{-4}	0.0614	0.0614	0.1228	0.1228	0.3069	0.3070	0.6105	0.6105
4.0×10^{-4}	0.0709	0.0709	0.1418	0.1418	0.3545	0.3545	0.6999	0.6999
5.0×10^{-4}	0.0793	0.0793	0.1585	0.1585	0.3963	0.3963	0.7756	0.7757
6.0×10^{-4}	0.0868	0.0868	0.1737	0.1737	0.4340	0.4340	0.8414	0.8413
8.0×10^{-4}	0.1003	0.1003	0.2005	0.2005	0.5007	0.5007	0.9515	0.9515
1.0×10^{-3}	0.1121	0.1121	0.2243	0.2243	0.5588	0.5588	1.0417	1.0417
1.5×10^{-3}	0.1373	0.1373	0.2746	0.2746	0.6790	0.6790	1.2145	1.2145
2.0×10^{-3}	0.1585	0.1585	0.3171	0.3171	0.7756	0.7757	1.3427	1.3427
3.0×10^{-3}	0.1942	0.1942	0.3883	0.3883	0.9261	0.9261	1.5294	1.5294
4.0×10^{-3}	0.2243	0.2242	0.4482	0.4482	1.0417	1.0417	1.6650	1.6650
5.0×10^{-3}	0.2507	0.2507	0.5007	0.5007	1.1355	1.1355	1.7716	1.7716
6.0×10^{-3}	0.2746	0.2746	0.5477	0.5477	1.2145	1.2145	1.8594	1.8594
8.0×10^{-3}	0.3171	0.3171	0.6297	0.6298	1.3427	1.3427	1.9990	1.9990
1.0×10^{-2}	0.3545	0.3545	0.6999	0.6999	1.4447	1.4447	2.1080	2.1080
1.5×10^{-2}	0.4340	0.4342	0.8414	0.8414	1.6344	1.6344	2.3073	2.3073
2.0×10^{-2}	0.5008	0.5013	0.9515	0.9515	1.7716	1.7716	2.4494	2.4494
3.0×10^{-2}	0.6116	0.6140	1.1182	1.1183	1.9676	1.9676	2.6505	2.6505

TABLE 2.6.1 (Cont.)
UNIFORM-FLUX VERTICAL FRACTURE IN A BOUNDED RESERVOIR

t_{DA}	$A_D = 4$		$A_D = 16$		$A_D = 100$		$A_D = 400$	
	p_{wD} CIRCLE	p_{wD} SQUARE	p_{wD} CIRCLE	p_{wD} SQUARE	p_{wD} CIRCLE	p_{wD} SQUARE	p_{wD} CIRCLE	p_{wD} SQUARE
4.0×10^{-2}	0.7031	0.7002	1.2435	1.2442	2.1084	2.1086	2.7937	2.7940
5.0×10^{-2}	0.7860	0.7935	1.3454	1.3469	2.2174	2.2201	2.9043	2.9068
6.0×10^{-2}	0.8625	0.8708	1.4279	1.4355	2.3070	2.3140	2.9957	3.0016
8.0×10^{-2}	1.0038	1.0127	1.5857	1.5892	2.4699	2.4732	3.1584	3.1618
1.0×10^{-1}	1.1202	1.1458	1.7149	1.7273	2.6027	2.6136	3.2918	3.3025
1.5×10^{-1}	1.4444	1.4652	2.0392	2.0502	2.9281	2.9381	3.6173	3.6273
2.0×10^{-1}	1.7597	1.7801	2.3519	2.3655	3.2420	3.2537	3.9312	3.9429
3.0×10^{-1}	2.3876	2.4085	2.9827	2.9940	3.8700	3.8823	4.5592	4.5715
4.0×10^{-1}	3.0155	3.0369	3.6103	3.6224	4.4985	4.5106	5.1877	5.1998
5.0×10^{-1}	3.6433	3.6652	4.2383	4.2507	5.1271	5.1389	5.8163	5.8281
6.0×10^{-1}	4.2741	4.2935	4.8667	4.8790	5.7555	5.7672	6.4447	6.4564
8.0×10^{-1}	5.4815	5.5501	6.1232	6.1356	7.0120	7.0239	7.7012	7.7131
1.0×10^{-0}	6.7747	6.8068	7.3798	7.3923	8.2686	8.2805	8.9579	8.9697
1.5×10^{-0}	9.9256	9.9484	10.521	10.534	11.410	11.422	12.099	12.111
2.0×10^{-0}	13.068	13.090	13.663	13.675	14.552	14.564	15.241	15.253
3.0×10^{-0}	19.351	19.373	19.946	19.959	20.835	20.847	21.524	21.536
4.0×10^{-0}	25.634	25.656	26.229	26.242	27.118	27.130	27.807	27.819
5.0×10^{-0}	31.918	31.940	32.513	32.525	33.401	33.413	34.091	34.102
6.0×10^{-0}	38.201	38.223	38.796	38.808	39.685	39.696	40.374	40.386
8.0×10^{-0}	50.767	50.789	51.362	51.375	52.251	52.263	52.940	52.952

for square drainage regions.

<u>IV. Horizontal Well, Bounded Reservoir</u> The objective of considering this example is to discuss the computation of "double infinite Fourier series" that are typical of wells with limited entry (partially penetrating wells, horizontal wells, etc.). Since many unsuccessful experiences have been reported concerning the use of solutions involving double or multiple infinite series, we include an example of this kind. (One of the advantages of Newman's method discussed by Gringarten and Ramey[3] is that the computation of multiple infinite series is avoided.)

As shown in §2.3 (Eq. 2.3.8), the dimensionless pressure for a horizontal well in an isotropic ($k = k_x = k_y = k_z$) rectangular drainage region with sealed top and bottom boundaries is given by

$$\overline{p}_D = \overline{p}_{Df} + \overline{F}_1, \tag{2.6.42}$$

where $\overline{p}_{Df}$ is the fully penetrating vertical fracture solution given by Eq. 2.6.24 (or 2.6.29) and $\overline{F}_1$ is given by

$$\begin{aligned}
\overline{F}_1 = {} & \frac{2\pi}{x_{eD}s}\sum_{n=1}^{\infty}\cos n\pi z_D \cos n\pi z_{wD} \\
& \frac{ch\sqrt{u+a}\,(y_{eD}-|y_D-y_{wD}|)+ch\sqrt{u+a}[y_{eD}-(y_D+y_{wD})]}{\sqrt{u+a}\;sh\sqrt{u+a}\,y_{eD}} \\
& +\frac{8}{s}\sum_{n=1}^{\infty}\cos n\pi z_D\cos n\pi z_{wD}\sum_{k=1}^{\infty}\frac{1}{k}\sin k\pi\frac{1}{x_{eD}}\cos k\pi\frac{x_{wD}}{x_{eD}}\cos k\pi\frac{x_D}{x_{eD}} \\
& \frac{ch\sqrt{u+b}\,(y_{eD}-|y_D-y_{wD}|)+ch\sqrt{u+b}[y_{eD}-(y_D+y_{wD})]}{\sqrt{u+b}\;sh\sqrt{u+b}\,y_{eD}},
\end{aligned} \tag{2.6.43}$$

where $a = n^2\pi^2L_D^2$, $b = n^2\pi^2L_D^2 + k^2\pi^2/x_{eD}^2$, and z_D and L_D are defined by Eqs. 2.6.6 and 2.6.7 respectively. In Eq. 2.6.42 the bottom left hand corner of the reservoir is assumed to be the origin. The location of the well center is determined by x_{wD}, y_{wD}, and z_{wD}. The measures of the sides of the rectangular drainage region are x_{eD} and y_{eD}. $ch(x)$ and $sh(x)$ denote hyperbolic cosine and hyperbolic sine functions respectively.

Points pertinent to the computation of the fracture solution, $\overline{p}_{Df}$, have been discussed above. Similar to the computation of the fracture solution, $\overline{p}_{Df}$ (Eqs. 2.6.24 and 2.6.29), we have found that for $t_{DA} \geq 10^{-2}$, $\overline{F}_1$ can be computed from Eq. 2.6.43 without difficulty provided that the relations given by Eqs. 2.6.25 - 2.6.27 are used to compute the ratio of hyperbolic functions, $ch(\alpha)/sh(\beta)$, when the arguments of the hyperbolic functions become large.

We now consider the computation of $\overline{F}_1$ for small times ($t_{DA} < 10^{-2}$). Using the relation given by Eq. 2.6.27, we can write $\overline{F}_1$ as

$$\overline{F}_1 = \frac{2\pi}{x_{eD}s}\sum_{n=1}^{\infty}\frac{\cos n\pi z_D \cos n\pi z_{wD}}{\sqrt{u+n^2\pi^2L_D^2}}\exp\left(-\sqrt{u+n^2\pi^2L_D^2}|y_D-y_{wD}|\right)$$

$$+\overline{F}_2+\overline{F}_{b1}+\overline{F}_{b2}, \tag{2.6.44}$$

where

$$\overline{F}_2 = \frac{4}{s}\sum_{n=1}^{\infty}\cos n\pi z_D\cos n\pi z_{wD}\sum_{k=1}^{\infty}\frac{1}{k}\frac{\sin k\pi\frac{1}{x_{eD}}\cos k\pi\frac{x_{wD}}{x_{eD}}\cos k\pi\frac{x_D}{x_{eD}}}{\sqrt{u+n^2\pi^2L_D^2+\frac{k^2\pi^2}{x_{eD}^2}}}$$

$$\exp\left(-\sqrt{u+n^2\pi^2L_D^2+\frac{k^2\pi^2}{x_{eD}^2}}|y_D-y_{wD}|\right), \tag{2.6.45}$$

$$\overline{F}_{b1} = \frac{2\pi}{x_{eD}s}\sum_{n=1}^{\infty}\frac{\cos n\pi z_D\cos n\pi z_{wD}}{\sqrt{u+n^2\pi^2L_D^2}}\left\{\left[e^{-\sqrt{u+n^2\pi^2L_D^2}(y_D+y_{wD})}\right.\right.$$

$$\left.+e^{-\sqrt{u+n^2\pi^2L_D^2}|2y_{eD}-(y_D+y_{wD})|}+e^{-\sqrt{u+n^2\pi^2L_D^2}(2y_{eD}-|y_D-y_{wD}|)}\right]$$

$$\left[1+\sum_{m=1}^{\infty}\exp\left(-2m\sqrt{u+n^2\pi^2L_D^2}y_{eD}\right)\right]$$

$$\left.+e^{-\sqrt{u+n^2\pi^2L_D^2}|y_D-y_{wD}|}\sum_{m=1}^{\infty}\exp\left(-2m\sqrt{u+n^2\pi^2L_D^2}y_{eD}\right)\right\}, \tag{2.6.46}$$

and

$$\overline{F}_{b2} = \frac{4}{s}\sum_{n=1}^{\infty}\cos n\pi z_D\cos n\pi z_{wD}\sum_{k=1}^{\infty}\frac{1}{k}\frac{\sin k\pi\frac{1}{x_{eD}}\cos k\pi\frac{x_D}{x_{eD}}\cos k\pi\frac{x_{wD}}{x_{eD}}}{\sqrt{u+n^2\pi^2L_D+\frac{k^2\pi^2}{x_{eD}^2}}}$$

$$\left\{\left[e^{-\sqrt{u+n^2\pi^2L_D^2+\frac{k^2\pi^2}{x_{eD}^2}}(y_D+y_{wD})}+e^{-\sqrt{u+n^2\pi^2L_D^2+\frac{k^2\pi^2}{x_{eD}^2}}|2y_{eD}-(y_D+y_{wD})|}\right.\right.$$

$$\left.+e^{-\sqrt{u+n^2\pi^2L_D^2+\frac{k^2\pi^2}{x_{eD}^2}}(2y_{eD}-|y_D-y_{wD}|)}\right]$$

$$\left[1+\sum_{m=1}^{\infty}\exp\left(-2m\sqrt{u+n^2\pi^2L_D^2+\frac{k^2\pi^2}{x_{eD}^2}}y_{eD}\right)\right]$$

$$\left.+e^{-\sqrt{u+n^2\pi^2L_D^2+\frac{k^2\pi^2}{x_{eD}^2}}|y_D-y_{wD}|}\sum_{m=1}^{\infty}\exp\left(-2m\sqrt{u+n^2\pi^2L_D^2+\frac{k^2\pi^2}{x_{eD}^2}}y_{eD}\right)\right\}. \tag{2.6.47}$$

Consider now $\overline{F}_2$ given by Eq. 2.6.45. We can write $\overline{F}_2$ as

$$\overline{F}_2=\frac{4}{s}\sum_{n=1}^{\infty}\cos n\pi z_D\cos n\pi z_{wD}\frac{\pi}{2x_{eD}}\int_{x_{wD}-1}^{x_{wD}+1}\sum_{k=1}^{\infty}\frac{\cos k\pi\frac{x'_{wD}}{x_{eD}}\cos n\pi\frac{x_D}{x_{eD}}}{\sqrt{u+n^2\pi^2L_D^2+\frac{k^2\pi^2}{x_{eD}^2}}}$$

$$\exp\left(-\sqrt{u+n^2\pi^2L_D^2+\frac{k^2\pi^2}{x_{eD}^2}}|y_D-y_{wD}|\right)dx'_{wD}. \tag{2.6.48}$$

Using the relation given by Eq. 2.5.14 in §2.5 and making the change of variable $\alpha=x_{wD}-x'_{wD}$, we can put $\overline{F}_2$ in the following form:

$$\overline{F}_2=\frac{1}{s}\sum_{n=1}^{\infty}\cos n\pi z_D\cos n\pi z_{wD}$$

$$\int_{-1}^{+1}\sum_{k=-\infty}^{+\infty}\left\{K_0\left[\sqrt{(x_D-x_{wD}-2kx_{eD}-\alpha)^2+(y_D-y_{wD})^2}\sqrt{u+n^2\pi^2L_D^2}\right]\right.$$

$$\left.+K_0\left[\sqrt{(x_D+x_{wD}-2kx_{eD}-\alpha)^2+(y_D-y_{wD})^2}\sqrt{u+n^2\pi^2L_D^2}\right]\right\}d\alpha$$

$$-\frac{2\pi}{x_{eD}s}\sum_{n=1}^{\infty}\frac{\cos n\pi z_D\cos n\pi z_{wD}}{\sqrt{u+n^2\pi^2L_D^2}}\exp\left(-\sqrt{u+n^2\pi^2L_D^2}|y_D-y_{wD}|\right). \tag{2.6.49}$$

Then we can write

$$\overline{F}_2=\overline{F}+\overline{F}_{b3}-\frac{2\pi}{x_{eD}s}\sum_{n=1}^{\infty}\frac{\cos n\pi z_D\cos n\pi z_{wD}}{\sqrt{u+n^2\pi^2L_D^2}}\exp\left(-\sqrt{u+n^2\pi^2L_D^2}|y_D-y_{wD}|\right), \tag{2.6.50}$$

where

$$\overline{F} = \frac{1}{s}\sum_{n=1}^{\infty} \cos n\pi z_D \cos n\pi z_{wD} \int_{-1}^{+1} K_0\left[\sqrt{(x_D - x_{wD} - \alpha)^2 + (y_D - y_{wD})^2}\sqrt{u + n^2\pi^2 L_D^2}\right] d\alpha, \tag{2.6.51}$$

and

$$\begin{aligned}\overline{F}_{b3} = \frac{1}{s}\sum_{n=1}^{\infty} \cos n\pi z_D \cos n\pi z_{wD} \\ \left\{\int_{-1}^{+1} K_0\left[\sqrt{(x_D + x_{wD} - \alpha)^2 + (y_D - y_{wD})^2}\sqrt{u + n^2\pi^2 L_D^2}\right] d\alpha\right. \\ + \sum_{k=1}^{\infty}\int_{-1}^{+1}\left\{K_0\left[\sqrt{(x_D - x_{wD} - 2kx_{eD} - \alpha)^2 + (y_D - y_{wD})^2}\sqrt{u + n^2\pi^2 L_D^2}\right]\right. \\ + K_0\left[\sqrt{(x_D + x_{wD} - 2kx_{eD} - \alpha)^2 + (y_D - y_{wD})^2}\sqrt{u + n^2\pi^2 L_D^2}\right] \\ + K_0\left[\sqrt{(x_D - x_{wD} + 2kx_{eD} - \alpha)^2 + (y_D - y_{wD})^2}\sqrt{u + n^2\pi^2 L_D^2}\right] \\ \left.\left. + K_0\left[\sqrt{(x_D + x_{wD} + 2kx_{eD} - \alpha)^2 + (y_D - y_{wD})^2}\sqrt{u + n^2\pi^2 L_D^2}\right]\right\} d\alpha\right\}.\end{aligned} \tag{2.6.52}$$

From Eqs. 2.6.44 and 2.6.50, we obtain

$$\overline{F}_1 = \overline{F} + \overline{F}_b, \tag{2.6.53}$$

where

$$\overline{F}_b = \overline{F}_{b1} + \overline{F}_{b2} + \overline{F}_{b3} \tag{2.6.54}$$

and $\overline{F}$, $\overline{F}_{b1}$, $\overline{F}_{b2}$, and $\overline{F}_{b3}$ are defined respectively by Eqs. 2.6.51, 2.6.46, 2.6.47, and 2.6.52. In Eq. 2.6.53, the function $\overline{F}$ is the pseudoskin function for a horizontal well in an infinite reservoir. The function $\overline{F}_b$ physically represents the influence of the reservoir boundaries on the pseudoskin function, $\overline{F}$. Then, basically this procedure involves writing $\overline{F}_1$ in a form similar to Eq. 2.6.19.

To compute the integrals appearing in Eqs. 2.6.51 and 2.6.52 at $y_D = y_{wD}$, the relations given in §2.5 can be used. For example, for $|x_D - x_{wD}| \leq 1$ and $y_D = y_{wD}$, using Eqs. 2.5.1 and 2.5.2, Eqs. 2.6.51 and 2.6.52 can be written respectively as

$$\overline{F}(z_D, z_{wD}, L_D) = \frac{1}{s}\sum_{n=1}^{\infty} \frac{\cos n\pi z_D \cos n\pi z_{wD}}{\sqrt{u + n^2\pi^2 L_D^2}} \left[\int_0^{\sqrt{u+a}|1-(x_D-x_{wD})|} K_0(z)dz + \int_0^{\sqrt{u+a}|1+(x_D-x_{wD})|} K_0(z)dz\right], \tag{2.6.55}$$

and

$$\overline{p}_{Db3} = \frac{1}{s}\sum_{n=1}^{\infty} \frac{\cos n\pi z_D \cos n\pi z_{wD}}{\sqrt{u+a}} \left\{\int_0^{\sqrt{u+a}(x_D+x_{wD}+1)} K_0(z)\,dz - \int_0^{\sqrt{u+a}(x_D+x_{wD}-1)} K_0(z)\,dz \right.$$
$$+ \sum_{k=1}^{\infty}\left[\int_0^{\sqrt{u+a}(2kx_{eD}-x_D+x_{wD}+1)} K_0(z)dz - \int_0^{\sqrt{u+a}(2kx_{eD}-x_D+x_{wD}-1)} K_0(z)dz \right.$$
$$+ \int_0^{\sqrt{u+a}(2kx_{eD}+x_D-x_{wD}+1)} K_0(z)dz - \int_0^{\sqrt{u+a}(2kx_{eD}+x_D-x_{wD}-1)} K_0(z)dz$$
$$+ \int_0^{\sqrt{u+a}(2kx_{eD}-x_D-x_{wD}+1)} K_0(z)dz - \int_0^{\sqrt{u+a}(2kx_{eD}-x_D-x_{wD}-1)} K_0(z)dz$$
$$\left.\left. + \int_0^{\sqrt{u+a}(2kx_{eD}+x_D+x_{wD}+1)} K_0(z)dz - \int_0^{\sqrt{u+a}(2kx_{eD}+x_D+x_{wD}-1)} K_0(z)dz\right]\right\}, \tag{2.6.56}$$

where $a = n^2\pi^2 L_D^2$. In light of the remarks following Eq. 2.6.9, using Eqs. 2.5.6 and 2.5.14, we finally obtain the following alternate forms of the functions $\overline{F}$ and $\overline{F}_{b3}$ to be used for small values of time for $|x_D - x_{wD}| \leq 1$ and $y_D = y_{wD}$:

$$\overline{F} = \frac{1}{2L_D s}\sum_{n=-\infty}^{+\infty}\left[K_0\left(\frac{|z_D - z_{wD} - 2n|\sqrt{u}}{L_D}\right) + K_0\left(\frac{|z_D + z_{wD} - 2n|\sqrt{u}}{L_D}\right)\right]$$
$$- \frac{\pi}{2s\sqrt{u}} - \frac{1}{s}\sum_{n=1}^{\infty}\frac{\cos n\pi z_D \cos n\pi z_{wD}}{\sqrt{u+a}}$$
$$\left\{Ki_1\left[\sqrt{u+a}\,[1-(x_D-x_{wD})]\right] + Ki_1\left[\sqrt{u+a}\,[1+(x_D-x_{wD})]\right]\right\}, \tag{2.6.57}$$

and

$$\overline{p}_{Db3} = \frac{1}{s}\sum_{n=1}^{\infty}\frac{\cos n\pi z_D \cos n\pi z_{wD}}{\sqrt{u+a}}$$

$$\left\{Ki_1\left[\sqrt{u+a}(x_D+x_{wD}+1)\right] - Ki_1\left[\sqrt{u+a}(x_D+x_{wD}-1)\right]\right.$$

$$+\sum_{k=1}^{\infty}\left[Ki_1\left[\sqrt{u+a}(2kx_{eD}-x_D+x_{wD}+1)\right]\right.$$

$$-Ki_1\left[\sqrt{u+a}(2kx_{eD}-x_D+x_{wD}-1)\right]$$

$$+Ki_1\left[\sqrt{u+a}(2kx_{eD}+x_D-x_{wD}+1)\right]$$

$$-Ki_1\left[\sqrt{u+a}(2kx_{eD}+x_D-x_{wD}-1)\right]$$

$$+Ki_1\left[\sqrt{u+a}(2kx_{eD}-x_D-x_{wD}+1)\right]$$

$$-Ki_1\left[\sqrt{u+a}(2kx_{eD}-x_D-x_{wD}-1)\right]$$

$$+Ki_1\left[\sqrt{u+a}(2kx_{eD}+x_D+x_{wD}+1)\right]$$

$$\left.\left.-Ki_1\left[\sqrt{u+a}(2kx_{eD}+x_D+x_{wD}-1)\right]\right]\right\}. \qquad (2.6.58)$$

In practical terms, correspondents have suggested to us that boundary effects may not be ignored when tests in horizontal wells are analyzed because horizontal well lengths are comparable to the dimensions of the reservoir. Thus the computational techniques suggested above should be extremely useful.

Tabulations of horizontal well responses computed with the aid of Eqs. 2.6.42 and 2.6.53 for all times (infinite acting and boundary-dominated flow periods) are given in Table 2.6.2. The well is assumed to be located at the center of a homogeneous ($u = s$), closed square drainage region ($x_{eD} = y_{eD}$, $x_{wD} = y_{wD} = x_{eD}/2$, $z_{wD} = 0.5$). The dimensionless horizontal well half-length, $L_D = 10$, and the dimensionless wellbore radius, $r_{wD} = r/h = 2 \times 10^{-3}$. The dimensionless time, t_{DA}, used in Table 2.6.2 is defined by Eq. 2.6.28 [with $A_D = (2x_e/L_h)^2$]. The responses shown in Table 2.6.2 are for the uniform-flux case; that is, we computed well responses at $x_D = 0$, $y_D = 0$, and $z_D = z_{wD} + r_{wD}$ (see Ref. 5 and Chapter III for

details). Also shown in Table 2.6.2 are the responses computed from the real time solution obtained by using the source functions of Ref. 3. The appropriate solution is given by

$$p_D = \frac{2\pi}{x_{eD}y_{eD}} \int_0^{t_D} \left[1 + 2\sum_{n=1}^{\infty} \exp\left(-\frac{n^2\pi^2}{y_{eD}^2}\tau\right) \cos n\pi \frac{y_{wD}}{y_{eD}} \cos n\pi \frac{y_D}{y_{eD}}\right]$$
$$\left[1 + \frac{2x_{eD}}{\pi} \sum_{n=1}^{\infty} \frac{1}{n} \exp\left(-\frac{n^2\pi^2}{x_{eD}^2}\tau\right) \sin n\pi \frac{1}{x_{eD}} \cos n\pi \frac{x_{wD}}{x_{eD}} \cos n\pi \frac{x_D}{x_{eD}}\right] \qquad (2.6.59)$$
$$\left[1 + 2\sum_{n=1}^{\infty} \exp\left(-\frac{n^2\pi^2}{h_D^2}\tau\right) \cos n\pi z_{wD} \cos n\pi z_D\right] d\tau.$$

The responses computed by using the Laplace domain solution (Eq. 2.6.42) and the real time solution (Eq. 2.6.59) are in excellent agreement for all times and for all reservoir sizes considered (x_{eD} = 2, 4, 10, and 20). (Unlike Eq. 2.6.59, however, Eq. 2.6.42 can be readily extended to solve more complicated problems.) Early time responses given in Table 2.6.2 are also in excellent agreement with infinite reservoir system responses noted in Ref. 5 and in Chapter III. Results for horizontal wells in bounded reservoirs are not discussed in the literature. The results given in Table 2.6.2 are intended to serve as a reference to other researchers.

In the subsequent sections of this chapter, we will consider further applications and extensions of the solutions presented in the previous pages. This will include obtaining asymptotic forms of our solutions by using the properties of the Laplace transformation technique and the extension of the solutions to situations that incorporate wellbore storage and skin effects and to the case where production is at a constant wellbore pressure.

2.7 Asymptotic Approximations

One well documented advantage of obtaining solutions by the Laplace transformation technique is that it is possible to readily obtain solutions that are useful for small and large values of time. The principal advantage of the asymptotic solutions is that they provide information on the structure of the solutions and thus are useful for correlating purposes. Of immediate importance to our work, the asymptotic

TABLE 2.6.2
UNIFORM-FLUX HORIZONTAL WELL IN A CLOSED SQUARE
$L_D = 10$
$z_{wD} = 0.5$
$r_{wD} = 2 \times 10^{-3}$

t_{DA}	$x_{eD} = 2$		$x_{eD} = 4$		$x_{eD} = 10$		$x_{eD} = 20$	
	p_{wD} Eq. 2.6.42	p_{wD} Eq. 2.6.59	p_{wD} Eq. 2.6.42	p_{wD} Eq. 2.6.59	p_{wD} Eq. 2.6.42	p_{wD} Eq. 2.6.59	p_{wD} Eq. 2.6.42	p_{wD} Eq. 2.6.59
1.0×10^{-4}	0.2505	0.2505	0.2897	0.2897	0.3961	0.3961	0.5733	0.5733
1.5×10^{-4}	0.2608	0.2608	0.3057	0.3057	0.4359	0.4359	0.6529	0.6529
2.0×10^{-4}	0.2684	0.2684	0.3191	0.3191	0.4695	0.4695	0.7196	0.7195
3.0×10^{-4}	0.2801	0.2801	0.3416	0.3416	0.5258	0.5258	0.8293	0.8293
4.0×10^{-4}	0.2897	0.2897	0.3606	0.3606	0.5733	0.5733	0.9187	0.9188
5.0×10^{-4}	0.2981	0.2981	0.3774	0.3774	0.6152	0.6151	0.9945	0.9945
6.0×10^{-4}	0.3057	0.3057	0.3925	0.3925	0.6529	0.6529	1.0602	1.0602
8.0×10^{-4}	0.3191	0.3191	0.4194	0.4194	0.7196	0.7195	1.1704	1.1703
1.0×10^{-3}	0.3309	0.3309	0.4430	0.4430	0.7775	0.7776	1.2605	1.2605
1.5×10^{-3}	0.3561	0.3561	0.4934	0.4934	0.8979	0.8979	1.4333	1.4333
2.0×10^{-3}	0.3774	0.3774	0.5359	0.5359	0.9945	0.9945	1.5617	1.5616
3.0×10^{-3}	0.4130	0.4130	0.6071	0.6071	1.1450	1.1450	1.7482	1.7482
4.0×10^{-3}	0.4430	0.4430	0.6670	0.6670	1.2605	1.2605	1.8838	1.8838
5.0×10^{-3}	0.4695	0.4695	0.7196	0.7195	1.3544	1.3544	1.9904	1.9904
6.0×10^{-3}	0.4934	0.4934	0.7665	0.7665	1.4333	1.4333	2.0781	2.0782
8.0×10^{-3}	0.5359	0.5359	0.8485	0.8486	1.5617	1.5616	2.2178	2.2178
1.0×10^{-2}	0.5733	0.5733	0.9187	0.9188	1.6636	1.6635	2.3268	2.3268
1.5×10^{-2}	0.6530	0.6530	1.0602	1.0602	1.8531	1.8532	2.5261	2.5262
2.0×10^{-2}	0.7202	0.7202	1.1704	1.1703	1.9904	1.9904	2.6681	2.6683
3.0×10^{-2}	0.8328	0.8329	1.3372	1.3372	2.1866	2.1865	2.8695	2.8694

TABLE 2.6.2 (Cont.)
UNIFORM-FLUX HORIZONTAL WELL IN A CLOSED SQUARE
$L_D = 10$
$z_{wD} = 0.5$
$r_{wD} = 2 \times 10^{-3}$

t_{DA}	$x_{eD} = 2$		$x_{eD} = 4$		$x_{eD} = 10$		$x_{eD} = 20$	
	p_{wD} Eq. 2.6.42	p_{wD} Eq. 2.6.59	p_{wD} Eq. 2.6.42	p_{wD} Eq. 2.6.59	p_{wD} Eq. 2.6.42	p_{wD} Eq. 2.6.59	p_{wD} Eq. 2.6.42	p_{wD} Eq. 2.6.59
4.0×10^{-2}	0.9280	0.9280	1.4631	1.4631	2.3274	2.3275	3.0128	3.0128
5.0×10^{-2}	1.0124	1.0124	1.5658	1.5658	2.4388	2.4389	3.1254	3.1257
6.0×10^{-2}	1.0898	1.0896	1.6543	1.6544	2.5326	2.5328	3.2203	3.2205
8.0×10^{-2}	1.2315	1.2316	1.8078	1.8081	2.6917	2.6921	3.3803	3.3806
1.0×10^{-1}	1.3646	1.3646	1.9461	1.9461	2.8325	2.8325	3.5213	3.5214
1.5×10^{-1}	1.6842	1.6841	2.2692	2.2690	3.1572	3.1570	3.8465	3.8461
2.0×10^{-1}	1.9993	1.9990	2.5846	2.5844	3.4732	3.4726	4.1619	4.1618
3.0×10^{-1}	2.6274	2.6274	3.2131	3.2129	4.1011	4.1011	4.7889	4.7903
4.0×10^{-1}	3.2558	3.2557	3.8411	3.8412	4.7293	4.7294	5.4185	5.4180
5.0×10^{-1}	3.8842	3.8840	4.4694	4.4695	5.3578	5.3577	6.0470	6.0469
6.0×10^{-1}	4.5124	4.5124	5.0978	5.0979	5.9862	5.9861	6.6753	6.6753
8.0×10^{-1}	5.7692	5.7690	6.3544	6.3545	7.2428	7.2427	7.9318	7.9319
1.0×10^{0}	7.0254	7.0256	7.6115	7.6111	8.4995	8.4993	9.1887	9.1885
1.5×10^{0}	10.168	10.167	10.753	10.753	11.640	11.641	12.330	12.330
2.0×10^{0}	13.309	13.309	13.895	13.894	14.783	14.783	15.472	15.472
3.0×10^{0}	19.592	19.592	20.179	20.178	21.067	21.066	21.755	21.755
4.0×10^{0}	25.876	25.875	26.462	26.461	27.350	27.349	28.038	28.038
5.0×10^{0}	32.159	32.158	32.745	32.744	33.635	33.632	34.322	34.321
6.0×10^{0}	38.439	38.442	39.024	39.027	39.918	39.915	40.605	40.604
8.0×10^{0}	51.012	51.008	51.594	51.593	52.479	52.482	53.171	53.171
1.0×10^{1}	63.578	63.574	64.162	64.160	65.048	65.048	65.738	65.737

expressions derived here enable us to compute shape factors and effective wellbore radii for many systems of interest. As a direct result of the long time approximations of vertically fractured well and horizontal well solutions in cylindrical coordinates, expressions to compute the shape factors for vertically fractured wells and horizontal wells in cylindrical reservoirs are obtained. Most interesting (and surprising), the closed form expressions we present for the shape factors for vertical wells and vertically fractured wells in rectangular drainage areas are much simpler than those given in the literature. We also present an expression to compute the shape factor for a horizontal well in a closed rectangular drainage volume. These expressions are extremely useful for computing stabilized inflow equations for various systems of interest.

Before proceeding further, we make note of the fact that we examine responses in a naturally fractured reservoir. Thus, we first note the asymptotic forms of the function $f(s)$ given by Eq. 2.1.23. As s becomes large, it can be shown that the function $f(s)$ approaches w sufficiently fast and therefore we can write the following:

$$\lim_{s \to \infty} f(s) = w \tag{2.7.1}$$

Similarly for small values of s, the function $f(s)$ can be approximated, by

$$\lim_{s \to 0+} f(s) = 1. \tag{2.7.2}$$

We will employ the relations given by Eqs. 2.7.1 and 2.7.2 in the following examples.

<u>I. Short Time Approximations</u> As noted in §2.6, solutions for bounded reservoirs can be expressed in the following form:

$$\overline{p}_D = \overline{p}_{Dinf} + \overline{p}_{Db}, \tag{2.7.3}$$

where $\overline{p}_{Dinf}$ is the appropriate solution for an infinite reservoir and $\overline{p}_{Db}$ represents the terms due to the boundaries of the reservoir. Once the bounded system solutions are written in the form given by Eq. 2.7.3, it can be easily shown that the

contribution of the term $\bar{p}_{Db}$ representing the influence of the boundaries is negligible at early times ($s \to \infty$). For example, examining the appropriate relations given in §2.6 (Eqs. 2.6.22, 2.6.40, and 2.6.54), we can decide that $\bar{p}_{Db} = f\left[K_0(a\sqrt{u+b})\right]$ and since $\lim_{x\to\infty} K_0(x) = 0$, $\bar{p}_{Db} = 0$. Therefore, the short time approximation of the bounded system solutions are obtained in the same fashion as in the case of infinite system solutions. An alternative approach to obtain the short time approximations of the solutions for rectangular drainage areas is discussed in Appendix C. This approach basically involves replacing the ratios of hyperbolic functions appearing in the solutions given in Table 3 of Appendix A and then approximating the resulting expression for small values of time. Here we will only examine the procedure to obtain the short time approximation of the solutions for laterally infinite resevoirs. We will consider two examples: a fully penetrating vertically fractured well and a horizontal well in an isotropic reservoir with impermeable top and bottom boundaries. We will assume that the center of the well is at the origin ($x_{wD} = y_{wD} = 0$).

We first examine the short time approximation of the vertically fractured well solution given by Eq. 2.6.1 and repeated below for convenience.

$$\bar{p}_D = \frac{1}{2s}\int_{-1}^{+1} K_0\left[\sqrt{u}\sqrt{(x_D-\alpha)^2+y_D^2}\right] d\alpha. \tag{2.7.4}$$

Using the integral representeation of $K_0(x)$ given by[23]

$$K_0(x) = \frac{1}{2}\int_0^\infty \exp\left(-\xi - \frac{x^2}{4\xi}\right)\frac{d\xi}{\xi}\ ; \quad [R(x^2)>0], \tag{2.7.5}$$

and

$$\int_{-1}^{+1} \exp\left[-\frac{(z-\alpha)^2 u}{4\xi}\right] d\alpha = \frac{\sqrt{\pi\xi}}{\sqrt{u}}\left[\mathrm{erf}\frac{(1-z)\sqrt{u}}{2\sqrt{\xi}} + \mathrm{erf}\frac{(1+z)\sqrt{u}}{2\sqrt{\xi}}\right], \tag{2.7.6}$$

Eq. 2.7.4 can be put in the following form:

$$\bar{p}_D = \frac{\sqrt{\pi}}{4s}\int_0^\infty \exp(-\xi)\exp\left(-\frac{uy_D^2}{4\xi}\right)\left[\mathrm{erf}\frac{(1+x_D)\sqrt{u}}{2\sqrt{\xi}} + \mathrm{erf}\frac{(1-x_D)\sqrt{u}}{2\sqrt{\xi}}\right]\frac{d\xi}{\sqrt{\xi u}}. \tag{2.7.7}$$

In order to obtain a short time approximation, we evaluate Eq. 2.7.7 as $s \to \infty$. By using Eq. 2.7.1, we first replace u by sw in Eq. 2.7.7. Also noting that

$$\lim_{s \to \infty} \left[\operatorname{erf} \frac{(1+x_D)\sqrt{sw}}{2\sqrt{\xi}} + \operatorname{erf} \frac{(1-x_D)\sqrt{sw}}{2\sqrt{\xi}} \right] = \beta, \tag{2.7.8}$$

where

$$\beta = \begin{cases} 2 \text{ for } |x_D| < 1, \\ 1 \text{ for } |x_D| = 1, \\ 0 \text{ for } |x_D| > 1, \end{cases} \tag{2.7.9}$$

we can approximate Eq. 2.7.7 as $s \to \infty$ by the following expression:

$$\overline{p}_D = \frac{\sqrt{\pi}\beta}{4s} \int_0^\infty \exp(-\xi) \exp\left(-\frac{wsy_D^2}{4\xi}\right) \frac{d\xi}{\sqrt{ws\xi}}. \tag{2.7.10}$$

Evaluating the integral in the right hand side of Eq. 2.7.10, we obtain

$$\overline{p}_D = \frac{\pi\beta}{4\sqrt{w}s^{3/2}} \exp\left(-|y_D|\sqrt{ws}\right). \tag{2.7.11}$$

Applying the inversion theorem for the Laplace transformation to Eq. 2.7.11, we finally obtain the following short time approximation for the vertical fracture solution:

$$p_D = \frac{\beta}{2} \left[\sqrt{\pi t_D/w} \exp\left(-\frac{y_D^2}{4t_D/w}\right) - \frac{\pi}{2\sqrt{w}} |y_D| \operatorname{erfc}\left(\frac{|y_D|}{2\sqrt{t_D/w}}\right) \right]. \tag{2.7.12}$$

For $w = 1$, Eq. 2.7.12 is identical to the short time approximation given by Ref. 10 for vertically fractured well solution (the expression in Ref. 10, Eq. 10 contains a misprint).

We now consider the short time approximation of the horizontal well solution given by Eq. 2.6.5. We can write the solution given by Eq. 2.6.5 in the following form:

$$\overline{p}_D = \overline{p}_{Df} + \overline{F}, \tag{2.7.13}$$

where $\overline{p}_{Df}$ is the vertically fractured well solution given by Eq. 2.7.4 and $\overline{F}$ is given by

$$\begin{aligned} \overline{F} = & \frac{1}{s} \sum_{n=1}^{\infty} \cos n\pi z_D \cos n\pi z_{wD} \\ & \int_{-1}^{+1} K_0 \left[\sqrt{u + n^2\pi^2 L_D^2} \sqrt{(x_D - \alpha)^2 + y_D^2} \right] d\alpha. \end{aligned} \tag{2.7.14}$$

In Eq. 2.7.14, z_D and L_D are defined by Eqs. 2.6.6 and 2.6.7. The short time approximation of $\overline{p}_{Df}$ has been obtained above and is given by the right hand side of Eq. 2.7.11. To obtain a short time approximation for $\overline{F}$ we first replace u by sw in Eq. 2.7.14 in accordance with Eq. 2.7.1. Using Eqs. 2.7.5, 2.7.6, and 2.7.8, we can approximate $\overline{F}$ as $s \to \infty$ by the following expression:

$$\overline{F} = \frac{\pi\beta}{2s} \sum_{n=1}^{\infty} \cos n\pi z_D \cos n\pi z_{wD} \int_0^{\infty} \exp(-\xi) \exp\left[-\frac{(ws + n^2\pi^2 L_D^2)\, y_D^2}{4\xi}\right] \frac{d\xi}{\sqrt{(ws + n^2\pi^2 L_D^2)\,\xi}}. \tag{2.7.15}$$

where β is defined by Eq. 2.7.9. Evaluating the integral in the right hand side of Eq. 2.7.15, we obtain

$$\overline{F} = \frac{\pi\beta}{2s} \sum_{n=1}^{\infty} \frac{\cos n\pi z_D \cos n\pi z_{wD}}{\sqrt{ws + n^2\pi^2 L_D^2}} \exp\left(-|y_D|\sqrt{ws + n^2\pi^2 L_D^2}\right). \tag{2.7.16}$$

If we now use the relation given by Eq. 2.5.14 in §2.5, we can recast Eq. 2.7.16 in the following form:

$$\overline{F} = \frac{\beta}{4L_D s} \sum_{n=-\infty}^{+\infty} \left\{ K_0\left[\sqrt{(z_D - z_{wD} - 2n)^2 / L_D^2 + y_D^2}\sqrt{ws}\right] + K_0\left[\sqrt{(z_D + z_{wD} - 2n)^2 / L_D^2 + y_D^2}\sqrt{ws}\right] \right\} - \frac{\pi\beta}{4\sqrt{w}s^{3/2}} \exp\left(-|y_D|\sqrt{ws}\right). \tag{2.7.17}$$

Substiuting the short time approximation of $\overline{p}_{Df}$ given by the right hand side of Eq. 2.7.11 and the short time approximation of $\overline{F}$ given by Eq. 2.7.17 into Eq. 2.7.13, we obtain the following short time approximation for the horizontal well solution:

$$\overline{p}_D = \frac{\beta}{4L_D s} \sum_{n=-\infty}^{+\infty} \left\{ K_0\left[\sqrt{(z_D - z_{wD} - 2n)^2 / L_D^2 + y_D^2}\sqrt{ws}\right] + K_0\left[\sqrt{(z_D + z_{wD} - 2n)^2 / L_D^2 + y_D^2}\sqrt{ws}\right] \right\}. \tag{2.7.18}$$

For large s, we can also assume that

$$K_0\left[\sqrt{(z_D \pm z_{wD} - 2n)^2 / L_D^2 + y_D^2}\sqrt{ws}\right] \ll K_0\left[\sqrt{(z_D - z_{wD})^2 / L_D^2 + y_D^2}\sqrt{ws}\right], \tag{2.7.19}$$

for $n > 0$ (physically, this assumption means that the influence of the top and bottom reservoir boundaries is not felt). Therefore, using the assumption stated by Eq. 2.7.19, we obtain the following short time approximation for the horizontal well solution:

$$\overline{p}_D = \frac{\beta}{4L_D s} K_0 \left[\sqrt{(z_D - z_{wD})^2 / L_D^2 + y_D^2} \sqrt{ws} \right]. \tag{2.7.20}$$

Applying the inversion theorem of the Laplace transformation to Eq. 2.7.20, we obtain the following expression in real time domain describing the short time pressure response of a horizontal well:

$$p_D = \frac{\beta}{8L_D} \mathrm{Ei} \left[-\frac{(z_D - z_{wD})^2 / L_D^2 + y_D^2}{4t_D / w} \right]. \tag{2.7.21}$$

For $w = 1$ (homogeneous reservoir), the short time approximation given by Eq. 2.7.21 is identical to that obtained in Refs. 37, 38, and 5 by using the source function approach of Gringarten and Ramey. The short time pressure behavior of horizontal wells will be discussed in Chapter III in detail.

II. Long Time Approximations, Infinite Reservoirs Here we derive the long time approximations for vertical wells, vertically fractured wells, and horizontal wells in reservoirs with impermeable top and bottom boundaries. Although the long time approximations of vertical well and vertically fractured well solutions are well known, and the long time pressure behavior of horizontal wells in infinite reservoirs will be discussed in detail later in Chapter III, this information is presented here mainly to help develop some of the ideas in the following parts of this section.

We first consider the long time approximation of the vertically fractured well solution given by Eq. 2.7.4. For small s (late times), replacing u by s as indicated by Eq. 2.7.2, and using the following approximation for the Bessel function $K_0(x)$ suitable for small arguments

$$K_0 \left(a\sqrt{z} \right) = -\ln \left(e^{\gamma} a\sqrt{z}/2 \right), \tag{2.7.22}$$

where γ is Euler's constant ($\gamma = 0.5772...$), we can write

$$K_0(\tilde{r}_D\sqrt{s}) = -\ln\left(e^{\gamma}\tilde{r}_D\sqrt{s}/2\right). \tag{2.7.23}$$

Using Eq. 2.7.23 in Eq. 2.7.4 and evaluating the integral, we obtain the following expression in Laplace domain describing the long time pressure behavior of vertically fractured wells in infinite reservoirs:

$$\bar{p}_D = -\frac{1}{2s}\ln s + \frac{1}{2s}\ln 4 - \frac{\gamma}{s} + \frac{1+\sigma\left(x_D, y_D\right)}{s}, \tag{2.7.24}$$

where $\sigma(x_D, y_D)$ is defined by

$$\begin{aligned}\sigma\left(x_D, y_D\right) = 0.25\Bigg\{&\left(x_D-1\right)\ln\left[\left(x_D-1\right)^2+y_D^2\right] \\ &-\left(x_D+1\right)\ln\left[\left(x_D+1\right)^2+y_D^2\right] - 2y_D\arctan\frac{2y_D}{x_D^2+y_D^2-1}\Bigg\},\end{aligned} \tag{2.7.25}$$

and is the pseudoskin factor defined by Eq. 22 of Ref. 10. Evaluating the Laplace inverse of the expression given by Eq. 2.7.24, we obtain the following long time approximation for the vertically fractured well solution:

$$p_D = 0.5\left(\ln t_D + 0.80907\right) + 1 + \sigma\left(x_D, y_D\right). \tag{2.7.26}$$

where t_D is the dimensionless time based on the fracture half length, L_{x_f}. Eq. 2.7.26 is identical to the long time approximation given by Eq. 14 of Ref. 10.

If we replace $\tilde{r}_D$ by r_D in Eq. 2.7.4, we obtain the solution for a vertical well. Using Eq. 2.7.23 (with $\tilde{r}_D$ replaced by r_D) in the resulting form of Eq. 2.7.4 and applying the inversion theorem of the Laplace transformation, we obtain the following well-known long time approximation for the vertical well solution:

$$p_D = 0.5\left(\ln t_D + 0.80907\right) - \ln r_D. \tag{2.7.27}$$

where t_D is based on the wellbore radius, r_w.

To obtain a long time approximation for the horizontal well solution given by Eq. 2.7.13, we assume that s is small enough that $\sqrt{u + n^2\pi^2 L_D^2} \approx n\pi L_D$ (where

we use Eq. 2.7.2 to replace u by s for small s). Then the appropriate approximation for $\overline{F}$ (Eq. 2.7.14) for small values of s is given by

$$\overline{F} = \frac{1}{s} \sum_{n=1}^{\infty} \cos n\pi z_D \cos n\pi z_{wD} \int_{-1}^{+1} K_0 \left[n\pi L_D \sqrt{(x_D - \alpha)^2 + y_D^2} \right] d\alpha. \quad (2.7.28)$$

Using the long time approximation of the fracture solution given by Eq. 2.7.24 and the long time approximation of $\overline{F}$ given by Eq. 2.7.28 in Eq. 2.7.13 and then applying the inversion theorem of the Laplace transformation to the resulting expression, we obtain the following approximation describing the long time pressure behavior of horizontal wells in an infinite reservoir with impermeable top and bottom boundaries:

$$p_D = 0.5 \left(\ln t_D + 0.80907 \right) + 1 + \sigma \left(x_D, y_D \right) + F \left(x_D, y_D, z_D, z_{wD}, L_D \right), \quad (2.7.29)$$

where $\sigma(x_D, y_D)$ is defined by Eq. 2.7.25 and $F(x_D, y_D, z_D, z_{wD}, L_D)$ is given by

$$F(x_D, y_D, z_D, z_{wD}, L_D) = \sum_{n=1}^{\infty} \cos n\pi z_D \cos n\pi z_{wD} \int_{-1}^{+1} K_0 \left[n\pi L_D \sqrt{(x_D - \alpha)^2 + y_D^2} \right] d\alpha. \quad (2.7.30)$$

Computational issues involved in the evaluation of the function F has been discussed in §§2.5 and 2.6 and will not be repeated here. We note, however, from Eqs 2.6.11 and 2.6.12 given in §2.6 that for the evaluation of the wellbore responses ($|x_D| \leq 1, y_D = 0, z_D = z_{wD} + r_{wD}$), F can be written as

$$F \left(|x_D| \leq 1, y_D = 0, z_D = z_{wD} + r_{wD} \right) = \frac{1}{L_D} \sum_{n=1}^{\infty} \frac{\cos n\pi \left(z_{wD} + r_{wD} \right) \cos n\pi z_{wD}}{n}$$

$$- \frac{1}{\pi L_D} \sum_{n=1}^{\infty} \frac{\cos n\pi \left(z_{wD} + r_{wD} \right) \cos n\pi z_{wD}}{n}$$

$$\left\{ Ki_1 \left[n\pi L_D \left(1 + x_D \right) \right] + Ki_1 \left[n\pi L_D \left(1 - x_D \right) \right] \right\}. \quad (2.7.31)$$

(In obtaining the form of F given by Eq. 2.7.31, we replaced $u + n^2\pi^2 L_D^2$ by $n^2\pi^2 L_D^2$ in Eqs. 2.6.11 and 2.6.12 as discussed above and then applied the inversion theorem

of the Laplace transformation to the resulting form of Eqs. 2.6.11 and 2.6.12.) Using the relations[36]

$$\cos n\pi z_{wD} \cos n\pi (z_{wD} + r_{wD}) = 0.5 \left[\cos n\pi \left(2z_{wD} + r_{wD}\right) + \cos n\pi r_{wD}\right] \quad (2.7.32)$$

and

$$\sum_{k=1}^{\infty} \frac{\cos kx}{k} = \frac{1}{2} \ln \frac{1}{2\left(1 - \cos x\right)}; \quad [0 < x < 2\pi] \quad (2.7.33)$$

we can write Eq. 2.7.31 as

$$\begin{aligned} &F\left(|x_D| \leq 1, y_D = 0, z_D = z_{wD} + r_{wD}\right) = \\ &-\frac{1}{2L_D} \ln \left[4 \sin \frac{\pi}{2} \left(2z_{wD} + r_{wD}\right) \sin \frac{\pi}{2} r_{wD}\right] - \varphi\left(x_D, 0, z_{wD}, r_{wD}, L_D\right), \end{aligned} \quad (2.7.34)$$

where

$$\begin{aligned} \varphi\left(x_D, 0, z_{wD}, r_{wD}, L_D\right) = &\frac{1}{\pi L_D} \sum_{n=1}^{\infty} \frac{\cos n\pi \left(z_{wD} + r_{wD}\right) \cos n\pi z_{wD}}{n} \\ &\left\{Ki_1 \left[n\pi L_D \left(1 + x_D\right)\right] + Ki_1 \left[n\pi L_D \left(1 - x_D\right)\right]\right\}. \end{aligned} \quad (2.7.35)$$

Eq. 2.7.34 defines the pseudoskin factor for a horizontal well and is discussed in detail in Chapter III.

Prats[39] and Prats *et al.*[40] showed that the behavior of infinite-conductivity vertical fractures can be represented by that of an unstimulated vertical well with wellbore radius equal to one-quarter of the length of the fracture. The expression for the equivalent wellbore radius, r'_{wf}, for vertically fractured wells can be obtained by rearranging the long time approximation given by Eq. 2.7.26 as follows:

$$p_{wD} = 0.5 \left(\ln \tilde{t}_D + 0.80907\right) - \ln \frac{L_{x_f}}{r'_{wf} \exp\left[1 + \sigma\left(x_D, 0\right)\right]}, \quad (2.7.36)$$

where $\tilde{t}_D$ is the dimensionless time based on the equivalent wellbore radius, r'_{wf}; that is,

$$\tilde{t}_D = t_D \left(\frac{L_{x_f}}{r'_{wf}}\right)^2. \quad (2.7.37)$$

Comparing Eq. 2.7.36 with the late time response of a vertical well given by Eq. 2.7.27, we can decide that the long time performance of a vertically fractured well can be represented by that of a vertical well with the equivalent wellbore radius, r'_{wf}, given by

$$r'_{wf} = L_{x_f} \exp\left[-1 - \sigma\left(x_D, 0\right)\right]. \tag{2.7.38}$$

The concept of equivalent wellbore radius can also be extended to horizontal wells. Rearranging Eq. 2.7.29 and using Eqs. 2.7.34 and 2.7.35, we can write

$$p_{wD} = 0.5\left(\ln \tilde{t}_D + 0.80907\right) - 0.5 \ln \frac{\left(L_h/2\right)^2 \left[4 \sin \pi\left(z_{wD} + \frac{\tilde{r}_{wD}}{2}\right) \sin \pi\left(\frac{\tilde{r}_{wD}}{2}\right)\right]^{1/L_D}}{{r'_{wh}}^2 \exp\left[2\left(1 + \sigma - \varphi\right)\right]}, \tag{2.7.39}$$

where σ and φ are given by Eqs. 2.7.25 and 2.7.35, respectively, and $\tilde{t}_D$ is the dimensionless time based on the equivalent wellbore radius, r'_{wh}; that is,

$$\tilde{t}_D = t_D \left(\frac{L_h}{2r'_{wh}}\right)^2. \tag{2.7.40}$$

Comparing Eq. 2.7.39 with the response of a vertical well (Eq. 2.7.27), we can decide that a horizontal well is equivalent to a vertical well with the equivalent wellbore radius given by

$$r'_{wh} = \frac{L_h/2}{\exp\left(1 + \sigma - \varphi\right)} \left[4 \sin \pi \left(z_{wD} + \frac{r_{wD}}{2}\right) \sin \pi \frac{r_{wD}}{2}\right]^{\frac{1}{2L_D}}. \tag{2.7.41}$$

To our knowledge, the expression given by Eq. 2.7.41 has not been reported in the literature.

<u>III. Long Time Approximations, Cylindrical Reservoirs</u> Here we derive the long time approximations for vertically fractured wells and horizontal wells in closed cylindrical reservoirs. Although it is well known, the long time approximation of the vertical well solution is also presented here for continuity.

We first consider the long time approximation of the vertically fractured well solution given by Eq. 2.6.20 and repeated below for convenience.

$$\bar{p}_D = \frac{1}{2s} \int_{-1}^{+1} \left[K_0\left(\tilde{r}_D \sqrt{u}\right) + \frac{I_0\left(\tilde{r}_D \sqrt{u}\right) K_1\left(r_{eD} \sqrt{u}\right)}{I_1\left(r_{eD} \sqrt{u}\right)}\right] d\alpha. \tag{2.7.42}$$

In Eq. 2.7.42, r_{eD} is the dimensionless drainage radius and $\tilde{r}_D = \sqrt{(x_D - \alpha)^2 + y_D^2}$. The long time approximation of Eq. 2.7.42 can be obtained by evaluating it at the limit as $s \rightarrow 0$. Following Ref. 16, if we neglect the terms of the order of $x^2 \ln x$ and higher, then we can approximate the Bessel functions in Eq. 2.7.42 by the following relations when their arguments become small:

$$K_0\left(a\sqrt{z}\right) = -\ln\left(e^{\gamma} a\sqrt{z}/2\right), \tag{2.7.43}$$

$$K_1\left(a\sqrt{z}\right) = \frac{1}{a\sqrt{z}} + \frac{a\sqrt{z}}{2}\left(\ln\frac{e^{\gamma} a\sqrt{z}}{2} - \frac{1}{2}\right), \tag{2.7.44}$$

$$I_0\left(a\sqrt{z}\right) = 1 + a^2 z/4, \tag{2.7.45}$$

and

$$I_1\left(a\sqrt{z}\right) = \frac{a\sqrt{z}}{2} + \frac{a^3 z^{3/2}}{16}. \tag{2.7.46}$$

In Eqs. 2.7.43 and 2.7.44, γ is Euler's constant ($\gamma = 0.5772...$). Using Eqs. 2.7.43 - 2.7.46 and Eq. 2.7.2, we can write the following expression as $s \rightarrow 0$:

$$\lim_{s \rightarrow 0}\left[K_0\left(\tilde{r}_D\sqrt{s}\right) + \frac{I_0\left(\tilde{r}_D\sqrt{s}\right) K_1\left(r_{eD}\sqrt{s}\right)}{I_1\left(r_{eD}\sqrt{s}\right)}\right] = \frac{2}{r_{eD}^2 s} + \ln\frac{r_{eD}}{\tilde{r}_D} - \frac{3}{4} + \frac{\tilde{r}_D^2}{2r_{eD}^2}. \tag{2.7.47}$$

In obtaining the right hand side of Eq. 2.7.47, we have neglected the terms of the order $s^{3/2}$. Substituting the right hand side of Eq. 2.7.47 in Eq. 2.7.42 yields the following relation as $s \rightarrow 0$:

$$\bar{p}_D = \frac{2}{r_{eD}^2 s^2} + \frac{1}{s}\left(\ln r_{eD} - \frac{3}{4}\right) + \frac{1 + \sigma(x_D, y_D)}{s} + \frac{\delta(x_D, y_D, r_{eD})}{s}, \tag{2.7.48}$$

where σ is defined by Eq. 2.7.49 and

$$\delta\left(x_D, y_D, r_{eD}\right) = \frac{y_D^2}{2r_{eD}^2} + \frac{(x_D + 1)^3 - (x_D - 1)^3}{12 r_{eD}^2}. \tag{2.7.49}$$

Applying the inversion theorem for Laplace transformation to Eq. 2.7.48 and defining

$$t_{DA} = \frac{t_D}{\pi r_{eD}^2}, \tag{2.7.50}$$

we obtain the following long time approximation for the pressure distribution in a closed cylindrical reservoir produced via a fully penetrating vertically fractured well:

$$p_D = 2\pi t_{DA} + \ln r_{eD} - 3/4 + 1 + \sigma\left(x_D, y_D\right) + \delta\left(x_D, y_D, r_{eD}\right). \tag{2.7.51}$$

The general solution for a vertically fractured well in a closed cylindrical reservoir given by Eq. 2.7.42 and its long time approximation given by Eq. 2.7.51 have not been reported in the literature. If we compare the numerical values obtained from Eq. 2.7.51 with those given in Table 2.6.1 (Cols. 1, 3, 5, and 7) at late times, we obtain identical values.

We now consider the long time approximation of the horizontal well solution in an isotropic closed cylindrical reservoir. The general solution is obtained from Table 2-E of Appendix A by using $L = L_h/2$ and is given by

$$\overline{p}_D = \overline{p}_{Df} + \overline{F} + \overline{F}_b, \tag{2.7.52}$$

where $\overline{p}_{Df}$ is the vertically fractured well solution given by Eq. 2.7.42 and $\overline{F}$ and $\overline{F}_b$ are defined respectively by

$$\begin{aligned}\overline{F}(x_D, y_D, z_D, z_{wD}, L_D) = \frac{1}{s}\sum_{n=1}^{\infty} \cos n\pi z_D \cos n\pi z_{wD} \\ \int_{-1}^{+1} K_0\left(\tilde{r}_D\sqrt{u + n^2\pi^2 L_D^2}\right) d\alpha,\end{aligned} \tag{2.7.53}$$

and

$$\begin{aligned}\overline{F}_b(x_D, y_D, z_D, z_{wD}, L_D, r_{eD}) = \frac{1}{s}\sum_{n=1}^{\infty} \cos n\pi z_D \cos n\pi z_{wD} \\ + \int_{-1}^{+1} \frac{I_0\left(\tilde{r}_D\sqrt{u + n^2\pi^2 L_D^2}\right) K_1\left(r_{eD}\sqrt{u + n^2\pi^2 L_D^2}\right)}{I_1\left(r_{eD}\sqrt{u + n^2\pi^2 L_D^2}\right)} d\alpha.\end{aligned} \tag{2.7.54}$$

In Eqs. 2.7.53 and 2.7.54, r_{eD} is the dimensionless drainage area and $\tilde{r}_D = \sqrt{(x_D - \alpha)^2 + y_D^2}$.

The long time approximation of the fracture solution, p_{Df}, has been obtained above and is given by the right hand side of Eq. 2.7.51. The long time approximations of the functions $\overline{F}$ and $\overline{F}_b$ are obtained by first replacing u by s in accordance with Eq. 2.7.2 and then assuming that s is small enough that $s+n^2\pi^2L_D^2 = n^2\pi^2L_D^2$. Evaluating the Laplace inversion of the resulting expressions, we obtain the following long time approximations for F and F_b in real time domain:

$$F(x_D, y_D, z_D, z_{wD}, L_D) = \sum_{n=1}^{\infty} \cos n\pi z_D \cos n\pi z_{wD} \int_{-1}^{+1} K_0\left(n\pi L_D \tilde{r}_D\right) d\alpha, \tag{2.7.55}$$

and

$$\begin{aligned} F_b(x_D, y_D, z_D, z_{wD}, L_D, r_{eD}) &= \sum_{n=1}^{\infty} \cos n\pi z_D \cos n\pi z_{wD} \\ &+ \int_{-1}^{+1} \frac{I_0\left(n\pi L_D \tilde{r}_D\right) K_1\left(n\pi L_D r_{eD}\right)}{I_1\left(n\pi L_D r_{eD}\right)} d\alpha. \end{aligned} \tag{2.7.56}$$

Note that the function F defined by Eq. 2.7.55 is the pseudoskin factor for a horizontal well in an infinite reservoir (see §2.7 II). Using Eqs. 2.7.51, 2.7.55, and 2.7.56 in Eq. 2.7.52, we obtain the following long time approximation of the horizontal well solution:

$$p_D = 2\pi t_{DA} + \ln r_{eD} - 3/4 + 1 + \sigma\left(x_D, y_D\right) + \delta\left(x_D, y_D, r_{eD}\right) + F + F_b. \tag{2.7.57}$$

In Eq. 2.7.57, t_{DA} is defined by Eq. 2.7.50.

Due to their simplicity, Eqs. 2.7.51 and 2.7.57 can also be used to define the shape factors for vertically fractured wells and horizontal wells at the center of a cylindrical reservoir. In the following, we shall derive the appropriate expressions for the shape factors for vertically fractured wells and horizontal wells in closed cylindrical reservoirs.

If we replace $\tilde{r}_D$ in Eq. 2.7.42 by r_D, then we obtain the solution for a fully penetrating vertical line source well in a closed cylindrical reservoir. Substitution of Eq. 2.7.47 (with $\tilde{r}_D$ replaced by r_D) in Eq. 2.7.42 and evaluation of the inverse Laplace transform of the resulting expression yields the following well-known long

time approximation for a vertical well:

$$p_D = 2\pi t_{DA} + \ln \frac{r_{eD}}{r_D} - 3/4 + \frac{r_D}{2r_{eD}^2}. \tag{2.7.58}$$

In Eq. 2.7.58, t_{DA} is defined by Eq. 2.7.50. (In this case, the reference length, $L = r_w$ where r_w is wellbore radius.) When considering wellbore responses ($r_D = 1$), assuming that $r_{eD} \gg 1$, we can neglect the last term in the right hand side of Eq. 2.7.58 and write the following well-known expression:

$$p_{wD} = 2\pi t_{DA} + \ln r_{eD} - 3/4. \tag{2.7.59}$$

We will now derive the expressions for the shape factors for the systems under consideration. The long time expression for the wellbore response of vertical wells (Eq. 2.7.59) can be written as[41]

$$p_{wD} = 2\pi t_{DA} + 0.5 \ln \frac{4A}{e^{\gamma} C_A L^2}. \tag{2.7.60}$$

Here A is the drainage area, γ is Euler's constant ($\gamma = 0.5772...$), C_A is the shape factor which depends only on the geometry of the drainage area and the location of the well within the drainage area (for a vertical well in a circular reservoir, $L = r_w$ and $C_A = 31.62$). Eq. 2.7.60 also implicitly assumes that $\sqrt{A}/r_w$ is large. By analogy to Eq. 2.7.60 the dimensionless pressure on the surface of a fully penetrating vertical fracture ($|x_D| < 1, y_D = 0$) can be written from Eq. 2.7.51 as

$$p_{wD} = 2\pi t_{DA} + 0.5 \ln \frac{4Ae^{2[1+\sigma(x_D,0)+\delta(x_D,0,r_{eD})]}}{e^{\gamma} C_A L_{x_f}^2}. \tag{2.7.61}$$

In many instances[10,39,40,42], an effective wellbore radius, r'_w has been defined by

$$r'_w = L_{x_f} \exp\left[-1 - \sigma\left(x_D, 0\right)\right] \tag{2.7.62}$$

and used in combination with Eq. 62 with $L = r'_w$ to determine the productivities of vertically fractured wells. As noted in Ref. 10 and shown above (see Eq. 2.7.38), however, the effective wellbore radius formula given by Eq. 2.7.62 can be rigorously established only for fractured wells in infinite reservoirs during the pseudoradial flow

period. Comparison of Eqs. 2.7.51 and 2.7.60 suggests that, during pseudosteady flow period, the effective wellbore radius, r'_w, should be defined by

$$r'_w = L_{x_f} \exp\left[-1 - \sigma\left(x_D, 0\right) - \delta\left(x_D, 0, r_{eD}\right)\right]. \tag{2.7.63}$$

Eq. 2.7.63 indicates, as noted in Ref. 10, that the effective wellbore radius, r'_w, is a function of the fracture penetration ratio, L_{x_f}/r_e, during pseudosteady flow period. If we wish to preserve the definition of the effective wellbore radius, r'_w, given by Eq. 2.7.62 during the pseudosteady flow period, then it is possible to define a shape factor, C_{Af}, for fractured wells as in Refs. 43 and 44. In this case, by combining Eqs. 2.7.61, 2.7.62, and 2.7.63, the shape factor for a vertically fractured well, C_{Af}, can be related to that for a vertical well, C_A, by the following relation:

$$C_{Af} = C_A \exp\left[-2\delta\left(x_D, 0, r_{eD}\right)\right]. \tag{2.7.64}$$

For small ratios of fracture penetration in the lateral direction, L_{x_f}/r_e, $\delta \to 0$ and we have $C_{fA} \approx C_A$[45]. Eq. 2.7.64 is the defining equation for the shape factor for a vertically fractured well in a closed cylindrical reservoir.

By similar arguments, we can write the horizontal well solution given by Eq. 2.7.57 as follows:

$$p_{wD} = 2\pi t_{DA} + 0.5 \ln \frac{4Ae^{2[1+\sigma(x_D,0)+\delta(x_D,0,r_{eD})+F+F_b]}}{e^{\gamma} C_A \left(L_h/2\right)^2}. \tag{2.7.65}$$

Eq. 2.7.65 suggests that the effective wellbore radius for a horizontal well during pseudosteady flow period be defined by

$$r'_w = \frac{L_h}{2} \exp\left[-1 - \sigma\left(x_D, 0\right) - \delta\left(x_D, 0, r_{eD}\right) - F - F_b\right]. \tag{2.7.66}$$

If we wish to preserve the definition of the effective wellbore radius determined in §2.7 II from pseudoradial flow equations given by

$$\begin{aligned} r'_w &= \frac{L_h/2}{\exp\left(1 + \sigma - \varphi\right)} \left[4 \sin \pi \left(z_{wD} + \frac{r_{wD}}{2}\right) \sin \pi \frac{r_{wD}}{2}\right]^{\frac{1}{2L_D}} \\ &= \frac{L_h}{2} \exp\left[-1 - \sigma\left(x_D, 0\right) - F\right], \end{aligned} \tag{2.7.67}$$

then we can can define the shape factor for horizontal wells in closed cylindrical reservoirs by the following relation

$$C_{Ah} = C_A \exp[-2\delta\,(x_D, 0, r_{eD}) - 2F_b], \tag{2.7.68}$$

where C_A is the shape factor for a vertical well. The shape factor expressions given by Eqs. 2.7.64 and 2.7.68 have not been reported in the literature.

<u>IV. Long Time Approximations, Rectangular Drainage Areas</u> Here, we limit our discussion to obtaining long time approximations for vertical wells, vertically fractured wells, and horizontal wells. We then derive expressions for shape factors for these three well configurations. For discussion, assuming isotropy, the pressure distributions in a closed rectangular drainage area produced via a vertical well, a vertically fractured well, and a horizontal well are given, respectively, by (see §2.3)

$$\begin{aligned}\overline{p}_{Dv} &= HT \\ &+ \frac{2\pi}{x_{eD}s}\sum_{k=1}^{\infty}\cos k\pi\frac{x_D}{x_{eD}}\cos k\pi\frac{x_{wD}}{x_{eD}} \\ &\frac{ch\sqrt{u+\frac{k^2\pi^2}{x_{eD}^2}}\,(y_{eD}-|y_D-y_{wD}|)+ch\sqrt{u+\frac{k^2\pi^2}{x_{eD}^2}}[y_{eD}-(y_D+y_{wD})]}{\sqrt{u+\frac{k^2\pi^2}{x_{eD}^2}}\;sh\sqrt{u+\frac{k^2\pi^2}{x_{eD}^2}}\,y_{eD}},\end{aligned} \tag{2.7.69}$$

$$\begin{aligned}\overline{p}_{Df} &= HT \\ &+ \frac{2}{s}\sum_{k=1}^{\infty}\frac{1}{k}\sin k\pi\frac{1}{x_{eD}}\cos k\pi\frac{x_D}{x_{eD}}\cos k\pi\frac{x_D}{x_{eD}} \\ &\frac{ch\sqrt{u+\frac{k^2\pi^2}{x_{eD}^2}}\,(y_{eD}-|y_D-y_{wD}|)+ch\sqrt{u+\frac{k^2\pi^2}{x_{eD}^2}}[y_{eD}-(y_D+y_{wD})]}{\sqrt{u+\frac{k^2\pi^2}{x_{eD}^2}}\;sh\sqrt{u+\frac{k^2\pi^2}{x_{eD}^2}}\,y_{eD}},\end{aligned} \tag{2.7.70}$$

and

$$\overline{p}_{Dh} = \overline{p}_{Df} + \overline{F}_1, \tag{2.7.71}$$

where

$$\overline{F}_1 = \frac{2\pi}{x_{eD}s}\sum_{n=1}^{\infty}\cos n\pi z_D\cos n\pi z_{wD}$$

$$\frac{ch\sqrt{u+a}\,(y_{eD}-|y_D-y_{wD}|)+ch\sqrt{u+a}[y_{eD}-(y_D+y_{wD})]}{\sqrt{u+a}\,sh\sqrt{u+a}y_{eD}}$$

$$+\frac{4}{s}\sum_{n=1}^{\infty}\cos n\pi z_D\cos n\pi z_{wD}\sum_{k=1}^{\infty}\sin k\pi\frac{1}{x_{eD}}\cos k\pi\frac{x_{wD}}{x_{eD}}\cos k\pi\frac{x_D}{x_{eD}}$$

$$\frac{ch\sqrt{u+b}\,(y_{eD}-|y_D-y_{wD}|)+ch\sqrt{u+b}[y_{eD}-(y_D+y_{wD})]}{\sqrt{u+b}\,sh\sqrt{u+b}y_{eD}}, \qquad (2.7.72)$$

with $a=n^2\pi^2L_D^2$ and $b=n^2\pi^2L_D^2+k^2\pi^2/x_{eD}^2$. In Eqs. 2.7.69 - 2.7.71, subscripts v, f, and h refer to vertical well, vertically fractured well, and horizontal well respectively, and HT is given by

$$HT=\frac{\pi}{x_{eD}s}\left\{\frac{ch\sqrt{u}\,[y_{eD}-(y_D+y_{wD})]+ch\sqrt{u}\,(y_{eD}-|y_D-y_{wD}|)}{\sqrt{u}\,sh\sqrt{u}y_{eD}}\right\}. \qquad (2.7.73)$$

If we note that[36]

$$\sum_{k=1}^{\infty}\frac{\cos kx}{k^2+a^2}=\frac{\pi}{2a}\frac{ch\;a(\pi-x)}{sh\;a\pi}-\frac{1}{2a^2},\quad [0\le x\le 2\pi], \qquad (2.7.74)$$

then we can write

$$\frac{1}{\sqrt{u}}\left[\frac{ch\sqrt{u}\,(y_{eD}-\tilde{y}_D)}{sh\sqrt{u}\;y_{eD}}\right]=\frac{2}{y_{eD}}\sum_{k=1}^{\infty}\frac{\cos k\pi\frac{\tilde{y}_D}{y_{eD}}}{u+\frac{k^2\pi^2}{y_{eD}^2}}+\frac{1}{uy_{eD}}. \qquad (2.7.75)$$

Using Eq. 2.7.75, we can recast Eq. 2.7.73 in the following form:

$$HT=\frac{2\pi}{x_{eD}y_{eD}su}+\frac{2\pi}{x_{eD}y_{eD}s}\sum_{m=1}^{\infty}\frac{\cos m\pi\frac{|y_D-y_{wD}|}{y_{eD}}+\cos m\pi\frac{y_D+y_{wD}}{y_{eD}}}{u+\frac{m^2\pi^2}{y_{eD}^2}}. \qquad (2.7.76)$$

For small s, replacing u by s (see Eq. 2.7.2) and $s+a$ by s (that is, neglecting s compared to a) and noting the relation[36]

$$\sum_{k=1}^{\infty}\frac{\cos kx}{k^2}=\frac{\pi^2}{6}-\frac{\pi x}{2}+\frac{x^2}{4},\quad [0\le x\le 2\pi], \qquad (2.7.77)$$

we can obtain an approximation for HT given by Eq. 2.7.73 when s is small as follows:

$$HT=\frac{2\pi}{x_{eD}y_{eD}s^2}$$

$$+\frac{2y_{eD}}{\pi x_{eD}s}\sum_{m=1}^{\infty}\frac{1}{m^2}\left(\cos m\pi\frac{|y_D-y_{wD}|}{y_{eD}}+\cos m\pi\frac{y_D+y_{wD}}{y_{eD}}\right) \qquad (2.7.78)$$

$$=\frac{2\pi}{x_{eD}y_{eD}s^2}+\frac{2\pi y_{eD}}{x_{eD}s}\left(\frac{1}{3}-\frac{y_D}{y_{eD}}+\frac{y_D^2+y_{wD}^2}{2y_{eD}^2}\right).$$

Similarly, when s is large, replacing $u + a$ by s in Eqs. 2.7.69, 2.7.70, and 2.7.72 and then applying the inversion theorem of Laplace transformation to Eqs. 2.7.69 - 2.7.72 and Eq. 2.7.73, we obtain the following long time approximations for vertical well, vertically fractured well, and horizontal well solutions given respectively by:

$$p_{Dv} = 2\pi t_{DA} + 2\pi \frac{y_{eD}}{x_{eD}} \left(\frac{1}{3} - \frac{y_D}{y_{eD}} + \frac{y_D^2 + y_{wD}^2}{2y_{eD}^2} \right)$$

$$+2 \sum_{k=1}^{\infty} \frac{1}{k} \cos k\pi \frac{x_D}{x_{eD}} \cos k\pi \frac{x_{wD}}{x_{eD}} \frac{ch\ k\pi \left(\frac{y_{eD} - |y_D - y_{wD}|}{x_{eD}} \right) + ch\ k\pi \left[\frac{y_{eD} - (y_D + y_{wD})}{x_{eD}} \right]}{sh\ k\pi \frac{y_{eD}}{x_{eD}}}, \tag{2.7.79}$$

$$p_{Df} = 2\pi t_{DA} + 2\pi \frac{y_{eD}}{x_{eD}} \left(\frac{1}{3} - \frac{y_D}{y_{eD}} + \frac{y_D^2 + y_{wD}^2}{2y_{eD}^2} \right)$$

$$+ \frac{2x_{eD}}{\pi} \sum_{k=1}^{\infty} \frac{1}{k^2} \sin k\pi \frac{1}{x_{eD}} \cos k\pi \frac{x_{wD}}{x_{eD}} \cos k\pi \frac{x_D}{x_{eD}}$$

$$\frac{ch\ k\pi \left(\frac{y_{eD} - |y_D - y_{wD}|}{x_{eD}} \right) + ch\ k\pi \left[\frac{y_{eD} - (y_D + y_{wD})}{x_{eD}} \right]}{sh\ k\pi \frac{y_{eD}}{x_{eD}}}, \tag{2.7.80}$$

and

$$p_{Dh} = p_{Df} + F_1, \tag{2.7.81}$$

where

$$F_1 = \frac{2}{x_{eD} L_D} \sum_{n=1}^{\infty} \frac{1}{n} \cos n\pi z_D \cos n\pi z_{wD}$$

$$\frac{ch\ n\pi L_D \left(y_{eD} - |y_D - y_{wD}| \right) + ch\ n\pi L_D \left[y_{eD} - (y_D + y_{wD}) \right]}{sh\ n\pi L_D y_{eD}}$$

$$+4 \sum_{n=1}^{\infty} \cos n\pi z_D \cos n\pi z_{wD} \sum_{k=1}^{\infty} \frac{1}{k} \frac{\sin k\pi \frac{1}{x_{eD}} \cos k\pi \frac{x_{wD}}{x_{eD}} \cos k\pi \frac{x_D}{x_{eD}}}{\sqrt{b}}$$

$$\frac{ch\sqrt{b} \left(y_{eD} - |y_D - y_{wD}| \right) + ch\sqrt{b} \left[y_{eD} - (y_D + y_{wD}) \right]}{sh\sqrt{b} y_{eD}}, \tag{2.7.82}$$

with $b = n^2\pi^2 L_D^2 + k^2\pi^2 / x_{eD}^2$. In Eqs. 2.7.79 - 2.7.80, t_{DA} is the dimensionless time based on drainage area $[t_{DA} = t_D / A_D = t_D / (x_{eD} y_{eD})]$.

The long time solutions given by Eqs. 2.7.79 and 2.7.80 can be computed without difficulty if the relations given by Eqs. 2.6.25 - 2.6.27 are used to compute the

ratio of hyperbolic functions when their arguments become large. The convergence of the series in Eq. 2.7.82, however, is slow. Note that it is also possible to obtain a long time approximation for the function $\overline{F}_1$ from the relation given by Eq. 2.6.53 in §2.6 IV (this only requires that $u + a$ be replaced by s in Eq. 2.6.53). This procedure yields the following alternate expression for F_1 to be used for computational purposes:

$$F_1 = F + F_{b1} + F_{b2} + F_{b3}. \tag{2.7.83}$$

Expressions for F, F_{b1}, F_{b2}, and F_{b3} are given respectively by

$$F = \sum_{n=1}^{\infty} \cos n\pi z_D \cos n\pi z_{wD}$$

$$\int_{-1}^{+1} K_0 \left[n\pi L_D \sqrt{(x_D - x_{wD} - \alpha)^2 + (y_D - y_{wD})^2} \right] d\alpha, \tag{2.7.84}$$

$$F_{b1} = \frac{2}{x_{eD} L_D} \sum_{n=1}^{\infty} \frac{1}{n} \cos n\pi z_D \cos n\pi z_{wD}$$

$$\left\{ \left[e^{-n\pi L_D (y_D + y_{wD})} + e^{-n\pi L_D (2y_{eD} - |y_D - y_{wD}|)} + e^{-n\pi L_D |2y_{eD} - (y_D + y_{wD})|} \right] \right.$$

$$\left[1 + \sum_{m=1}^{\infty} \exp\left(-2mn\pi L_D y_{eD}\right) \right]$$

$$\left. + e^{-n\pi L_D |y_D - y_{wD}|} \sum_{m=1}^{\infty} \exp\left(-2mn\pi L_D y_{eD}\right) \right\}, \tag{2.7.85}$$

$$F_{b2} = 4 \sum_{n=1}^{\infty} \cos n\pi z_D \cos n\pi z_{wD} \sum_{k=1}^{\infty} \frac{1}{k} \frac{\sin k\pi \frac{1}{x_{eD}} \cos k\pi \frac{x_D}{x_{eD}} \cos k\pi \frac{x_{wD}}{x_{eD}}}{\sqrt{n^2\pi^2 L_D + \frac{k^2\pi^2}{x_{eD}^2}}}$$

$$\left\{ \left[e^{-\sqrt{n^2\pi^2 L_D^2 + \frac{k^2\pi^2}{x_{eD}^2}} (y_D + y_{wD})} + e^{-\sqrt{n^2\pi^2 L_D^2 + \frac{k^2\pi^2}{x_{eD}^2}} |2y_{eD} - (y_D + y_{wD})|} \right.\right.$$

$$\left. \left. + e^{-\sqrt{n^2\pi^2 L_D^2 + \frac{k^2\pi^2}{x_{eD}^2}} (2y_{eD} - |y_D - y_{wD}|)} \right] \left[1 + \sum_{m=1}^{\infty} \exp\left(-2m \sqrt{n^2\pi^2 L_D^2 + \frac{k^2\pi^2}{x_{eD}^2}} y_{eD} \right) \right] \right.$$

$$\left. + e^{-\sqrt{n^2\pi^2 L_D^2 + \frac{k^2\pi^2}{x_{eD}^2}} |y_D - y_{wD}|} \sum_{m=1}^{\infty} \exp\left(-2m \sqrt{n^2\pi^2 L_D^2 + \frac{k^2\pi^2}{x_{eD}^2}} y_{eD} \right) \right\}, \tag{2.7.86}$$

and

$$F_{b3} = \sum_{n=1}^{\infty} \cos n\pi z_D \cos n\pi z_{wD}$$

$$\left\{ \int_{-1}^{+1} K_0 \left[n\pi L_D \sqrt{(x_D + x_{wD} - \alpha)^2 + (y_D - y_{wD})^2} \right] d\alpha \right.$$

$$+ \sum_{k=1}^{\infty} \int_{-1}^{+1} \left\{ K_0 \left[n\pi L_D \sqrt{(x_D - x_{wD} - 2kx_{eD} - \alpha)^2 + (y_D - y_{wD})^2} \right] \right.$$

$$+ K_0 \left[n\pi L_D \sqrt{(x_D + x_{wD} - 2kx_{eD} - \alpha)^2 + (y_D - y_{wD})^2} \right]$$

$$+ K_0 \left[n\pi L_D \sqrt{(x_D - x_{wD} + 2kx_{eD} - \alpha)^2 + (y_D - y_{wD})^2} \right]$$

$$\left. \left. + K_0 \left[n\pi L_D \sqrt{(x_D + x_{wD} + 2kx_{eD} - \alpha)^2 + (y_D - y_{wD})^2} \right] \right\} d\alpha \right\}. \qquad (2.7.87)$$

To compute the functions F and F_{b3} given by Eqs. 2.7.84 and 2.7.87 respectively at $y_D = y_{wD}$, the relations given by Eqs. 2.5.1 – 2.5.3 in §2.5 I are useful. Our computations indicate that the use of the relation given by Eq. 2.7.83 to compute the function F_1 improves the speed of the computations remarkably.

To our knowledge, the only source that reports long time approximations for pressure distributions in closed rectangular reservoirs produced via a vertically fractured well and a vertical well is Ref. 43. Solutions given by Eqs. 2.7.79 and 2.7.80, however, are considerably simpler than the ones given in Ref. 43. The long time approximation of the horizontal well solution given by Eq. 2.7.81 is new and no other approximation has come to our attention in the literature.

Eqs. 2.7.79 – 2.7.81 can also be used to obtain expressions for the shape factors for vertical wells, vertically fractured wells, and horizontal wells. If we assume that the long time pressure behavior can be described by Eq. 2.7.60 and let C define the shape factor for the appropriate well type, we can write

$$p_{wD} = 2\pi t_{DA} + 0.5 \ln \frac{4A}{e^{\gamma} C L^2}. \qquad (2.7.88)$$

Combining Eq. 2.7.88 with Eq. 2.7.79, 2.7.80, or 2.7.81 and noting the appropriate characteristic length, L ($L = r_w$, L_{x_f}, and $L_h/2$ for vertical well, vertically

fractured well, and horizontal well, respectively), we obtain the following shape factors in a rectangular drainage region for a vertical well, C_A, for a vertically fractured well, C_{Af}, and for a horizontal well, C_{Ah}, respectively:

$$\ln C_A = \ln \frac{4A}{e^{\gamma} r_w^2} - 4\pi \frac{y_{eD}}{x_{eD}} \left(\frac{1}{3} - \frac{y_D}{y_{eD}} \frac{y_D^2 + y_{wD}^2}{2y_{eD}^2} \right)$$

$$-4 \sum_{k=1}^{\infty} \frac{1}{k} \cos k\pi \frac{x_D}{x_{eD}} \cos k\pi \frac{x_{wD}}{x_{eD}} \frac{ch\ k\pi \left(\frac{y_{eD} - |y_D - y_{wD}|}{x_{eD}} \right) + ch\ k\pi \left[\frac{y_{eD} - (y_D + y_{wD})}{x_{eD}} \right]}{sh\ k\pi \frac{y_{eD}}{x_{eD}}}, \tag{2.7.89}$$

$$\ln C_{A_f} = \ln \frac{4A}{e^{\gamma} L_{x_f}^2} - 4\pi \frac{y_{eD}}{x_{eD}} \left(\frac{1}{3} - \frac{y_D}{y_{eD}} + \frac{y_D^2 + y_{wD}^2}{2y_{eD}^2} \right)$$

$$-\frac{4x_{eD}}{\pi} \sum_{k=1}^{\infty} \frac{1}{k^2} \sin k\pi \frac{1}{x_{eD}} \cos k\pi \frac{x_{wD}}{x_{eD}} \cos k\pi \frac{x_D}{x_{eD}}$$

$$\frac{ch\ k\pi \left(\frac{y_{eD} - |y_D - y_{wD}|}{x_{eD}} \right) + ch\ k\pi \left[\frac{y_{eD} - (y_D + y_{wD})}{x_{eD}} \right]}{sh\ k\pi \frac{y_{eD}}{x_{eD}}}, \tag{2.7.90}$$

and

$$\ln C_{Ah} = \ln \frac{4A}{e^{\gamma} (L_h/2)^2} - 4\pi \frac{y_{eD}}{x_{eD}} \left(\frac{1}{3} - \frac{y_D}{y_{eD}} + \frac{y_D^2 + y_{wD}^2}{2y_{eD}^2} \right)$$

$$-\frac{4x_{eD}}{\pi} \sum_{k=1}^{\infty} \frac{1}{k^2} \sin k\pi \frac{1}{x_{eD}} \cos k\pi \frac{x_{wD}}{x_{eD}} \cos k\pi \frac{x_D}{x_{eD}}$$

$$\frac{ch\ k\pi \left(\frac{y_{eD} - |y_D - y_{wD}|}{x_{eD}} \right) + ch\ k\pi \left[\frac{y_{eD} - (y_D + y_{wD})}{x_{eD}} \right]}{sh\ k\pi \frac{y_{eD}}{x_{eD}}} - 2F_1, \tag{2.7.91}$$

where F_1 is defined by Eq. 2.7.82 or 2.7.83.

From Eq. 2.7.89 we conclude that the shape factor for a vertical well in a rectangular drinage region is a function of the well location, x_{wD}/x_{eD} and y_{wD}/y_{eD}, the wellbore radius (in the form $x_D/x_{eD}, y_D/x_{eD}$), the aspect ratio of the drainage area, y_{eD}/x_{eD}, and the dimensionless drainage area, $A_D = A/r_w^2$. Similarly, Eq. 2.7.90 indicates that the shape factor for a vertical fracture is a function of the well location in the drainage area, x_{wD}/x_{eD} and y_{wD}/x_{eD}, the fracture penetration in the lateral direction, $1/x_{eD} = L_{x_f}/x_e$, the aspect ratio of the drainage area, y_{eD}/x_{eD}, and the

dimensionless drainage area, $A_D = A/L_{x_f}^2$. The horizontal well shape factor given by Eq. 2.7.91 depends on the location of the well, $x_{wD}/x_{eD}, y_{wD}/x_{eD}, z_{wD}$, the well penetration in the lateral direction, $1/x_{eD} = L_h/(2x_e)$, the dimensionless wellbore radius, $r_{wD} = r_w/h$, the aspect ratio of the reservoir, y_{eD}/x_{eD}, the ratios of the reservoir height to the areal dimensions, $x_{eD}L_D$ and $y_{eD}L_D$, and the dimensionless drainage area, $A_D = A/L_{x_f}^2$. Shape factors for other boundary conditions may also be derived along the same lines.

In Table 2.7.1, we present the shape factors, computed by Eqs. 2.7.89 - 2.7.91 for vertical wells, vertical fractures, and horizontal wells located at the center of a closed square drainage region. A_D in Table 2.7.1 is the dimensionless drainage area defined by $A_D = A/L^2$ ($L = r_w$, L_{x_f}, and $L_h/2$ for vertical wells, vertical fractures, and horizontal wells respectively). Shape factors for vertical fractures and horizontal wells are given for both uniform-flux and infinite-conductivity idealizations. The horizontal well half length considered in Table 2.7.1 is $L_D = 5$ and the dimensionless wellbore radius is $r_{wD} = 2 \times 10^{-3}$. It is assumed that the horizontal well is located midway between the top and bottom boundaries of the reservoir ($z_{wD} = 0.5$). The shape factors for vertical wells and vertical fractures presented in Table 2.7.1 are in very good agreement with those presented in Ref. 43. Until now, no information has been published in the literature regarding the shape factors for horizontal wells. Since horizontal well lengths can be comparable to the dimensions of the drainage area, the use of Eq. 2.7.60 with an effective wellbore radius, r'_w, determined from pseudoradial flow equations may lead to erroneous results. The use of the correct expression for the shape factor for horizontal wells presented in Eq. 2.7.91 is thus extremely important.

The shape factor expressions presented above can also be used to obtain production rates for wells producing at a constant pressure in a bounded reservoir. The appropriate relation is given by

$$q_D = \frac{141.2q(t)\mu}{kh(p_i - p_{wf})}$$
$$= \frac{1}{0.5\ln\frac{4A}{e^\gamma C L^2}} \exp\left(-\frac{2\pi t_{DA}}{0.5\ln\frac{4A}{e^\gamma C L^2}}\right), \qquad (2.7.92)$$

TABLE 2.7.1
SHAPE FACTORS FOR WELLS AT THE CENTER
OF A CLOSED SQUARE DRAINAGE REGION

A_D	Vertical Well	Vertical Fracture		Horizontal Well*	
		Uniform-Flux	Infinite-Conductivity	Uniform-Flux	Infinite-Conductivity
4.0×10^{0}	15.475	3.1525	3.1525	1.3173	1.3173
1.6×10^{1}	25.532	3.9098	6.3485	1.6337	2.6527
1.0×10^{2}	29.931	4.1357	7.3957	1.7281	3.0903
4.0×10^{2}	30.640	4.1684	7.5491	1.7417	3.1544
1.0×10^{4}	30.872	4.1687	7.6062	1.7419	3.1782

* $z_{wD} = 0.5$

$r_{wD} = 2 \times 10^{-3}$

$L_D = 5$

where C is C_A, C_{Af}, or C_{Ah}, and L is the appropriate charateristic length.

2.8 Applications

As noted before, one of our objectives in obtaining the Laplace transformation of pressure distributions for a wide variety of conditions is that it is possible to readily extend constant rate solutions to more complicated boundary conditions such as the inclusion of wellbore storage effects or the study of variable rate production; for example, constant pressure production. Here we consider the application of the solutions derived in §§2.1 – 2.3 to obtain some new solutions. Specifically, we consider wellbore storage effects and variable rate production for vertically fractured wells and horizontal wells. It is not our intention to document the characteristics of the solutions in great detail. Our objective is much more limited; we only wish to demonstrate the utility of our suggestion and present results in tabular form for some cases to enable others to verify the accuracy of their solutions.

I. Wellbore Storage and Skin Effects In 1949, van Everdingen and Hurst[16] showed that the response of a well with storage and skin can be obtained from the following relation:

$$\overline{p}_{wD} = \frac{s\overline{p}_D + S}{s + S_D s^2 (s\overline{p}_D + S)}. \tag{2.8.1}$$

In Eq. 2.8.1, $\overline{p}_D$ is the response of a well without storage and skin (in Laplace space), S is the skin factor, and S_D is the dimensionless wellbore storage constant defined by

$$S_D = \frac{5.615\widetilde{S}}{2\pi\phi c_t h L^2}, \tag{2.8.2}$$

where $\widetilde{S}$ is the unit storage factor and L is the appropriate characteristic length.

Two asymptotic cases of Eq. 2.8.1 are noteworthy. As $s \to \infty$ (small times), Eq. 2.8.1 yields

$$\overline{p}_{wD} \approx \frac{1}{s^2 S_D}, \tag{2.8.3}$$

and its Laplace inversion is given by

$$p_{wD} \approx t_D/S_D. \tag{2.8.4}$$

As $s \rightarrow 0$ (late times), the following relation is obtained from Eq. 2.8.1:

$$\overline{p}_{wD} \approx \overline{p}_D + \frac{S}{s}, \tag{2.8.5}$$

of which the Laplace inversion yields

$$p_{wD} \approx p_D + S. \tag{2.8.6}$$

With the aid of a Laplace inversion routine, such as the one suggested by Stehfest[9], Eq. 2.8.1 has been successfully used in the literature to compute the responses of wells with storage and skin where analytical expressions are available for the Laplace transform of the responses without storage and skin, $\overline{p}_D$. Here we consider two examples: vertically fractured well and horizontal well responses under the influence of wellbore storage and skin.

Vertically Fractured Wells Although vertically fractured wells are very common in practice, due to difficulties involved in obtaining the Laplace transform of vertically fractured well solution given by Ref. 10, Eq. 2.8.1 has not been directly applied to vertically fractured wells. Ref. 12, for example, uses a finite difference procedure to compute the responses of vertically fractured wells with wellbore storage effects. Ref. 11 presents a generalized procedure which, for all practical purposes, is a finite difference representation of Duhamel's principle. The dimensionless pressures documented in Ref. 11 are obtained by discretizing the constant rate solution in time. With the expectation that wellbore storage would only affect the early flow behavior, Raghavan[13] obtained analytical expressions for the response of vertically fractured wells during storage-dominated flow period. As noted earlier, an analytical expression for the Laplace transform of the fracture solution given by Ref. 10 is presented in Ref 28. Kuchuk[28] has also suggested that Eq. 2.8.1 can be used to obtain the responses with storage and skin.

We shall now consider the computation of wellbore pressure responses using Eq. 2.6.1 for a homogeneous reservoir. In this case, we have $f(s) = 1$; that is, $u = s$, and the pressure distribution is given by

$$\overline{p}_D\left(|x_D| \leq 1, y_D = 0\right) = \frac{1}{2s}\int_{-1}^{+1} K_0\left[\sqrt{s}\sqrt{(x_D-\alpha)^2}\right] d\alpha. \tag{2.8.7}$$

We computed the responses of uniform-flux ($x_D = 0$) and infinite-conductivity ($x_D = 0.732$) vertical fractures with storage effects by using the Stehfest algorithm[9] to numerically invert the Laplace space solution given by Eqs. 2.8.1 and 2.8.7. Table 2.8.1 presents results for the uniform-flux case for $S_D = 1.0$ and $S = 0$. Results obtained by using Eq. 2.8.7 are documented in Col. 2. In Cols. 3 and 4, solutions obtained by Refs. 11 and 13, respectively, are documented. Results from all three sources presented in Table 2.8.1 are in good agreement. In Table 2.8.2, we document results for the infinite-conductivity idealization for the $S_D = 10^{-3}$ and $S = 0$ case. Our results are presented in Col. 2, those presented in Ref. 12 (the finite difference solution) are given in Col. 3, and the results obtained from the approximate solution of Raghavan[13] are documented in Col. 4. The agreement between the responses obtained in this study and from the solution given by Ref. 13 is very good (note that the linear flow assumption used by Ref. 13 does not hold at late times and thus responses for late times are not shown in Col. 4 of Table 2.8.2). Responses computed in Ref. 12 appear to be significantly lower than the responses computed in this study and those obtained from the solution of Ref. 13 at early times. At later times, agreement between the results of Ref. 12 and our study is better. Similar results are obtained for other values of S_D when we compare our results with those documented in Ref. 12.

Fig. 2.8.1 presents a typical set of dimensionless pressure responses, p_{wD}, of infinite-conductivity vertical fractures vs. dimensionless time, t_D. The skin factor considered in Fig. 2.8.1 is $S = 0$ and the variable of interest is the dimensionless storage constant, S_D. As expected from Eq. 2.8.4, at early times, the dimensionless response curves depict a unit slope line on log-log coordinates (this behavior is evident for large values of S_D in Fig. 2.8.1; for small values of S_D this behavior

TABLE 2.8.1
UNIFORM-FLUX VERTICAL FRACTURE
WITH WELLBORE STORAGE
$S = 0.0$
$S_D = 1.0$

t_D	p_{wD} This Study	p_{wD} Ref. 11	p_{wD} Ref. 13
1.010×10^{-4}	1.0054×10^{-4}	1.0095×10^{-4}	1.0042×10^{-4}
2.014×10^{-4}	2.0005×10^{-4}	2.0105×10^{-4}	1.9988×10^{-4}
3.004×10^{-4}	2.9799×10^{-4}	2.9895×10^{-4}	2.9778×10^{-4}
4.015×10^{-4}	3.9773×10^{-4}	3.9866×10^{-4}	3.9749×10^{-4}
6.050×10^{-4}	5.9800×10^{-4}	5.9889×10^{-4}	5.9769×10^{-4}
1.007×10^{-3}	9.9243×10^{-4}	9.9330×10^{-4}	9.9204×10^{-4}
2.009×10^{-3}	1.9666×10^{-3}	1.9672×10^{-3}	1.9660×10^{-3}
3.027×10^{-3}	2.9490×10^{-3}	2.9495×10^{-3}	2.9483×10^{-3}
4.005×10^{-3}	3.8868×10^{-3}	3.8872×10^{-3}	3.8860×10^{-3}
6.034×10^{-3}	5.8175×10^{-3}	5.8176×10^{-3}	5.8164×10^{-3}
1.005×10^{-2}	9.5866×10^{-3}	9.5866×10^{-3}	9.5850×10^{-3}
2.003×10^{-2}	1.8756×10^{-2}	1.8754×10^{-2}	1.8753×10^{-2}
3.019×10^{-2}	2.7852×10^{-2}	2.7849×10^{-2}	2.7848×10^{-2}
4.034×10^{-2}	3.6772×10^{-2}	3.6769×10^{-2}	3.6769×10^{-2}
6.019×10^{-2}	5.3788×10^{-2}	5.3784×10^{-2}	5.3785×10^{-2}
1.002×10^{-1}	8.6833×10^{-2}	8.6832×10^{-2}	8.6840×10^{-2}
2.018×10^{-1}	1.6517×10^{-1}	1.6515×10^{-1}	1.6544×10^{-1}

TABLE 2.8.2
INFINITE-CONDUCTIVITY VERTICAL FRACTURE
WITH WELLBORE STORAGE
$S = 0.0$
$S_D = 0.001$

t_D	p_{wD} This Study	p_{wD} Ref. 12	p_{wD} Ref. 13
1.0×10^{-6}	6.6671×10^{-4}	5.6025×10^{-4}	6.6663×10^{-4}
1.5×10^{-6}	9.2786×10^{-4}	8.2249×10^{-4}	9.2775×10^{-4}
2.0×10^{-6}	1.1656×10^{-3}	1.0579×10^{-3}	1.1654×10^{-3}
3.0×10^{-6}	1.5924×10^{-3}	1.4754×10^{-3}	1.5922×10^{-3}
4.0×10^{-6}	1.9734×10^{-3}	1.8491×10^{-3}	1.9732×10^{-3}
6.0×10^{-6}	2.6446×10^{-3}	2.4987×10^{-3}	2.6444×10^{-3}
8.0×10^{-6}	3.2332×10^{-3}	3.0722×10^{-3}	3.2330×10^{-3}
1.0×10^{-5}	3.7645×10^{-3}	3.5925×10^{-3}	3.7643×10^{-3}
1.5×10^{-5}	4.9240×10^{-3}	4.7060×10^{-3}	4.9239×10^{-3}
2.0×10^{-5}	5.9226×10^{-3}	5.6733×10^{-3}	5.9226×10^{-3}
3.0×10^{-5}	7.6255×10^{-3}	7.3119×10^{-3}	7.6258×10^{-3}
4.0×10^{-5}	9.0788×10^{-3}	8.7179×10^{-3}	9.0795×10^{-3}
6.0×10^{-5}	1.1539×10^{-2}	1.1084×10^{-2}	1.1541×10^{-2}
8.0×10^{-5}	1.3627×10^{-2}	1.3105×10^{-2}	1.3617×10^{-2}
1.0×10^{-4}	1.5474×10^{-2}	1.4903×10^{-2}	1.5257×10^{-2}
1.5×10^{-4}	1.9418×10^{-2}	1.8696×10^{-2}	1.9241×10^{-2}
2.0×10^{-4}	2.2753×10^{-2}	2.1911×10^{-2}	2.2599×10^{-2}
3.0×10^{-4}	2.8359×10^{-2}	2.7299×10^{-2}	2.8232×10^{-2}
4.0×10^{-4}	3.3091×10^{-2}	3.1862×10^{-2}	3.2982×10^{-2}
6.0×10^{-4}	4.1039×10^{-2}	3.9482×10^{-2}	4.0949×10^{-2}
8.0×10^{-4}	4.7743×10^{-2}	4.5903×10^{-2}	4.7665×10^{-2}
1.0×10^{-3}	5.3654×10^{-2}	5.1576×10^{-2}	5.3583×10^{-2}
1.5×10^{-3}	6.6240×10^{-2}	6.3578×10^{-2}	6.6179×10^{-2}
2.0×10^{-3}	7.6847×10^{-2}	7.3695×10^{-2}	7.6799×10^{-2}
3.0×10^{-3}	9.4651×10^{-2}	9.0568×10^{-2}	9.4614×10^{-2}
4.0×10^{-3}	1.0966×10^{-1}	1.0473×10^{-1}	1.0963×10^{-1}
6.0×10^{-3}	1.3477×10^{-1}	1.2860×10^{-1}	1.3483×10^{-1}
8.0×10^{-3}	1.5577×10^{-1}	1.4866×10^{-1}	1.5607×10^{-1}
1.0×10^{-2}	1.7407×10^{-1}	1.6629×10^{-1}	1.7478×10^{-1}
1.5×10^{-2}	2.1219×10^{-1}	2.0333×10^{-1}	2.1461×10^{-1}
2.0×10^{-2}	2.4330×10^{-1}	2.3418×10^{-1}	2.4820×10^{-1}
3.0×10^{-2}	2.9332×10^{-1}	2.8490×10^{-1}	-
4.0×10^{-2}	3.3358×10^{-1}	3.2676×10^{-1}	-
6.0×10^{-2}	3.9773×10^{-1}	-	-
8.0×10^{-2}	4.4913×10^{-1}	-	-
1.0×10^{-1}	4.9280×10^{-1}	-	-

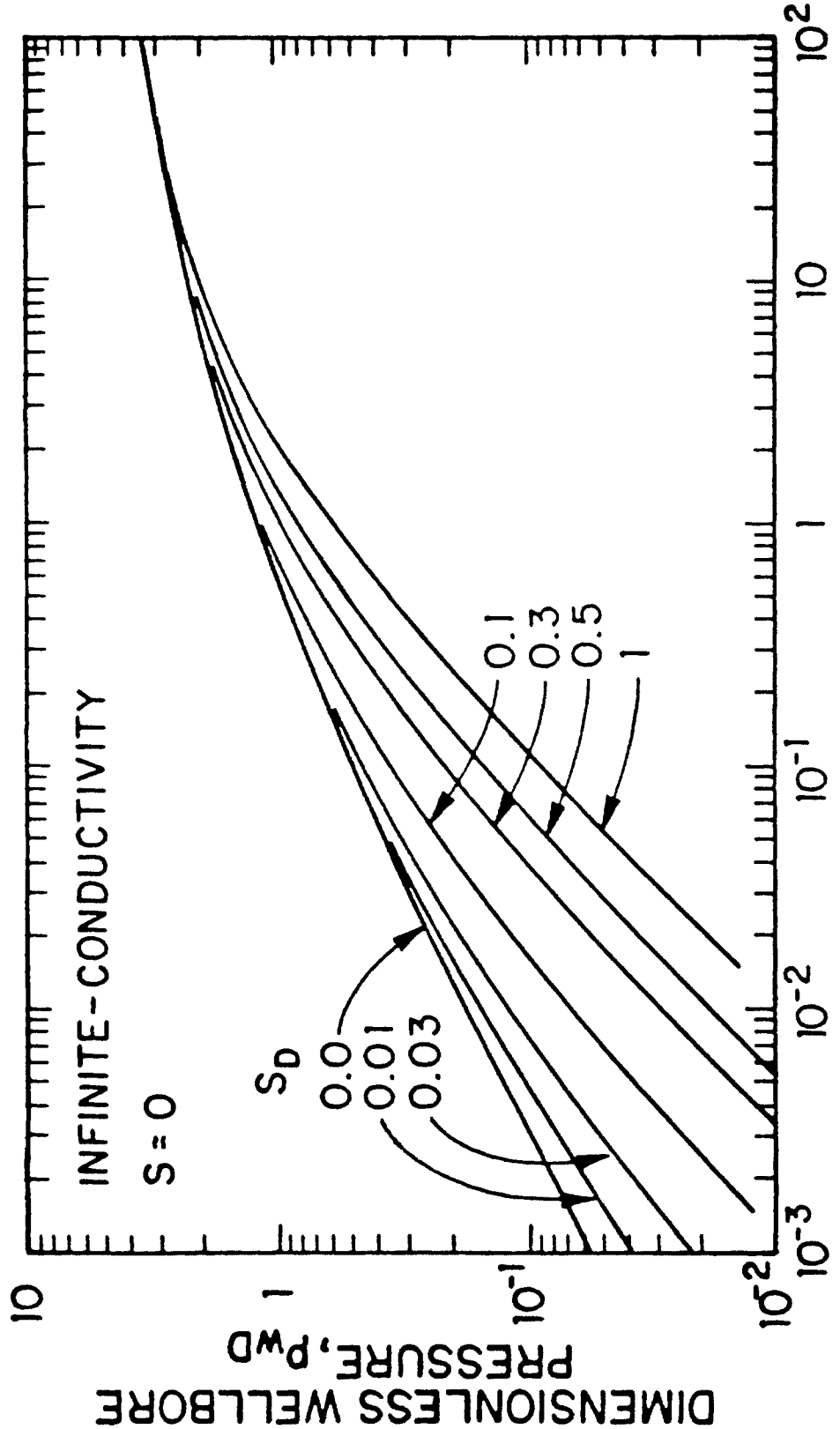

Fig. 2.8.1 - Influence of Wellbore Storage on Pressure Responses of Vertically Fractured Wells.

exists at times earlier than those considered in Fig. 2.8.1). At late times, all the response curves merge to follow the responses corresponding to the case for $S_D = 0$. This behavior is also predicted by Eq. 2.8.6. The appropriate expression describing the pressure response at late times has been obtained in §2.7 (Eq. 2.7.26) and is given by

$$p_D = \frac{1}{2}\left(\ln t_D + 2.80907\right) + \sigma\left(x_D, y_D\right), \tag{2.8.8}$$

where $\sigma(x_D, y_D)$ is defined by Eq. 2.6.25 Using Eq. 2.8.8 in Eq. 2.8.6 and rearranging the resulting expression, we obtain the following result:

$$p_{wD} \approx \frac{1}{2}\left(\ln \frac{t_D}{S_D} + 2.80907\right) + \frac{1}{2}\ln\left[S_D \exp\left(2S\right)\right] + \sigma\left(x_D, 0\right). \tag{2.8.9}$$

Eqs. 2.8.4 and 2.8.9 indicate that the pressure response curves for different values of S_D should merge to yield a unit slope line at early times on a log-log plot of p_{wD} vs. t_D/S_D. At the end of the storage-dominated flow period, pressure responses for different values of $S_D \exp(2S)$ would deviate from the initial unit slope line and when the pseudoradial flow is established, the pressure responses would be uniquely determined by t_D/S_D and $S_D \exp(2S)$ (see Eq. 2.8.9). The pressure responses shown by the unbroken lines of Fig. 2.8.2 clearly demonstrate this behavior for the special case of $S = 0$. Three values of S_D are considered; $S_D = 0.005$, 0.05, and 0.5. The derivative responses, $dp_{wD}/d\ln t_D$ vs. t_D/S_D, shown by the dashed lines of Fig. 2.8.2 merge with the pressure response curves at early times and also display a unit slope line (see Eq. 2.8.4). When pseudoradial flow is attained, the derivative responses assume the constant value 0.5 as indicated by Eq. 2.8.9. The shape of the derivative response curves during the transitional period between the storage-dominated and pseudoradial flow periods is dictated by the value of S_D. Characteristics of the derivative responses are also discussed in Refs. 46 and 47. The third set of curves (chain dotted curves) in Fig. 2.8.2 are the responses plotted in terms of the Chow[4] pressure group, $p_{wD}/(2dp_{wD}/d\ln t_D)$. Chow's approach is also discussed in Refs. 5 – 8. The advantage of Chow's approach is that the ordinates of the field curve and the type curve are identical since $p_{wD}/(2dp_{wD}/d\ln t_D) = \Delta p_{wf}/(2dp_{wf}/d\ln t)$. Thus, type curve matching becomes easier since the vertical

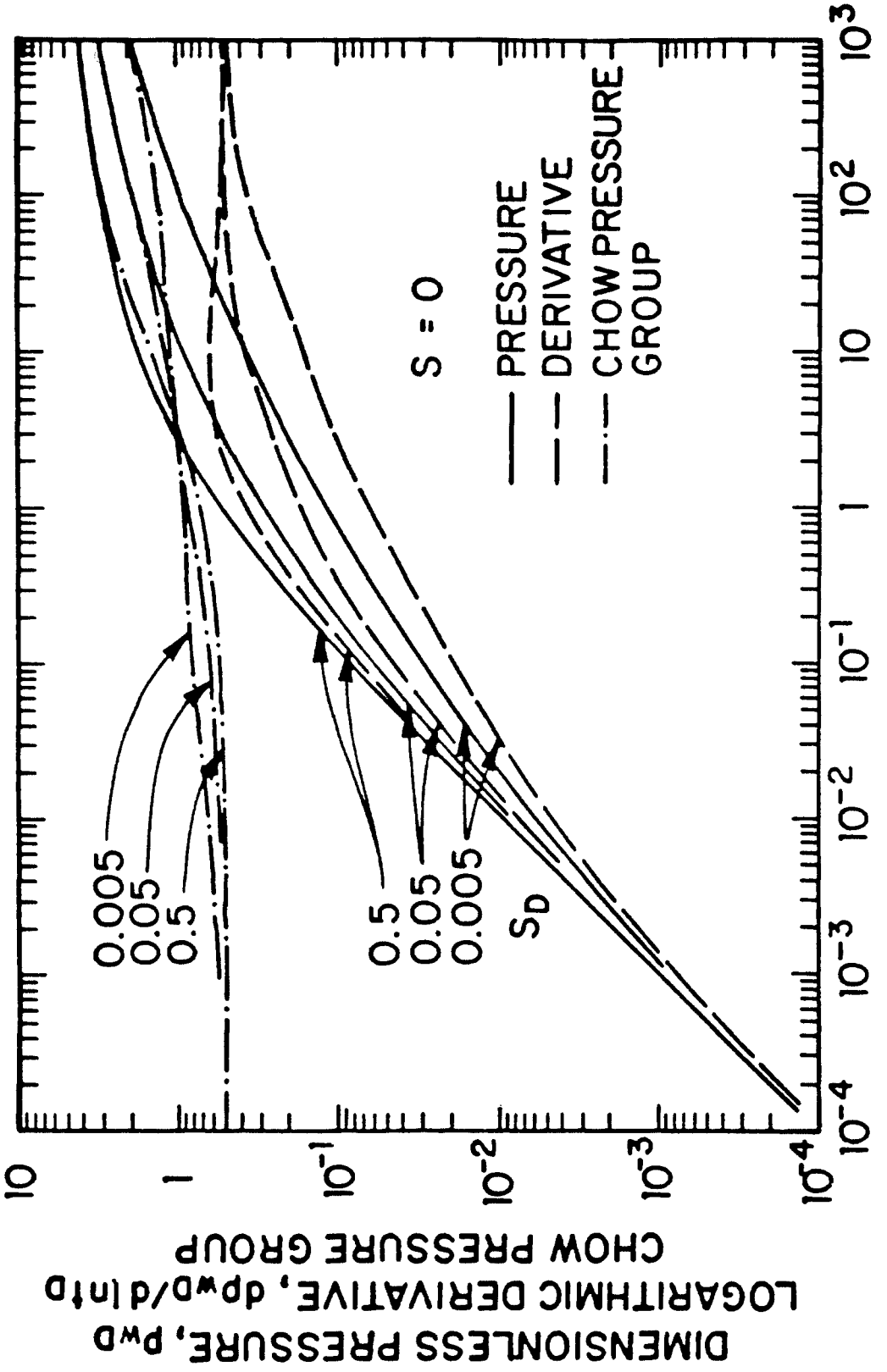

Fig. 2.8.2 - Influence of Wellbore Storage on Vertically Fractured Well Responses.

axes of the field data plot and the type curve can be aligned, and the field data curve may then be shifted horizontally until the best match is obtained. Details are discussed in Chapter III and in the references listed above. As expected from Eq. 2.8.4 and displayed by the chain-dotted lines of Fig. 2.8.2, the responses in terms of the Chow pressure group attain the constant value of 0.5 at early times for all values of S_D. At the end of the storage-dominated flow period, the responses deviate from the constant value 0.5 and at the onset of the pseudoradial flow period they merge with the corresponding pressure response curve since $2dp_{wD}/d\ln t_D = 1$.

Horizontal Wells The second example we consider is horizontal well responses with storage effects. We assume that the well produces an isotropic ($k = k_x = k_y = k_z$) and homogeneous reservoir ($u = s$). The pertinent solution for horizontal well responses in absence of storage and skin effects, $\bar{p}_D$, is given by Eq. 2.6.8 (or Eq. 2.6.18 for use at especially early times). We computed the horizontal well responses with storage effects by using Eq. 2.6.8 in Eq. 2.8.1. Figs. 2.8.3 and 2.8.4 present horizontal well responses for $L_D = 5$ and 100, respectively, under the influence of wellbore storage for an undamaged ($S = 0$) well. In both figures, the well is assumed to be located midway between the impermeable top and bottom boundaries ($z_{wD} = 0.5$) and the dimensionless wellbore radius, $r_{wD} = 2 \times 10^{-3}$. Three values of dimensionless storage constant, S_D, are considered; $S_D = 0.5$, 0.05, and 0.005. The unbroken lines are the dimensionless pressure responses, p_{wD} vs. t_D/S_D, the dashed lines correspond to logarithmic derivative responses, $dp_{wD}/d\ln t_D$ vs. t_D/S_D, and the chain-dotted lines are the responses in terms of the Chow pressure group, $p_{wD}/(2dp_{wD}/d\ln t_D)$. The characteristics of horizontal well responses shown in Figs. 2.8.3 and 2.8.4 are qualitatively similar to those of vertically fractured wells discussed in connection with Fig. 2.8.2 and will not be repeated here.

In Refs. 5 and 38, it is noted that the differences in the late time responses of long horizontal wells ($L_D \geq 4$) and vertically fractured wells are negligible. If wellbore storage effects dominate early time responses, then differences in the two solutions will be obscured even further. Early time responses of long horizontal wells and vertically fractured wells under the influence of wellbore storage are shown in

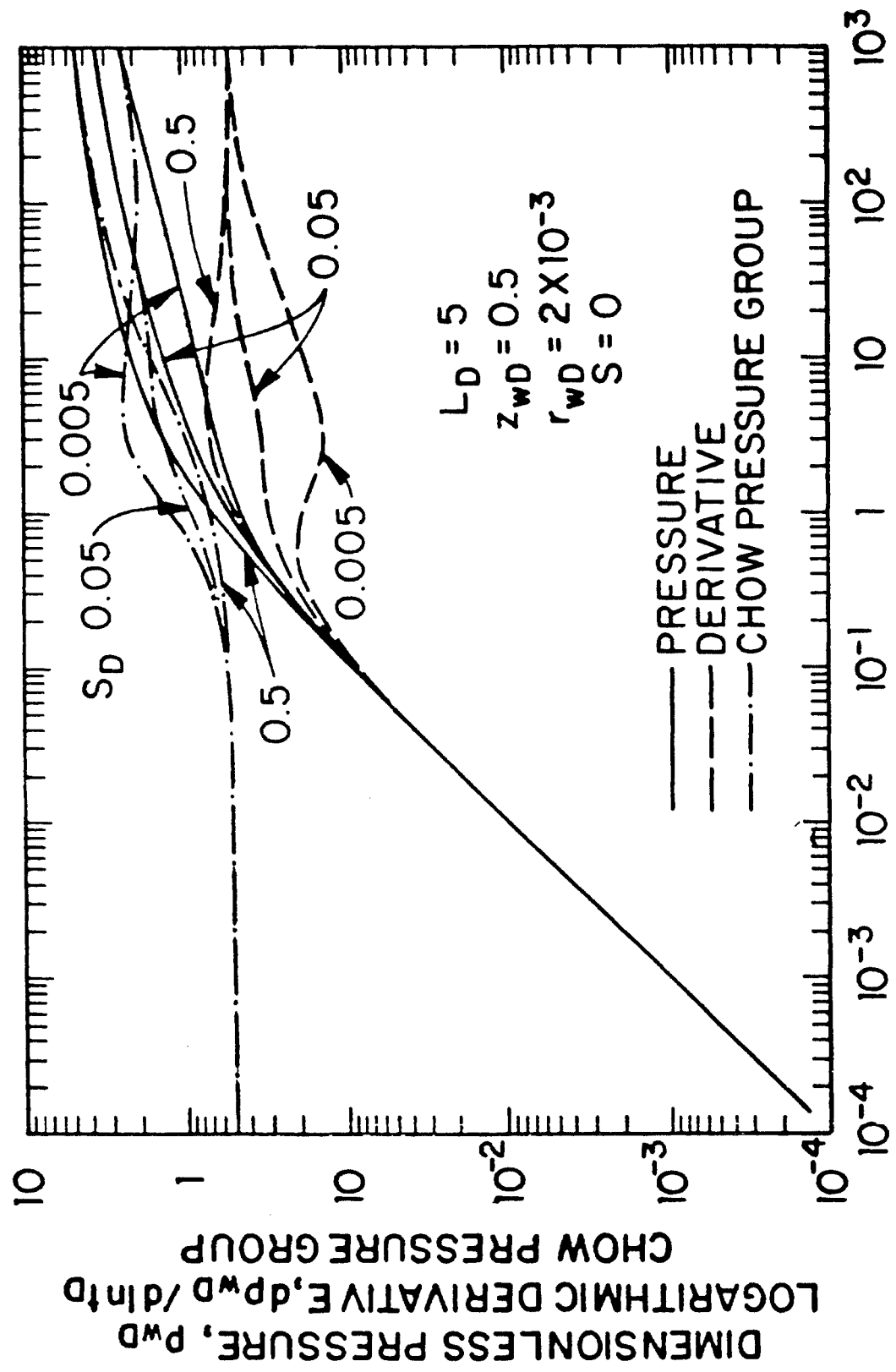

Fig. 2.8.3 - Influence of Wellbore Storage on Horizontal Well Responses ($L_D = 5$).

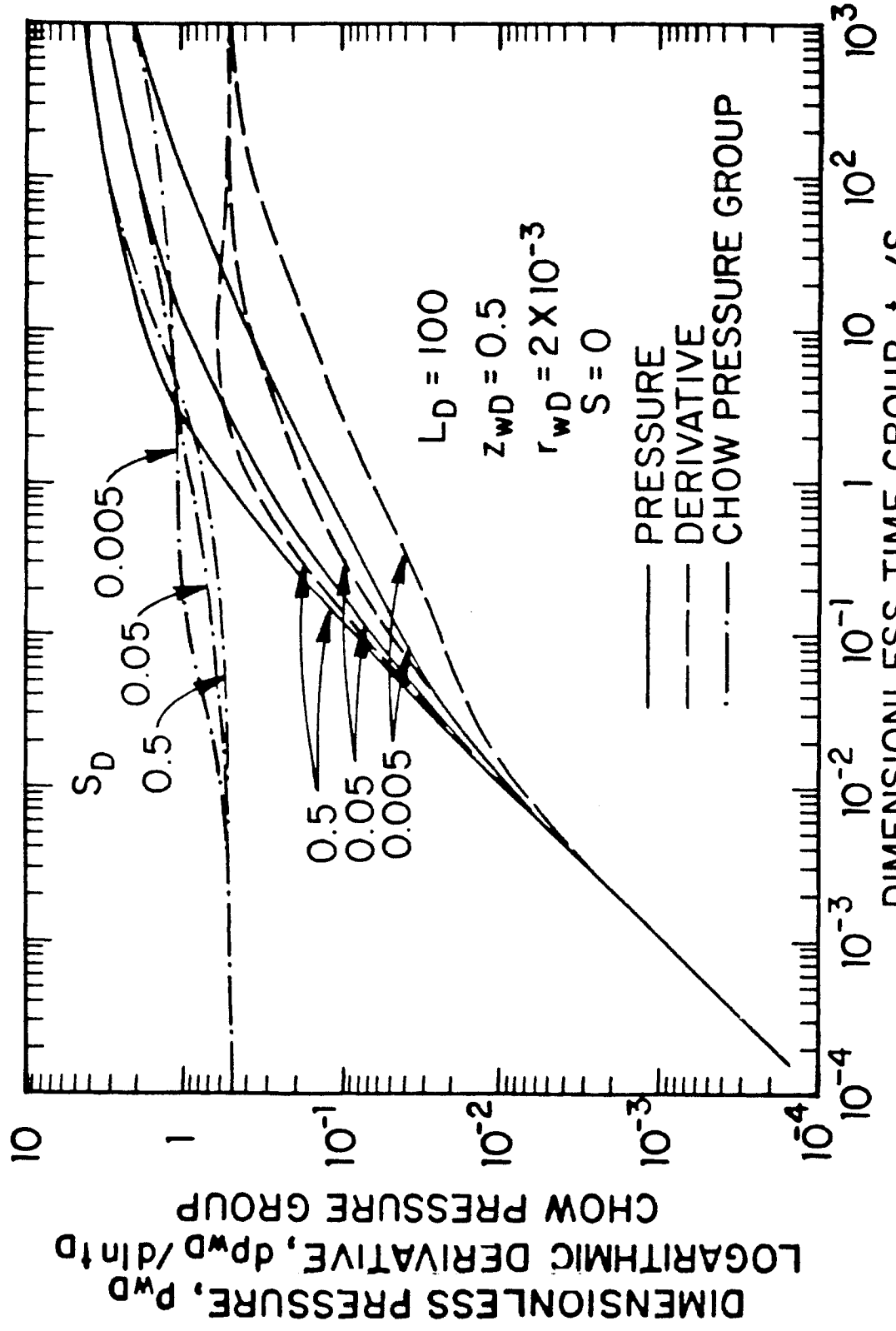

Fig. 2.8.4 - Influence of Wellbore Storage on Horizontal Well Responses ($L_D = 100$).

Fig. 2.8.5. Both the horizontal well and vertically fractured well are assumed to have infinite-conductivity and to be undamaged ($S = 0$). The horizontal well half-length, $L_D = 100$, the dimensionless wellbore radius, $r_{wD} = 2 \text{ x } 10^{-3}$, and $z_{wD} = 0.5$ (well is located midway between the top and bottom boundaries). We present results in terms of the logarithmic derivative principally because differences can be more readily highlighted. For $S_D = 0.5$, not unexpectedly, the derivative responses for long horizontal wells and vertical fractures are essentially identical for all times. For smaller values of S_D, the horizontal well responses and vertical fracture responses are initially identical (see Eq. 2.8.4). The fractured well responses deviate from the unit slope line earlier indicating that, all conditions being identical, the storage-dominated flow period for fractured wells ends earlier than that for horizontal wells. When pseudoradial flow conditions are attained, the two responses again become indistinguishable.

The examples considered above clearly demonstrate the utility of the solutions developed in this chapter. Both examples, vertically fractured well and horizontal well solutions with wellbore storage, are very common in practice and the use of Laplace domain solutions developed in this chapter eliminates the difficulties involved in obtaining convenient and reliable solutions for an otherwise very complex problem. The procedure discussed here can also be used to compute slug test responses[48]. In the following, we consider another complex problem - production at prescribed pressure - for which the appropriate solutions can be conveniently obtained if Laplace domain solutions are available.

<u>II. Production At Prescribed Pressure</u> Here we consider a specific case of the variable rate production problem - production at a prescribed pressure. By using Duhamel's principle (superposition theorem), van Everdingen and Hurst[16] have shown the following relation in Laplace domain between the wellbore pressure responses under constant rate production condition, $\overline{p}_{wD}$, and the rate responses

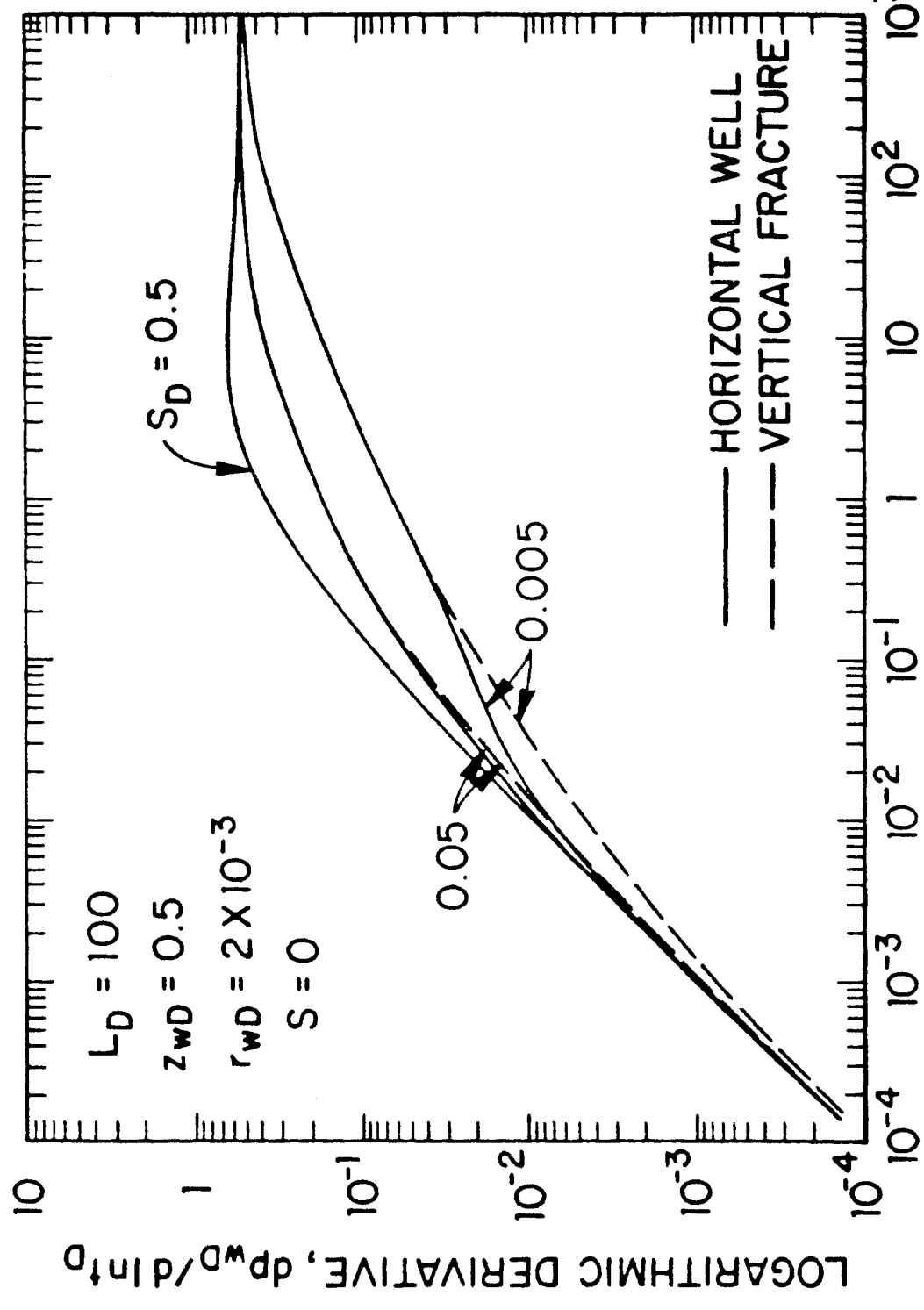

Fig. 2.8.5 - Comparison of Horizontal Well and Vertically Fractured Well Responses – Wellbore Storage.

under constant pressure production condition, $\overline{q}_D$:

$$\overline{p}_{wD}\overline{q}_D = \frac{1}{s^2} \tag{2.8.10}$$

In Eq. 2.8.10, $\overline{p}_{wD}$ and $\overline{q}_D$ are defined, respectively, by

$$\overline{p}_{wD} = \frac{2\pi kh}{q\mu}\overline{\Delta p}_{wf}(s), \tag{2.8.11}$$

and

$$\overline{q}_D = \frac{\overline{q}(s)\,\mu}{2\pi kh\Delta p_{wf}}. \tag{2.8.12}$$

Using the relation given by Eq. 2.8.10 and the Laplace domain solutions for $\overline{p}_{wD}$ developed in §§2.1 – 2.3, the rate responses, q_D, for a variety of wells can be obtained without difficulty.

Fig. 2.8.6 shows dimensionless reciprocal rate responses, $1/q_D$, vs. dimensionless time group t_D/w for an infinite-conductivity vertically fractured well in an isotropic ($k = k_x = k_y = k_z$) naturally fractured reservoir. To compute the responses shown in Fig. 2.8.6, we used the dimensionless pressure solution given by Eq. 2.6.2 (at $x_D = 0.732$) and Eq. 2.8.10. These responses correspond to dimensionless storativity, $w = 10^{-2}$ and the dimensionless transfer coefficient, λ, is the variable of interest. Since our intent is to show the use of our solutions, detailed discussion of the responses shown in Fig. 2.8.6 is outside the scope of this section. We only note that these responses do display all the characteristics of vertically fractured wells and naturally fractured reservoirs. They display the linear flow behavior, typical of vertically fractured wells at early times, a transition period characterized by approximately constant values of q_D, typical of the Warren and Root[18] model, and ultimately pseudoradial flow.

The procedure outlined above can be applied to various well types considered in this chapter. For those who wish to compare their results obtained by using the solutions presented in this chapter, we include a table of horizontal well rate responses in homogeneous and naturally fractured reservoirs. To compute the responses given in Table 2.8.3 we used the horizontal well pressure response solution given by Eq. 2.6.8 (at $x_D = 0.732$). Pertinent information on the well and reservoir properties is presented in Table 2.8.3.

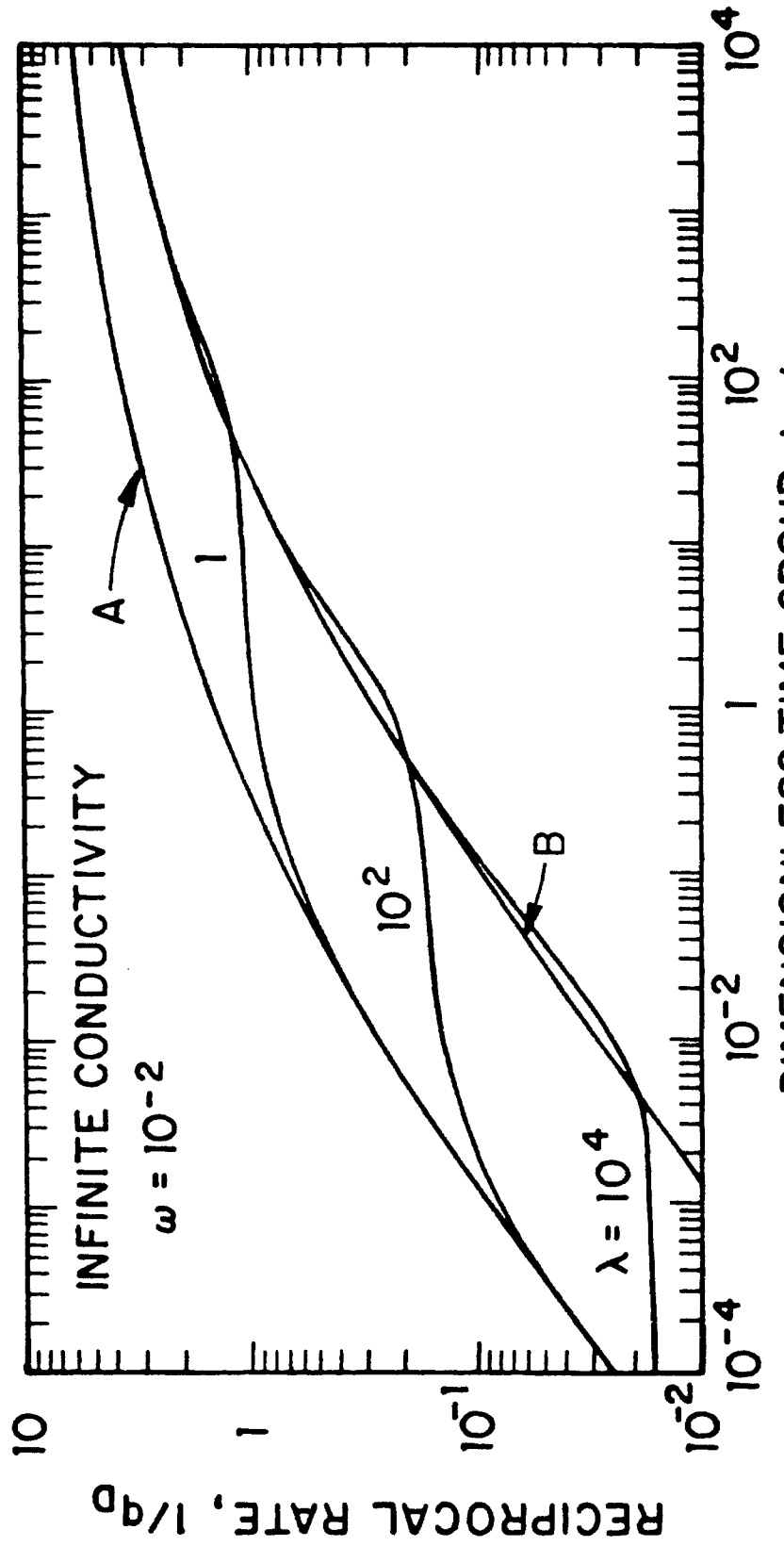

Fig. 2.8.6 - Vertically Fractured Well Responses in Fractured Reservoirs – Constant Pressure Production.

TABLE 2.8.3
INFINITE-CONDUCTIVITY HORIZONTAL WELL
$L_D = 5$
$z_{wD} = 0.5$
$r_{wD} = 2 \times 10^{-3}$

t_D/w	q_D			
	HOMOGENEOUS RESERVOIR, $w = 1$	NATURALLY FRACTURED RESERVOIR, $w = 10^{-2}$		
		$\lambda = 1$	$\lambda = 10^2$	$\lambda = 10^4$
1.0×10^{-4}	2.6603	2.6604	2.6652	3.0622
1.5×10^{-4}	2.5294	2.5294	2.5358	3.0216
2.0×10^{-4}	2.4437	2.4438	2.4516	3.0043
3.0×10^{-4}	2.3320	2.3321	2.3426	2.9899
4.0×10^{-4}	2.2585	2.2586	2.2716	2.9831
5.0×10^{-4}	2.2045	2.2047	2.2200	2.9781
6.0×10^{-4}	2.1622	2.1624	2.1799	2.9736
8.0×10^{-4}	2.0986	2.0988	2.1206	2.9649
1.0×10^{-3}	2.0517	2.0520	2.0777	2.9565
1.5×10^{-3}	1.9715	1.9719	2.0068	2.9356
2.0×10^{-3}	1.9178	1.9182	1.9616	2.9154
3.0×10^{-3}	1.8431	1.8438	1.9031	2.8769
4.0×10^{-3}	1.7884	1.7892	1.8643	2.8406
5.0×10^{-3}	1.7436	1.7446	1.8357	2.8066
6.0×10^{-3}	1.7051	1.7063	1.8134	2.7745
8.0×10^{-3}	1.6405	1.6422	1.7811	2.7159
1.0×10^{-2}	1.5875	1.5897	1.7593	2.6637
1.5×10^{-2}	1.4861	1.4895	1.7289	2.5562
2.0×10^{-2}	1.4116	1.4163	1.7146	2.4735
3.0×10^{-2}	1.3056	1.3129	1.7029	2.3556
4.0×10^{-2}	1.2308	1.2407	1.6981	2.2756
5.0×10^{-2}	1.1736	1.1859	1.6951	2.2170
6.0×10^{-2}	1.1273	1.1421	1.6927	2.1717
8.0×10^{-2}	1.0558	1.0754	1.6882	2.1045
1.0×10^{-1}	1.0014	1.0257	1.6838	2.0558
1.5×10^{-1}	0.9055	0.9409	1.6729	1.9734
2.0×10^{-1}	0.8402	0.8859	1.6621	1.9184
3.0×10^{-1}	0.7532	0.8178	1.6413	1.8426
4.0×10^{-1}	0.6962	0.7775	1.6215	1.7875
5.0×10^{-1}	0.6552	0.7512	1.6025	1.7426
6.0×10^{-1}	0.6241	0.7331	1.5842	1.7042
8.0×10^{-1}	0.5792	0.7104	1.5500	1.6399

TABLE 2.8.3 (Cont.)
INFINITE-CONDUCTIVITY HORIZONTAL WELL
$L_D = 5$
$z_{wD} = 0.5$
$r_{wD} = 2 \times 10^{-3}$

t_D/w	q_D			
	HOMOGENEOUS RESERVOIR, $w = 1$	NATURALLY FRACTURED RESERVOIR, $w = 10^{-2}$		
		$\lambda = 1$	$\lambda = 10^2$	$\lambda = 10^4$
1.0×10^0	0.5480	0.6973	1.5184	1.5871
1.5×10^0	0.4984	0.6819	1.4493	1.4859
2.0×10^0	0.4681	0.6757	1.3916	1.4116
3.0×10^0	0.4309	0.6708	1.3002	1.3056
4.0×10^0	0.4078	0.6685	1.2306	1.2309
5.0×10^0	0.3914	0.6667	1.1752	1.1736
6.0×10^0	0.3789	0.6651	1.1297	1.1274
8.0×10^0	0.3606	0.6620	1.0583	1.0558
1.0×10^1	0.3476	0.6590	1.0037	1.0014
1.5×10^1	0.3260	0.6514	0.9074	0.9056
2.0×10^1	0.3122	0.6441	0.8419	0.8402
3.0×10^1	0.2946	0.6302	0.7547	0.7532
4.0×10^1	0.2831	0.6171	0.6975	0.6962
5.0×10^1	0.2748	0.6048	0.6564	0.6552
6.0×10^1	0.2684	0.5932	0.6251	0.6241
8.0×10^1	0.2588	0.5720	0.5800	0.5792
1.0×10^2	0.2523	0.5559	0.5509	0.5503
1.5×10^2	0.2405	0.5168	0.5007	0.5003
2.0×10^2	0.2327	0.4871	0.4700	0.4698
3.0×10^2	0.2225	0.4455	0.4325	0.4324
4.0×10^2	0.2158	0.4183	0.4092	0.4091
5.0×10^2	0.2108	0.3992	0.3927	0.3926
6.0×10^2	0.2069	0.3849	0.3801	0.3801
8.0×10^2	0.2011	0.3646	0.3617	0.3617
1.0×10^3	0.1968	0.3505	0.3486	0.3486

CHAPTER III

HORIZONTAL WELL PRESSURE ANALYSIS

A review of production performance over the past few years, conclusively establishes the advantages of horizontal wells and drainholes[49]. Drainholes are normally drilled from existing vertical wells and extend 100 feet to 500 feet in either direction. Horizontal wells involve the drilling of new wells and are usually 1000 feet to 2000 feet long. Both completions, like fractured wells, are intended to provide a larger surface area for fluid withdrawal and thus improve productivity. These completions have been found to be effective in *(i)* some naturally fractured reservoirs, *(ii)* reservoirs wherein gas and/or water coning problems preclude the efficient operation of vertical wells, *(iii)* thin reservoirs, and *(iv)* reservoirs with high vertical permeability. Disadvantages of these completions include high drilling costs and the inability to produce contigious zones separated by impermeable layers via a single wellbore.

For purposes of modeling well behavior, horizontal wells and drainholes can be treated similarly. Thus, unless specifically stated, the term horizontal well will include both types of completions.

To be a commercial method of completion, at least for primary recovery, horizontal well productivity must be comparable to the productivity of a vertically fractured well. It is not sufficient to compare horizontal well productivity with unstimulated vertical wells. Similar observations have been made in Refs. 1 and 2. Thus, in this work responses for vertically fractured wells are used as a basis for comparison. (A horizontal well may be viewed as a fracture with limited height, however, this does not imply that horizontal well productivity will never be comparable to that of a vertically fractured well.)

The transient behavior of horizontal wells and the characteristics of response curves have been considered in Refs. 5, 37, 38, and 50. The central new results of this chapter concern the development of analytical expressions and correlations for the pseudoskin factor, and the development of new methods of analysis to determine formation properties and well characteristics. In particular, we discuss new applications of the derivative approach suggested by Chow[4] – the pressure normalized by its derivative. In this chapter, we refer to this method as the normalized pressure procedure. Although it is probably the oldest derivative method, Chow's approach was not known in the petroleum engineering literature until recently. Here we restrict our discussion to the applications of Chow's procedure to analyze the pressure responses of horizontal wells and vertically fractured wells as in Ref. 5. The procedure suggested by Chow, however, has a much broader range of applicability (see also Refs. 6 – 8).

3.1 Problem Formulation

The mathematical model considered here is identical to that examined in Refs. 37 and 38. We consider the flow of a slightly compressible fluid to a horizontal well of length L_h in a homogeneous reservoir of height h. The well is assumed to be parallel to the top and bottom boundaries. Gravity effects are considered to be negligible. The well is assumed to be located at any location, z_w, within the vertical interval and is considered to be a line source (Fig. 3.1.1). Two boundary conditions on the well surface are considered – infinite-conductivity and uniform-flux. The consequences of using these boundary conditions are discussed in §§3.3 and 3.7.

The solution for pressure distribution in the reservoir has been obtained in Refs. 37 and 38 by using the source function approach of Ref. 3. Assuming anisotropy in the three principal directions, x, y, and z (that is, $k_x \neq k_y \neq k_z$ and $k_x \neq k_z$), the

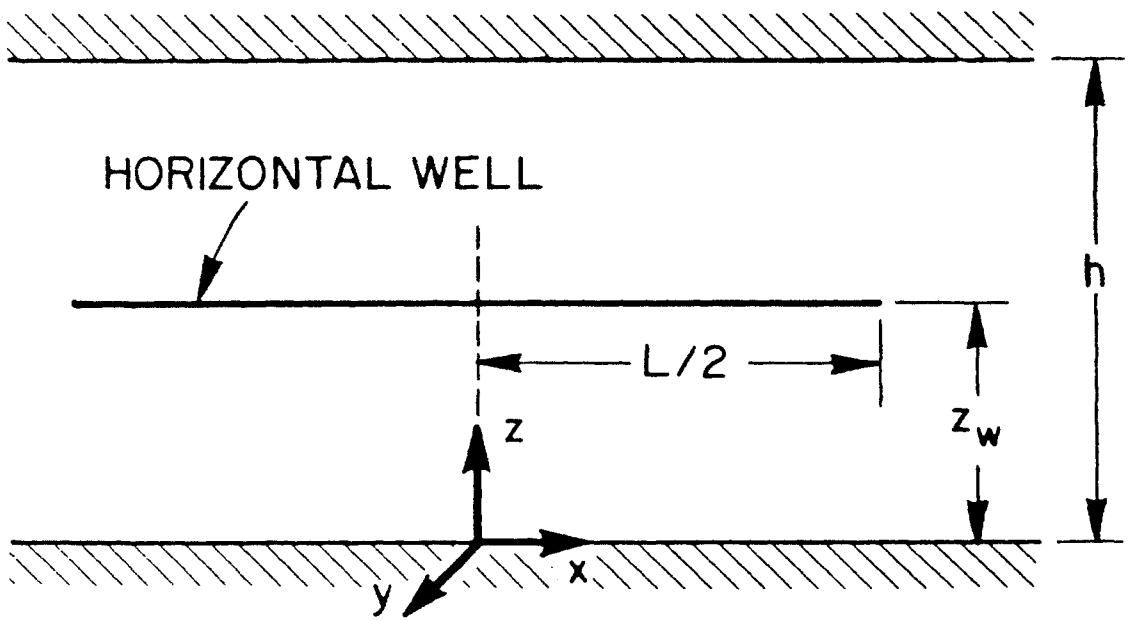

Fig. 3.1.1 - Schematic of the Horizontal Well-Reservoir System

solution given by Eq. $A-6$ of Ref. 38 can be written as

$$p_D\left(x_D, y_D, z_D, z_{wD}, L_D, t_D\right) = \frac{\sqrt{\pi}}{4}\sqrt{\frac{k}{k_y}}\int_0^{t_D}\left[\operatorname{erf}\frac{\left(\sqrt{k/k_x}+x_D\right)}{2\sqrt{\tau}}+\operatorname{erf}\frac{\left(\sqrt{k/k_x}-x_D\right)}{2\sqrt{\tau}}\right]\left[\exp\left(-\frac{y_D^2}{4\tau}\right)\right] \left[1+2\sum_{n=1}^{\infty}\exp\left(-n^2\pi^2L_D^2\tau\right)\cos n\pi z_D\cos n\pi z_{wD}\right]\frac{d\tau}{\sqrt{\tau}}. \quad (3.1.1)$$

Here p_D is the dimensionless pressure at any point in the reservoir and t_D is dimensionless time based on one-half the well length, $L_h/2$. p_D and t_D are defined by the following equations:

$$p_D\left(x_D, y_D, z_D, z_{wD}, L_D, t_D\right) = \frac{kh}{141.2qB\mu}\left[p_i - p\left(x, y, z, z_w, L_h, t\right)\right], \quad (3.1.2)$$

and

$$t_D = \frac{0.001055kt}{\phi c_t \mu L_h^2}. \quad (3.1.3)$$

Dimensionless distances x_D and y_D are based on the well half length, L_h, and z_D is based on formation thickness, h. The center of the well is assumed to be at $(0, 0, z_w)$. Thus, x_D, y_D, and z_D are defined by the following relations, respectively:

$$x_D = \frac{2x}{L_h}\sqrt{\frac{k}{k_x}}, \quad (3.1.4)$$

$$y_D = \frac{2y}{L_h}\sqrt{\frac{k}{k_y}}, \quad (3.1.5)$$

and

$$z_D = \frac{z}{h}. \quad (3.1.6)$$

The symbol L_D denotes the dimensionless well half length and is given by the following relation:

$$L_D = \frac{L_h}{2h}\sqrt{\frac{k_z}{k}}. \quad (3.1.7)$$

In Eqs. 3.1.1 – 3.1.7, k_x, k_y, and k_z denote the permeabilities in x, y, and z directions, respectively. k is an arbitrary constant and it may be chosen as the permeability of an equivalent isotropic system ($k = \sqrt[3]{k_x k_y k_z}$) or it may be chosen

as the equivalent horizontal permeability ($k = \sqrt{k_x k_y}$). Its definition is dictated by the system under study. In the rest of this chapter, we will define k as the equivalent horizontal permeability; that is, $k = \sqrt{k_x k_y}$. Note that the dimensionless well half length, L_D, incorporates the anisotropy of the formation. If the formation is isotropic, and L_D is 0.5, then the surface area available for fluid production is identical to that of a fully penetrating vertical well.

Note that the solution given by Eq. 3.1.1 is different from that given by Eq. 9 of Ref. 38. Eq. 9 of Ref. 38 can be obtained from Eq. $A-6$ of the same reference if $k_x = k_y$ and therefore their work assumes that the reservoir is isotropic in the horizontal plane.

3.2 Asymptotic Approximations

In Chapter II, we derived a solution in Laplace domain for the same problem considered here (see Table 2.2.1 and Eq. 2.6.5). There we also noted short and long time approximations for the pressure distribution (see Eqs. 2.7.21 and 2.7.29). Short and long time approximations for the pressure distribution can also be derived from the real time solution given by Eq. 3.1.1 by using the methods outlined in Refs. 3 and 10.

I. Short Time Approximation Using the short time approximations for the source functions[3] used to construct the solution given by Eq. 3.1.1, the short time approximation for the pressure distribution has been obtained in Ref. 38 and is given by

$$p_D\left(x_D, y_D, z_D, z_{wD}, L_D, t_D\right) = -\frac{\beta}{8L_D}\sqrt{\frac{k}{k_y}}\,\mathrm{Ei}\left[-\frac{\left(z_D - z_{wD}\right)^2/L_D^2 + y_D^2}{4t_D}\right], \tag{3.2.1}$$

where

$$\beta = \begin{cases} 2 \text{ for } |x_D| < \sqrt{k/k_x}, \\ 1 \text{ for } |x_D| = \sqrt{k/k_x}, \\ 0 \text{ for } |x_D| > \sqrt{k/k_x}. \end{cases} \tag{3.2.2}$$

The duration for which Eq. 3.2.1 is valid is a function of x_D, z_D, z_{wD}, and L_D. The duration of this flow period, the initial radial flow period, is given by the following equation[38]:

$$t_D \leq \min \begin{cases} \delta_D^2/20, \\ (z_D + z_{wD})^2 / (20L_D^2), \\ [(z_D + z_{wD}) - 2]^2 / (20L_D^2). \end{cases} \tag{3.2.3}$$

Here $\delta_D = \sqrt{k/k_x} - |x_D|$ if $|x_D| < \sqrt{k/k_x}$, and $\delta_D = 2\sqrt{k/k_x}$ if $|x_D| = \sqrt{k/k_x}$. These expressions are approximate and the actual times for which Eq. 3.2.1 is valid can be determined only via computations. If we assume three dimensional anisotropy ($k_x \neq k_y \neq k_z$), then the counterpart of Eq. 3.2.1 in dimensional form is given by the following expression for $|x| < L_h/2$:

$$\frac{\sqrt{k_y k_z} L_h \left[p_i - p\left(|x| < L_h/2, y, z, z_w, t\right)\right]}{141.2qB\mu} = -\frac{1}{2}\mathrm{Ei}\left[-\frac{y^2 k_z + (z - z_w)^2 k_y}{4\left(0.0002637\eta_y \eta_z t\right)}\right]. \tag{3.2.4}$$

Here $\eta_j = k_j/(\phi c_t \mu)$, where $j = z$ or y. Eq. 3.2.4 suggests that the early time response will be identical to that of a vertical well in a formation with thickness equal to L_h; that is, the well behaves as if it is located in an infinite reservoir of height L_h (infinite-acting radial flow). This flow period has been identified in Refs. 37, 38, and 50. If this flow period can be identified on a well test, then it is possible to determine $\sqrt{k_y k_z}$ from the slope of the semilog straight line. An examination of Eqs. 3.2.1 – 3.2.4 indicates that this initial radial flow period ends when the effect of the closest physical boundary (the top or the bottom reservoir boundary) is felt or when flow across the well tips ($x = \pm L_h/2$) affects the pressure response. Detailed information on the duration of this flow period is given in §3.7.

II. Long Time Approximation In §2.7, we obtained a long time approximation for the pressure distribution (Eq. 2.7.29) by using the Laplace domain solution for the problem under consideration (Eq. 2.6.5). A long time approximation for Eq. 3.1.1 has also been obtained in Ref. 38 by using the procedure outlined in Ref. 3. As discussed in Chapter II, in many cases, the procedure given in Ref. 3 does not yield closed form expressions for the long time approximations of solutions

(the result of this procedure is usually in the form of a fairly complicated integral as in the case of the long time approximation of Eq. 3.1.1 reported by Ref. 38). Here we obtain the long time approximation of Eq. 3.1.1 by using the properties of Laplace transforms. Our objective in rederiving the long time approximation already obtained in §2.7 (Eq. 2.7.29) is to briefly demonstrate a procedure that can be also used to obtain the Laplace transform of some of the solutions constructed by using the source function approach of Ref. 3.

We first note that the dimensionless pressure for the horizontal well given by Eq. 3.1.1 can be written as

$$p_D\left(x_D, y_D, z_D, z_{wD}, L_D, t_D\right) = p_{Df}\left(x_D, y_D, t_D\right)$$

$$+F'\left(x_D, y_D, z_D, z_{wD}, L_D, t_D\right), \tag{3.2.5}$$

where p_{Df} is the dimensionless pressure drop due to production from a fully penetrating vertically fractured well and is given by[10]

$$p_{Df} = \frac{\sqrt{\pi}}{4}\sqrt{\frac{k}{k_y}}\int_0^{t_D}\left[\operatorname{erf}\frac{\left(\sqrt{k/k_x}+x_D\right)}{2\sqrt{\tau}} + \operatorname{erf}\frac{\left(\sqrt{k/k_x}-x_D\right)}{2\sqrt{\tau}}\right]\left[\exp\left(-\frac{y_D^2}{4\tau}\right)\right]\frac{d\tau}{\sqrt{\tau}}. \tag{3.2.6}$$

The function, F', is defined by

$$\begin{aligned} &F'(x_D, y_D, z_D, z_{wD}, L_D, t_D) = \\ &\frac{\sqrt{\pi}}{4}\sqrt{\frac{k}{k_y}}\int_0^{t_D}\left[2\sum_{n=1}^{\infty}\exp\left(-n^2\pi^2 L_D^2\tau\right)\cos n\pi z_D \cos n\pi z_{wD}\right] \\ &\left[\operatorname{erf}\frac{\left(\sqrt{k/k_x}+x_D\right)}{2\sqrt{\tau}} + \operatorname{erf}\frac{\left(\sqrt{k/k_x}-x_D\right)}{2\sqrt{\tau}}\right]\left[\exp\left(-\frac{y_D^2}{4\tau}\right)\right]\frac{d\tau}{\sqrt{\tau}}. \end{aligned} \tag{3.2.7}$$

The long time approximation for the vertically fractured well solution, p_{Df}, (Eq. 3.2.6) has been obtained in Ref. 10 (Eq. 14 of Ref. 10) and is given by the following expression:

$$p_{Df} = \frac{1}{2}\left(\ln t_D + 2.80907\right) + \sigma\left(x_D, y_D\right), \tag{3.2.8}$$

where

$$\sigma\left(x_D, y_D\right) = 0.25\Bigg\{\left(x_D - \sqrt{k/k_x}\right) \ln\left[\left(x_D - \sqrt{k/k_x}\right)^2 + y_D^2\right]$$

$$- \left(x_D + \sqrt{k/k_x}\right) \ln\left[\left(x_D + \sqrt{k/k_x}\right)^2 + y_D^2\right] - 2y_D \operatorname{arctg} \frac{2y_D}{x_D^2 + y_D^2 - \sqrt{k/k_x}}\Bigg\}. \tag{3.2.9}$$

Eq. 3.2.8 is valid when

$$t_D \geq \max \begin{cases} 25\left[\left(x_D - \sqrt{k/k_x}\right)^2 + y_D^2\right], \\ 25\left[\left(x_D + \sqrt{k/k_x}\right)^2 + y_D^2\right]. \end{cases} \tag{3.2.10}$$

Using the relation

$$\left[\operatorname{erf}\frac{\left(\sqrt{k/k_x} + x_D\right)}{2\sqrt{\tau}} + \operatorname{erf}\frac{\left(\sqrt{k/k_x} - x_D\right)}{2\sqrt{\tau}}\right] =$$

$$\frac{\sqrt{k/k_x}}{\sqrt{\pi\tau}} \int_{-1}^{+1} \exp\left[-\frac{\left(x_D - \alpha\sqrt{k/k_x}\right)^2}{4\tau}\right] d\alpha, \tag{3.2.11}$$

we can write the function F' (Eq. 3.2.7) as

$$F'(x_D, y_D, z_D, z_{wD}, L_D, t_D) = \frac{1}{2} \sum_{n=1}^{\infty} \cos n\pi z_D \cos n\pi z_{wD}$$

$$\int_{-1}^{+1} \int_0^{t_D} \exp\left(-n^2\pi^2 L_D^2 \tau\right) \exp\left[-\frac{\left(x_D - \alpha\sqrt{k/k_x}\right)^2 + y_D^2}{4\tau}\right] \frac{d\tau}{\tau} d\alpha. \tag{3.2.12}$$

Taking the Laplace transform of Eq. 3.2.12 with respect to t_D, we obtain

$$\overline{F'}\left(s\right) = \frac{1}{s} \sum_{n=1}^{\infty} \cos n\pi z_D \cos n\pi z_{wD} \int_{-1}^{+1} K_o\left(\tilde{r}_D \sqrt{s + n^2\pi^2 L_D^2}\right) d\alpha, \tag{3.2.13}$$

where $\overline{F'}(s)$ is the Laplace Transform of F' and $\tilde{r}_D$ is given by

$$\tilde{r}_D^2 = \left(x_D - \alpha\sqrt{k/k_x}\right)^2 + y_D^2. \tag{3.2.14}$$

If

$$s \leq 0.01\pi^2 L_D^2, \tag{3.2.15}$$

or accordingly when

$$t_D \geq \frac{100}{\pi^2 L_D^2}, \tag{3.2.16}$$

we can assume that $s + n^2\pi^2 L_D^2 \approx n^2\pi^2 L_D^2$ and thus the long time approximation of $\overline{F'}$ is given by

$$\overline{F'}(s \to 0) = \frac{1}{s}\sum_{n=1}^{\infty} \cos n\pi z_D \cos n\pi z_{wD} \int_{-1}^{+1} K_o\left(\tilde{r}_D n\pi L_D\right) d\alpha. \tag{3.2.17}$$

Letting F denote the long time approximation of the function F' and evaluating the inverse Laplace transform of Eq. 3.2.17, we obtain the following expression:

$$F(x_D, y_D, z_D, z_{wD}, L_D) = \sum_{n=1}^{\infty} \cos n\pi z_D \cos n\pi z_{wD} \int_{-1}^{+1} K_o\left(\tilde{r}_D n\pi L_D\right) d\alpha. \tag{3.2.18}$$

Using Eqs. 3.2.8 and 3.2.18 in Eq. 3.2.5, the long time approximation for the horizontal well dimensionless pressure can be written as

$$p_D\left(x_D, y_D, z_D, z_{wD}, L_D, t_D\right) = \frac{1}{2}\left(\ln t_D + 2.80907\right)$$

$$+\sigma\left(x_D, y_D\right) + F\left(x_D, y_D, z_D, z_{wD}, L_D\right), \tag{3.2.19}$$

when

$$t_D \geq \max\begin{cases} 100/\left(\pi L_D\right)^2, \\ 25\left[\left(x_D + \sqrt{k/k_x}\right)^2 + y_D^2\right], \\ 25\left[\left(x_D - \sqrt{k/k_x}\right)^2 + y_D^2\right]. \end{cases} \tag{3.2.20}$$

It must be emphasized that the restrictions given by Eq. 3.2.20 are approximate; different arrangements of Eq. 3.1.1 and the use of different approximations during the course of derivations will lead to the expression given by Eq. 3.2.19, but Eq. 3.2.20 would be different. Our calculations indicate that the time restrictions given by Eq. 3.2.20 provide the highest order of accuracy, especially in computing the pseudoskin factor (see §3.4).

Eq. 3.2.19 indicates that at long times a semilog plot of p_D vs. t_D will be a straight line with slope equal to 1.151 – the pseudoradial flow period. If data during this flow period are available, then formation permeability, k or $\sqrt{k_x k_y}$ in case we

consider anisotropy in the x-y plane, can be determined. Formation permeability, k, can also be obtained by type curve matching. If k_z were known, and the initial radial flow period can be analyzed to obtain $\sqrt{k_y k_z}$, then the possibility to determine k_x, k_y and k_z exists. Eq. 3.2.19 also permits us to obtain an analytical expression for the pseudoskin factor (see §3.4).

3.3 Computation of Well Responses

Without loss of generality, in the following, we assume that the formation is isotropic. As mentioned earlier, in this study we model the horizontal well as a line source. First we note the similarity between the short time approximation for the horizontal well solution given by Eq. 3.2.1 and the line source approximation for a vertical well in an infinite reservoir. Then by analogy to vertical well solution, we can decide that the line source approximation of a horizontal well of finite radius is acceptable when

$$t_D \geq 25\left[\left(z_D - z_{wD}\right)^2 / L_D^2 + y_D^2\right], \tag{3.3.1}$$

which is satisfied for most practical applications of well testing. We also note from Eq. 3.3.1 that if we define a circle with the origin at $y_D = z_D - z_{wD} = 0$ and the dimensionless radius

$$r_D = \sqrt{\left(z_D - z_{wD}\right)^2 / L_D^2 + y_D^2} = 2r_w / L_h, \tag{3.3.2}$$

where r_w is the radius of the horizontal well, then the pressure drop calculated at any point on the circumference of this circle will be the same at early times. This suggests that we define the dimensionless wellbore radius, r_{wD}, from Eq. 3.3.2 and calculate the well responses at $r_D = r_{wD}$. It is not obvious from the long time approximation of horizontal well solution (Eq. 3.2.19), however, that this definition of the wellbore radius would be correct for all times. But one can readily decide that when the line source assumption for the finite radius horizontal well becomes acceptable, then the error introduced in the definition of wellbore pressure measurement point would not have a major impact on the accuracy of the results.

Our computations for dimensionless pressure defined by Eq. 3.1.1 proved that the dimensionless pressure never changes more than 0.005 along the circumference of the wellbore defined by Eq. 3.3.2.

In Refs. 37 and 38, wellbore pressures are computed at the point $z_D = z_{wD}$ and $y_D = r_{wD}$. Eq. 3.3.2 and the discussion following it, however, indicates that the point $y_D = 0$ and $(z_D - z_{wD})/L_D = r_{wD}$ could also be chosen to compute wellbore responses. Numerical computations prove that the wellbore pressures computed at $z_D = z_{wD}$ and $y_D = r_{wD}$ and $(z_D - z_{wD})/L_D = r_{wD}$ and $y_D = 0$ are essentially the same. In this work, we use both definitions to compute wellbore responses. Mainly for the purpose of comparison with the published data[37,38], we choose the point $z_D = z_{wD}$ and $y_D = r_{wD}$ to compute the well responses when we present our results. As will be shown in §3.4, however, use of the point $z_D = z_{wD} + r_{wD}L_D$ and $y_D = 0$ for the evaluation of the analytical expressions for the long time approximation and the pseudoskin factor is more advantageous. In this case, for convenience we define the dimensionless wellbore radius by $r_{wDz} = r_{wD}L_D$. Note that, in terms of real variables, r_{wD} and r_{wDz} are defined respectively by

$$r_{wD} = \frac{2r_w}{L_h}\sqrt{\frac{k}{k_y}}, \tag{3.3.3}$$

and

$$r_{wDz} = r_{wD}L_D = \frac{r_w}{h}\sqrt{\frac{k_z}{k_y}}. \tag{3.3.4}$$

Therefore, there exists a simple conversion between the results computed at r_{wD} and r_{wDz}.

The fact that the wellbore pressure is computed at a finite radius, r_w, has ramifications which deserve consideration. The vertical fracture solutions given in the literature ignore the existence of the wellbore. It is possible to compute the response of a vertically fractured well at $x_D = 0$, $y_D = 0$ and specify the pressure at this point to be the wellbore pressure. (Mathematically this implies that it is possible to compute pressures on the source and that these solutions are bounded for all values of time.) For the horizontal well case, however, since it is assumed

to be a line source, it is not possible to compute pressure drops on the source. Pressure drops have to be computed at some finite radius, r. Thus consideration must be given to two factors in the analysis of the results. First, the horizontal well solutions are a function of the variable, r_w. (This is also true for fractured wells and is usually ignored.) Second, since the vertical fracture solutions and the horizontal well solutions are not computed at the same point, it can be shown that in some cases the productivity of a horizontal well will exceed that of a vertically fractured well, all other conditions being identical. This unrealistic result is obtained mainly because of the locations at which the pressure drops are computed and should not be construed to imply that horizontal well productivity can be greater than that of a vertically fractured well. Other considerations (reservoir heterogeneity, fluid contacts, etc.) may result in horizontal well productivity being higher than that of a vertically fractured well.[51] It should be noted that the latter consideration cannot be avoided even if we assume that the horizontal well has a finite radius.

The next consideration in the computation of the well responses is the representation of the horizontal well by the uniform-flux or the infinite-conductivity idealization. It should be realized that the method of sources and sinks[3] used to construct the solution given by Eq. 3.1.1 assumes that the flux distribution along the well surface is uniform. To compute well responses for the uniform-flux case, we assume that $x_D = 0$. This solution should be applicable to drainholes that extend equal distances on either side of the vertical well. The uniform-flux solution does not appear to be appropriate for analyzing horizontal well responses. If we assume that the uniform-flux solution is valid for the horizontal well case, then we should assume that the pressure at $|x| = L_h/2$ would represent the wellbore pressure. Note that the uniform-flux solution, Eq. 3.1.1, predicts that pressure will vary along the length of the well and the pressure is the lowest at the well center ($x_D = 0$). Although the method of sources and sinks[3] used to develop Eq. 3.1.1 provides no information regarding the ultimate extraction of fluid once fluid enters the vertical fracture or horizontal well, the assumption that pressure is measured at the tip should imply that fluid from the reservoir is extracted at this point. This assump-

tion will result in the unrealistic implication that fluid can move from a region of lower pressure ($x = 0$) to that of higher pressure ($|x| = L_h/2$).

It was shown in Refs. 52, 53 and 3 that the response of infinite-conductivity wells can be closely approximated by using the solutions for uniform-flux wells. In §3.5, we will present a discussion of the procedure to compute the infinite-conductivity well responses by using the uniform-flux well solution. To set the stage for this discussion, we first derive an analytical expression for the horizontal well pseudoskin factor.

3.4 Pseudoskin Factor and Effective Wellbore Radius

In this section, we obtain analytical expressions for the horizontal well pseudoskin factor and effective wellbore radius. These expressions are extremely useful to determine the long term productivity of horizontal wells and to compare the performance of horizontal wells to that of vertically fractured wells and unstimulated vertical wells.

I. Pseudoskin Factor As stated before, for a horizontal well to be a commercial method of completion, its productivity must be comparable to the productivity of a vertically fractured well. Therefore, the pseudoskin factors considered in this work are based on the appropriate vertically fractured well solution; that is, we define the pseudoskin factor as the additional pressure drop caused by the fact that a horizontal well is a partially penetrating fracture at the limit. Here we will present a simplified formula to evaluate the pseudoskin factor at the well location.

Consider the long time approximation of the horizontal well solution given by Eq. 3.2.19. In light of the discussion on the computation of wellbore responses presented above (§3.3) , if we choose the point $y_D = 0$, $z_D = z_{wD} + r_{wDz}$ to compute the wellbore pressures, then the dimensionless wellbore pressure, p_{wD}, is defined by

$$p_{wD} = 0.5\left(\ln t_D + 2.80907\right) + \sigma\left(x_D, 0\right) + F\left(x_D, 0, z_{wD}, r_{wDz}, L_D\right). \qquad (3.4.1)$$

If we note that the first two terms on the right hand side of Eq. 3.4.1 define the pressure drop on the surface of a vertically fractured well[10], then the function F defines the pseudoskin factor for a horizontal well:

$$F(x_D,0,z_{wD},r_{wDz},L_D)=\sum_{n=1}^{\infty}\cos n\pi(z_{wD}+r_{wDz})\cos n\pi z_{wD}$$

$$\int_{-1}^{+1}K_0\left[n\pi L_D\sqrt{\left(x_D-\alpha\sqrt{k/k_x}\right)^2}\right]d\alpha. \tag{3.4.2}$$

As noted in Chapter II, evaluation of the integral in the right hand side of Eq. 3.4.2 can pose dificulties. These difficulties, however, can be avoided if we follow the lines suggested in §§2.5 and 2.6. Using the relation given by Eq. 2.5.1, we can recast Eq. 3.4.2 in the following form:

$$F(|x_D|\le\sqrt{k/k_x},0,z_{wD},r_{wDz},L_D)=$$
$$\frac{1}{\pi L_D\sqrt{k/k_x}}\sum_{n=1}^{\infty}\frac{\cos n\pi(z_{wD}+r_{wDz})\cos n\pi z_{wD}}{n} \tag{3.4.3}$$
$$\left[\int_0^{n\pi L_D\left(\sqrt{k/k_x}+x_D\right)}K_0(u)\,du+\int_0^{n\pi L_D\left(\sqrt{k/k_x}-x_D\right)}K_0(u)\,du\right].$$

Note that the case for $|x_D|>\sqrt{k/k_x}$ can also be handled in a similar fashion by using Eq. 2.5.2. In §2.5 I, we also showed that

$$\int_0^x K_0(u)\,du=\frac{\pi}{2}-Ki_1(x), \tag{3.4.4}$$

where

$$Ki_1(x)=\int_x^{\infty}K_0(u)\,du. \tag{3.4.5}$$

Then, Eq. 3.4.3 can be also written as

$$F\left(|x_D|\le\sqrt{k/k_x},0,z_{wD},r_{wDz},L_D\right)=$$
$$\frac{1}{L_D\sqrt{k/k_x}}\sum_{n=1}^{\infty}\frac{\cos n\pi\left(z_{wD}+r_{wDz}\right)\cos n\pi z_{wD}}{n}-\varphi(x_D,0,z_{wD},r_{wDz},L_D), \tag{3.4.6}$$

where

$$\varphi(x_D,0,z_{wD},r_{wDz},L_D)=\frac{1}{\pi L_D\sqrt{k/k_x}}\sum_{n=1}^{\infty}\frac{\cos n\pi\left(z_{wD}+r_{wDz}\right)\cos n\pi z_{wD}}{n}$$

$$\left\{Ki_1\left[n\pi L_D\left(\sqrt{k/k_x}+x_D\right)\right]+Ki_1\left[n\pi L_D\left(\sqrt{k/k_x}-x_D\right)\right]\right\}. \tag{3.4.7}$$

If we write

$$\cos n\pi z_{wD}\cos n\pi(z_{wD}+r_{wDz})=0.5\left[\cos n\pi\left(2z_{wD}+r_{wDz}\right)+\cos n\pi r_{wDz}\right] \tag{3.4.8}$$

and use the relation[36]

$$\sum_{k=1}^{\infty}\frac{\cos kx}{k}=\frac{1}{2}\ln\frac{1}{2\left(1-\cos x\right)};\quad [0<x<2\pi], \tag{3.4.9}$$

then we can write Eq. 3.4.7 as

$$F\left(|x_D|\le\sqrt{k/k_x},0,z_{wD},r_{wDz},L_D\right)=$$
$$-\frac{1}{2L_D\sqrt{k/k_x}}\ln\left[4\sin\frac{\pi}{2}\left(2z_{wD}+r_{wDz}\right)\sin\frac{\pi}{2}r_{wDz}\right]-\varphi\left(x_D,0,z_{wD},r_{wDz},L_D\right). \tag{3.4.10}$$

To our knowledge, the expression for the horizontal well pseudoskin factor given by Eq. 3.4.10 has not been reported in the literature. As will be discussed later in detail, our computations indicate that for $L_D\sqrt{k/k_x}\ge 5$, the pseudoskin factor, F, becomes negligible and the differences between the late time responses of vertically fractured wells and horizontal wells vanish for practical purposes. In physical terms, the logarithmic term in the right hand side of Eq. 3.4.10 represents the contribution of the early time radial flow period in the vertical plane (see Eq. 3.2.1) to the pseudoskin factor. Similarly, the terms denoted by φ (Eq. 3.4.7) represent the contribution of the three dimensional flow period between the early time radial flow and late time pseudoradial flow periods.

In §2.5 I, we noted that $Ki_1(x)$ can be neglected compared to $\pi/2$ within 1 % when $x\ge 3.6$ (see the discussion following Eq. 2.5.7). Then the function φ becomes negligible compared to the first term on the right hand side of Eq. 3.4.6, within 1 %, when

$$L_D\ge\frac{3.6}{\pi\left(\sqrt{k/k_x}-|x_D|\right)}. \tag{3.4.11}$$

When the condition given by Eq. 3.4.11 holds, we can approximate the horizontal well pseudoskin factor by

$$F\left[|x_D|\le\sqrt{k/k_x},0,z_{wD},r_{wDz},L_D\ge 1.15/\left(\sqrt{k/k_x}-|x_D|\right)\right]\approx$$

$$-\frac{1}{2L_D\sqrt{k/k_x}}\ln\left[4\sin\frac{\pi}{2}\left(2z_{wD}+r_{wDz}\right)\sin\frac{\pi}{2}r_{wDz}\right]. \qquad (3.4.12)$$

There is field evidence[49] that most horizontal well lengths would satisfy the condition stated by Eq. 3.4.11 and therefore the use of the approximate relation given by Eq. 3.4.12 would be satisfactory for the computation of the pseudoskin factor.

II. Effective Wellbore Radius To obtain a comparison between vertical well and horizontal well productivities, it is often useful to define an effective wellbore radius which is the wellbore radius of an unstimulated vertical well to yield the same productivity as that of a horizontal well. The concept of effective wellbore radius was used by Prats[39] and Prats *et al.*[40] to show that the behavior of infinite-conductivity vertical fractures can be represented by that of an unstimulated vertical well with wellbore radius equal to one-quarter of the length of the fracture. In §2.7 II, we extended this idea to horizontal wells in isotropic reservoirs (see Eq. 2.7.41). If we consider three dimensional anisotropy ($k_x \neq k_y \neq k_z$), then combining Eqs. 3.4.1 and 3.4.10, we can write the following expression:

$$\begin{aligned} p_{wD} =& 0.5\left(\ln\tilde{t}_D + 0.80907\right) \\ &- 0.5\ln\frac{\left(L_h/2\right)^2\left[4\sin\pi\left(z_{wD}+\frac{r_{wDz}}{2}\right)\sin\pi\left(\frac{r_{wDz}}{2}\right)\right]^{\frac{1}{L_D}\sqrt{\frac{k_x}{k}}}}{r_w'^{\,2}\exp\left[2\left(1+\sigma-\varphi\right)\right]} \end{aligned} \qquad (3.4.13)$$

where $\tilde{t}_D$ is the dimensionless time based on the equivalent wellbore radius, r_w'; that is,

$$\tilde{t}_D = t_D\left(\frac{L_h}{2r_w'}\right)^2. \qquad (3.4.14)$$

The late time response of an unstimulated vertical well is given by

$$p_{wD} = 0.5\left(\ln t_D + 0.80907\right). \qquad (3.4.15)$$

Comparing Eq. 3.4.13 with Eq. 3.4.15, we can decide that a horizontal well is equivalent to a vertical well with wellbore radius given by

$$r_w' = \frac{L_h/2}{\exp\left(1+\sigma-\varphi\right)}\left[4\sin\frac{\pi}{h}\left(z_w+\frac{r_w}{2}\sqrt{\frac{k_z}{k_y}}\right)\sin\frac{\pi}{2h}r_w\sqrt{\frac{k_z}{k_y}}\right]^{\frac{h}{L_h}\sqrt{\frac{k_x}{k_z}}}. \qquad (3.4.16)$$

Note from Eqs. 3.4.11 and 3.4.12 that for $L_D \geq 1.15/(\sqrt{k/k_x} - |x_D|)$, we have $\varphi \approx 0$ and Eq. 3.4.16 can be written as

$$r'_w = \frac{L_h/2}{\exp(1+\sigma)} \left[4 \sin \frac{\pi}{h} \left(z_w + \frac{r_w}{2} \sqrt{\frac{k_z}{k_y}} \right) \sin \frac{\pi}{2h} r_w \sqrt{\frac{k_z}{k_y}} \right]^{\frac{h}{L_h}\sqrt{\frac{k_x}{k_z}}} . \quad (3.4.17)$$

Note also from Eq. 3.4.10 that as $L_D \to \infty$, $F \to 0$; horizontal well pressure response approaches the vertically fractured well response, and Eq. 3.4.16 yields

$$r'_w = \frac{L_h/2}{\exp(1+\sigma)}, \quad (3.4.18)$$

where $1 + \sigma = 1$ and $\ln 2$ for uniform-flux and infinite-conductivity conditions, respectively. Eq. 3.4.18 defines the effective wellbore radius for a vertically fractured well (see Refs. 39, 40, 42, and 10). A similar expression to that given by Eq. 3.4.17 has been obtained in Refs. 54 and 55 by using an approximate solution for long horizontal wells.

3.5 Computation of Infinite-Conductivity Well Responses

In obtaining the solution given by Eq. 3.1.1, we assumed that the flux distribution along the surface of the horizontal well (or drainhole) was uniform (uniform-flux well idealization). As discussed in §3.3, however, the conductivity of horizontal wells would be close to infinity and hence the pressure distribution, instead of the flux distribution, would be uniform along the well surface (infinite-conductivity well). It is shown in Refs. 52, 53, and 3 that the solution for the infinite-conductivity idealization can be obtained from the uniform-flux solution by dividing the well length into small segments each with uniform flux per unit area and then adjusting the strength of the source in each segment so that the resulting pressure distribution would be approximately uniform along the well. In most well-reservoir systems of interest, the pressure drop can be shown to be independent of the flux condition on the well surface initially (for example, during the linear flow period in fractured wells and radial flow period that is concentric with the well axis in partially penetrating wells and horizontal wells). Subsequently, for infinite-conductivity wells,

the flux distribution becomes a function of time and ultimately it stabilizes along the well length. Gringarten *et al.*[10] noted that once the stabilized flux distribution is attained, then it is possible to find a point along the axis of a uniform-flux well at which the pressure drop created by a uniform-flux well and an infinite-conductivity well would be the same. This point is usually referred to as the equivalent pressure point and is used to obtain wellbore pressures of infinite-conductivity wells by using the solutions developed under the uniform-flux well assumption. A similar procedure can be used for all times; however, in this case the equivalent pressure point would be a function of time. Ref. 10 suggests that the use of the stabilized flux distribution (and therefore the equivalent pressure point obtained during stabilized flow period) for all times would not introduce significant error.

In the following, we summarize the procedure to obtain the stabilized flux distribution and to determine the equivalent pressure point for horizontal wells. The development presented below is similar to that given in Ref. 10 and additional details can be found in the quoted reference.

For discussion, if we assume that the reservoir is isotropic in the horizontal plane ($k_x = k_y$), then we can write the solution given by Eq. 3.1.1 as

$$p_D = p_{Df} + F', \tag{3.5.1}$$

where p_{Df} is the vertically fractured well solution given by

$$p_{Df} = \frac{\sqrt{\pi}}{4} \int_0^{t_D} \left[\text{erf} \frac{(1+x_D)}{2\sqrt{\tau}} + \text{erf} \frac{(1-x_D)}{2\sqrt{\tau}} \right] \left[\exp\left(-\frac{y_D^2}{4\tau} \right) \right] \frac{d\tau}{\sqrt{\tau}}, \tag{3.5.2}$$

and

$$F' = \frac{\sqrt{\pi}}{4} \int_0^{t_D} \left[2 \sum_{n=1}^{\infty} \exp\left(-n^2 \pi^2 L_D^2 \tau \right) \cos n\pi z_D \cos n\pi z_{wD} \right]$$
$$\left[\text{erf} \frac{(1+x_D)}{2\sqrt{\tau}} + \text{erf} \frac{(1-x_D)}{2\sqrt{\tau}} \right] \left[\exp\left(-\frac{y_D^2}{4\tau} \right) \right] \frac{d\tau}{\sqrt{\tau}}. \tag{3.5.3}$$

Using the relation given by Eq. 3.2.11, the vertically fractured well solution, p_{Df}, can also be written as

$$p_{Df} = -0.25 \int_{-1}^{+1} \text{Ei} \left[-\frac{(x_D - \alpha)^2 + y_D^2}{4t_D} \right] d\alpha. \tag{3.5.4}$$

If we replace the $\mathrm{Ei}(-x)$ function in the right hand side of Eq. 3.5.4 by its logarithmic approximation suitable for small values of its argument (large times), then we can write the long time approximation of the fracture solution as

$$p_{Df} = 0.25 \int_{-1}^{+1} \left[\ln \frac{t_D}{(x_D - \alpha)^2 + y_D^2} + 0.80907 \right] d\alpha. \tag{3.5.5}$$

In §3.2, we showed that the long time approximation of the function F' is given by

$$F = \sum_{n=1}^{\infty} \cos n\pi z_D \cos n\pi z_{wD} \int_{-1}^{+1} K_0 \left[n\pi L_D \sqrt{(x_D - \alpha)^2 + y_D^2} \right] d\alpha. \tag{3.5.6}$$

Using the relations given by Eqs. 3.5.5 and 3.5.6 in Eq. 3.5.1, the long time approximation of the horizontal well solution can be written as

$$p_D = \int_{-1}^{+1} \left\{ \left[\ln \frac{t_D}{(x_D - \alpha)^2 + y_D^2} + 0.80907 \right] \right.$$

$$\left. + \sum_{n=1}^{\infty} \cos n\pi z_D \cos n\pi z_{wD} K_0 \left[n\pi L_D \sqrt{(x_D - \alpha)^2 + y_D^2} \right] \right\} d\alpha. \tag{3.5.7}$$

If we divide the half length of the well, $L_h/2$, into M equal segments, then the pressure drop due to production from the m^{th} uniform-flux element extending from $(m-1)\,L_h/\,(2M)$ to $mL_h/\,(2M)$ is given by

$$p_D = q_m \int_{(m-1)/M}^{m/M} \left\{ 0.25 \left[\ln \frac{t_D}{(x_D - \alpha)^2 + y_D^2} + 0.80907 \right] \right.$$

$$\left. + \sum_{n=1}^{\infty} \cos n\pi z_D \cos n\pi z_{wD} K_0 \left[n\pi L_D \sqrt{(x_D - \alpha)^2 + y_D^2} \right] \right\} d\alpha, \tag{3.5.8}$$

where q_m is defined by

$$q_m = \frac{\tilde{q}_m L_h}{q}. \tag{3.5.9}$$

In Eq. 3.5.9, $\tilde{q}_m$ is the strength of the differential flux elements (or point sources) located along the flux element (and assumed to be constant for the flux element) and q is the production rate from the total length of the horizontal well.

Due to symmetry with respect to the center of the well (assumed to be at $x_D = 0$), we consider another flux element extending from $-(m-1)L_h/(2M)$ to $-mL_h/(2M)$ that yields a pressure drop given by

$$p_D = -q_m \int_{-(m-1)/M}^{-m/M} \left\{ 0.25 \left[\ln \frac{t_D}{(x_D-\alpha)^2 + y_D^2} + 0.80907 \right] \right.$$

$$\left. + \sum_{n=1}^{\infty} \cos n\pi z_D \cos n\pi z_{wD} K_0 \left[n\pi L_D \sqrt{(x_D-\alpha)^2 + y_D^2} \right] \right\} d\alpha. \qquad (3.5.10)$$

The pressure drop due to mutual production from the m^{th} flux elements in the positive and the negative x direction is then obtained by superposing Eqs. 3.5.8 and 3.5.10 and is given by the following relation.

$$p_D = q_m \left[\int_{(m-1)/M}^{m/M} - \int_{-(m-1)/M}^{-m/M} \right] \left\{ 0.25 \left[\ln \frac{t_D}{(x_D-\alpha)^2 + y_D^2} + 0.80907 \right] \right.$$

$$\left. + \sum_{n=1}^{\infty} \cos n\pi z_D \cos n\pi z_{wD} K_0 \left[n\pi L_D \sqrt{(x_D-\alpha)^2 + y_D^2} \right] \right\} d\alpha. \qquad (3.5.11)$$

If we note that

$$\left[\int_{(m-1)/M}^{m/M} - \int_{-(m-1)/M}^{-m/M} \right] f(\alpha) d\alpha = \left[\int_{-m/M}^{m/M} - \int_{-(m-1)/M}^{(m-1)/M} \right] f(\alpha) d\alpha \qquad (3.5.12)$$

and define

$$p_{Dm} = \int_{-m/M}^{m/M} \left\{ 0.25 \left[\ln \frac{t_D}{(x_D-\alpha)^2 + y_D^2} + 0.80907 \right] \right.$$

$$\left. + \sum_{n=1}^{\infty} \cos n\pi z_D \cos n\pi z_{wD} K_0 \left[n\pi L_D \sqrt{(x_D-\alpha)^2 + y_D^2} \right] \right\} d\alpha, \qquad (3.5.13)$$

then Eq. 3.5.11 can be written as

$$p_D = q_m \left(p_{Dm} - p_{Dm-1} \right). \qquad (3.5.14)$$

Finally, considering all the flux elements along the well, the resulting pressure drop can be formulated as

$$p_D = \sum_{m=1}^{M} q_m \left(p_{Dm} - p_{Dm-1} \right), \qquad (3.5.15)$$

and the resulting production rate from the total length of the well, q, is given by $q = \sum_{m=1}^{M} (\tilde{q}_m L_h/M)$ or

$$\sum_{m=1}^{M} q_m = M. \tag{3.5.16}$$

If we now choose q_m in Eq. 3.5.15 such that p_D would be approximately constant along the surface of the well, then Eq. 3.5.15 gives the pressure distribution due to production from an infinite-conductivity horizontal well. In order to obtain q_m to be used in Eq. 3.5.15, we impose the condition along the well surface ($y_D = 0$, $z_D = z_{wD} + r_{wDz}$; see §3.3) that the pressure drop measured in the middle of the m^{th} flux element be equal to that in the middle of the $(m+1)^{st}$ flux element; that is

$$p_{wD}\left(x_D = \frac{2j-1}{2M}\right) = p_{wD}\left(x_D = \frac{2j+1}{2M}\right) \quad [j = 1, M-1]. \tag{3.5.17}$$

Note from Eq. 3.5.13 that

$$\begin{aligned} p_{Dm} - p_{Dm-1} =& \frac{2}{M}(\ln t_D + 2.80907) + \sigma(x_D, y_D) \\ &+ F(x_D, y_D, z_D, z_{wD}, L_D) \end{aligned} \tag{3.5.18}$$

where

$$\begin{aligned} \sigma(x_D, y_D) =& 0.25\Bigg\{\left(x_D - \frac{m}{M}\right)\ln\left[\left(x_D - \frac{m}{M}\right)^2 + y_D^2\right] \\ &- \left(x_D + \frac{m}{M}\right)\ln\left[\left(x_D + \frac{m}{M}\right)^2 + y_D^2\right] \\ &+ \left(x_D + \frac{m-1}{M}\right)\ln\left[\left(x_D + \frac{m-1}{M}\right)^2 + y_D^2\right] \\ &- \left(x_D - \frac{m-1}{M}\right)\ln\left[\left(x_D - \frac{m-1}{M}\right)^2 + y_D^2\right] \\ &- 2y_D \arctan\left[\frac{2y_D}{M}\frac{x_D^2 + y_D^2 + \frac{m(m-1)}{M^2}}{\left(x_D^2 + y_D^2 - \frac{m^2}{M^2}\right)\left(x_D^2 + y_D^2 - \frac{(m-1)^2}{M^2}\right) + \frac{4m(m-1)}{M^2}y_D^2}\right]\Bigg\} \end{aligned} \tag{3.5.19}$$

and

$$F_m(x_D, y_D, z_D, z_{wD}, L_D) = \sum_{n=1}^{\infty} \cos n\pi z_D \cos n\pi z_{wD}$$

$$\left[\int_{-m/M}^{m/M} - \int_{-(m-1)/M}^{(m-1)/M}\right] K_0\left[n\pi L_D\sqrt{(x_D-\alpha)^2+y_D^2}\right] d\alpha. \tag{3.5.20}$$

Then the condition given by Eq. 3.5.17 can also be expressed in the following form:

$$\begin{aligned}&\sum_{m=1}^{M} q_m\left[\sigma(x_D,0)+F_m(x_D,0,z_{wD},r_{wDz},L_D)\right]_{x_D=\frac{2j-1}{2M}} = \\ &\sum_{m=1}^{M} q_m\left[\sigma(x_D,0)+F_m(x_D,0,z_{wD},r_{wDz},L_D)\right]_{x_D=\frac{2j+1}{2M}} \quad [j=1,M-1].\end{aligned} \tag{3.5.21}$$

Using the additional condition that

$$\sum_{m=1}^{M} q_m = M, \tag{3.5.22}$$

the system of equations given by Eqs. 3.5.21 and 3.5.22 can be solved to obtain the stabilized flux distribution, q_m. (To avoid difficulties in computing the function F_m given by Eq. 3.5.20 at $y_D = 0$, relations given by Eqs. 2.5.1 - 2.5.3 should be useful.)

Once the stabilized flux distribution, q_m, is obtained, Eq. 3.5.15 can be solved to obtain the wellbore pressure of an infinite-conductivity horizontal well. To find the equivalent pressure point, we compute the pressure distribution along the surface of a uniform-flux horizontal well from Eq. 3.2.19. The equivalent pressure point is then found to be the point at which the uniform-flux and infinite-conductivity solutions yield the same pressure drop.

In Refs. 5, 38, and 50, the infinite-conductivity responses are computed from the uniform-flux solution at the equivalent pressure point $x_D = 0.732$. Justification for this value of the equivalent pressure point is based on the work of Gringarten *et al.*[10] who showed that the uniform-flux solution can be used to compute the response of a well intercepted by an infinite-conductivity vertical fracture if $x_D = 0.732$. To investigate the basis of the assumption made in Refs. 5, 38, and 50, let us consider the long time approximation of the horizontal well solution given by

$$p_{wD} = p_{Df} + F(x_D,0,z_{wD},r_{wDz},L_D), \tag{3.5.23}$$

where p_{Df} is the long time approximation of the vertically fractured well solution and F is the pseudoskin factor for a horizontal well given by (see §3.4):

$$F(x_D,0,z_{wD},r_{wDz},L_D) = -\frac{1}{2L_D}\ln\left[4\sin\frac{\pi}{2}(2z_{wD}+r_{wDz})\sin\frac{\pi}{2}r_{wDz}\right] - \varphi(x_D,0,z_{wD},r_{wDz},L_D). \tag{3.5.24}$$

In Eq. 3.5.24, φ is defined by

$$\varphi(x_D,0,z_{wD},r_{wDz},L_D) = \frac{1}{\pi L_D}\sum_{n=1}^{\infty}\frac{\cos n\pi(z_{wD}+r_{wDz})\cos n\pi z_{wD}}{n} \left\{Ki_1[n\pi L_D(1+x_D)] + Ki_1[n\pi L_D(1-x_D)]\right\}. \tag{3.5.25}$$

In §3.4, we discussed that if $L_D \geq 5$, then the pseudoskin factor, F, is negligible and therefore the long time responses of vertically fractured wells and horizontal wells are practically the same. This result suggests that the equivalent pressure point $x_D = 0.732$ for a vertically fractured well can also be used for long horizontal wells ($L_D \geq 4$). In §3.4, we also showed that the function φ becomes negligible if $L_D \geq 1.15/(1-|x_D|)$ and the long time response of a horizontal well is given by

$$p_{wD}[L_D \geq 1.15/(1-|x_D|)] = p_{Df} - \frac{1}{2L_D}\ln\left[4\sin\frac{\pi}{2}(2z_{wD}+r_{wDz})\sin\frac{\pi}{2}r_{wDz}\right]. \tag{3.5.26}$$

Note that the second term in the right hand side of Eq. 3.5.26 (the horizontal well pseudoskin factor) is independent of flow in the x direction. This suggests that the point $x_D = 0.732$ obtained by Ref. 10 for vertically fractured wells can be used as the equivalent pressure point for horizontal wells if $L_D \geq 1.15/(1-|x_D|)$.

In this work, as in Refs. 5, 38, and 50, we use the point $x_D = 0.732$ to compute the infinite-conductivity well responses by using the uniform-flux well solution given by Eq. 3.1.1. The equivalent pressure point for horizontal wells is also obtained in Ref. 56 by computing the stabilized flux distribution as outlined before in this section. Ref. 56 presents the equivalent pressure points for the range of horizontal well lengths $2.5 \leq L_D \leq 20$. The values of the equivalent pressure point given in Ref. 56 appear to be in conflict with our observations presented above that

based on the investigation of the analytical expression for the pseudoskin factor, for $L_D \geq 1.15/(1 - |x_D|)$, $x_D = 0.732$.

3.6 Pressure Derivative Analysis

The advent of sensitive pressure gauges makes it possible to use the pressure derivative as a practical method of analysis. In this section, we present an alternate approach to analyze well test data via the derivative method. This approach involves plotting $\Delta p / [2\partial (\Delta p) / \partial \ln t]$ with respect to time. To our knowledge, this procedure was first presented in the groundwater literature in 1952 by Chow[4]. This method has a wide range of applicability and should improve our ability to analyze data, particularly with regard to heterogeneous reservoirs. In this chapter, we refer to Chow's method as the normalized pressure procedure. The normalized pressure procedure should eliminate some of the nonuniqueness problems often encountered in type-curve matching pressure data; for example, data affected by storage and skin, fractured well and horizontal well responses. This method is also extremely useful in identifying semilog straight lines, particularly if producing times are short. In this work, however, we restrict our attention to the problem under consideration and consider applications to three cases: the exponential integral solution, the horizontal well solution, and the vertically fractured well solution. Applications of this procedure to other situations can also be found in Refs. 6 – 8. In the following, we first examine the line source well solution to discuss the basis of Chow's procedure. This development is similar to that presented by Chow[4]. We then examine the applicability of this method to the horizontal well solutions. Since we compare horizontal well responses with that of vertically fractured wells, a discussion of the vertically fractured well case is also presented. For simplicity, throughout the following discussion, we assume that the reservoir is isotropic in the horizontal plane $(k_x = k_y)$.

I. The Line Source Solution The line source well solution is given by

$$p_D\left(r_D, t_D\right) = -\frac{1}{2}\mathrm{Ei}\left(-\frac{r_D^2}{4t_D}\right). \tag{3.6.1}$$

Taking the derivative of p_D with respect to $\ln t_D$ and dividing both sides of Eq. 3.6.1 by $2\left(\partial p_D/\partial \ln t_D\right)$, we obtain

$$\frac{p_D}{2\left(\partial p_D/\partial \ln t_D\right)} = -\frac{1}{2}\exp\left(\frac{r_D^2}{4t_D}\right)\mathrm{Ei}\left(-\frac{r_D^2}{4t_D}\right). \tag{3.6.2}$$

If

$$\frac{r_D^2}{4t_D} \leq 0.01, \tag{3.6.3}$$

then

$$\exp\left(\frac{r_D^2}{4t_D}\right) = 1, \tag{3.6.4}$$

within 1 %. When the condition given by Eq. 3.6.3 is satisfied, the exponential integral function, $\mathrm{Ei}(-x)$, can be replaced by the logarithmic approximation within 1 %. Thus, we can write

$$\frac{p_D}{2\left(\partial p_D/\partial \ln t_D\right)} \approx p_D = \frac{1}{2}\left(\ln\frac{t_D}{r_D^2} + 0.80907\right). \tag{3.6.5}$$

Eqs. 3.6.1 - 3.6.5 teach us the following. First, if the semilog straight line exists, then a plot of $\Delta p/\left(2\partial\Delta p/\partial \ln t\right)$ vs. $\log t$ should be a straight line with slope equal to 1.151. Thus, this procedure permits us to identify the semilog straight line in a straightforward manner, should it exist. If we consider the dimensional form of Eq. 3.6.2, we obtain

$$\frac{\Delta p}{2\left(\partial\Delta p/\partial \ln t\right)} = -\frac{1}{2}\exp\left(\frac{r^2}{4\eta t}\right)\mathrm{Ei}\left(-\frac{r^2}{4\eta t}\right). \tag{3.6.6}$$

Comparing Eqs. 3.6.2 and 3.6.6, it is clear that when $\left(r^2/\eta t\right) = \left(r_D^2/t_D\right)$, the left hand sides of the functions given by Eqs. 3.6.2 and 3.6.6 are equal. This indicates that it is possible to prepare a type curve based on Eq. 3.6.2 and use it to match data in the conventional way. In this case, we would plot $\Delta p/(2\partial\Delta p/\partial \ln t)$ vs. time, t. If the semilog straight line does not exist, then it is possible to determine

hydraulic diffusivity, η, by aligning the vertical axes. (Note that the vertical axis for the type curve and the field curve are dimensionless.) Once η is determined, pressure data can be used to match the well response to obtain kh (the time axes are now fixed) and the $\phi c_t h$ product can be determined from the estimates of kh and η. To apply this procedure, we generate a plot of $p_D/\left(2\partial p_D/\partial \ln t_D\right)$ vs. t_D/r_D^2 (log-log or semilog coordinates). Then type curve matching can be performed as follows:

1. Plot $\Delta p/\left(2\partial \Delta p/\partial \ln t\right)$ vs. t with the same scale as that of the type curve.

2. Align the $\Delta p/\left(2\partial \Delta p/\partial \ln t\right)$ axis with the $p_D/\left(2\partial p_D/\partial \ln t_D\right)$ axis (the vertical axes) and match the field data with the type curve by horizontal movement of the field curve.

3. Once the match is obtained, choose a match point, record the values of t and t_D/r_D^2 and determine the value of the diffusivity constant, η.

4. Using the match determined in step 3 align the time axes (horizontal axes) of the field curve and the type curve and then match the pressure response curve (Δp vs. t) with the conventional log-log type curve by vertical movement of the field curve. Once this match is obtained, then kh and $\phi c_t h$ can be obtained in the conventional manner.

Although we have considered the exponential integral solution, this method is applicable to other situations.

<u>II. Application to Horizontal Wells</u> The dimensionless pressure and its derivative with respect to $\ln t_D$ for a horizontal well are given, respectively, by

$$\begin{aligned} &p_D(x_D, y_D, z_D, z_{wD}, L_D, t_D) = \\ &\frac{\sqrt{\pi}}{4}\int_0^{t_D}\left[\operatorname{erf}\frac{(1+x_D)}{2\sqrt{\tau}} + \operatorname{erf}\frac{(1-x_D)}{2\sqrt{\tau}}\right]\left[\exp\left(-\frac{y_D^2}{4\tau}\right)\right] \\ &\left[1 + 2\sum_{n=1}^{\infty}\exp\left(-n^2\pi^2 L_D^2\tau\right)\cos n\pi z_D \cos n\pi z_{wD}\right]\frac{d\tau}{\sqrt{\tau}}, \end{aligned} \tag{3.6.7}$$

and

$$\frac{\partial p_D}{\partial \ln t_D} = \frac{\sqrt{\pi t_D}}{4}\left[\operatorname{erf}\frac{(1+x_D)}{2\sqrt{t_D}} + \operatorname{erf}\frac{(1-x_D)}{2\sqrt{t_D}}\right]\left[\exp\left(-\frac{y_D^2}{4t_D}\right)\right]$$

$$\left[1+2\sum_{n=1}^{\infty}\exp\left(-n^2\pi^2L_D^2t_D\right)\cos n\pi z_D\cos n\pi z_{wD}\right]. \tag{3.6.8}$$

Dividing Eq. 3.6.7 by 3.6.8 and multiplying by 0.5, we obtain

$$\frac{p_D}{2\left(\partial p_D/\partial \ln t_D\right)}=\frac{1}{2\sqrt{t_D}}\left\{\int_0^{t_D}\left[\exp\left(-\frac{y_D^2}{4\tau}\right)\right]\right.$$

$$\left[1+2\sum_{n=1}^{\infty}\exp\left(-n^2\pi^2L_D^2\tau\right)\cos n\pi z_D\cos n\pi z_{wD}\right]$$

$$\left.\left[\operatorname{erf}\frac{(1+x_D)}{2\sqrt{\tau}}+\operatorname{erf}\frac{(1-x_D)}{2\sqrt{\tau}}\right]\frac{d\tau}{\sqrt{\tau}}\right\}$$

$$\left\{\left[1+2\sum_{n=1}^{\infty}\exp\left(-n^2\pi^2L_D^2t_D\right)\cos n\pi z_D\cos n\pi z_{wD}\right]\right.$$

$$\left.\left[\operatorname{erf}\frac{(1+x_D)}{2\sqrt{t_D}}+\operatorname{erf}\frac{(1-x_D)}{2\sqrt{t_D}}\right]\left[\exp\left(-\frac{y_D^2}{4t_D}\right)\right]\right\}^{-1}. \tag{3.6.9}$$

In §3.2 I, it is shown that when

$$t_D\le\min\begin{cases}\delta_D^2/20,\\ \left(z_D+z_{wD}\right)^2/\left(20L_D^2\right),\\ \left[\left(z_D+z_{wD}\right)-2\right]^2/\left(20L_D^2\right),\end{cases} \tag{3.6.10}$$

where $\delta_D=1-|x_D|$ if $|x_D|<1$, and $\delta_D=2$ if $|x_D|=1$, the horizontal well solution can be approximated by

$$p_D\left(x_D,y_D,z_D,z_{wD},L_D,t_D\right)=-\frac{\beta}{8L_D}\operatorname{Ei}\left[-\frac{\left(z_D-z_{wD}\right)^2/L_D^2+y_D^2}{4t_D}\right], \tag{3.6.11}$$

where

$$\beta=\begin{cases}2 \text{ for } |x_D|<1,\\ 1 \text{ for } |x_D|=1,\\ 0 \text{ for } |x_D|>1.\end{cases} \tag{3.6.12}$$

Therefore, for the time range determined by Eq. 3.6.10 and $|x_D|\le 1$, Eq. 3.6.9 can be approximated by

$$\frac{p_D}{2\left(\partial p_D/\partial \ln t_D\right)}=-\frac{1}{2}\exp\left[\frac{\left(z_D-z_{wD}\right)^2/L_D^2+y_D^2}{4t_D}\right]$$

$$\mathrm{Ei}\left[-\frac{(z_D - z_{wD})^2/L_D^2 + y_D^2}{4t_D}\right]. \tag{3.6.13}$$

Note that when

$$\frac{(z_D - z_{wD})^2/L_D^2 + y_D^2}{4t_D} \leq 0.01, \tag{3.6.14}$$

the right hand side of Eq. 3.6.13 can be approximated by

$$\frac{p_D}{2\left(\partial p_D/\partial \ln t_D\right)} \approx 2L_D p_D = \frac{1}{2}\left\{\ln\left[\frac{t_D}{(z_D - z_{wD})^2/L_D^2 + y_D^2}\right] + 0.80907\right\}. \tag{3.6.15}$$

In dimensional form, Eq. 3.6.13 becomes

$$\frac{\Delta p}{2\left(\partial \Delta p/\partial \ln t\right)} = -\frac{1}{2}\exp\left[\frac{(z - z_w)^2 + (y - y_w)^2}{4\eta t}\right] \mathrm{Ei}\left[-\frac{(z - z_w)^2 + (y - y_w)^2}{4\eta t}\right]. \tag{3.6.16}$$

Eq. 3.6.16 indicates that, when the short-time approximation for the horizontal well solution given by Eq. 3.6.11 becomes valid, then a plot of $\Delta p/\left(2\partial \Delta p/\partial \ln t\right)$ vs. t is independent of $2h/L_h$; that is, the normalized responses on dimensionless coordinates at early times are independent of L_D (see Figs. 3.7.3 and 3.7.7). Furthermore, when the condition given by Eq. 3.6.14 is satisfied, the slope of the plot of $\Delta p/\left(2\partial \Delta p/\partial \ln t\right)$ vs. $\log t$ is 1.151. This observation can be used to identify the initial radial flow period.

For times determined by

$$t_D \geq \max\begin{cases} 100/(\pi L_D)^2, \\ 25\left[(x_D + 1)^2 + y_D^2\right], \\ 25\left[(x_D - 1)^2 + y_D^2\right], \end{cases} \tag{3.6.17}$$

the horizontal well solution can be approximated by (see §3.2)

$$p_D = \frac{1}{2}\left(\ln t_D + 2.80907\right) + \sigma\left(x_D, y_D\right) + F(x_D, y_D, z_D, z_{wD}, L_D). \tag{3.6.18}$$

Then, during the time range given by Eq. 3.6.17, Eq. 3.6.9 can be approximated by

$$\frac{p_D}{2\left(\partial p_D/\partial \ln t_D\right)} = \frac{1}{2}\left(\ln t_D + 2.80907\right) + \sigma\left(x_D, y_D\right) + F(x_D, y_D, z_D, z_{wD}, L_D). \tag{3.6.19}$$

Eq. 3.6.19 suggests that at long times the normalized responses will merge with the pressure responses. Furthermore, if the pseudoradial flow period is evident, then a plot of normalized responses with respect to time will yield a semilog straight line with slope equal to 1.151.

III. Application to Fractured Wells The dimensionless pressure solution for a vertically fractured well is given by[10]

$$p_D = \frac{\sqrt{\pi}}{4}\int_0^{t_D}\left[\mathrm{erf}\frac{(1-x_D)}{2\sqrt{\tau}} + \mathrm{erf}\frac{(1+x_D)}{2\sqrt{\tau}}\right]\left[\exp\left(-\frac{y_D^2}{4\tau}\right)\right]\frac{d\tau}{\sqrt{\tau}}. \tag{3.6.20}$$

Thus, we have

$$\frac{\partial p_D}{\partial \ln t_D} = \frac{\sqrt{\pi t_D}}{4}\left[\mathrm{erf}\frac{(1-x_D)}{2\sqrt{t_D}} + \mathrm{erf}\frac{(1+x_D)}{2\sqrt{t_D}}\right]\left[\exp\left(-\frac{y_D^2}{4t_D}\right)\right]. \tag{3.6.21}$$

At very early times, we can use the approximation given by Ref. 10 (note that Eq. 10 of Ref. 10 contains a misprint):

$$p_D = \beta\left[\sqrt{\pi t_D}\exp\left(-\frac{y_D^2}{4t_D}\right) - \frac{\pi}{2}|y_D|\mathrm{erfc}\left(\frac{|y_D|}{2\sqrt{t_D}}\right)\right], \tag{3.6.22}$$

where $\beta = 1$ and 0.5 for $|x_D| < 1$ and $|x_D| = 1$, respectively. For $|x_D| > 1$, $p_D = 0$ at early times. Therefore, at early times for $|x_D| \leq 1$, we can write

$$\frac{p_D}{2\left(\partial p_D/\partial \ln t_D\right)} = 1 - \frac{\pi|y_D|}{2\sqrt{\pi t_D}}\exp\left(\frac{y_D^2}{4t_D}\right)\mathrm{erfc}\left(\frac{|y_D|}{2\sqrt{t_D}}\right). \tag{3.6.23}$$

We note that on the fracture plane ($y_D = 0$), Eq. 3.6.23 yields

$$\frac{p_D}{2\left(dp_D/d\ln t_D\right)} = 1. \tag{3.6.24}$$

This indicates that the ordinate of the normalized plot of fracture responses is approximately unity at early times (see Figs. 3.7.3 and 3.7.7).

It is shown in Ref. 10 that during pseudoradial flow period, pressure distribution in the reservoir is given by

$$p_D = 0.5(\ln t_D + 2.80907) + \sigma(x_D, y_D), \tag{3.6.25}$$

where $\sigma(x_D, y_D)$ is defined by Eq. 3.2.9. Therefore at late times, the normalized vertically fractured well responses are defined by the following expression:

$$\frac{p_D}{2\left(\partial p_D/\partial \ln t_D\right)} \approx p_D = \frac{1}{2}\left(\ln t_D + 2.80907\right) + \sigma\left(x_D, y_D\right). \qquad (3.6.26)$$

As in the other cases, Eq. 3.6.26 suggests that at late times the normalized plot will merge with the pressure response curve and will yield a semilog straight line with slope equal to 1.151.

3.7 Results

Here we present the results of our investigation of the responses of horizontal wells based on the analytical developments presented in the previous sections. Our main objective in this section is to provide physical insight of the parameters that govern the performance of horizontal wells and to discuss the procedures to analyze the pressure responses of horizontal wells. We consider both infinite-conductivity and uniform-flux wells. Based on the discussion presented in §3.5, the infinite conductivity results are obtained from the uniform-flux well solution given by Eq. 3.1.1 at $x_D = 0.732$. For the purpose of continuity and comparison with the results presented in Refs. 37 and 38, we use the point $z_D = z_{wD}$ and $y_D = r_{wD}$ (see Eq. 3.3.3) to compute the wellbore pressures. The results presented throughout this section assume that the reservoir is isotropic in the horizontal plane; that is, $k = k_x = k_y$.

I. Infinite-Conductivity Well Responses Fig. 3.7.1 shows typical pressure responses of infinite-conductivity horizontal wells. The variable of interest is the dimensionless horizontal well length, L_D, $(0.1 \leq L_D \leq 100)$. The solutions shown here are for a well located at the reservoir mid-height $(z_{wD} = 0.5)$ and $r_{wD} = 10^{-4}$. The bottom curve in this figure is the response of a fully penetrating vertically fractured well. The figure shows that the $L_D \geq 50$ solutions are indistinguishable from the vertically fractured well solution for $t_D \geq 2.3 \times 10^{-1}$ (relative difference

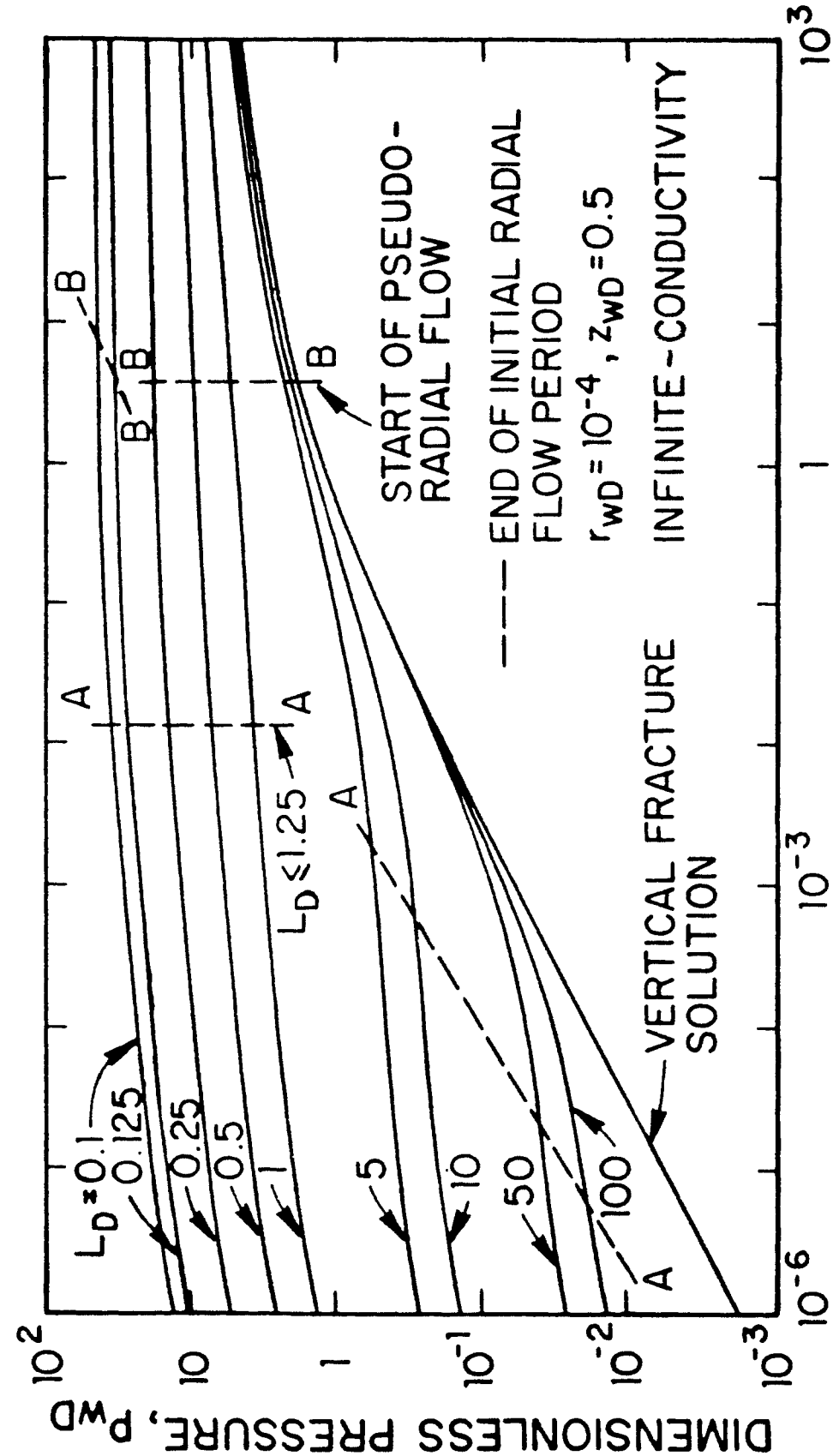

Fig. 3.7.1 - Typical Responses of Horizontal Wells – Infinite-Conductivity.

is less than or equal to 5 percent), i.e., at long times, the pressure responses of long horizontal wells are almost identical to the responses of fully penetrating vertically fractured wells. Our computations indicate that the difference between the horizontal well responses and vertically fractured well responses at late times is less than 10 percent if $L_D \geq 4$.

The dashed lines on the left hand side, lines marked AA, of this figure, denote the end of the initial radial flow period, Eq. 3.2.1. As already mentioned, during this period, the well behaves as if it were a vertical well completely penetrating a formation of thickness L_h. The end of this flow period was determined by computing slopes and the lines marked AA reflect times at which slopes differ from 1.151 by 5 percent. The end of this flow period is determined by two factors. First, movement of fluid across the well tips ($|x_D| = 1$) can distort the isopotential lines that are concentric with the well axis. In this case, the end of this flow period will be independent of L_D. Intuitively we would expect this to be the case for small values of L_D (h large and/or k_z small). This period can also end if upper and/or lower boundaries influence the well response. Under such circumstances, we would expect L_D to have an influence on the end of this period. Intuitively speaking, we would expect the boundaries to influence the well behavior early if L_D is large (h small and/or k_z large). These results are consistent with the time ranges given by the right hand side of Eq. 3.2.3.

The chain-dotted lines, lines marked BB, on the right hand side of the figure denote the beginning of the pseudoradial flow period. Data beyond this time period can be used to obtain formation permeability and skin factor by conventional semilog analysis techniques. If $L_D \geq 0.25$, the beginning of this flow period is independent of L_D; in this case the upper and lower reservoir boundaries do not influence the beginning of this flow period. The basis for this result can be understood if we examine the derivative of p_{wD}. Fig. 3.7.2 is a plot of $dp_{wD}/d\ln t_D$ vs. t_D. Note that the derivative plot has a value equal to $0.25/L_D$ at early times (Eq. 3.2.1) and 0.5 at late times (Eq. 3.2.19). The letter x ($t_D = 4.13$) in Fig. 3.7.2 represents the time for the start of pseudoradial flow for horizontal wells for

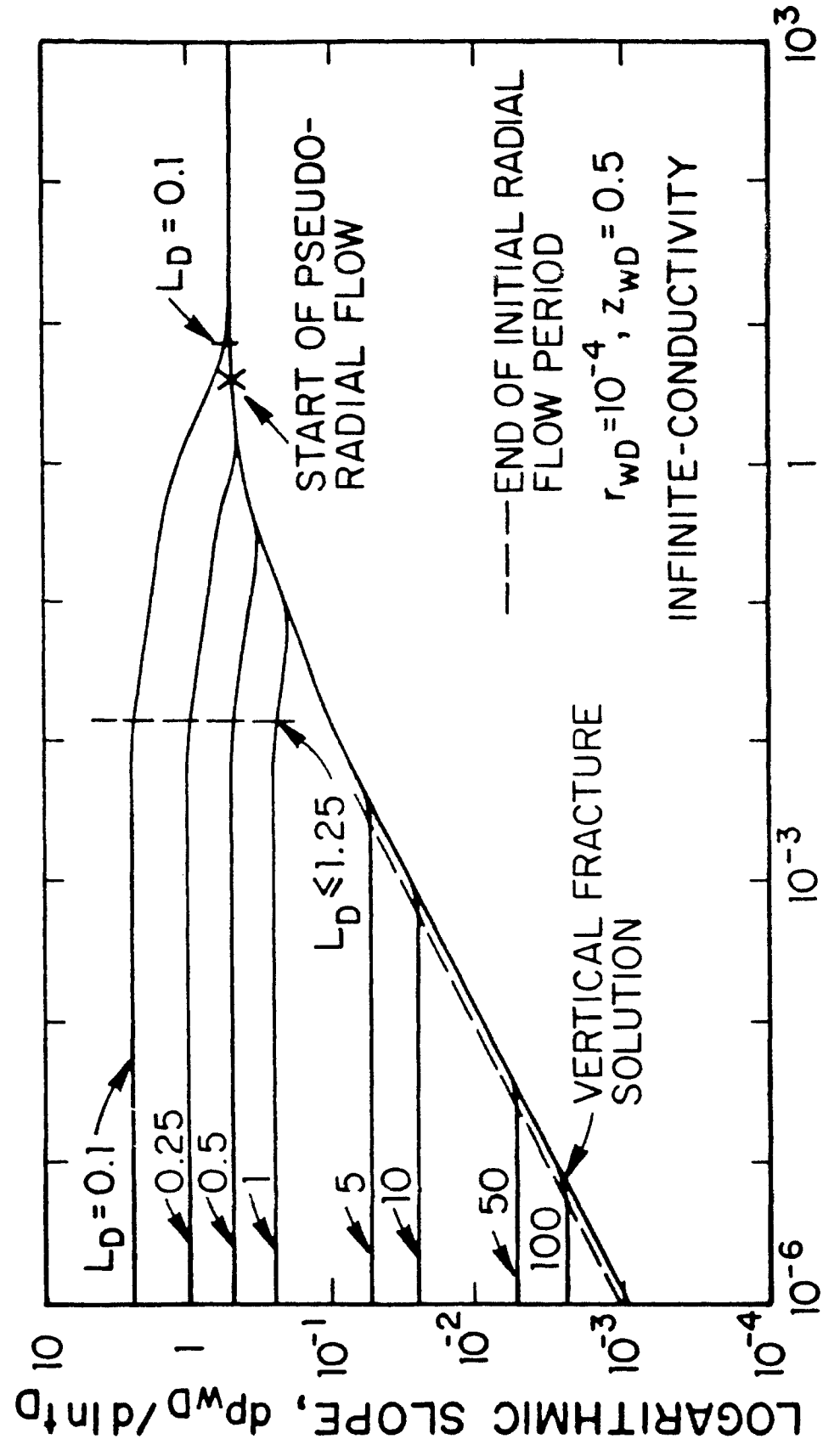

Fig. 3.7.2 - Horizontal Well Derivative Responses – Infinite-Conductivity.

$L_D \geq 0.25$. It also represents the time for the start of pseudoradial flow for a vertically fractured well. This result implies that for $L_D \geq 0.25$, the formation thickness, h, and the ratio k_z/k do not affect the beginning of this flow period; thus, it is the length of the horizontal well, L_h, that governs the start of the pseudoradial flow period and not surprisingly this time is identical to the start of the pseudoradial flow period for a vertically fractured well. If L_D is small ($L_D < 0.25$), then the upper and lower boundaries also control the time for the beginning of pseudoradial flow and thus L_D (vertical permeability and reservoir thickness) has an influence on the beginning of the pseudoradial flow period. These observations may also be interpreted as follows. If the initial radial flow period ends because of the influence of the top or bottom boundary (large L_D), then our results show that the start of pseudoradial flow is independent of L_D and is governed by the value of L_h (via t_D). The reverse argument is also true.

Based on an examination of the responses shown in Figs. 3.7.1 and 3.7.2, the following conclusions may be derived. First, if L_D is large, then it may not be possible to distinguish the horizontal well solutions from the vertically fractured well solutions. The results shown in Fig. 3.7.1 and other computations suggest that if $L_D \geq 50$ then the two solutions may be indistinguishable. The fact that the horizontal well solutions are for all practical purposes identical to the fully penetrating vertical fracture solution at late times for large L_D values deserves comment. We have noted earlier that a horizontal well may be viewed as a vertical fracture of zero height in the limit. Thus it may be surprising that the two solutions are for all practical purposes identical for certain values of L_D. Physically, this result implies that flow in the vertical direction is negligibly small. Also, the magnitude of the additional pressure drop reflecting convergence to the wellbore depends on the manner in which the fluid converges toward the wellbore. At large distances from the well center, velocities are small, and if convergence takes place where velocities are small then the additional pressure drop that reflects convergence is small. In the horizontal well case, fluid begins to converge at large distances from the well and thus the additional pressure drop is small. In the case of vertical wells, fluid

converges toward the wellbore where velocities are high, and if all conditions are identical (r_w, h, k_z, and k), the corresponding additional pressure drop would be much higher. It is for this reason that a horizontal well may reduce water or gas coning problems (see Refs. 57 and 58).

Although not directly pertinent to this work, the observations in the preceeding paragraphs and the results in Figs. 3.7.1 and 3.7.2 have a bearing on the performance of vertically fractured wells. These results suggest that the long term productivity of a vertically fractured well is governed principally by the length (and conductivity) of the vertical fracture rather than the height of the fracture. The results given here imply that if lateral penetration is significant, penetration in the vertical plane is not germane to long term productivity (see also Ref. 59).

The second conclusion that can be drawn from the responses shown in Figs. 3.7.1 and 3.7.2 is that, if L_D is small, then the characteristic shape of the well response will be indistinguishable from that of an unfractured vertical well. The well responses display features similar to that of an unfractured vertical well. If L_D is small enough, type curve matching of pressure data may be virtually impossible. Also, from the derivative plot, we may not be able to distinguish the specific radial flow period (initial or pseudoradial) if all measured data are taken during one of these flow periods. Fig. 3.7.2, however, suggests that the derivative plot would be beneficial if data during the transitional period are available. In the following, we suggest a procedure to identify the appropriate semilog straight line and also improve our ability to type curve match pressure data.

Normalized Pressure Plots Fig. 3.7.3 is a composite of the normalized pressure responses discussed in §3.6 (unbroken lines) and the pressure responses (dashed lines). At early times the normalized pressure responses are identical; the influence of L_D is negligible. This result follows directly from Eq. 3.6.15. As time increases, the normalized pressure responses diverge and ultimately merge with the appropriate p_{wD} curve (see Eq. 3.6.19). Note that the ordinate of the normalized pressure responses does not involve formation or well parameters. This result implies that it is possible to conduct type curve matching of normalized pressure data by aligning

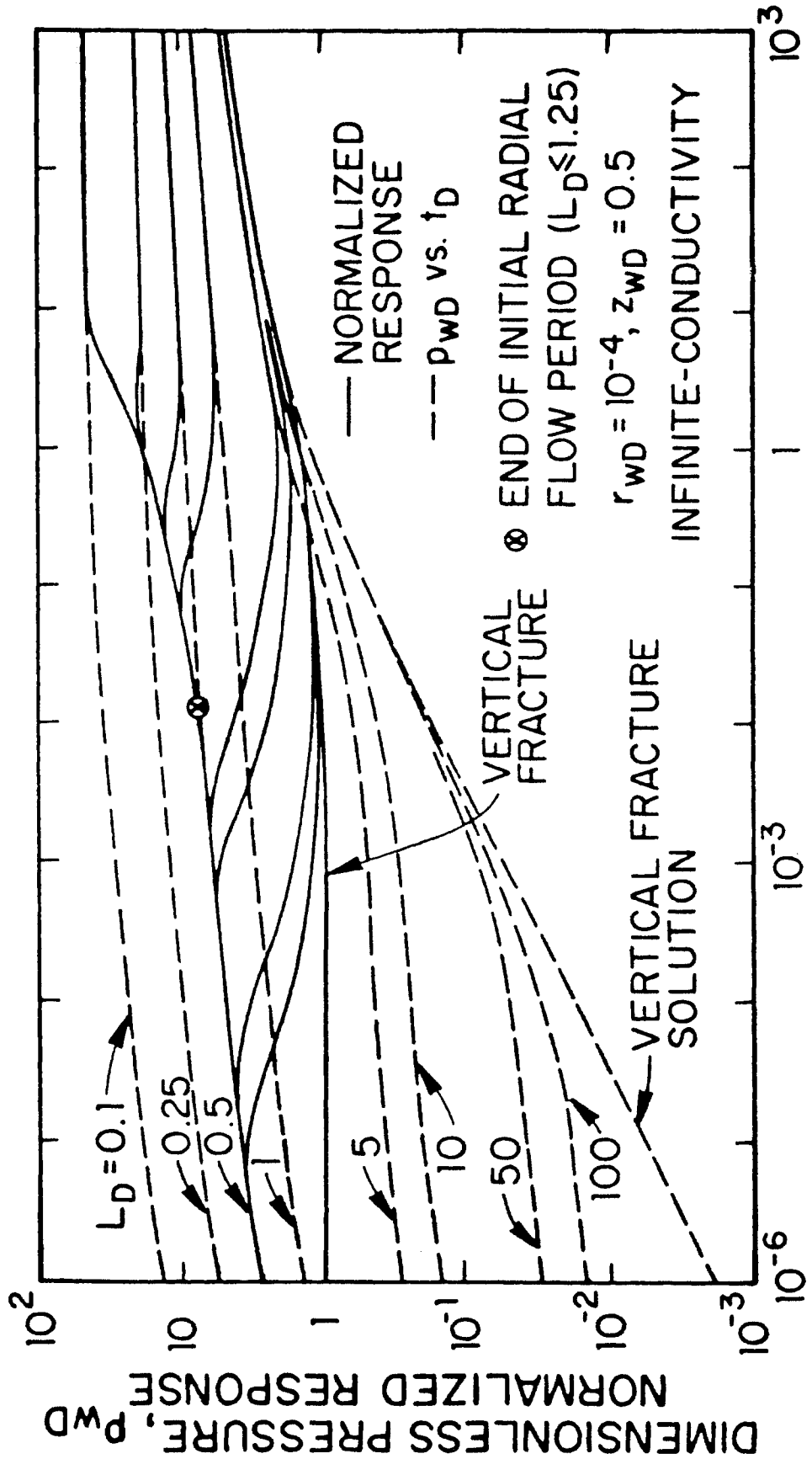

Fig. 3.7.3 - Composite Pressure and Normalized Response Type Curve – Infinite-Conductivity.

the vertical scales of the field curve and the type curve (Fig. 3.7.3). The circle circumscribing the letter x on Fig. 3.7.3 reflects the end of the initial radial flow period for $L_D \leq 1.25$. From Fig. 3.7.3, we note that the normalized responses are for all practical purposes identical to the pressure responses during the pseudoradial flow period (Eq. 3.6.19). Thus, by type curve matching data with the normalized pressure plots, the appropriate semilog straight lines, should they exist, can be identified.

Influence of Well Radius, r_w, on Well Response The results presented in Figs. 3.7.1 – 3.7.3 assume that $r_{wD} = 10^{-4}$. We have chosen this value of r_{wD} principally because we believe that $r_{wD} = 10^{-4}$ is representative of the value of the dimensionless wellbore radius that will be encountered in practice, particularly for long horizontal wells. In field applications, the wellbore diameter will be dictated by the drilling constraints but will not vary by more than a factor of two. To evaluate the influence of changes in wellbore radius, we computed pressure responses for r_{wD} values in the range $5 \times 10^{-5} \leq r_{wD} \leq 5 \times 10^{-4}$. Typical responses for two values of L_D, L_D =10 and 1 are shown in Tables 3.7.1 and 3.7.2, respectively. Considering the results in Table 3.7.1, we note that at early times the differences are significant. (In actual practice, the difference at early times may not be as large as that shown here. For a well of finite radius we would expect the differences to be smaller.) Long term productivity, however, is unaffected. For example, at $t_D = 10^4$ the change in dimensionless pressure is only 1.3 percent. For small values of L_D (Table 3.7.2), r_{wD} has a greater influence on long term productivity. In this case, for the ranges considered in Table 3.7.2, dimensionless pressures vary by approximately 10 percent. The results presented in Tables 3.7.1 and 3.7.2 cover a wide range of r_{wD} values and for a given value of L_D, one will not encounter such large variations in r_{wD}. The tabulations are presented to emphasize the importance of r_{wD}, particularly on the early time pressure response.

Influence of Well Location, z_{wD}, on Well Response Tables 3.7.3 and 3.7.4 are intended to provide information on the influence of the well location, z_{wD}, for two values of L_D. In each table, four horizontal well locations are considered, $z_{wD} = 0.5$,

TABLE 3.7.1

THE INFLUENCE OF WELLBORE RADIUS ON PRESSURE RESPONSE

OF AN INFINITE-CONDUCTIVITY HORIZONTAL WELL

(L_D = 10, z_{wD} = 0.5)

	Dimensionless Wellbore Pressure, p_{wD}		
Dimensionless Well Radius, r_{wD}	5×10^{-5}	10^{-4}	5×10^{-4}
Dimensionless Time, t_D			
1E-6	0.1700	0.1354	0.05642
1E-5	0.2276	0.1929	0.1126
1E-4	0.2851	0.2505	0.1700
1E-3	0.3439	0.3093	0.2288
1E-2	0.4646	0.4300	0.3495
1E-1	0.7827	0.7480	0.6675
1E0	1.491	1.457	1.376
1E1	2.556	2.521	2.440
1E2	3.697	3.662	3.582
1E3	4.847	4.813	4.732
1E4	5.999	5.964	5.884

TABLE 3.7.2

THE INFLUENCE OF WELLBORE RADIUS ON PRESSURE RESPONSE

OF AN INFINITE-CONDUCTIVITY HORIZONTAL WELL

(L_D = 1, z_{wD} = 0.5)

	Dimensionless Wellbore Pressure, p_{wD}		
Dimensionless Well Radius, r_{wD}	5×10^{-5}	10^{-4}	5×10^{-4}
Dimensionless Time, t_D			
1E-6	1.700	1.354	0.5642
1E-5	2.276	1.929	1.126
1E-4	2.851	2.505	1.700
1E-3	3.427	3.080	2.276
1E-2	4.000	3.654	2.849
1E-1	4.501	4.155	3.350
1E0	5.212	4.865	4.060
1E1	6.276	5.929	5.125
1E2	7.418	7.071	6.266
1E3	8.568	8.221	7.417
1E4	9.719	9.372	8.568

TABLE 3.7.3

INFLUENCE OF WELL LOCATION ON

PRESSURE RESPONSE OF AN INFINITE-CONDUCTIVITY HORIZONTAL WELL

(L_D = 25, r_{wD} = 1E-04)

	Dimensionless Wellbore Pressure, p_{wD}			
Well Location, z_{wD}	0.5	0.25	0.125	0.0625
Dimensionless Time, t_D				
2E-6	0.06109	0.06109	0.06109	0.06119
1E-5	0.07717	0.07717	0.07742	0.08149
1E-4	0.1033	0.1024	0.1106	0.1228
1E-3	0.1391	0.1460	0.1583	0.1718
1E-2	0.2595	0.2665	0.2787	0.2922
1E-1	0.5776	0.5845	0.5968	0.6103
1E0	1.286	1.293	1.305	1.319
1E1	2.350	2.357	2.370	2.383
1E2	3.492	3.499	3.511	3.525
1E3	4.642	4.649	4.662	4.675
1E4	5.794	5.801	5.813	5.826
1E5	6.945	6.952	6.964	6.978

TABLE 3.7.4

THE INFLUENCE OF WELL LOCATION ON

PRESSURE RESPONSE OF AN INFINITE-CONDUCTIVITY HORIZONTAL WELL

(L_D = 0.25, r_{wD} = 1E-04)

Dimensionless Time	Dimensionless Wellbore Pressure, P_{wD}			
	Dimensionless Well Location, z_{wD}			
	0.5	0.25	0.125	0.0625
2E-6	6.109	6.109	6.109	6.109
1E-5	7.717	7.717	7.717	7.717
1E-4	10.02	10.02	10.02	10.02
1E-3	12.32	12.32	12.32	12.32
1E-2	14.61	14.61	14.61	14.61
1E-1	16.58	16.58	16.60	16.92
1E0	17.99	18.10	18.59	19.42
1E1	19.07	19.36	19.99	20.87
1E2	20.21	20.50	21.14	22.02
1E3	21.37	21.65	22.29	23.17
1E4	22.52	22.80	23.44	24.32
1E5	23.67	23.95	24.59	25.47

0.25, 0.125, and 0.0625. The tabulations show that for these values of L_D, the pressure responses are insensitive to well location. These results suggest that the pseudoskin factor will be essentially independent of z_{wD}. This result may be explained if we note that for large values of L_D, the horizontal well solutions are essentially identical to the vertical fracture solution; i.e., flow in the vertical direction is negligibly small. Consequently the location of the wellbore within the productive interval is not significant. If we compare pressure responses for a smaller value of L_D (Table 3.7.4), then the pressure responses are independent of z_{wD} at early times. This result can be attributed to the fact that for small values of L_D the initial radial flow period exists for a very long time. At later times, differences become significant and at $t_D = 10^5$ the pressure drops differ by approximately eight percent (for $L_D = 25$, the difference at $t_D = 10^5$ is less than 0.5 percent). Although differences in p_{wD} values at late times are much larger than the differences in Table 3.7.3, the influence of z_{wD} on the pseudoskin factor may not be significant principally because the magnitudes of the dimensionless wellbore pressures during the pseudoradial flow period for small L_D values are much larger than the magnitudes of the dimensionless wellbore pressures for the vertical fracture solution at corresponding times. Thus, we expect the percent change in pseudoskin factor to be of the same order of magnitude as the dimensionless wellbore pressure. It is interesting that in this case the pressure response is, for all practical purposes, relatively independent of z_{wD} for $0.125 \leq z_{wD} \leq 0.875$. The effect of r_{wD} on the pressure response for various well locations is similar to that discussed above.

The Pseudoskin Factor As noted earlier, pseudoskin factors of horizontal wells are calculated by comparing their late time pressure responses with that of a fully penetrating vertical fracture. Fig. 3.7.4 shows the variation in pseudoskin factor, F, as a function of dimensionless well length, L_D ($z_{wD} = 0.5$). The variable of interest is the dimensionless well radius, r_{wD}. We have considered values of r_{wD} as large as 10^{-2}, principally because we wish to provide solutions for short drainholes. It should be noted, however, that if the drainhole is short, then the upper limit for L_D will be much smaller than the upper limit considered in this study. As

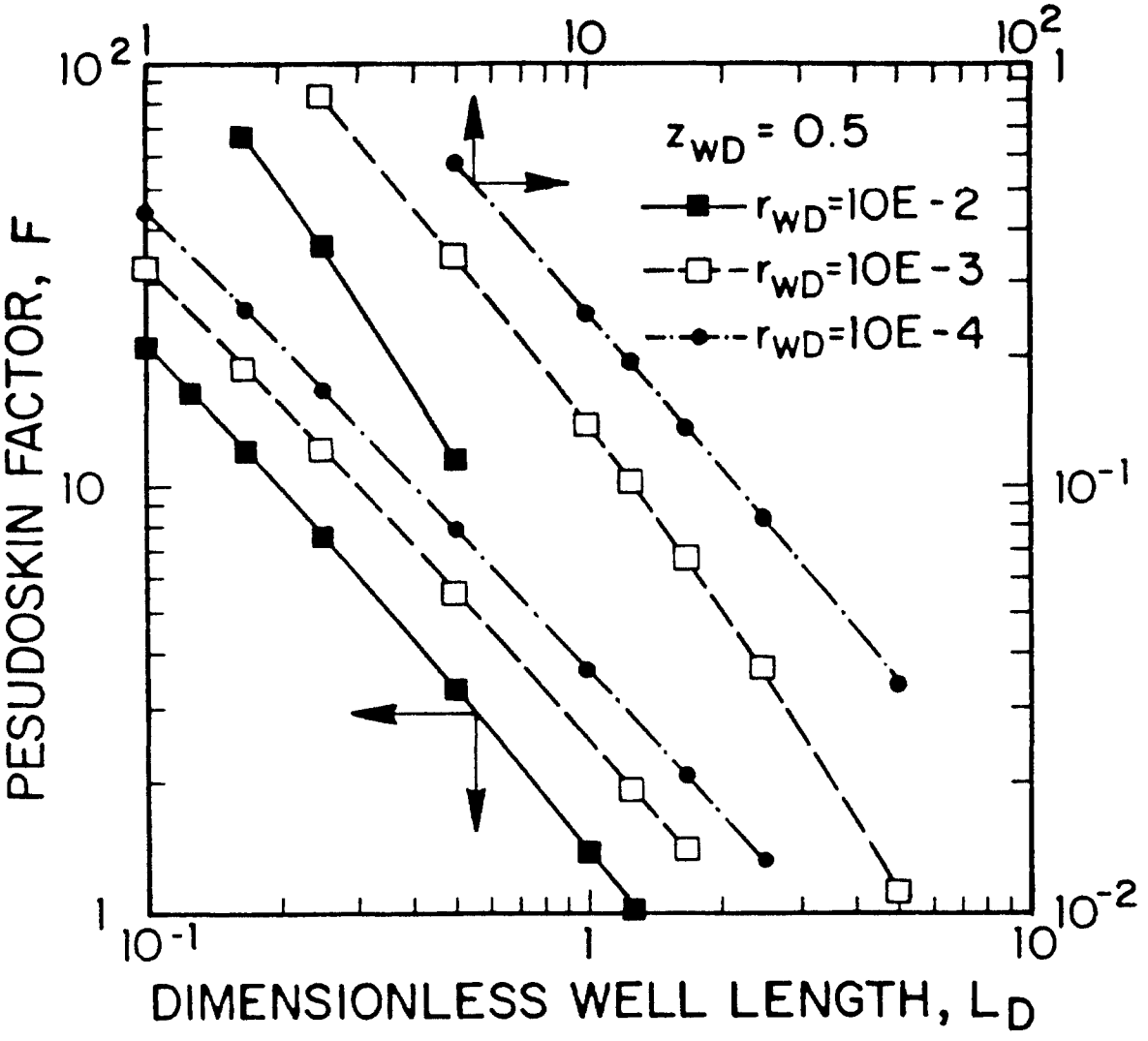

Fig. 3.7.4 - Influence of Dimensionless Well Radius on Pseudoskin Factor.

expected from the results given earlier, for a fixed value of r_{wD}, the pseudoskin factor increases as L_D decreases. Also for a fixed value of L_D, pseudoskin factors decrease as r_{wD} increases. An increase in r_{wD} should be viewed as an increase in the wellbore diameter, all other variables being fixed. It should be noted that if r_{wD} is chosen large enough, then pseudoskin factors would be negative for some values of L_D. Under the assumptions of this work, this result is obtained primarily because well responses are computed at different points for the horizontal well and vertical fracture solutions. (Actually, one may view the vertical fracture solutions in the literature to be computed at $r_{wD} = 0$.) For reasons mentioned earlier, we believe that these results are unrealistic and have not considered them in this work.

Fig. 3.7.5 depicts the variation in pseudoskin factor for various values of z_{wD} ($r_{wD} = 10^{-4}$). Similar results are obtained for other values of r_{wD}. For large values of L_D, pseudoskin factors are negligibly small and thus the well location does not impact the magnitude of the pseudoskin factor. On a percent basis, however, the variation in pseudoskin factor is 10 percent. For smaller values of L_D, we note that the pseudoskin factor for a well located at $z_{wD} = 0.5$ is large; for example, $F \approx 40.5$ for $L_D = 0.1$. The additional pressure drops caused by the proximity of the upper or lower boundary does not appear to be significant. Large values of pseudoskin factors for small values of L_D may be explained as follows. For simplicity, if we assume an isotropic reservoir, then values of $L_D < 0.5$ would represent well lengths less than the reservoir height. Such wells can be viewed as limited entry vertical wells. In such cases, large pseudoskin factors are reasonable.

Influence of Well Length, L_h, on the Well Response As is evident from the results presented thus far, the well length has a dominant effect on well productivity. If we wish to examine the influence of length on productivity, then some care should be taken because a change in well length influences both r_{wD} and L_D, all other parameters being constant. For example, if we consider a system with $L_D = 10$ and $r_{wD} = 5 \times 10^{-5}$ (Col. 2, Table 3.7.1) and wish to examine the effect of reducing the well length, L_h, by a factor of 10, then we must consider the solution for $L_D = 1$, $r_{wD} = 5 \times 10^{-4}$ (Col. 4, Table 3.7.2). If we compare responses for these two

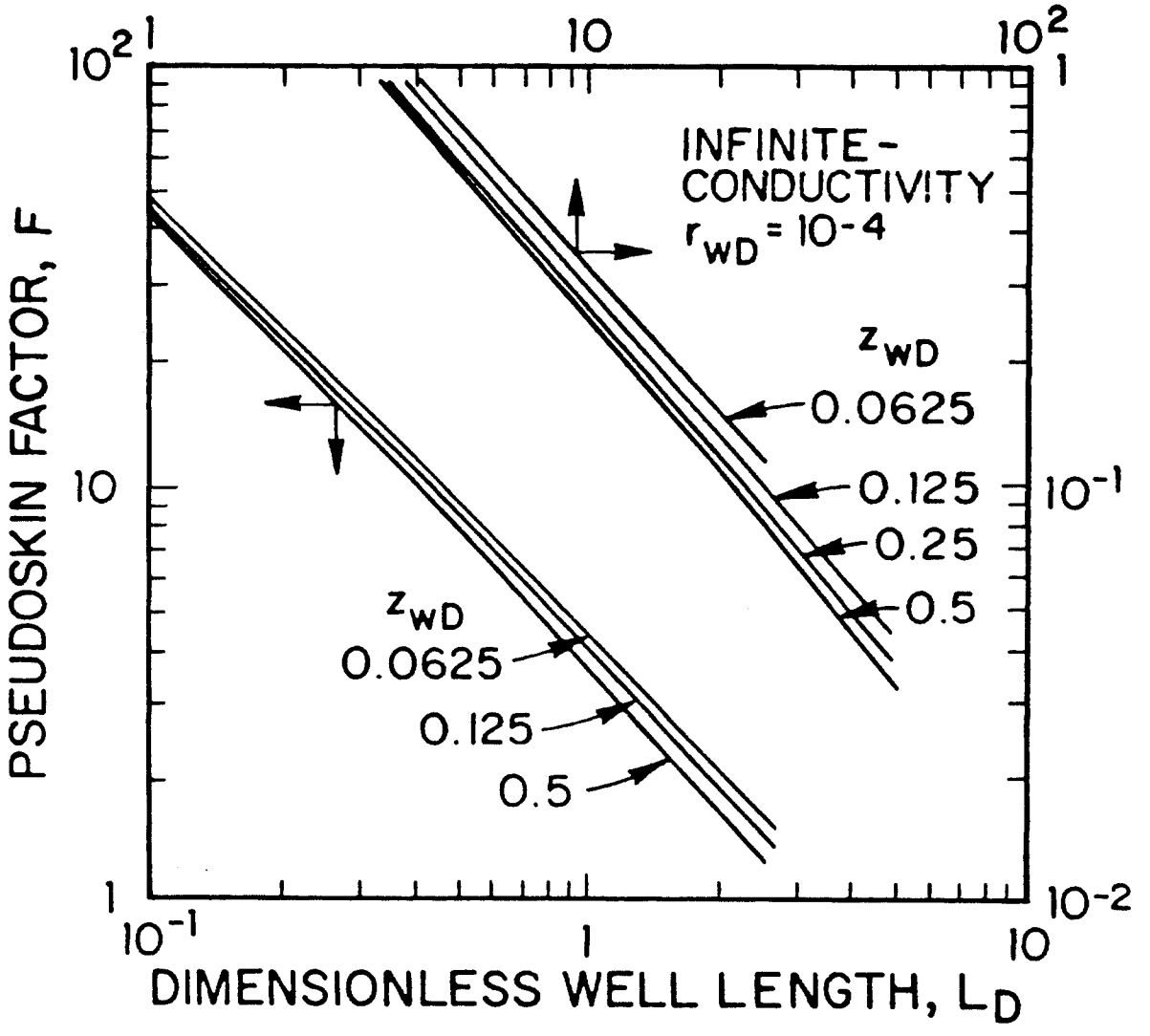

Fig. 3.7.5 - Influence of Well Location on Pseudoskin Factor.

cases we find that the pseudoskin factor changes from 0.2881 to 2.857, a change of approximately 900 percent.

II. Uniform-Flux Well Responses Based on the responses of vertically fractured wells[10], we expect the characteristics of the response curves for the uniform-flux case to be similar to those of the response curves for the infinite-conductivity case. Fig. 3.7.6 presents solutions for the uniform-flux case. The well is assumed to be at the center of the reservoir ($z_{wD} = 0.5$). As mentioned earlier, these solutions may be applicable to drainholes which extend on either side of a vertical well. If we compare the magnitude of the pressure drops with the corresponding cases in Fig. 3.7.1, we find that the pressure drops, in general, are greater than or equal to the corresponding infinite-conductivity solution. During the initial radial flow period, the responses would be identical since the conductivity has no influence on the well response. The dashed lines on the left side of this figure, lines AA, denote the end of the initial radial flow period. In this case also, the duration of this period was determined by computing the slope of the pressure trace. For $L_D \geq 1$, these times are essentially identical to the times for the infinite-conductivity case. For intermediate values of L_D, $0.5 < L_D \leq 1$, this flow period exists for a longer time.

The chain dotted lines on the right, lines BB, denote the beginning of the pseudoradial flow period. As in the infinite-conductivity case, the beginning of this flow period is independent of L_D if $L_D \geq 0.5$. In this case, the pseudoradial flow period begins earlier ($t_D \approx 1.6$ as compared to 4.13 for the infinite-conductivity case). For $L_D < 0.5$, the upper and lower boundaries also determine the start of the pseudoradial flow period, and, thus, these times depend on L_D.

Fig. 3.7.7 is a composite of the pressure responses and normalized pressure responses. The characteristics of the normalized pressure curves are similar to those considered in Fig. 3.7.3. The circle cirscumscribing the letter x on this plot denotes the end of the initial radial flow for $L_D \leq 0.5$. At late times, the normalized pressure curves merge with the pressure response curves (Eq. 3.6.19). The normalized pressure plots should enable us to identify the appropriate radial flow periods and

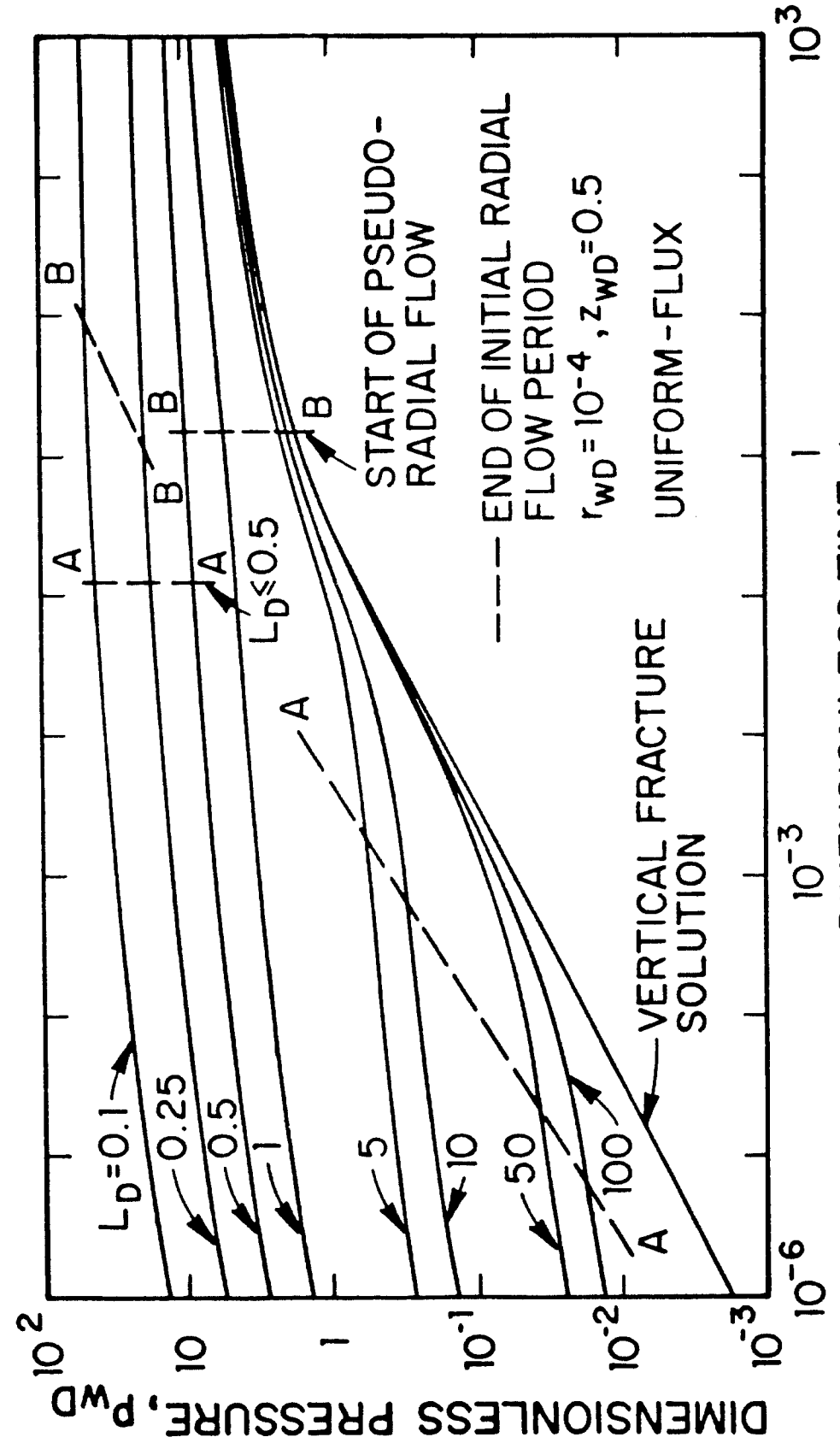

Fig. 3.7.6 - Typical Responses of Horizontal Wells – Uniform-Flux.

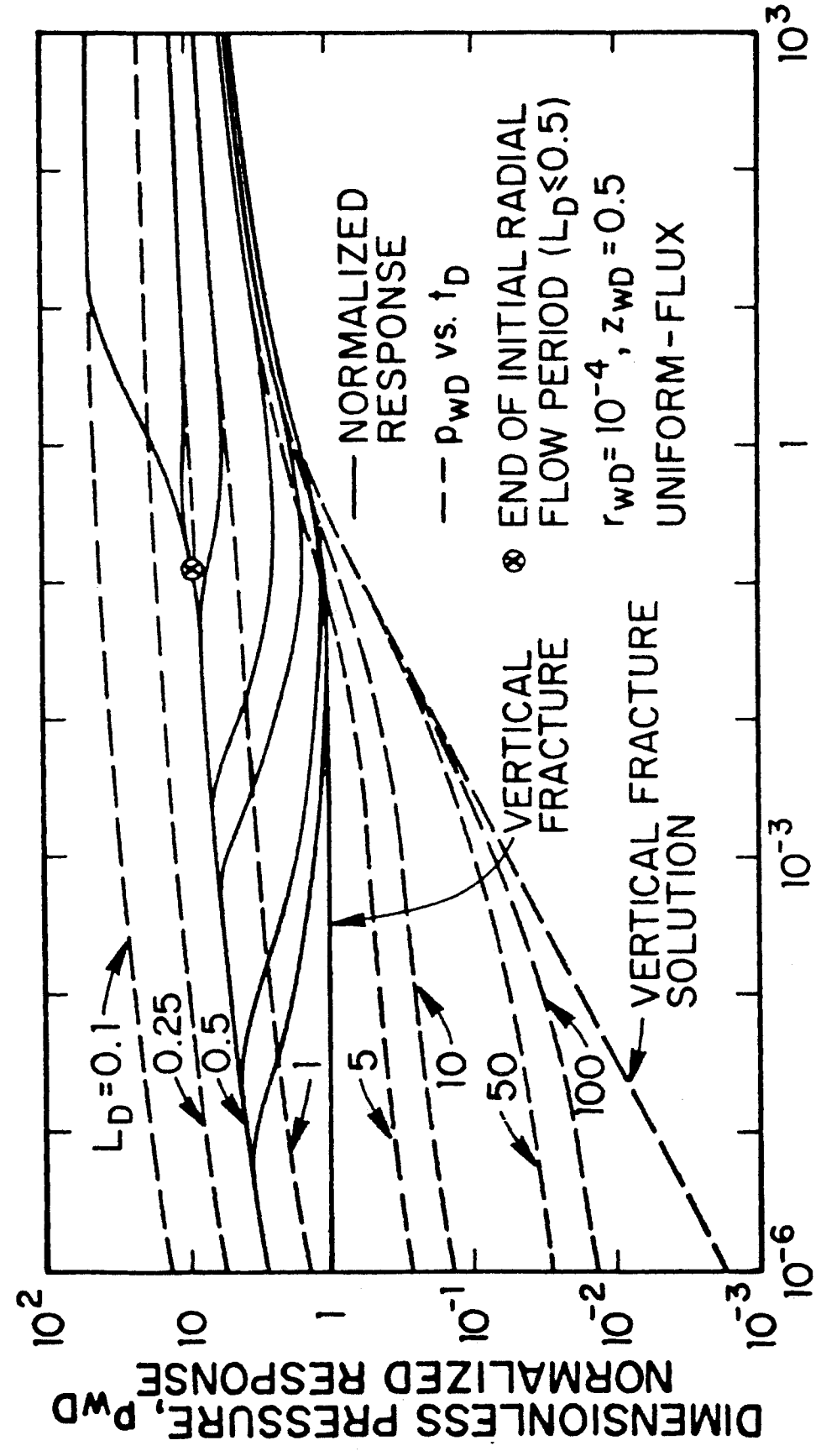

Fig. 3.7.7 - Composite Pressure and Normalized Response Type Curve – Uniform-Flux.

also enable us to choose the appropriate L_D curve to match pressure data if L_D is small. The type curve matching procedure is identical to that discussed earlier.

Since the characteristics of the well responses for the uniform-flux case are similar to those for the infinite-conductivity case, it does not appear worthwhile to document the influence of z_{wD}, r_{wD}, etc. in detail.

As mentioned earlier, computation of responses at $|x_D| = 1$, does not appear to be worthwhile for the uniform-flux case. Table 3.7.5 compares well responses at $x_D = 0$ and at $|x_D| = 1$, at $t_D = 10^5$. The results demonstrate that the dimensionless pressures at the well tips are less than those at the well center (see also Eq. 3.2.1). Thus, for a single drainhole or a single horizontal well, where produced fluids are pumped out from the well tip ($|x_D| = 1$), the uniform-flux assumption is an unrealistic boundary condition since the point in a wellbore from where fluid is pumped to the surface must be the point of lowest pressure within the well. The infinite-conductivity assumption is the only viable boundary condition for single drainholes or horizontal wells. Since the pressure at the well center ($x_D = 0$) is the lowest, the uniform-flux boundary condition can be used as an alternative to the infinite-conductivity idealization for two equal length drainholes, drilled in diametrically opposite directions from a single vertical well.

3.8 Example Application

In this section a simulated example is presented to demonstrate the application of the solutions obtained in this chapter. Table 3.8.1 presents well completion data pertinent to this test. Fig. 3.8.1 is a type curve match of pressure buildup data with a type curve similar to that shown in Fig. 3.7.3. The unbroken lines represent the normalized pressure responses of the drawdown type curve. (The dimensionless pressure curves are not shown here.) The circles represent the normalized pressure responses. To compute the normalized pressure responses for the "field" curve we computed derivatives with respect to the Horner[60] Time Ratio, HR. The square data points represent pressure responses and are shown principally for continuity and

TABLE 3.7.5

DIMENSIONLESS PRESSURES AT $t_D = 10^{-5}$, AT $x_D = 0$ AND $|x_D| = 1$

(UNIFORM-FLUX SOLUTION)

($z_{wD} = 0.5$, $r_{wD} = 1E\text{-}4$)

Dimensionless Well Length, L_D	Dimensionless Pressure, P_{wD}	
	Well Center, $x_D = 0$	Well Tip, $x_D = 1$
0.1	53.263	37.00
1.0	10.85	8.988
10.0	7.415	6.662
50.0	7.196	6.499
Vertical Fracture	7.161	6.468

TABLE 3.8.1

RESERVOIR AND WELL DATA

Porosity, ϕ, Fraction of Bulk Volume	0.22
Thickness, h, Feet	50.
System Compressibility, c_t, psi^{-1}	6×10^{-5}
Formation Volume Factor, B, RB/STB	1.01
Flow Rate, q, STB/D	2000
Viscosity, μ, cp	1
Well Radius, r_w, Feet	0.33
Producing Time, t, Hours	500

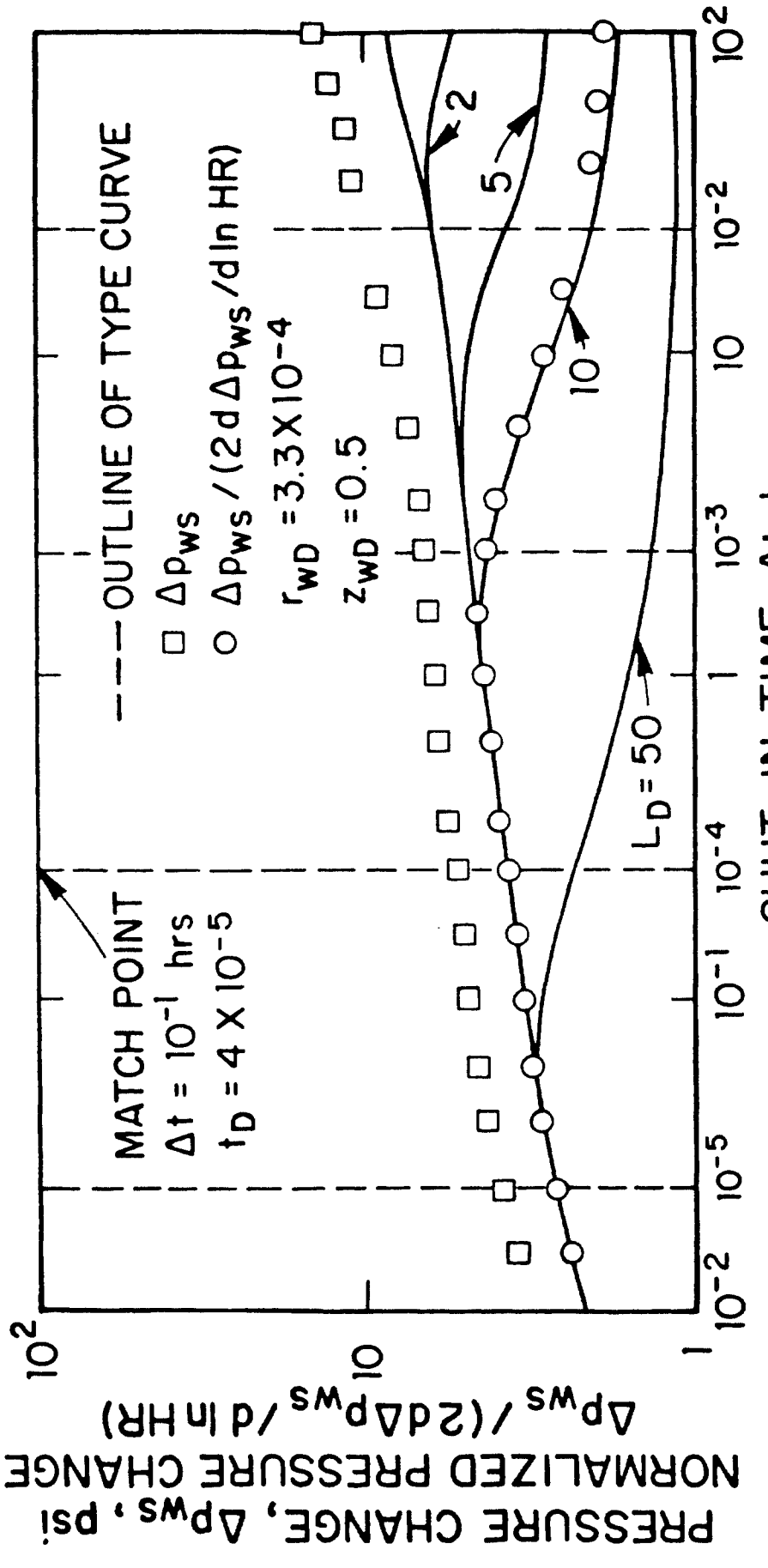

Fig. 3.8.1 - Type Curve Match of Normalized Responses – Example Application.

convenience. The match of the normalized pressure responses was conducted after aligning the ordinates of the "field" curve and the type curve and then sliding the "field" curve in the horizontal direction. Deviations at large values of Δt represent the effect of producing time[61]. The match shown in Fig. 3.8.1 indicates that $L_D = 10$, and $\Delta t = 10^{-1}$ hrs. at $t_D = 4 \times 10^{-5}$. Using these values, the pressure responses were matched as shown in Fig. 3.8.2. The circular data points in Fig. 3.8.2 are the pressure responses and the square data points are the normalized pressure responses. From the match point shown, we obtain the following results: $kh = 983.5$ md-ft., $L_h = 2000$ feet and $k_z/k = 0.25$.

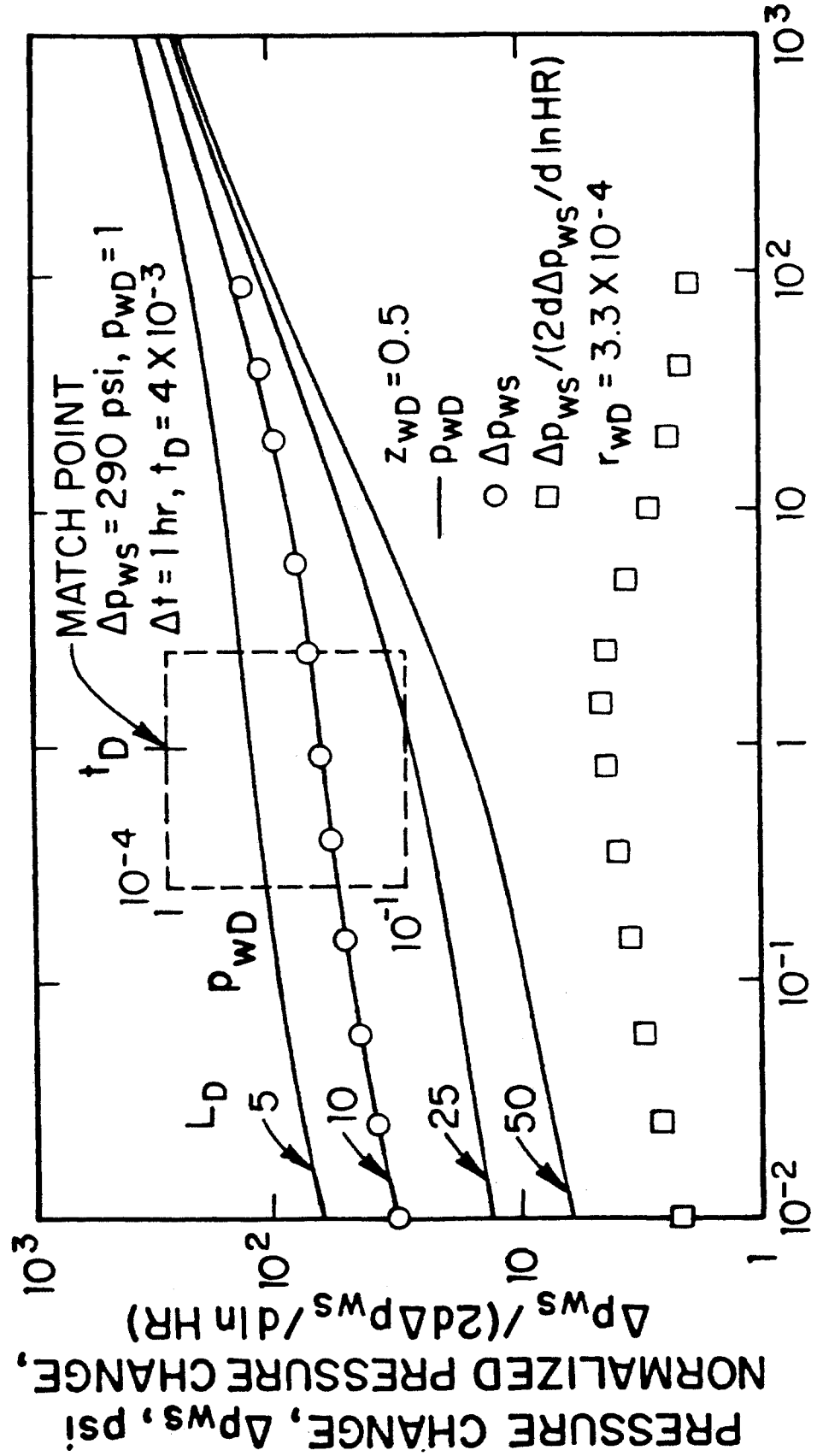

Fig. 3.8.2 - Type Curve Match of Pressure Responses – Example Application.

CHAPTER IV

PERFORMANCE OF HORIZONTAL WELLS SUBJECT TO BOTTOM WATER DRIVE

It is proposed in the literature that a horizontal well is an attractive option in situations where bottom water will play a major role on production characteristics. The objective of this chapter is to present information that enables the engineer to decide on the productivity improvements that may be expected from horizontal well completions under bottom water drive. As noted in Chapter III, when there is no fluid intrusion into the reservoir across the boundaries of the reservoir, pseudoskin factors can be used to determine the productivity improvement that can be expected from horizontal well completions. The behavior of water drive reservoirs poses a more complicated problem and an investigation of the productivities of the wells operating under such conditions requires a different treatment. In such a system, bottom water will tend to encroach into the oil zone and after some time, reach the well. Therefore, the producing history of the wells operating in the presence of contiguous water can be divided into two phases. The first phase is characterized by water-free oil production, while during the following phase, water production starts increasing at an accelerated rate. Since our primary objective is to compare horizontal and vertical well productivities with a view of developing guidelines similar to those presented in Chapter III, we only consider the first phase.

Three papers[62-64] have appeared in the literature that investigate the encroachment of water into the oil zone due to production from a horizontal well. Ref. 62 extends the classic treatment of the water coning phenomena as presented

by Muskat and Wyckoff[65] to horizontal wells operating under edge water drive conditions. Refs. 63 and 64 use the method of hodographs[52] to take into account the deformed shape of the oil-water boundary due to production from a horizontal well. Ref. 64 (also 63) states that the pattern of flow lines for the bottom water drive mechanism is the same as that for the lateral edge water drive mechanism in the vicinity of the well and hence the shape of the oil-water boundary obtained for the latter can be used for the former in the neighborhood of the well. This observation appears to be in conflict with Muskat's comparison of the two water drive mechanisms[53,66]. Our work suggests that the streamlines for edge water drive systems are significantly different from those for bottom water drive systems. In this work, we recognize the distinct flow characteristics of bottom water drive reservoirs. Although our analysis involves the assumptions used by Refs. 53 and 66, the model used here takes into account the basic phenomena underlying the behavior of wells producing under bottom water drive conditions.

In this chapter, we first develop analytical expressions describing the pressure behavior of horizontal wells subject to bottom water drive, and discuss the characteristics of horizontal well responses under bottom water drive conditions. Recently, Kuchuk *et al.*[67] have considered the pressure behavior of horizontal wells under bottom water drive. Solutions presented by Ref. 67 only consider a laterally infinite reservoir whereas this study also investigates the influence of no-flow boundaries. This aspect is particularly important for deliverability predictions.

Except the work of Muskat[66], the differences between the bottom water drive and the edge water drive mechanisms have not been discussed in detail in the literature. In this chapter, we also present a comparison of the basic phenomena underlying the bottom water drive and the edge water drive mechanisms. We then investigate the overall performance of horizontal wells under bottom water drive conditions. Comparison of horizontal and vertical well performances under bottom water drive conditions is also provided.

4.1 Transient Flow Behavior

Here we develop the analytical expressions that describe the pressure behavior of horizontal wells subject to bottom water drive. Asymptotic forms of the solution for pressure distribution suitable during the transient flow period are derived. We also investigate the conditions under which the lateral boundaries of the reservoir do not have an impact on the production characteristics of horizontal wells if the movement of bottom water is the driving force. The results presented here are for uniform-flux wells. The consequences of using the infinite-conductivity well idealization are discussed in §4.3.

I. Problem Formulation The mathematical model we consider here is similar to the one examined in Chapter III. We consider the flow of a slightly compressible fluid to a horizontal well of length L_h in a reservoir of height h. The well is assumed to be parallel to the top and the bottom boundaries of the rectangular drainage region and is located at an elavation z_w within the vertical interval. The well is modeled to be a line source. We assume that the well is produced at a constant rate. The reservoir boundary at the top of the formation ($z = h$) and the boundaries at the lateral extent of the formation ($x = y = 0$ and $x = x_e$ and $y = y_e$) are assumed to be impermeable. It is assumed that an active aquifer at the bottom of the reservoir ($z = 0$) would yield an effect identical to that of a constant pressure boundary located at the original water-oil contact and the pressure is above the bubble point. Therefore, the production is merely by virtue of the movement of the water-oil interface, not by internal dissolved gas.

To obtain a solution for pressure distribution, we use the source function approach discussed in Ref. 3. Under the assumptions stated above, we can visualize the horizontal well as the intersection of three sources: *(i)* Infinite slab source in an infinite slab reservoir:

$$S_x(x,t) = \frac{L_h}{x_e}\left[1 + \frac{4x_e}{\pi L_h}\sum_{n=1}^{\infty}\frac{1}{n}\exp\left(-\frac{n^2\pi^2\eta_x t}{x_e^2}\right)\sin n\pi\frac{L_h}{2x_e}\cos n\pi\frac{x_w}{x_e}\cos n\pi\frac{x}{x_e}\right]. \tag{4.1.1}$$

(ii) Infinite plane source in an infinite slab reservoir:

$$S_y(y,t) = \frac{1}{y_e}\left[1 + 2\sum_{n=1}^{\infty} \exp\left(-\frac{n^2\pi^2\eta_y t}{y_e^2}\right) \cos n\pi \frac{y_w}{y_e} \cos n\pi \frac{y}{y_e}\right]. \tag{4.1.2}$$

(iii) Infinite plane source in an infinite slab reservoir:

$$S_z(z,t) = \frac{2}{h}\sum_{n=1}^{\infty} \exp\left[-\frac{(2n-1)^2\pi^2\eta_z t}{4h^2}\right] \sin(2n-1)\pi\frac{z_w}{2h} \sin(2n-1)\pi\frac{z}{2h}. \tag{4.1.3}$$

The pressure drop at any point in the reservoir (except at the source location, $x = x_w, y = y_w, z = z_w$) is given by[3]

$$\Delta p(x,y,z,t) = \frac{1}{\phi c_t}\int_0^t q(\tau)\, S(t-\tau)\, d\tau \tag{4.1.4}$$

where $S(t)$ is the horizontal well source function for the problem under consideration and, by the Newman's product solution method[3], is given by

$$S(t) = S_x(x,t)\, S_y(y,t)\, S_z(z,t). \tag{4.1.5}$$

If we assume that the flux distribution along the well surface is uniform and the production from the horizontal well is at a constant rate, then $q(t) = q/L_h$. If we further assume that $k = k_x = k_y \neq k_z$, then using Eqs. 4.1.1 – 4.1.5, we obtain the following solution for the dimensionless pressure:

$$p_D = \frac{4\pi}{\tilde{x}_{eD}\tilde{y}_{eD}}\int_0^{t_D}\left[1 + 2\sum_{n=1}^{\infty}\exp\left(-\frac{n^2\pi^2\tau}{\tilde{y}_{eD}^2}\right)\cos n\pi\frac{\tilde{y}_{wD}}{\tilde{y}_{eD}}\cos n\pi\frac{\tilde{y}_D}{\tilde{y}_{eD}}\right]$$

$$\left[1 + \frac{2\tilde{x}_{eD}}{\pi}\sum_{n=1}^{\infty}\frac{1}{n}\exp\left(-\frac{n^2\pi^2\tau}{\tilde{x}_{eD}^2}\right)\sin n\pi\frac{1}{\tilde{x}_{eD}}\cos n\pi\frac{\tilde{x}_{wD}}{\tilde{x}_{eD}}\cos n\pi\frac{\tilde{x}_D}{\tilde{x}_{eD}}\right]$$

$$\sum_{n=1}^{\infty}\exp\left[-(2n-1)^2\pi^2\frac{L_D^2}{4}\tau\right]\sin(2n-1)\frac{\pi}{2}z_{wD}\sin(2n-1)\frac{\pi}{2}z_D\, d\tau. \tag{4.1.6}$$

Here p_D is the dimensionless pressure at any point in the reservoir, t_D is the dimensionless time based on the well half length, $L_h/2$, $\tilde{x}_D$ and $\tilde{y}_D$ are the dimensionless horizontal distances based on the well half length, z_D is the vertical distance based

on the formation thickness, h, and L_D is the dimensionless well half length. The well is assumed to be centered at $\tilde{x}_{wD}, \tilde{y}_{wD}, z_{wD}$. The location of the reservoir boundaries in the lateral extent of the system is defined by $\tilde{x}_{eD}$ and $\tilde{y}_{eD}$ (Fig. 4.1.1). The definitions of the dimensionless variables are given by the following equations:

$$p_D = \frac{kh}{141.2qB\mu}\left[p_i - p\left(x, y, z, z_w, L_h, t\right)\right], \tag{4.1.7}$$

$$t_D = \frac{0.001055kt}{\phi c_t \mu L_h^2}, \tag{4.1.8}$$

$$\tilde{x}_D = 2x/L_h, \tag{4.1.9}$$

$$\tilde{y}_D = 2y/L_h, \tag{4.1.10}$$

$$z_D = z/h, \tag{4.1.11}$$

and

$$L_D = \frac{L_h}{2h}\sqrt{\frac{k_z}{k}}. \tag{4.1.12}$$

Eqs. 4.1.6 – 4.1.12 assume that the vertical permeability, k_z, is different from the horizontal permeability, k, and $k = k_x = k_y$. The effect of two dimensional anisotropy of the formation is incorporated in the definition of the dimensionless well half length, L_D. [If one wishes to consider anisotropy in all three directions, then k in Eqs. 4.1.6 – 4.1.12 should be replaced by $\sqrt[3]{k_x k_y k_z}$ or $\sqrt{k_x k_y}$ and the right hand side of Eq. 4.1.6 must be multiplied by $\sqrt{k/k_y}$. This would also require that we define $\tilde{x}_D = (2x/L_h)\sqrt{k/k_x}$ and $\tilde{y}_D = (2y/L_h)\sqrt{k/k_y}$.]

<u>II. Asymptotic Approximations</u> As discussed in Ref. 3, the asymptotic forms of the solution given by Eq. 4.1.6 can be obtained by examining the asymptotic forms of the source functions used to construct the solution (Eqs. 4.1.1 – 4.1.3). The appropriate asymptotic expressions for the source functions given by Eqs. 4.1.1 – 4.1.3 can be obtained by considering the conditions under which the phsical boundaries of the reservoir do not influence the source response. In case of slab sources, it is also possible to consider the influence of flow across the tips of the slab source.

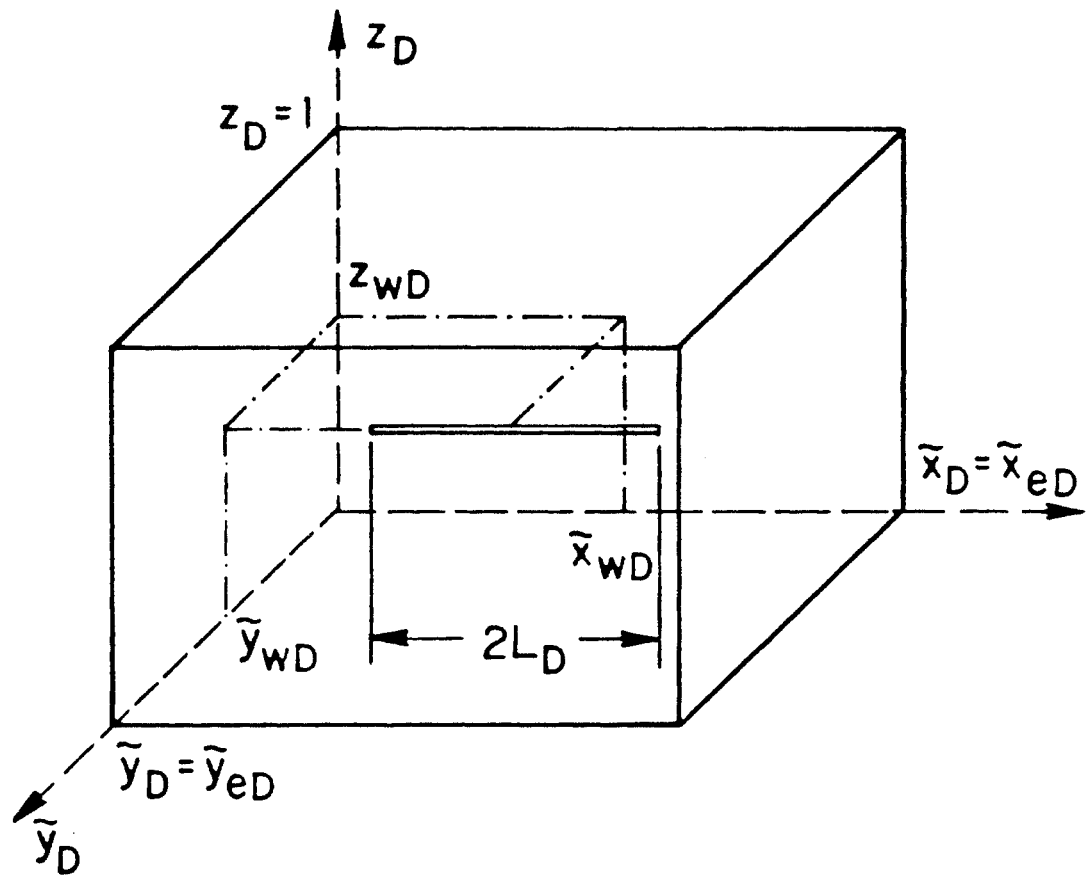

Fig. 4.1.1 - Coordinate System of Eq. 4.1.6.

We will first examine the situation where the lateral boundaries of the reservoir do not have an impact on the pressure distribution. In this case, we take into account the influence of the top and the bottom reservoir boundaries and the convergence of flow across the tips of the well. When the boundaries at $\tilde{y}_D = 0$ and $\tilde{y}_{eD}$ do not influence the pressure response, we can replace the source function S_y (Eq. 4.1.2) by its short time approximation given by[3]

$$S_y(y,t) = \frac{\exp\left[-\frac{(y-y_w)^2}{4\eta_y t}\right]}{2\sqrt{\pi\eta_y t}}. \tag{4.1.13}$$

The time period during which the influence of the boundaries in the y direction is not felt is defined by the condition for the source function S_y to be replaced by its short time approximation; that is,

$$t_D \leq \min \begin{cases} (\tilde{y}_D + \tilde{y}_{wD})^2 / 20, \\ [(\tilde{y}_D + \tilde{y}_{wD}) - 2\tilde{y}_{eD}]^2 / 20. \end{cases} \tag{4.1.14}$$

The source function S_x given by Eq. 4.1.1 involves two types of boundaries; the boundaries of the reservoir at $\tilde{x}_D = 0$ and $\tilde{x}_{eD}$, and the slab boundary (the tips of the well) at $\tilde{x}_D = \tilde{x}_{wD} - 1$ and $\tilde{x}_D = \tilde{x}_{wD} + 1$. Therefore, it is possible to make a two-step approximation for S_x. If we assume that the influence of the reservoir boundaries has not been felt yet but the influence of the slab boundary might have been felt, then the source function S_x can be replaced by an infinite slab source in an infinite reservoir[3]:

$$S_x(x,t) = \frac{1}{2}\left\{\text{erf}\left[\frac{L/2 + (x - x_w)}{2\sqrt{\eta_x t}}\right] + \text{erf}\left[\frac{L/2 - (x - x_w)}{2\sqrt{\eta_x t}}\right]\right\}. \tag{4.1.15}$$

Eq. 4.1.15 would approximate the source function S_x given by Eq. 4.1.1 for the dimensionless times given by

$$t_D \leq \min \begin{cases} (\tilde{x}_D + \tilde{x}_{wD})^2 / 20, \\ [(\tilde{x}_D + \tilde{x}_{wD}) - 2\tilde{x}_{eD}]^2 / 20. \end{cases} \tag{4.1.16}$$

If we replace the source functions S_x and S_y in Eq. 4.1.5 by the short time approximations given by Eqs. 4.1.13 and 4.1.15 and use the resulting form of Eq. 4.1.5 in Eq. 4.1.4, we obtain the following asymptotic approximation:

$$p_D = \frac{\sqrt{\pi}}{2}\int_0^{t_D}\left[\text{erf}\frac{(1+x_D)}{2\sqrt{\tau}} + \text{erf}\frac{(1-x_D)}{2\sqrt{\tau}}\right]\exp\left(-\frac{y_D^2}{4\tau}\right)$$

$$\sum_{n=1}^{\infty} \exp\left[-(2n-1)^2 \pi^2 \frac{L_D^2}{4}\tau\right] \sin(2n-1)\frac{\pi}{2} z_D \sin(2n-1)\frac{\pi}{2} z_{wD} \frac{d\tau}{\sqrt{\tau}}. \quad (4.1.17)$$

In physical terms, this solution represents the pressure distribution due to production from a horizontal well in a laterally infinite reservoir. Note that in Eq. 4.1.17, the definitions of the dimensionless distances in x and y directions are different from those used in Eq. 4.1.6 and are given, respectively, by (see Fig. 4.1.2)

$$x_D = 2(x - x_w)/L_h, \quad (4.1.18)$$

and

$$y_D = 2(y - y_w)/L_h. \quad (4.1.19)$$

This change is only introduced for convenience in presenting the results. The times for which Eq. 4.1.17 approximates Eq. 4.1.6 can be found by combining the conditions given in Eqs. 4.1.14 and 4.1.17 and are given by

$$t_D \leq \min \begin{cases} (\tilde{x}_D + \tilde{x}_{wD})^2/20, \\ [(\tilde{x}_D + \tilde{x}_{wD}) - 2\tilde{x}_{eD}]^2/20, \\ (\tilde{y}_D + \tilde{y}_{wD})^2/20, \\ [(\tilde{y}_D + \tilde{y}_{wD}) - 2\tilde{y}_{eD}]^2/20. \end{cases} \quad (4.1.20)$$

Assuming that the well is located at the center of the areal extent of the reservoir ($\tilde{x}_{wD} = \tilde{x}_{eD}/2 = x_{eD}$ and $\tilde{y}_{wD} = \tilde{y}_{wD}/2 = y_{eD}$; see Figs. 4.1.1 and 4.1.2), the minimum of the right hand side of Eq. 4.1.20 is given by

$$t_D \leq \min \begin{cases} x_{eD}^2/20, \\ y_{eD}^2/20. \end{cases} \quad (4.1.21)$$

Prior to the time the influence of the source boundary (well tips) is felt, the source function S_x can be replaced by the short time approximation of Eq. 4.1.15 given by[3]

$$S_x(x,t) = \frac{\beta}{2}, \quad (4.1.22)$$

where $\beta = 2$ for $|x - x_w| < L_h/2$, $\beta = 1$ for $|x - x_w| = L_h/2$, and $\beta = 0$ for $|x - x_w| > L_h/2$. The approximation given by Eq. 4.1.22 is applicable when

$$t_D \leq \delta_D^2/20, \quad (4.1.23)$$

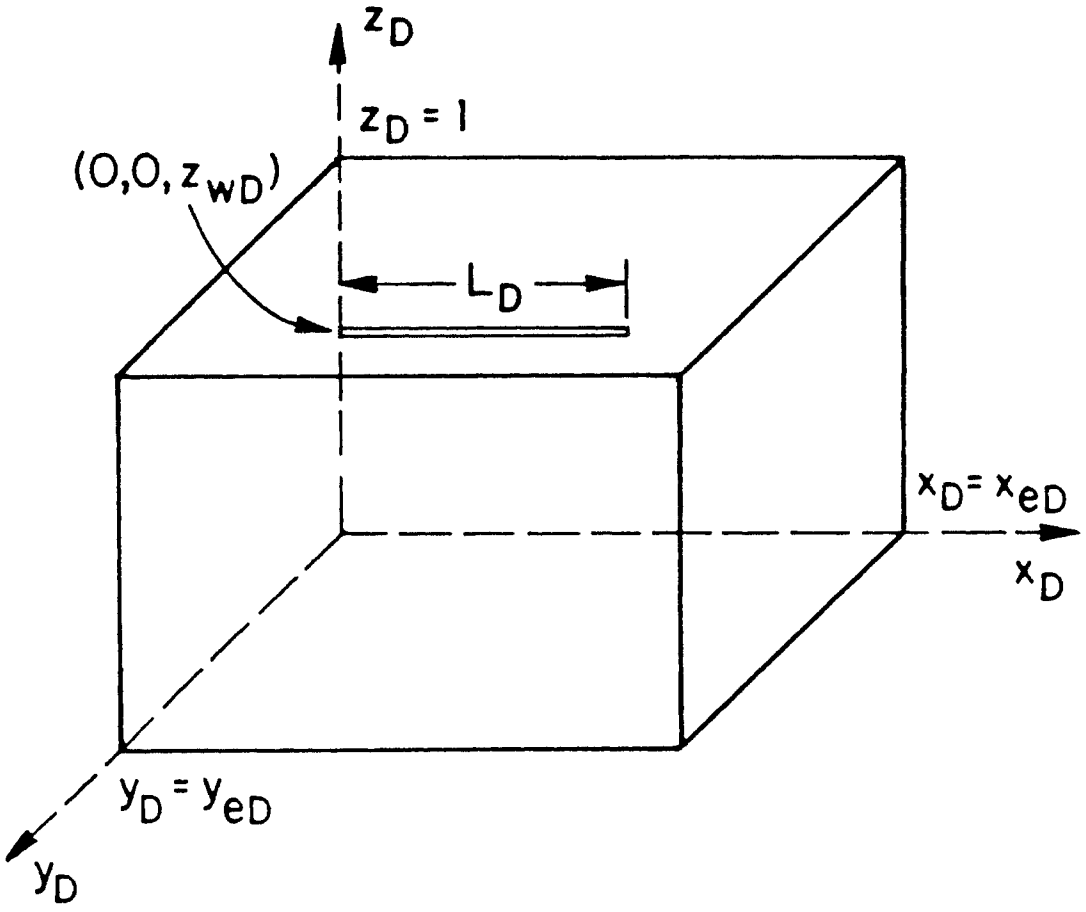

Fig. 4.1.2 - Coordinate System of Eq. 4.1.17.

where $\delta_D = 1 - |x_D|$ for $|x_D| < 1$ and $\delta_D = 2$ for $|x_D| = 1$. Using the short-time approximations for S_x and S_y given by Eqs. 4.1.22 and 4.1.13, respectively, and S_z given by Eq. 4.1.3, we obtain

$$p_D = \sqrt{\pi}\frac{\beta}{2}\int_0^{t_D} \exp\left(-\frac{y_D^2}{4\tau}\right)\sum_{n=1}^{\infty}\exp\left[-(2n-1)^2\pi^2\frac{L_D^2}{4}\tau\right]$$

$$\sin(2n-1)\frac{\pi}{2}z_D \sin(2n-1)\frac{\pi}{2}z_{wD}\frac{d\tau}{\sqrt{\tau}}. \tag{4.1.24}$$

The time limit for the approximation given by Eq. 4.1.24 to be valid is obtained by combining the conditions given by Eqs. 4.1.14 and 4.1.23 and is given by

$$t_D \leq \min\begin{cases} \delta_D^2/20, \\ (\tilde{y}_D + \tilde{y}_{wD})^2/20, \\ [(\tilde{y}_D + \tilde{y}_{wD}) - 2\tilde{y}_{eD}]^2/20. \end{cases} \tag{4.1.25}$$

Physically, this solution would represent the pressure distribution in a reservoir in which the flow in the x direction is negligible. We can argue that this would be the case where the horizontal well length is long enough for the influence of the horizontal boundaries of the reservoir to be felt prior to the influence of convergence of flow across the tips of the well.

At very early times, the convergence of flow toward the well would be from the close neighborhood of the well and therefore none of the physical boundaries of the reservoir (including the top and the bottom boundaries) and the tips of the well would influence the pressure response. Then, at very early times, we can replace the individual source functions by their appropriate short time approximations given in Ref. 3. The short time approximations of S_x and S_y are given by Eqs. 4.1.23 and 4.1.13, respectively. The short time approximation of S_z is also given by the right hand side of Eq. 4.1.23 with y replaced by z. The appropriate asymptotic form of Eq. 4.1.6 during this early flow period is defined by the following equation:

$$p_D(|x_D| \leq 1, y_D, z_D, z_{wD}, L_D, t_D) = -\frac{\beta}{8L_D}\ \mathrm{Ei}\left\{-\frac{[(z_D - z_{wD})/L_D]^2 + y_D^2}{4t_D}\right\}. \tag{4.1.26}$$

In Eq. 13, β is a constant equal to 2 for $|x_D| < 1$, 1 for $|x_D| = 1$, and 0 for $|x_D| > 1$. The approximate expression for the duration of this flow period is given by

$$t_D \leq \min \begin{cases} \delta_D^2/20, \\ \left(\tilde{y}_D + \tilde{y}_{wD}\right)^2/20, \\ \left[\left(\tilde{y}_D + \tilde{y}_{wD}\right) - 2\tilde{y}_{eD}\right]^2/20, \\ \left(z_D + z_{wD}\right)^2/\left(20L_D^2\right), \\ \left[\left(z_D + z_{wD}\right) - 2\right]^2/\left(20L_D^2\right). \end{cases} \tag{4.1.27}$$

Here $\delta_D = 1 - |x_D|$ and 2 for $|x_D| < 1$ and $|x_D| = 1$, respectively.

The asymptotic expressions given by Eqs. 4.1.17, 4.1.24, and 4.1.26, and the time limits for these expressions to be applicable (Eqs. 4.1.20, 4.1.25, and 4.1.27) are extremely useful in that they provide valuable information on the interaction of the physical boundaries of the system. Note that the asymptotic approximations given by Eqs. 4.1.17 and 4.1.24 take into account the influence of the constant pressure bottom boundary (in obtaining the approximations given by Eqs. 4.1.17 and 4.1.24, we used the exact expression for the source function S_z given by Eq. 4.1.3). The constant pressure bottom boundary of the reservoir would manifest its existence by stabilizing the pressure gradients developed by the convergence of flow toward the pressure sink created at the well location due to extraction of fluids from the well. This would bring the system to a steady state and the conditions at every point in the reservoir established at the onset of steady state would be preserved thereafter. We will investigate the steady flow behavior in §4.2. For our discussion in this section, we only note the onset of the stedy flow period.

Examining the expression for the source function S_z given by Eq. 4.1.3, we can decide that S_z becomes negligible (within 1 %) when the argument of the exponential function in Eq. 4.1.3 becomes less than -5. This indicates that the horizontal well source function (Eq. 4.1.5) $S(t) \approx 0$ when $t_D \geq 20/(\pi L_D)^2$, and from Eq. 4.1.4, we can decide that for times $t_D \geq 20/(\pi L_D)^2$, the pressure distribution in the reservoir is steady. Therefore, the onset of stedy state is determined by

$$t_D \geq \frac{20}{(\pi L_D)^2}. \tag{4.1.28}$$

In the following, we will use the relation given by Eq. 4.1.28 to determine the conditions under which one or several of the physical boundaries of the system

(including the tips of the well) would not affect the pressure distribution in the reservoir.

III. Boundary of Influence In light of the discussion presented above, it is clear that if steady state occurs prior to the time the influence of a closed boundary manifests itself, then the existence of that boundary will not be evident; that is, assuming that the well is located at the center of the areal extent of the reservoir, the lateral boundaries of the reservoir would not affect the pressure distribution if times predicted by Eq. 4.1.28 occur earlier than the times predicted by Eq. 4.1.21. If we denote the distances at which the influence of production from the well will not be evident in the x and y directions by x_{iD} and y_{iD}, respectively, then x_{iD} and y_{iD} may be obtained by equating the right hand sides of Eqs. 4.1.21 and 4.1.28:

$$x_{iD}L_D = \frac{x_i}{h}\sqrt{\frac{k_z}{k}} = \frac{20}{\pi} \tag{4.1.29}$$

and

$$y_{iD}L_D = \frac{y_i}{h}\sqrt{\frac{k_z}{k}} = \frac{20}{\pi}. \tag{4.1.30}$$

(Detailed computations suggest that Eqs. 4.1.29 and 4.1.30 overestimate the distance of "the influence limit" and, for all practical purposes, the constant $20/\pi$ on the right hand sides of Eqs. 4.1.29 and 4.1.30 can be replaced by $7.2/\pi$.) From Eqs. 4.1.29 and 4.1.30, it can be concluded that if $x_{iD} \leq x_{eD}$ and $y_{iD} \leq y_{eD}$, then Eq. 4.1.17 would represent the pressure behavior of the entire system for all times. Eq. 4.1.29 also indicates that the influence of flow across the tips of the well is negligible if $L_D \geq 20/\pi$ since in this case flow does not occur in the reservoir beyond the tips of the well ($x_i \geq L_h/2$ or $x_{iD} \geq 1$). Therefore, we can decide that the asymptotic approximation given by Eq. 4.1.24 can be used to represent the pressure behavior of the entire system for all times if $L_D \geq 20/\pi$.

The conclusion that can be derived from Eqs. 4.1.29 and 4.1.30 is that if bottom water drive dominates the well response, then regions beyond the distances given by Eqs. 4.1.29 and 4.1.30 will not be drained by the horizontal well. In other

words, the constant pressure bottom boundary establishes no-flow boundaries in the lateral directions without regard to the existence or nonexistence of a physical boundary, provided that such boundaries are far enough. Therefore the maximum drainage area of a horizontal well subject to bottom water drive is determined by the "boundary of influence" of the well (Eqs. 4.1.29 and 4.1.30), all other things being the same. It should be noted that this conclusion is independent of the rates of production. In essence, Eqs. 4.1.29 and 4.1.30 provide us with guidelines for spacing horizontal wells in a multiwell pattern. Actually, this observation is generic to bottom water drive systems; that is, it is not restricted to horizontal wells. If we note that Eqs. 4.1.29 and 4.1.30 were obtained by only noting the times for which the influence of the constant pressure boundary would dominate the well response before the influence of the no-flow boundaries becomes evident and also realize that these times would be independent of the type of well completion (see the time limits for the approximations of various source functions given in Ref. 3), we can conclude that the condition expressed by Eqs. 4.1.29 and 4.1.30 would also be independent of the type of well completion. We will investigate the consequences of this condition in more detail when we discuss the productivities of wells subject to bottom water drive. For now, we make two observations: First, Eqs. 4.1.29 and 4.1.30 indicate that if bottom water drive is the major producing mechanism, then small formation thickness or large vertical vs. horizontal permeability contrast reduces the maximum drainage area of the well. Second, the information obtained from the analysis of well test data, regardless of how long the test is run, may only reflect the properties of the part of the reservoir in the vicinity of the well.

<u>IV. Computation of Well Responses</u> In this study, the horizontal well is modeled as a line source. In §3.3, we discussed that the line source well approximation of a horizontal well of finite radius is acceptable when

$$t_D \geq 25\left[(z_D - z_{wD})^2 / L_D^2 + y_D^2\right]. \tag{4.1.31}$$

We also showed that for the case where the horizontal well is located between the

impermeable top and bottom boundaries, the circle with the radius

$$r_D = \sqrt{(z_D - z_{wD})^2 / L_D^2 + y_D^2}, \tag{4.1.32}$$

and located at $x_D = y_D = z_D - z_{wD} = 0$ can be used to define the wellbore radius. For an isotropic system, our computations indicate that when the bottom boundary of the reservoir is at a constant pressure, the dimensionless pressure computed by Eq. 4.1.17 never changes more than 0.7 % along the circumference of the wellbore defined by Eq. 4.1.32. For the range of variables, $0.1 \leq L_D \leq 100$, $0.0625 \leq z_{wD} \leq 1$, and $5 \times 10^{-5} \leq r_{wD} \leq 5 \times 10^{-4}$, we observed that the pressures computed at $z_D = z_{wD}$, $y_D = r_{wD}$, where $r_{wD} = 2r_w/L_h$, would best represent the average pressure at the circumference of the wellbore. Dimensionless pressures computed at $y_D = 0$, $z_D = z_{wD} + L_D r_{wD}$ and those computed at $y_D = r_{wD}$, $z_D = z_{wD}$, however, do differ approximately 0.2 %. In the rest of this text, we will use the point $y_D = 0$, $z_D = z_{wD} + L_D r_{wD}$ to compute wellbore pressures. We will define the dimensionless wellbore radius by the relation

$$r_{wDz} = L_D r_{wD} = \frac{r_w}{h}\sqrt{\frac{k_z}{k_y}}. \tag{4.1.33}$$

Note that r_{wDz} is based on the formation thickness, h, whereas r_{wD} is based on the horizontal well half length, $L_h/2$. Therefore the definition of the dimensionless wellbore radius as given by Eq. 4.1.33 is more convenient in presenting solutions with the dimensionless well half length being the variable of interest and in comparing horizontal well responses with the responses of unstimulated vertical wells.

The above discussion can be readily extended to anisotropic systems. Care must be taken in interpreting the results since in this case the equipotential surfaces are ellipses at early times; that is, we should not expect pressures to be identical for all values of y and z, for a fixed value of r_D (Eq. 4.1.32). This point is particularly important if we compare solutions given here with numerical solutions.

<u>V. Discussion of Well Responses</u> A typical set of pressure responses of horizontal wells, located at the reservoir mid-height ($z_{wD} = 0.5$), computed by Eq. 4.1.17

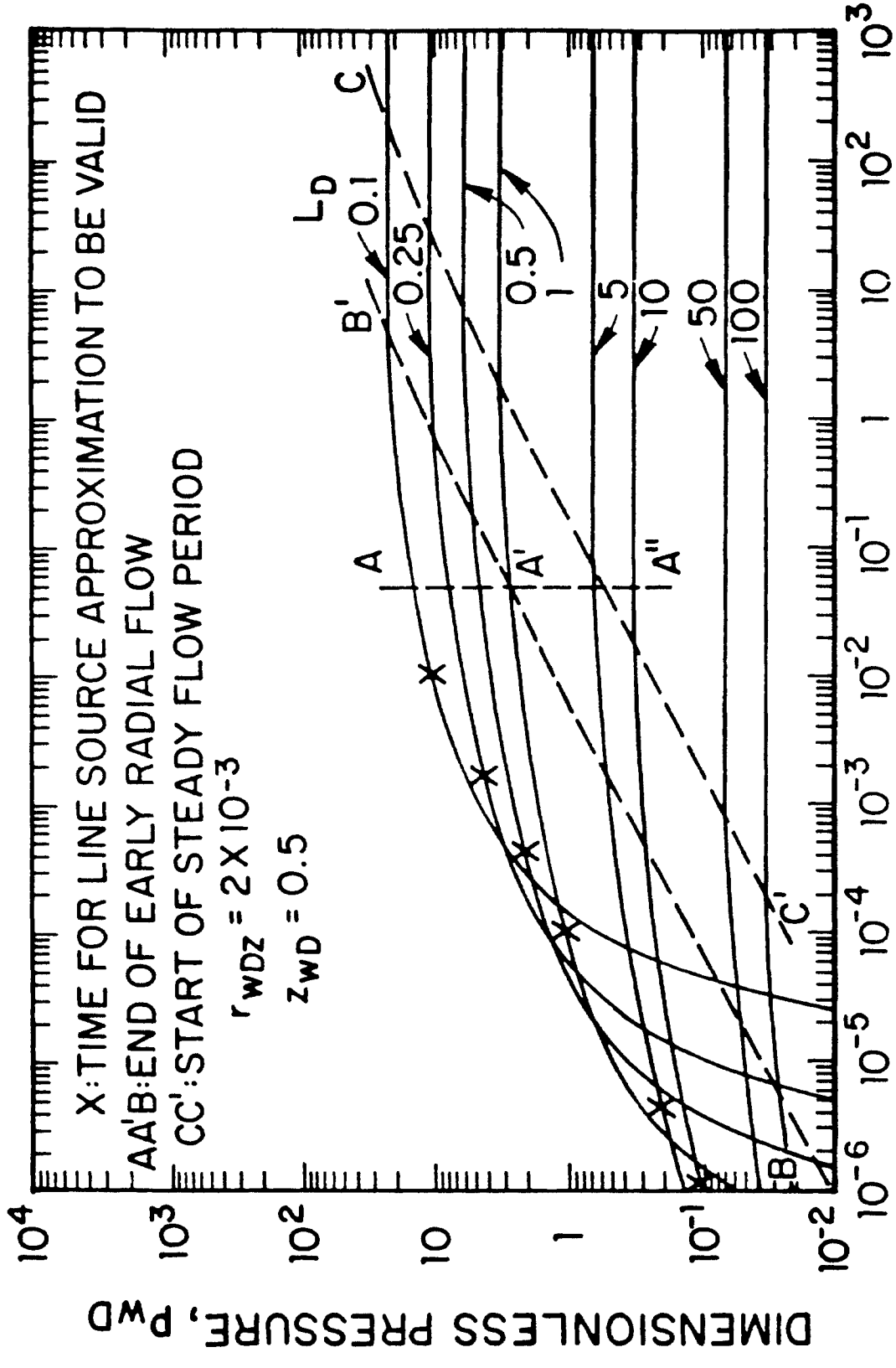

Fig. 4.1.3 - A Typical Set of Pressure Responses – Laterally Infinite Reservoir.

is plotted in Fig. 4.1.3. Each curve in this set of pressure responses corresponds to a specific value of the dimensionless well half length, L_D. We have considered well lengths in the range $0.1 \leq L_D \leq 100$. The dimensionless wellbore radius, r_{wDz}, used in this figure is 2×10^{-3}. The letter x indicates the times at which the line source well assumption becomes applicable for a finite radius horizontal well and is given by Eq. 4.1.31. The dashed lines marked AA' and $A'B$ denote the times for the end of the initial radial flow period (Eq. 4.1.26) and these times are given by Eq. 4.1.27. The line $AA'A''$ is given by $t_D = 1/20$ (the first condition of Eq. 4.1.27) and corresponds to the time at which flow across the well tips affects the pressure response. The line BB' is given by $t_D = \min\{(z_D + z_{wD})^2 / (20L_D^2), [(z_D + z_{wD}) - 2]^2 / (20L_D^2)\}$ (the last two conditions of Eq. 4.1.27) and corresponds to the time at which the boundaries located at the top and the bottom of the reservoir influence the well response. For the case shown here ($z_{wD} = 0.5$), the intersection point of the lines $AA'A''$ and BB' falls on the response curve for $L_D = 1$ and is denoted by A'. The figure indicates that the end of the early radial flow period is dictated by the top and the bottom boundaries for $L_D \geq 1$ and by the flow of fluid across the well tips if $L_D < 1$. Noting the differences between the times denoted by the letter x and the lines AA' and $A'B$, one can conclude that the exponential integral solution (Eq. 4.1.26) would not be very useful for analyzing the early time responses of ultra short horizontal wells ($L_D \leq 0.1$). As discussed in §4.4, the overall performance of ultra short horizontal wells shows more resemblence to point source wells (single perforation). Ultra short horizontal wells, however, may not have any conceivable use in oil production practices and this discussion is presented primarily for completeness. An extensive discussion of early radial flow period and the information that can be extracted from it is presented in Chapter III and will not be repeated here. Of primary interest here are the events that develop subsequent to the times predicted by Eq. 4.1.27 (or the lines AA' and $A'B$ on Fig. 4.1.3).

In physical terms, Eq. 4.1.27 represents the times for the isopotential lines concentric with the well axis to be distorted either because of movement of fluid across the well tips or because of the influence of the reservoir boundaries (the top

or the bottom boundary of the reservoir). As discussed above, at times predicted by Eq. 4.1.28, the influence of the constant pressure bottom boundary is established and the flow in the reservoir becomes steady. The dashed line marked CC' on Fig. 4.1.3 denotes the times for the beginning of the steady flow period and is only a function of L_D. Note from the first condition of Eq. 4.1.27 and Eq. 4.1.28 that the intersection point of the lines $AA'A''$ and CC' would approximately fall on the response curve for $L_D = 6.37$. Since there is no flow in the x direction prior to the times denoted by the line $AA'A''$ and the conditions existing in the reservoir at the instant denoted by the line CC' are preserved at subsequent times, it appears that there will be no flow in the x direction for all times if $L_D \geq 6.37$. In other words, for $L_D \geq 6.37$, flow occurs primarily in the vertical $(y - z)$ plane. (Our computations and the analytical results obtained during the investigation of the steady flow period presented in §4.2 suggest that, for $L_D \geq 7.2/\pi$, the contribution of the three-dimensional flow effects becomes negligible for all practical purposes.)

The responses shown in Fig. 4.1.3 are replotted in Fig. 4.1.4 as a function of the dimensionless time group $t_D L_D^2$. Note that $t_D L_D^2$ is independent of the well length, L_h, and the responses shown in Fig. 4.1.4 for different values of L_D correspond to the same range of the real time, t. Therefore, the dimensionless time group $t_D L_D^2$ is introduced here for convenience in discussing the influence of the well length, L_h. It is clear from the shape of the pressure response curves presented in Fig. 4.1.4 that, unless an estimate of L_D is available (that is, L_h, h, and k/k_z can be obtained by some independent means), type curve matching the pressure responses with the theoretical responses shown in Fig. 4.1.4 (or Fig. 4.4.3) may not provide reliable estimates of parameters. In order to alleviate this difficulty, in Fig. 4.1.4, we have included the pressure responses in terms of Chow's pressure group[4], $p_{wD}/\left[2\left(dp_{wD}/d\ln t_D\right)\right]$. For convenience, we refer to these responses as normalized responses. The procedure for type curve matching and the advantages of using Chow's pressure group for horizontal and vertically fractured wells are discussed in §3.6.

At early times (times predicted by Eq. 4.1.27), the normalized responses fol-

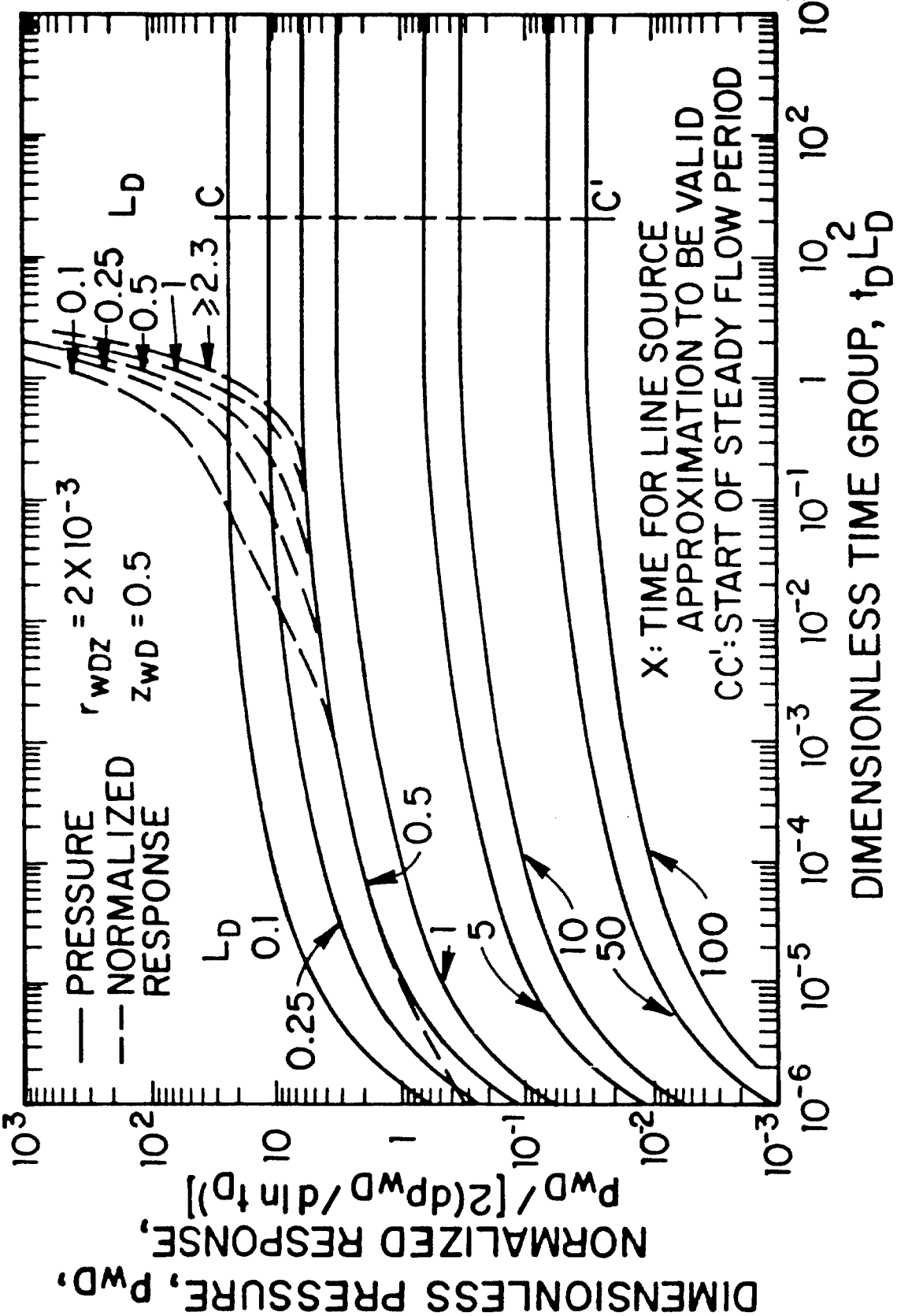

Fig. 4.1.4 - Pressure and Normalized Responses as a Function of $t_D L_D^2$ – Laterally Infinite Reservoir.

low the pressure responses corresponding to the case for $L_D = 0.5$. This result can be understood if we replace the exponential integral function in Eq. 4.1.26 by its logarithmic approximation during the period of time determined by Eqs. 4.1.27 and 4.1.31 and note that in this case $dp_{wD}/d\ln t_D = 1/(4L_D)$ and thus $p_{wD}/[2(dp_{wD}/d\ln t_D)] = 2L_D p_{wD}$. The normalized responses follow the pressure response curve for $L_D = 0.5$ until the end of the early radial flow period (Eq. 4.1.27 or the line $AA'B$ in Fig. 4.1.3). After deviating from the pressure responses for $L_D = 0.5$, the normalized responses bend upwards and eventually approach infinity at the onset of the steady flow period. Fig. 4.1.4 indicates that for $L_D \geq 2.3$, the normalized response curves merge to yield a single curve. As explained above, for $L_D \geq 2.3$, the contribution of flow across the tips of the well is negligible; hence, the well tips do not influence the flow characteristics of the well (and therefore the length of the well does not have influence on the shape of the response curves). The distinct character of the normalized response curves for $L_D < 2.3$, subsequent to deviations from the radial flow behavior, can be used to obtain an estimate of L_D. Obviously, for $L_D \geq 2.3$, the value of L_D cannot be obtained by type curve matching procedure if the bottom boundary is at a constant pressure.

The discussion presented on Figs. 4.1.3 and 4.1.4 assumes that the reservoir is either infinite in the areal extent or that $x_{eD} \geq x_{iD}$ and $y_{eD} \geq y_{iD}$. If we assume that $x_{eD} = y_{eD}$ (square drainage region), then from Eqs. 4.1.29 and 4.1.30, we can conclude that the lateral boundaries of the reservoir would not have an influence on the pressure responses if $x_{eD}L_D \geq 20/\pi$. In fact, as discussed above, for $L_D \geq 7.2/\pi$, flow across the tips of the well is negligible. Since the minimum value x_{eD} can take is 1, it is therefore reasonable to expect that the influence of the lateral boundaries would also be negligible if $x_{eD}L_D \geq 7.2/\pi$. In order to investigate the influence of the lateral boundaries, the pressure responses and the normalized responses computed by Eq. 4.1.6 for $L_D = 0.5$, $z_{wD} = 0.5$, and $r_{wDz} = 2 \times 10^{-3}$ are plotted in Fig. 4.1.5. The unbroken lines represent the pressure responses and the dashed lines represent the normalized responses. Pressure responses for $x_{eD} \geq 14.4/\pi$ are identical. Similar behavior is also observed for the normalized

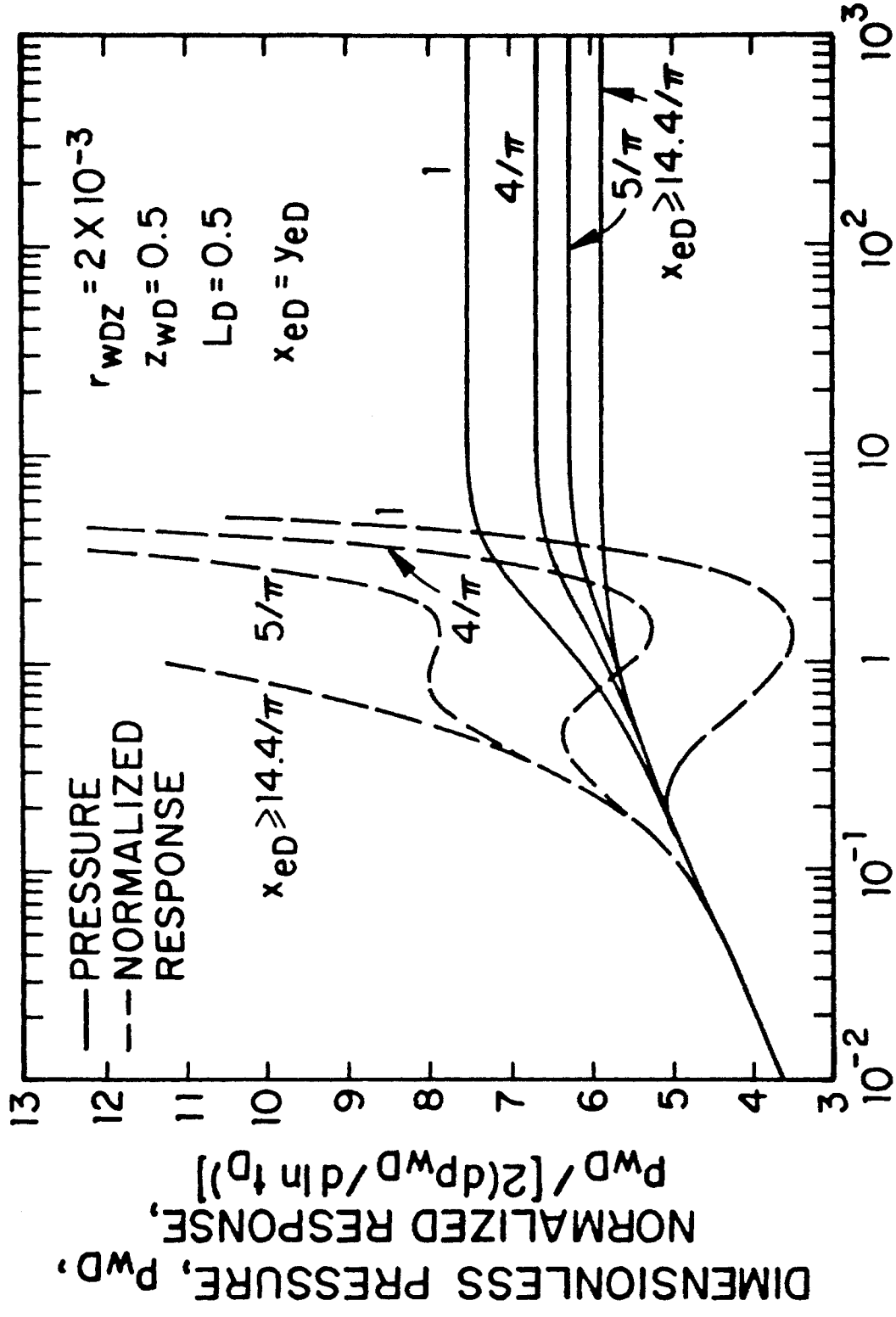

Fig. 4.1.5 - Influence of Lateral Boundaries on Pressure and Normalized Responses.

responses. For smaller values of x_{eD}, the pressure responses depart from the responses for $x_{eD} \geq 14.4/\pi$; the upward bend in this curves indicates that the system undergoes a depletion period due to the bounded nature of the reservoir. Ultimately steady flow prevails. The same behavior is evident in the normalized responses. The maxima and the minima shown by these responses are a consequence of the interplay of changes in flow regimes and the influence of various boundaries. A detailed discussion of the behavior of normalized responses is useful for they provide insight regarding the influence of flow regimes and the boundaries. For large values of x_{eD} ($x_{eD} \geq 14.4/\pi$), the constant pressure boundary dominates the well response and the normalized responses approach infinity asymptotically. The influence of the lateral boundaries, as already discussed, is negligible. For the solutions corresponding to $x_{eD} = 5/\pi$ and $4/\pi$ (in these cases $y_e > L_h/2$), the upward bend in the curves is caused by the flow across the well tips. The downward trend in the normalized responses reflects the influence of the lateral boundaries (for a completely bounded system, $p_{wD}/\left[2\left(dp_{wD}/d\ln t_D\right)\right] \rightarrow 0.5$ as t_D becomes large). When the constant pressure bottom boundary begins to provide pressure support, the normalized response curve begins to bend upwards and approaches infinity as steady state is attained. The normalized responses for $x_{eD} = 1$ represent the case where the well completely penetrates the formation in the x direction. In other words, this case is identical to that of a vertical well located in a reservoir surrounded by impermeable boundaries on three sides; the fourth boundary parallel to the well is kept at a constant pressure. As will be expected, for this case the normalized responses follow the pressure responses for a longer period of time compared to the other cases shown in this figure. When the bottom boundary begins to provide pressure support, the characteristics of the responses are similar to the other curves discussed here.

For completeness, the derivatives of the pressure responses shown on Fig. 4.1.5 with respect to the natural logarithm of time are plotted in Fig. 4.1.6. At early times, the derivative responses are constant and equal to $1/\left(4L_D\right)$. Following the end of the initial radial flow period, the responses for $x_{eD} \geq 14.4/\pi$ continuously decrease to the late time value, zero. The responses for $x_{eD} \leq 5/\pi$, on the other hand,

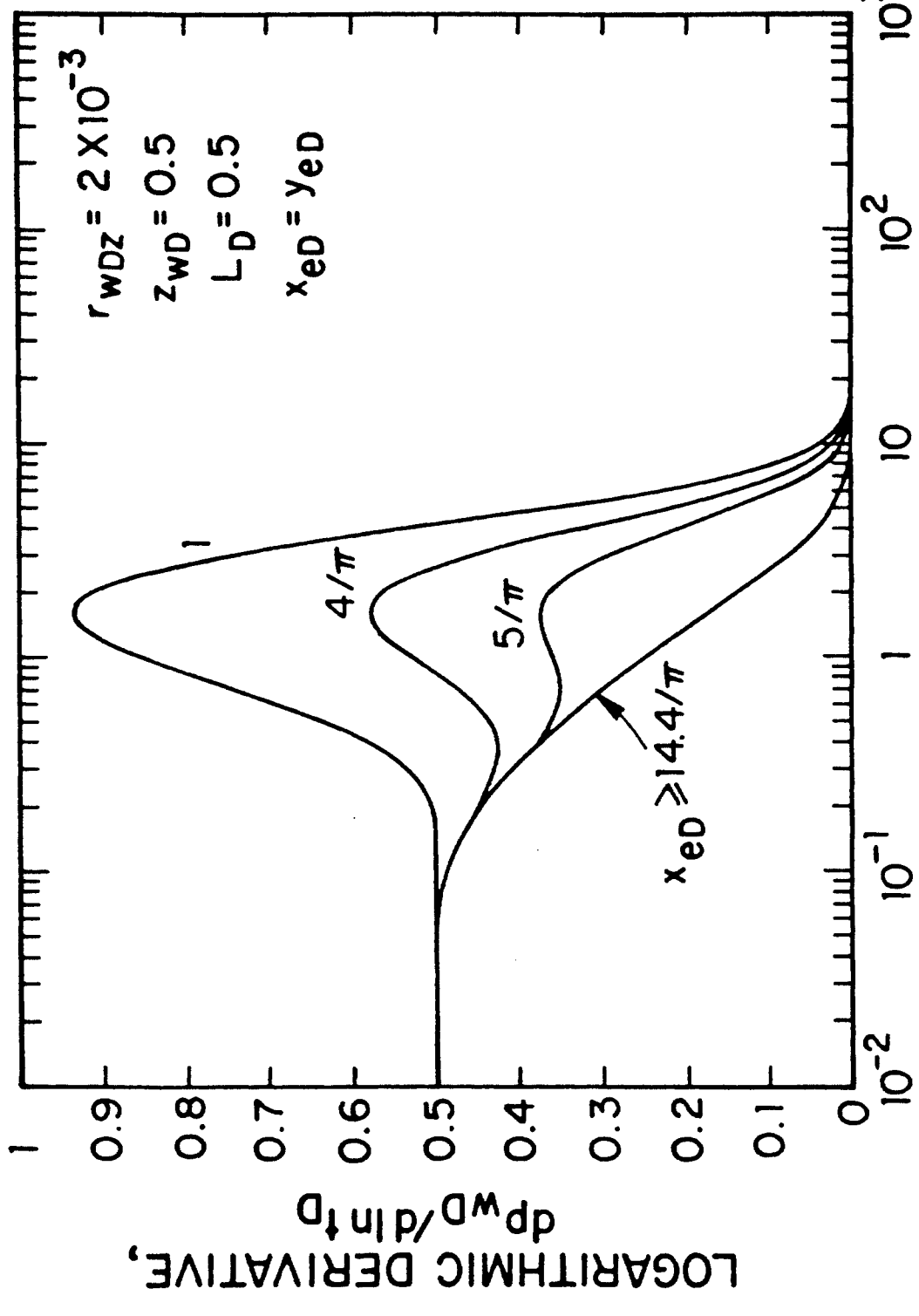

Fig. 4.1.6 - Influence of Lateral Boundaries on Derivative Responses.

display a peak, caused by the influence of the lateral boundaries of the reservoir, before they start rapidly dropping to zero (this behavior is not readily identifiable for $5/\pi < x_{eD} < 14.4/\pi$ because the influence of the lateral boundaries is masked by the influence of the constant pressure bottom boundary).

Qualitatively, the observations presented above also apply to other well locations. The expressions given above may be used to obtain the times for appropriate flow regimes to be evident. The observations also apply, in a qualitative sense, to infinite-conductivity wellbores (see §4.3). Solutions for the pressure responses for other well locations can be developed from Eqs. 4.1.6 and 4.1.17. Analysis procedures using pressure and normalized responses are identical to that discussed in Chapter III and will not be repeated here.

4.2 Steady Flow Behavior

As indicated by the results of the previous section, horizontal wells producing bottom water drive reservoirs ultimately reach a steady flow period at times dictated by the dimensionless horizontal well half length, L_D (that is, by the ratios of L_h/h and k_z/k). The appropriate asymptotic forms of Eqs. 4.1.6, 4.1.17, and 4.1.24 describing the steady flow behavior can be obtained by taking the Laplace transform of these expressions and then evaluating at the limit as the Laplace transform variable s approaches zero. In this section we first obtain the Laplace transform of the solutions given by Eqs. 4.1.6, 4.1.17, and 4.1.24. We then derive the expressions describing the steady flow behavior and present a discussion of the late time results.

I. Laplace Transforms of Solutions Here we briefly demonstrate the procedure to obtain the Laplace transform of the solutions given by Eqs. 4.1.6, 4.1.17, and 4.1.24. We first consider the Laplace transform of Eq. 4.1.6. If we define

$$S(\tau) = (1+g_1)(1+g_2)g_3 = g_3 + g_2g_3 + g_1g_3 + g_1g_2g_3, \qquad (4.2.1)$$

where

$$g_1 = 2\sum_{n=1}^{\infty} \exp\left(-\frac{n^2\pi^2\tau}{\tilde{y}_{eD}^2}\right) \cos n\pi \frac{\tilde{y}_{wD}}{\tilde{y}_{eD}} \cos n\pi \frac{\tilde{y}_D}{\tilde{y}_{eD}}, \tag{4.2.2}$$

$$g_2 = \frac{2\tilde{x}_{eD}}{\pi} \sum_{n=1}^{\infty} \frac{1}{n} \exp\left(-\frac{n^2\pi^2\tau}{\tilde{x}_{eD}^2}\right) \sin n\pi \frac{1}{\tilde{x}_{eD}} \cos n\pi \frac{\tilde{x}_{wD}}{\tilde{x}_{eD}} \cos n\pi \frac{\tilde{x}_D}{\tilde{x}_{eD}}, \tag{4.2.3}$$

and

$$g_3 = \sum_{n=1}^{\infty} \exp\left[-(2n-1)^2 \pi^2 \frac{L_D^2}{4}\tau\right] \sin(2n-1)\frac{\pi}{2} z_{wD} \sin(2n-1)\frac{\pi}{2} z_D, \tag{4.2.4}$$

then we can write Eq. 4.1.6 as

$$p_D = \frac{4\pi}{\tilde{x}_{eD}\tilde{y}_{eD}} \int_0^{t_D} S(\tau)\, d\tau. \tag{4.2.5}$$

The Laplace transform of Eq. 4.2.5 is given by

$$\mathcal{L}\{p_D\} = \frac{4\pi}{\tilde{x}_{eD}\tilde{y}_{eD}} \frac{1}{s} \mathcal{L}\{S(t_D)\}, \tag{4.2.6}$$

where s is the Laplace transform variable with respect to t_D.

The functions, g_2g_3, g_1g_3, and $g_1g_2g_3$, on the right hand side of Eq. 4.2.1 can be written as

$$g_2g_3 = \frac{2\tilde{x}_{eD}}{\pi} \sum_{n=1}^{\infty} \frac{1}{n} \sin n\pi \frac{1}{\tilde{x}_{eD}} \cos n\pi \frac{\tilde{x}_{wD}}{\tilde{x}_{eD}} \cos n\pi \frac{\tilde{x}_D}{\tilde{x}_{eD}}$$

$$\sum_{k=1}^{\infty} \exp\left\{-\left[(2k-1)^2 \pi^2 \frac{L_D^2}{4} + \frac{n^2\pi^2}{\tilde{x}_{eD}^2}\right]\tau\right\} \sin(2k-1)\frac{\pi}{2} z_{wD} \sin(2k-1)\frac{\pi}{2} z_D, \tag{4.2.7}$$

$$g_1g_3 = 2\sum_{n=1}^{\infty} \cos n\pi \frac{\tilde{y}_{wD}}{\tilde{y}_{eD}} \cos n\pi \frac{\tilde{y}_D}{\tilde{y}_{eD}}$$

$$\sum_{k=1}^{\infty} \exp\left\{-\left[(2k-1)^2 \pi^2 \frac{L_D^2}{4} + \frac{n^2\pi^2}{\tilde{y}_{eD}^2}\right]\tau\right\} \sin(2k-1)\frac{\pi}{2} z_{wD} \sin(2k-1)\frac{\pi}{2} z_D, \tag{4.2.8}$$

and

$$g_1g_2g_3 = \frac{4\tilde{x}_{eD}}{\pi} \sum_{n=1}^{\infty} \cos n\pi \frac{\tilde{y}_{wD}}{\tilde{y}_{eD}} \cos n\pi \frac{\tilde{y}_D}{\tilde{y}_{eD}} \sum_{k=1}^{\infty} \frac{1}{k} \sin k\pi \frac{1}{\tilde{x}_{eD}} \cos k\pi \frac{\tilde{x}_{wD}}{\tilde{x}_{eD}} \cos k\pi \frac{\tilde{x}_D}{\tilde{x}_{eD}}$$

$$\sum_{j=1}^{\infty} \exp\left\{ -\left[(2j-1)^2 \pi^2 \frac{L_D^2}{4} + \frac{n^2\pi^2}{\tilde{y}_{eD}^2} + \frac{k^2\pi^2}{\tilde{x}_{eD}^2} \right] \tau \right\}$$

$$\sin (2j-1)\frac{\pi}{2} z_{wD} \sin (2j-1)\frac{\pi}{2} z_D. \tag{4.2.9}$$

Then applying the Laplace transform property given by

$$\mathcal{L}\{\exp(-at)\} = \frac{1}{s+a} \tag{4.2.10}$$

to Eqs. 4.2.4 and 4.2.7 – 4.2.9, the Laplace transform of the function $S(t_D)$ on the right hand side of Eq. 4.2.6 can be easily obtained as

$$\mathcal{L}\{S(t_D)\} = \sum_{n=1}^{\infty} \frac{\sin (2n-1)\frac{\pi}{2} z_{wD} \sin (2n-1)\frac{\pi}{2} z_D}{s+a}$$

$$+\frac{2\tilde{x}_{eD}}{\pi} \sum_{n=1}^{\infty} \frac{1}{n} \sin n\pi \frac{1}{\tilde{x}_{eD}} \cos n\pi \frac{\tilde{x}_{wD}}{\tilde{x}_{eD}} \cos n\pi \frac{\tilde{x}_D}{\tilde{x}_{eD}}$$

$$\sum_{k=1}^{\infty} \frac{\sin (2k-1)\frac{\pi}{2} z_{wD} \sin (2k-1)\frac{\pi}{2} z_D}{s+b}$$

$$+2 \sum_{n=1}^{\infty} \cos n\pi \frac{\tilde{y}_{wD}}{\tilde{y}_{eD}} \cos n\pi \frac{\tilde{y}_D}{\tilde{y}_{eD}} \sum_{k=1}^{\infty} \frac{\sin (2k-1)\frac{\pi}{2} z_{wD} \sin (2k-1)\frac{\pi}{2} z_D}{s+c}$$

$$+\frac{4\tilde{x}_{eD}}{\pi} \sum_{n=1}^{\infty} \cos n\pi \frac{\tilde{y}_{wD}}{\tilde{y}_{eD}} \cos n\pi \frac{\tilde{y}_D}{\tilde{y}_{eD}} \sum_{k=1}^{\infty} \frac{1}{k} \sin k\pi \frac{1}{\tilde{x}_{eD}} \cos k\pi \frac{\tilde{x}_{wD}}{\tilde{x}_{eD}} \cos k\pi \frac{\tilde{x}_D}{\tilde{x}_{eD}}$$

$$\sum_{j=1}^{\infty} \frac{\sin (2j-1)\frac{\pi}{2} z_{wD} \sin (2j-1)\frac{\pi}{2} z_D}{s+d}. \tag{4.2.11}$$

In Eq. 4.2.11, a, b, c, and d are given, respectively, by

$$a = (2n-1)^2 \pi^2 \frac{L_D^2}{4}, \tag{4.2.12}$$

$$b = (2k-1)^2 \pi^2 \frac{L_D^2}{4} + \frac{n^2\pi^2}{\tilde{x}_{eD}^2}, \tag{4.2.13}$$

$$c = (2k-1)^2 \pi^2 \frac{L_D^2}{4} + \frac{n^2\pi^2}{\tilde{y}_{eD}^2}, \tag{4.2.14}$$

and

$$d = (2j-1)^2 \pi^2 \frac{L_D^2}{4} + \frac{n^2\pi^2}{\tilde{y}_{eD}^2} + \frac{k^2\pi^2}{\tilde{x}_{eD}^2}. \tag{4.2.15}$$

To obtain the Laplace transform of Eq. 4.1.17, we first note that

$$\text{erf}\frac{(1+x_D)}{2\sqrt{\tau}} + \text{erf}\frac{(1-x_D)}{2\sqrt{\tau}} = \frac{1}{\sqrt{\pi\tau}}\int_{-1}^{+1} \exp\left[-\frac{(x_D-\alpha)^2}{4\tau}\right] d\alpha. \tag{4.2.16}$$

Then, Eq. 4.1.17 can be written as

$$p_D = \frac{1}{2}\int_0^{t_D}\int_{-1}^{+1}\sum_{n=1}^{\infty} \exp\left[-(2n-1)^2\pi^2\frac{L_D^2}{4}\tau\right] \exp\left[-\frac{(x_D-\alpha)^2+y_D^2}{4\tau}\right]$$

$$\sin(2n-1)\frac{\pi}{2}z_D \sin(2n-1)\frac{\pi}{2}z_{wD}\, d\alpha\frac{d\tau}{\tau}. \tag{4.2.17}$$

Using the following Laplace transform relation[27]

$$\mathcal{L}\left\{\int_0^{t_D} \exp(-a^2\tau)\exp\left(-\frac{r_D^2}{4\tau}\right)\frac{d\tau}{\tau}\right\} = \frac{2}{s}\text{K}_0\left(r_D\sqrt{s+a}\right), \tag{4.2.18}$$

the Laplace transform of Eq. 4.1.17 is obtained as

$$\mathcal{L}\{p_D\} = \sum_{n=1}^{\infty}\sin(2n-1)\frac{\pi}{2}z_D \sin(2n-1)\frac{\pi}{2}z_{wD}$$

$$\int_{-1}^{+1}\frac{1}{s}\text{K}_0\left[\sqrt{(x_D-\alpha)^2+y_D^2}\sqrt{s+a}\right] d\alpha, \tag{4.2.19}$$

where a is defined by Eq. 4.2.12.

The Laplace transform of Eq. 4.1.24 can be easily obtained by using the relations given in any Laplace transform pairs table. Here we only report the resulting Laplace transform of Eq. 4.1.24:

$$\mathcal{L}\{p_D\} = \pi\frac{\beta}{2}\sum_{n=1}^{\infty}\sin(2n-1)\frac{\pi}{2}z_D \sin(2n-1)\frac{\pi}{2}z_{wD}\frac{\exp\left(-|y_D|\sqrt{s+a}\right)}{s\sqrt{s+a}}, \tag{4.2.20}$$

where a is given by Eq. 4.2.12 and $\beta = 2$, 1, and 0 for $|x_D| < 1$, $|x_D| = 1$, and $|x_D| > 1$, respectively.

II. Derivation of Steady Flow Equations In order to obtain expressions that describe the steady flow behavior of the system under consideration, we evaluate the solutions given by Eqs. 4.1.6, 4.1.17, and 4.1.24 at large values of time. This can be

accomplished most conveniently if we evaluate the counterparts of these equations in Laplace domain given by Eqs. 4.2.11, 4.2.19, and 4.2.20 as the Laplace transform variable $s \rightarrow 0$.

Consider first the Laplace domain solution given by Eq. 4.2.11. If we assume that the Laplace transform variable, s, becomes small so that the following condition is satisfied

$$s \leq \frac{a}{100}, \tag{4.2.21}$$

where a is defined by Eq. 4.2.12 (with $n = 1$), we can write the following approximation for $s^{-1}\mathcal{L}\{S(t_D)\}$:

$$\begin{aligned}\frac{1}{s}\mathcal{L}\{S(t_D)\} = \frac{1}{s}\Bigg\{ & \sum_{n=1}^{\infty} \frac{\sin(2n-1)\frac{\pi}{2}z_{wD}\sin(2n-1)\frac{\pi}{2}z_D}{a} \\ & + \frac{2\tilde{x}_{eD}}{\pi}\sum_{n=1}^{\infty}\frac{1}{n}\sin n\pi\frac{1}{\tilde{x}_{eD}}\cos n\pi\frac{\tilde{x}_{wD}}{\tilde{x}_{eD}}\cos n\pi\frac{\tilde{x}_D}{\tilde{x}_{eD}} \\ & \sum_{k=1}^{\infty}\frac{\sin(2k-1)\frac{\pi}{2}z_{wD}\sin(2k-1)\frac{\pi}{2}z_D}{b} \\ & + 2\sum_{n=1}^{\infty}\cos n\pi\frac{\tilde{y}_{wD}}{\tilde{y}_{eD}}\cos n\pi\frac{\tilde{y}_D}{\tilde{y}_{eD}}\sum_{k=1}^{\infty}\frac{\sin(2k-1)\frac{\pi}{2}z_{wD}\sin(2k-1)\frac{\pi}{2}z_D}{c} \\ & + \frac{4\tilde{x}_{eD}}{\pi}\sum_{n=1}^{\infty}\cos n\pi\frac{\tilde{y}_{wD}}{\tilde{y}_{eD}}\cos n\pi\frac{\tilde{y}_D}{\tilde{y}_{eD}}\sum_{k=1}^{\infty}\frac{1}{k}\sin k\pi\frac{1}{\tilde{x}_{eD}}\cos k\pi\frac{\tilde{x}_{wD}}{\tilde{x}_{eD}}\cos k\pi\frac{\tilde{x}_D}{\tilde{x}_{eD}} \\ & \sum_{j=1}^{\infty}\frac{\sin(2j-1)\frac{\pi}{2}z_{wD}\sin(2j-1)\frac{\pi}{2}z_D}{d}\Bigg\}. \end{aligned} \tag{4.2.22}$$

If we write

$$\begin{aligned}\frac{\sin(2n-1)\frac{\pi}{2}z_{wD}\sin(2n-1)\frac{\pi}{2}z_D}{a} = & \frac{2}{(2n-1)^2\pi^2 L_D^2} \\ & \left[\cos(2n-1)\frac{\pi}{2}(z_D - z_{wD}) - \cos(2n-1)\frac{\pi}{2}(z_D + z_{wD})\right], \end{aligned} \tag{4.2.23}$$

and note that[68]

$$\frac{2}{\pi^2 L_D^2}\sum_{n=1}^{\infty}\frac{\cos(2n-1)\frac{\pi}{2}\tilde{z}_D}{(2n-1)^2} = \frac{1}{4L_D^2}\left(1 - |\tilde{z}_D|\right); \quad [-2 \leq \tilde{z}_D \leq 2], \tag{4.2.24}$$

then we can write

$$\sum_{n=1}^{\infty} \frac{\sin(2n-1)\frac{\pi}{2} z_{wD} \sin(2n-1)\frac{\pi}{2} z_D}{a} = \frac{1}{4L_D^2} \left(z_D + z_{wD} - |z_D - z_{wD}|\right). \quad (4.2.25)$$

If we also use the relation[68]

$$\sum_{k=1}^{\infty} \frac{\cos(2k-1)\, x}{(2k-1)^2 + \xi^2} = \frac{\pi}{4\xi} \frac{sh\left[\left(\frac{\pi}{2} - x\right)\xi\right]}{ch\left(\frac{\pi}{2}\xi\right)}; [0 \le x \le \pi], \quad (4.2.26)$$

then Eq. 4.2.22 can be written as

$$\frac{1}{s}\mathcal{L}\{S(t_D)\} = \frac{1}{s}\Bigg\{ \frac{1}{4L_D^2}\left(z_D + z_{wD} - |z_D - z_{wD}|\right)$$

$$+ \frac{\tilde{x}_{eD}^2}{2\pi^2 L_D} \sum_{n=1}^{\infty} \frac{1}{n^2} \sin n\pi \frac{1}{\tilde{x}_{eD}} \cos n\pi \frac{\tilde{x}_{wD}}{\tilde{x}_{eD}} \cos n\pi \frac{\tilde{x}_D}{\tilde{x}_{eD}}$$

$$\frac{sh\left[\left(1 - |z_D - z_{wD}|\right)\frac{n\pi}{\tilde{x}_{eD} L_D}\right] - sh\left[\left(1 - z_D - z_{wD}\right)\frac{n\pi}{\tilde{x}_{eD} L_D}\right]}{ch\sqrt{\frac{n\pi}{\tilde{x}_{eD}^2 L_D^2}}}$$

$$+ \frac{\tilde{y}_{eD}}{2\pi L_D} \sum_{n=1}^{\infty} \frac{1}{n} \cos n\pi \frac{\tilde{y}_{wD}}{\tilde{y}_{eD}} \cos n\pi \frac{\tilde{y}_D}{\tilde{y}_{eD}}$$

$$\frac{sh\left[\left(1 - |z_D - z_{wD}|\right)\frac{n\pi}{\tilde{y}_{eD} L_D}\right] - sh\left[\left(1 - z_D - z_{wD}\right)\frac{n\pi}{\tilde{y}_{eD} L_D}\right]}{ch\sqrt{\frac{n\pi}{\tilde{y}_{eD}^2 L_D^2}}}$$

$$+ \frac{\tilde{x}_{eD}}{\pi} \sum_{n=1}^{\infty} \cos n\pi \frac{\tilde{y}_{wD}}{\tilde{y}_{eD}} \cos n\pi \frac{\tilde{y}_D}{\tilde{y}_{eD}} \sum_{k=1}^{\infty} \frac{1}{k} \sin k\pi \frac{1}{\tilde{x}_{eD}} \cos k\pi \frac{\tilde{x}_{wD}}{\tilde{x}_{eD}} \cos k\pi \frac{\tilde{x}_D}{\tilde{x}_{eD}}$$

$$\frac{sh\left[\left(1 - |z_D - z_{wD}|\right)\sqrt{e}\right] - sh\left[\left(1 - z_D - z_{wD}\right)\sqrt{e}\right]}{\sqrt{e}\, ch\sqrt{e}} \Bigg\}. \quad (4.2.27)$$

Here $e = \frac{n^2\pi^2}{\tilde{y}_{eD}^2} + \frac{k^2\pi^2}{\tilde{x}_{eD}^2}$. Substituting Eq. 4.2.27 into Eq. 4.2.6 for $s^{-1}\mathcal{L}\{S(t_D)\}$ and taking the inverse Laplace transform of the resulting expression, we obtain the following long time approximation

$$p_D = \frac{4}{\tilde{x}_{eD}\tilde{y}_{eD}} \Bigg\{ \frac{1}{4L_D^2}\left(z_D + z_{wD} - |z_D - z_{wD}|\right)$$

$$+\frac{\tilde{x}_{eD}^2}{2\pi^2 L_D}\sum_{n=1}^{\infty}\frac{1}{n^2}\sin n\pi\frac{1}{\tilde{x}_{eD}}\cos n\pi\frac{\tilde{x}_{wD}}{\tilde{x}_{eD}}\cos n\pi\frac{\tilde{x}_D}{\tilde{x}_{eD}}$$

$$\frac{sh\left[(1-|z_D-z_{wD}|)\frac{n\pi}{\tilde{x}_{eD}L_D}\right]-sh\left[(1-z_D-z_{wD})\frac{n\pi}{\tilde{x}_{eD}L_D}\right]}{ch\sqrt{\frac{n\pi}{\tilde{x}_{eD}^2L_D^2}}}$$

$$+\frac{\tilde{y}_{eD}}{2\pi L_D}\sum_{n=1}^{\infty}\frac{1}{n}\cos n\pi\frac{\tilde{y}_{wD}}{\tilde{y}_{eD}}\cos n\pi\frac{\tilde{y}_D}{\tilde{y}_{eD}}$$

$$\frac{sh\left[(1-|z_D-z_{wD}|)\frac{n\pi}{\tilde{y}_{eD}L_D}\right]-sh\left[(1-z_D-z_{wD})\frac{n\pi}{\tilde{y}_{eD}L_D}\right]}{ch\sqrt{\frac{n\pi}{\tilde{y}_{eD}^2L_D^2}}}$$

$$+\frac{\tilde{x}_{eD}}{\pi}\sum_{n=1}^{\infty}\cos n\pi\frac{\tilde{y}_{wD}}{\tilde{y}_{eD}}\cos n\pi\frac{\tilde{y}_D}{\tilde{y}_{eD}}\sum_{k=1}^{\infty}\frac{1}{k}\sin k\pi\frac{1}{\tilde{x}_{eD}}\cos k\pi\frac{\tilde{x}_{wD}}{\tilde{x}_{eD}}\cos k\pi\frac{\tilde{x}_D}{\tilde{x}_{eD}}$$

$$\left.\frac{sh\left[(1-|z_D-z_{wD}|)\sqrt{e}\right]-sh\left[(1-z_D-z_{wD})\sqrt{e}\right]}{\sqrt{e}ch\sqrt{e}}\right\}. \tag{4.2.28}$$

If we note that Eq. 4.2.27 would be applicable when the condition given by Eq. 4.2.21 holds, then we can conclude that Eq. 4.2.28 is valid when

$$t_D \geq \frac{400}{(\pi L_D)^2}. \tag{4.2.29}$$

In §4.1 II, we obtained another expression for the onset of stedy flow period (Eq. 4.1.28). The times determined by Eq. 4.1.28 are earlier than the times determined by Eq. 4.2.29 by a factor of 20. Our computations indicate that the time limit given by Eq. 4.1.28 is satisfactory for determining the onset of steady flow period for all practical purposes.

The long time approximation of Eq. 4.1.17 can also be obtained in a similar manner to that discussed above. If we assume that the condition given by Eq. 4.2.21 holds, then we can replace $s+a$ by a in Eq. 4.2.19 and taking the inverse Laplace transform of the resulting form of Eq. 4.2.19, we obtain

$$p_D = \sum_{n=1}^{\infty}\sin(2n-1)\frac{\pi}{2}z_D\sin(2n-1)\frac{\pi}{2}z_{wD}$$

$$\int_{-1}^{+1}\mathrm{K}_0\left[(2n-1)\frac{\pi}{2}L_D\sqrt{(x_D-\alpha)^2+y_D^2}\right]d\alpha. \tag{4.2.30}$$

Eq. 4.2.30, as it stands, is not convenient for computations at small values of y_D. In particular, difficulties arise if $y_D = 0$; that is, if pressure distributions are computed in the $x - z$ plane, the plane in which the well is located. These difficulties, however, can be eliminated by using the procedure outlined in §2.5 I. For example, using Eq. 2.5.1, we can write Eq. 4.2.30 at $y_D = 0$ and for $|x_D| < 1$ as

$$p_D\left(|x_D| < 1, y_D = 0\right) = \frac{2}{L_D}\sum_{n=1}^{\infty}\frac{\sin\left(2n-1\right)\frac{\pi}{2}z_D \sin\left(2n-1\right)\frac{\pi}{2}z_{wD}}{\left(2n-1\right)}$$

$$-\frac{2}{\pi L_D}\sum_{n=1}^{\infty}\frac{\sin\left(2n-1\right)\frac{\pi}{2}z_D \sin\left(2n-1\right)\frac{\pi}{2}z_{wD}}{\left(2n-1\right)}$$

$$\{\mathrm{Ki}_1\left[\left(2n-1\right)\frac{\pi}{2}L_D\left(1+x_D\right)\right] + \mathrm{Ki}_1\left[\left(2n-1\right)\frac{\pi}{2}L_D\left(1-x_D\right)\right]\}. \qquad (4.2.31)$$

Also using the relations[36]

$$\sin\left(2n-1\right)\frac{\pi}{2}z_D \sin\left(2n-1\right)\frac{\pi}{2}z_{wD} =$$

$$0.5\left[\cos\left(2n-1\right)\frac{\pi}{2}\left(z_D - z_{wD}\right) - \cos\left(2n-1\right)\frac{\pi}{2}\left(z_D + z_{wD}\right)\right] \qquad (4.2.32)$$

and

$$\sum_{k=1}^{\infty}\frac{\cos\left(2k-1\right)x}{2k-1} = \frac{1}{2}\ln\cot\frac{x}{2};\ \ [0 < x < \pi] \qquad (4.2.33)$$

Eq. 4.2.32 can be written in the following form:

$$p_D\left(|x_D| < 1, y_D = 0\right) = \frac{1}{2L_D}\ln\frac{\tan\frac{\pi}{4}\left(z_D + z_{wD}\right)}{\tan\frac{\pi}{4}|z_D - z_{wD}|}$$

$$-\frac{2}{\pi L_D}\sum_{n=1}^{\infty}\frac{\sin\left(2n-1\right)\frac{\pi}{2}z_D \sin\left(2n-1\right)\frac{\pi}{2}z_{wD}}{\left(2n-1\right)}$$

$$\left\{\mathrm{Ki}_1\left[\left(2n-1\right)\frac{\pi}{2}L_D\left(1+x_D\right)\right] + \mathrm{Ki}_1\left[\left(2n-1\right)\frac{\pi}{2}L_D\left(1-x_D\right)\right]\right\} \qquad (4.2.34)$$

Application of similar arguments to the cases where $|x_D| > 1$ and $|x_D| = 1$ leads to the following expressions:

$$p_D\left(|x_D| = 1, y_D = 0\right) = \frac{1}{4L_D}\ln\frac{\tan\frac{\pi}{4}\left(z_D + z_{wD}\right)}{\tan\frac{\pi}{4}|z_D - z_{wD}|}$$

$$-\frac{2}{\pi L_D}\sum_{n=1}^{\infty}\frac{\sin(2n-1)\frac{\pi}{2}z_D\sin(2n-1)\frac{\pi}{2}z_{wD}}{(2n-1)}\mathrm{Ki}_1\left[(2n-1)\frac{\pi}{2}L_D\right], \quad (4.2.35)$$

and

$$p_D(|x_D|>1, y_D=0)=\frac{2}{\pi L_D}\sum_{n=1}^{\infty}\frac{\sin(2n-1)\frac{\pi}{2}z_D\sin(2n-1)\frac{\pi}{2}z_{wD}}{(2n-1)}$$

$$\left\{\mathrm{Ki}_1\left[(2n-1)\frac{\pi}{2}L_D(|x_D|-1)\right]-\mathrm{Ki}_1\left[(2n-1)\frac{\pi}{2}L_D(|x_D|+1)\right]\right\}. \quad (4.2.36)$$

In Eqs. 4.2.34 - 4.2.36, the function $\mathrm{Ki}_1(z)$ is defined by

$$\mathrm{Ki}_1(z)=\int_z^{\infty}\mathrm{K}_0(t)\,dt. \quad (4.2.37)$$

It can be noted from Table 11.1 of Ref. 23 that

$$\frac{2}{\pi}\mathrm{Ki}_1(z)\leq 0.01, \quad (4.2.38)$$

and $(2/\pi)Ki_1(z)$ asymptoticaly approaches zero when

$$z\geq 3.6. \quad (4.2.39)$$

This indicates that the summation term on the right hand side of Eqs. 4.2.34 4.2.36 becomes negligible, within 1 %, when

$$L_D\geq\frac{7.2}{\pi(1-|x_D|)}. \quad (4.2.40)$$

It can be shown that, for large values of x_D and y_D, Eq. 4.2.30 and its derivatives with respect to x_D and y_D all vanish. This indicates that Eq. 4.2.30 approximately satisfies both the constant pressure and the no-flow conditions at $x_D=\pm x_{eD}$ and $y_D=\pm y_{eD}$ if x_{eD} and y_{eD} are large enough (see also Eqs. 4.1.29 and 4.1.30 and the discussion following these equations). Actually, if we follow Muskat[53,66], Eq. 4.2.30 can be readily extended to a bounded reservoir of radius r_e as given by the following equation:

$$p_D=\sum_{n=1}^{\infty}\sin(2n-1)\frac{\pi}{2}z_D\sin(2n-1)\frac{\pi}{2}z_{wD}$$

$$\int_{-1}^{+1}\left\{\mathrm{K}_0\left[(2n-1)\frac{\pi}{2}L_D\tilde{r}_D\right]+\frac{\mathrm{I}_0\left[(2n-1)\frac{\pi}{2}L_D\tilde{r}_D\right]\mathrm{K}_1\left[(2n-1)\frac{\pi}{2}L_Dr_{eD}\right]}{\mathrm{I}_1\left[(2n-1)\frac{\pi}{2}L_Dr_{eD}\right]}\right\}d\alpha, \tag{4.2.41}$$

where $\tilde{r}_D = \sqrt{(x_D-\alpha)^2+y_D^2}$ and $r_{eD} = \sqrt{x_{eD}^2+y_{eD}^2}$. Note that the second term inside the integral sign of Eq. 4.2.41 decreases exponentially with increasing values of L_Dr_{eD}. Although Eq. 4.2.41 assumes a circular drainage region, pressure distribution determined by Eq. 4.2.41 represents a very good approximation for a square drainage region. In the rest of our discussion, we will use Eq. 4.2.41, instead of Eq. 4.2.28, to investigate the steady flow behavior of the system under consideration.

As noted before, if horizontal well length is long, then the influence of the constant pressure bottom boundary becomes dominant before the flow across the well tips starts. In this case, the steady flow behavior will be independent of the x coordinate. The appropriate steady state expression for this case can be obtained by evaluating the inverse Laplace transform of Eq. 4.2.20 subject to the condition given by Eq. 4.2.21 and is given by

$$p_D = \frac{\beta}{L_D}\sum_{n=1}^{\infty}\frac{\sin(2n-1)\frac{\pi}{2}z_D\sin(2n-1)\frac{\pi}{2}z_{wD}}{(2n-1)}\exp\left[-(2n-1)\frac{\pi}{2}L_D|y_D|\right], \tag{4.2.42}$$

when

$$t_D \geq 20/(\pi L_D). \tag{4.2.43}$$

Using the relation given by Eq. 4.2.32 and[36]

$$\sum_{k=1}^{\infty}\frac{p^{2k-1}\cos(2k-1)x}{2k-1} = \frac{1}{4}\ln\frac{1+2p\cos x+p^2}{1-2p\cos x+p^2};\quad [0<x<2\pi, p^2\leq 1] \tag{4.2.44}$$

with

$$p = \exp\left(-\frac{\pi}{2}L_D|y_D|\right) \tag{4.2.45}$$

we can write Eq. 4.2.42 as

$$p_D = \frac{\beta}{8L_D}\left[\ln\frac{1+2\exp(-\pi L_D|y_D|/2)\cos\frac{\pi}{2}|z_D-z_{wD}|+\exp(-\pi L_D|y_D|)}{1-2\exp(-\pi L_D|y_D|/2)\cos\frac{\pi}{2}|z_D-z_{wD}|+\exp(-\pi L_D|y_D|)}\right.$$

$$-\ln\frac{1+2\exp\left(-\pi L_D|y_D|/2\right)\cos\frac{\pi}{2}\left(z_D+z_{wD}\right)+\exp\left(-\pi L_D|y_D|\right)}{1-2\exp\left(-\pi L_D|y_D|/2\right)\cos\frac{\pi}{2}\left(z_D+z_{wD}\right)+\exp\left(-\pi L_D|y_D|\right)}\Bigg]. \quad (4.2.46)$$

Note that in Eq. 4.2.46, we can not have $y_D = 0$ and $z_D = z_{wD}$ at the same time. If we use $y_D = 0$, and $z_D \neq z_{wD}$ in Eq. 4.2.46, we can show that Eq. 4.2.46 is the same as Eqs. 4.2.34 – 4.2.36 for large values of L_D.

II. Discussion of the Late-Time Results The transient flow behavior of horizontal wells producing bottom water drive fields presented in the previous sections should be useful for the analysis of well test data. In studying the productivities of the wells, however, late time flow characteristics rather than transient flow characteristics are of interest. Fig. 4.2.1 is intended to display the influence of the reservoir boundaries on the wellbore responses at late times. The responses shown in Fig. 4.2.1 were computed by Eq. 4.2.41 and are plotted as a function of the dimensionless well half length, L_D. It is assumed that the well is located midway between the top and the bottom reservoir boundaries ($z_{wD} = 0.5$) and at the center of a square drainage area ($x_{eD} = y_{eD}$). The dimensionless wellbore radius used in these computations is $r_{wDz} = 2 \times 10^{-3}$. The variable of interest is x_{eD}; that is, the ratio of the length of the reservoir in the x direction to the length of the horizontal well. The responses for $x_{eD} = 1$ correspond to the case where the well completely penetrates the reservoir in the x direction. Larger values of x_{eD} result from incomplete penetration of the reservoir in the x direction. Also shown in Fig. 4.2.1 are the responses of an infinite system ($x_{eD} \to \infty$, $y_{eD} \to \infty$). Note that the responses corresponding to the cases where $x_{eD} \geq 7.2/(\pi L_D)$ are identical to the responses for $x_{eD} = \infty$. Fig. 4.2.1 indicates that the pressure responses become independent of x_{eD} at large values of L_D and merge with the responses corresponding to $x_{eD} = \infty$. At smaller values of L_D, p_{wD} decreases as x_{eD} increases. Care should be taken, however, in interpreting these results since both x_{eD} and L_D are based on the well half length, $L_h/2$.

Fig. 4.2.2 is a replot of the responses shown in Fig. 4.2.1 except that the dimensionless pressure group $L_D p_{wD}$, instead of p_{wD}, is plotted vs. the dimension-

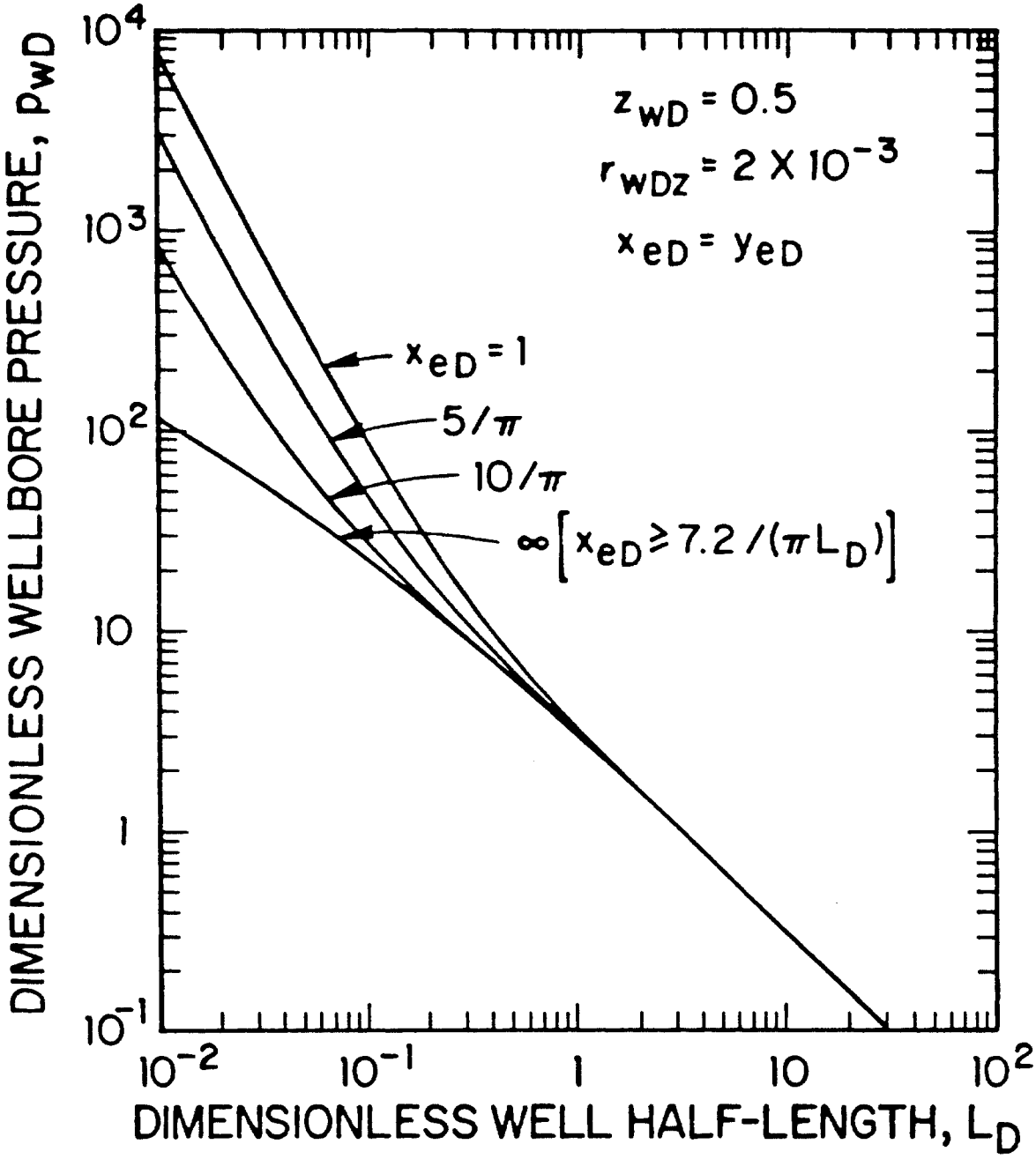

Fig. 4.2.1 - Influence of Lateral Boundaries on Pressure Responses – Steady Flow Period.

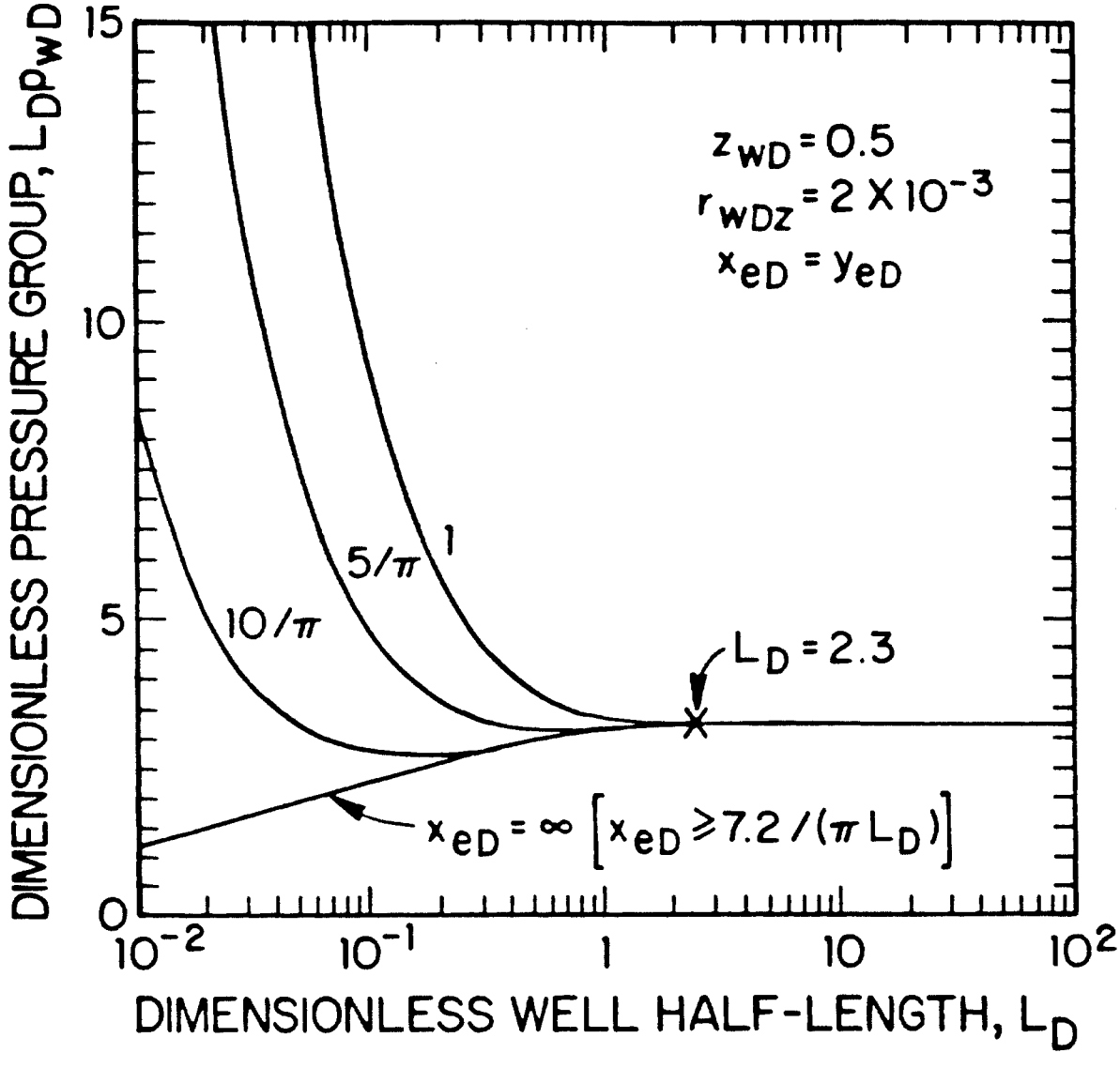

Fig. 4.2.2 - Influence of Lateral Boundaries on Pressure Responses – Steady Flow Period.

less well half length, L_D. As will be expected from Eqs. 4.2.34 – 4.2.36 and the remark following these equations that, for $L_D \geq 2.3$, the dimensionless pressure group $L_D p_{wD}$ becomes independent of the dimensionless well half length, L_D, at steady state. Fig. 4.2.2 also indicates that for $L_D \geq 7.2/(\pi x_{eD})$, the dimensionless distance to the boundary, x_{eD}, has no influence on pressure responses and the pressure responses become identical to that for $x_{eD} = \infty$.

4.3 Solution for Infinite-Conductivity Wells

In obtaining the solutions presented thus far, we assumed that the flux distribution along the well surface is uniform (uniform-flux well idealization). In §3.5, we noted that the solution for an infinite-conductivity horizontal well located between impermeable top and bottom boundaries can be obtained from uniform-flux solution by dividing the well half length, $L_h/2$, into small uniform-flux elements.[52,53,3] The same procedure as discussed in §3.5 can be used if the bottom boundary of the reservoir is at a constant pressure. For this case, using the laterally infinite system solution given by Eq. 4.2.30 at steady state, we can write the infinite-conductivity well solution as

$$p_D = \sum_{m=1}^{M} q_m (p_{Dm} - p_{Dm-1}). \tag{4.3.1}$$

Here p_{Dm} is given by

$$p_{Dm} = \sum_{n=1}^{\infty} \sin(2n-1)\frac{\pi}{2} z_D \sin(2n-1)\frac{\pi}{2} z_{wD}$$

$$\int_{-m/M}^{m/M} K_0 \left[(2n-1)\frac{\pi}{2} L_D \sqrt{(x_D - \alpha)^2 + y_D^2} \right] d\alpha, \tag{4.3.2}$$

and

$$q_m = \frac{\tilde{q} L_h}{q} \tag{4.3.3}$$

where $\tilde{q}_m$ is the strength of the differential flux elements (or point sources) located along the flux element (and assumed to be constant along the flux element) and q is the production rate from the total length of the well. In Eq. 4.3.1, the stabilized

flux distribution, q_m, should be chosen such that the resulting pressure distribution along the well surface is uniform. q_m to be used in Eq. 4.3.1 can be obtained from the solution of the following system of equations:

$$p_{wD}\left(x_D = \frac{2j-1}{2M}\right) = p_{wD}\left(x_D = \frac{2j+1}{2M}\right), \quad [j = 1, M-1], \tag{4.3.4}$$

and

$$\sum_{m=1}^{M} q_m = M. \tag{4.3.5}$$

As noted in §4.2 II, Eq. 4.3.2 is not convenient for computations at $y_D = 0$. We suggest that Eqs. 4.2.34 – 4.2.36, with the constant 1 in the argument of the $Ki_1(x)$ function replaced by m/M be used instead of Eq. 4.3.2.

Note that Eq. 4.3.1 represents an approximation to the infinite-conductivity solution and as the number of uniform flux elements, M, used in computations increases, the result should improve. Computational constraints, however, dictates and upper limit for the value of M (large values of M require excessive computation time and the accuracy of the results deteriorates due to rounding errors). In Fig. 4.3.1, we investigate the influence of M on the infinite-conductivity solution obtained from Eq. 4.3.1. In this figure, we show the dimensionless pressure distribution on the well surface ($y_D = 0$, $z_D = z_{wD} + r_{wDz}$, $x_D \leq 1$) and in the reservoir beyond the tip of the well ($x_D = 1$). The well is assumed to be located midway between the horizontal boundaries of the reservoir ($z_{wD} = 0.5$). The dimensionless wellbore radius is $r_{wDz} = 10^{-4}$ and the dimensionless well half length is $L_D = 1$. To obtain the infinite-conductivity results shown in Fig. 4.3.1 (unbroken line), we first solved the system of equations given by Eqs. 4.3.4 and 4.3.5 for the stabilized flux distribution, q_m, by using 10 uniform flux elements ($M = 10$). Then using the stabilized flux distribution, we solved Eq. 4.3.1 to obtain the dimensionless pressure distribution, p_D. Also shown in Fig. 4.3.1 is the pressure distribution for the uniform-flux case (dashed line) computed by Eq. 4.2.30. We first note from Fig. 4.3.1 that beyond the tip of the well ($x_D = 1$), the differences between the uniform-flux and infinite-conductivity responses cannot be distinguished for practical purposes. On the well surface, close to the well tip, we observe oscillations

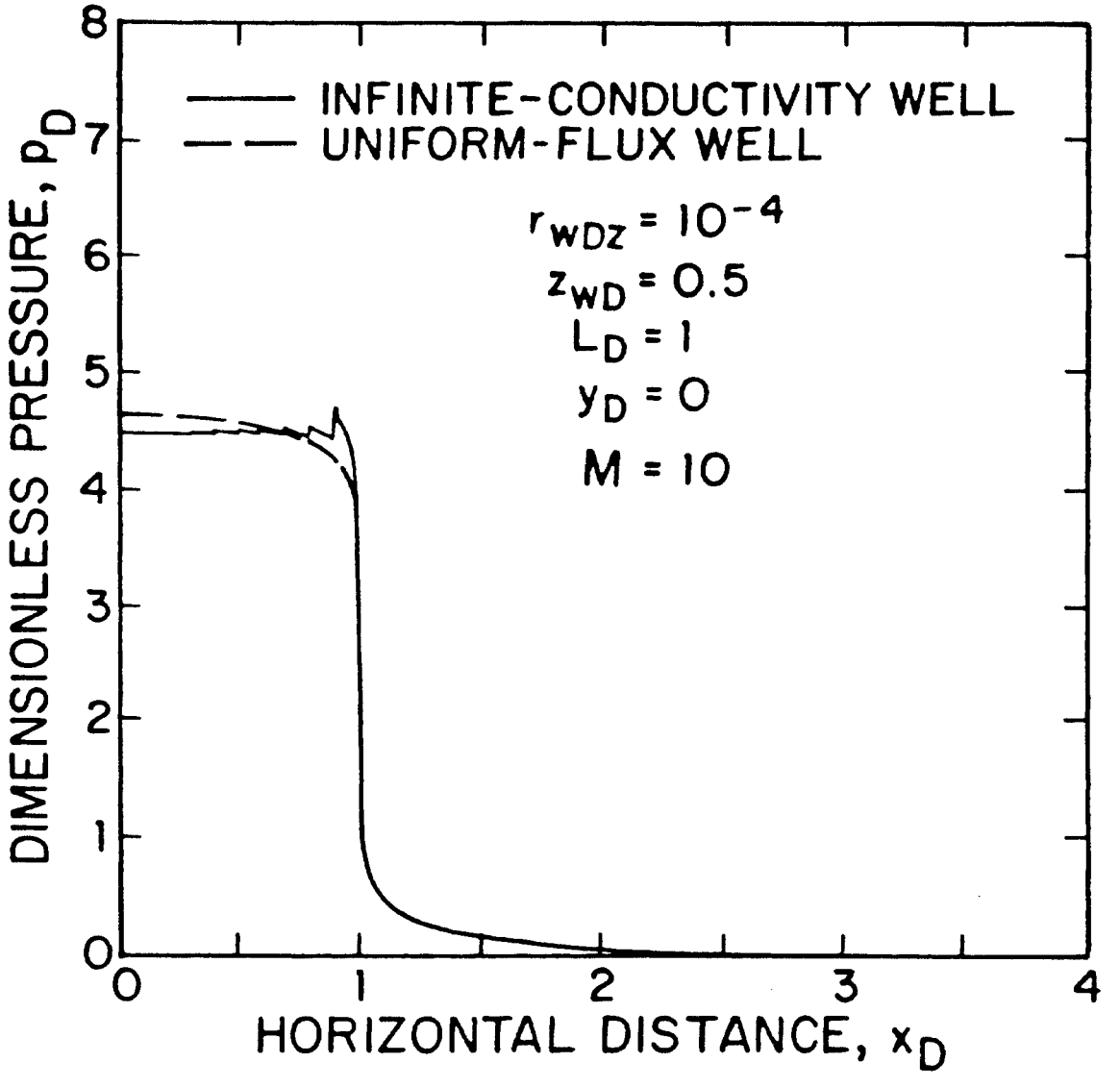

Fig. 4.3.1 - Influence of Number of Segments Used to Obtain Infinite-Conductivity Solution.

in the responses computed by Eq. 4.3.1. Close to the well center ($x_D = 0$), however, oscillations diminish and the dimensionless pressure distribution is uniform. Increasing the number of the uniform flux elements, M, used in these computations, we were able to obtain uniform pressure distribution in an extended portion of the well surface from the well center; yet we observed that the uniform pressures obtained close to the well center with $M = 10$ remained unaffected from the increase in the value of M (we obtained similar results for different values of L_D and z_{wD}). Therefore, in our computations hereafter, we used $M = 10$ and assumed that the pressure obtained for the first flux element from the well center represents the wellbore pressure of an infinite-conductivity horizontal well.

We computed dimensionless pressure responses of infinite-conductivity horizontal wells subject to bottom water drive at steady state by using the procedure outlined above. These responses are plotted as a function of the dimensionless distance x_D along the well surface ($y_D = 0$, $z_D = z_{wD} + r_{wDz}$) in Fig. 4.3.2 (the unbroken lines). The well is located midway between the top and bottom boundaries ($z_{wD} = 0.5$) and the dimensionless wellbore radius is $r_{wDz} = 10^{-4}$. Three values of L_D are considered: $L_D = 0.5, 1$, and 5. Also shown in Fig. 4.3.2 are the uniform-flux well solutions (dashed lines). $x_D = 1$ corresponds to the dimensionless location of the well tip. Fig. 4.3.2 indicates that as L_D increases the differences between the uniform-flux and infinite-conductivity solutions diminish; also flow beyond the tips of the well becomes negligible as L_D increases. This result should be expected in light of the discussion on the flow characteristics of uniform-flux wells presented in the previous sections. Earlier, we concluded that for $L_D \geq 6.37$ flow would take place only in the $y - z$ plane perpendicular to the well axis; that is, there would be no pressure gradient in the x direction. Pressure gradients in the x direction would develop in the region outlined by the line $AA'C$ in Fig. 4.1.3, and the duration of the flow in the x direction would increase as L_D decreases. Hence the influence the flux condition on the well surface become significant as L_D decreases.

The intersection point of the solutions for uniform-flux and infinite-conductivity

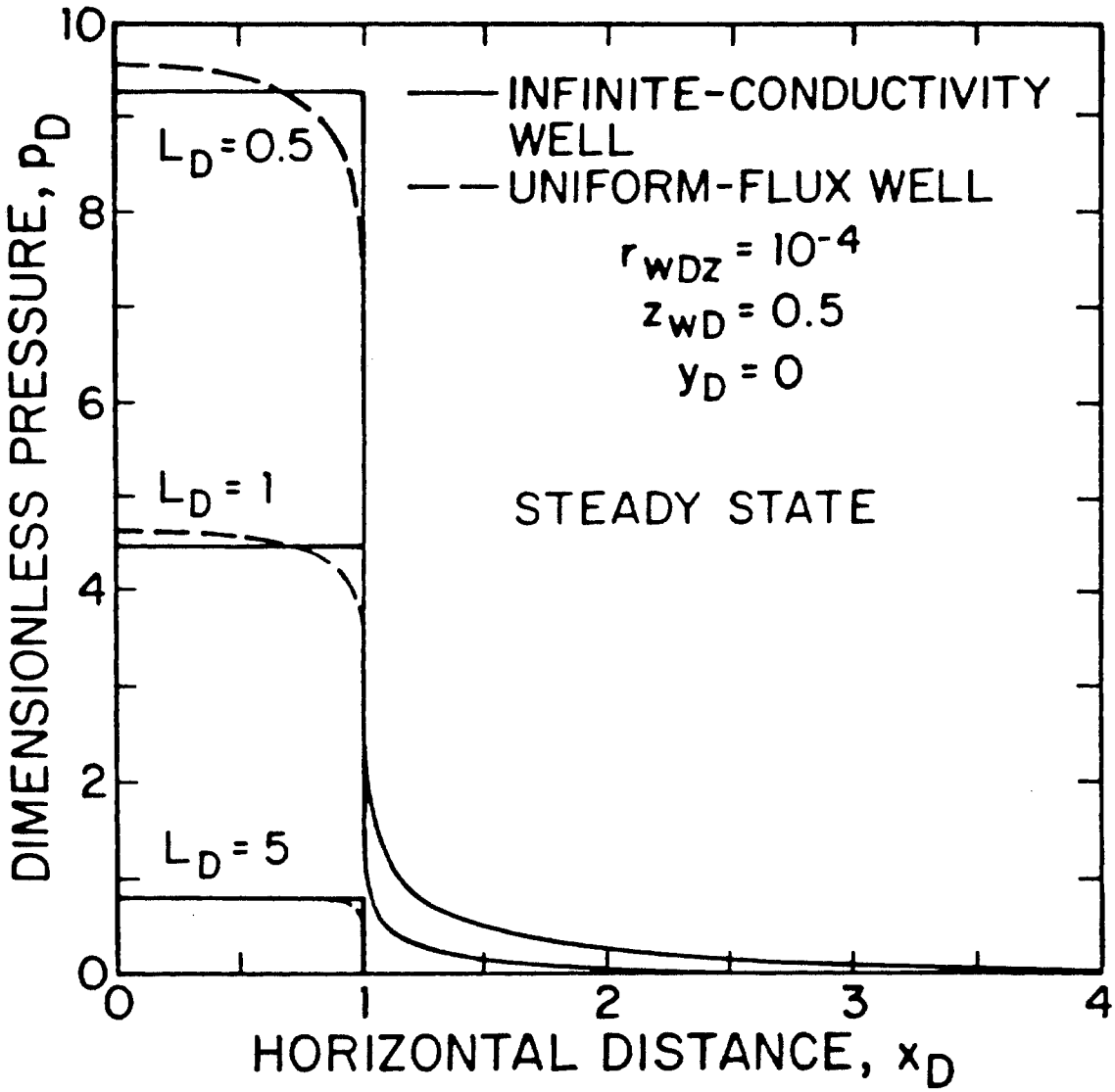

Fig. 4.3.2 - Influence of Flux Condition Along the Well Surface – Steady Flow Period.

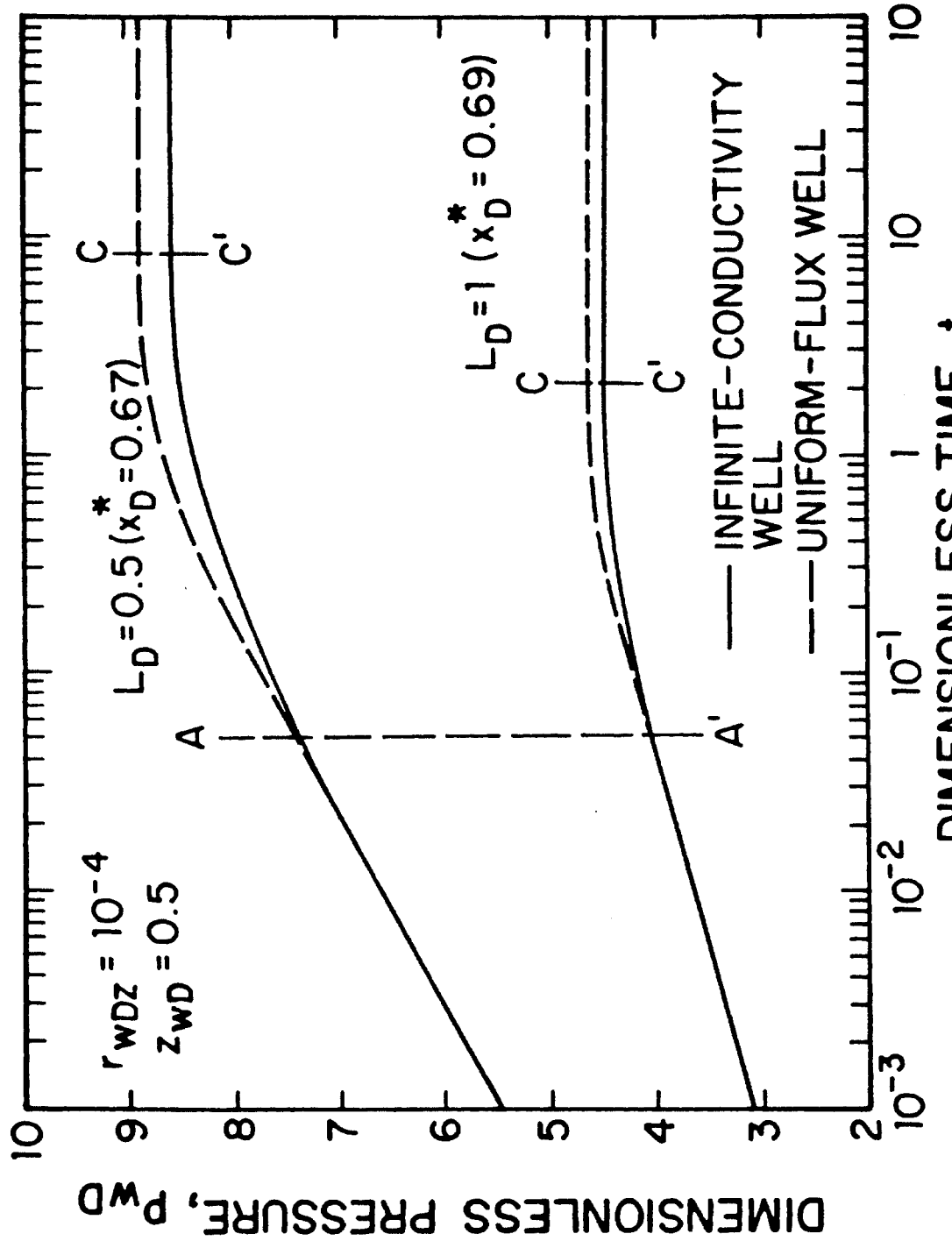

Fig. 4.3.3 - Comparison of Infinite-Conductivity and Uniform-Flux Results.

conditions are the equivalent pressure point denoted by x_D^* for the specific value of L_D corresponding to each case represented in Fig. 4.3.2. From the results shown in Fig. 4.3.2, we determined the equivalent pressure points as $x_D^* = 0.67$ and 0.69 for $L_D = 0.5$ and 1, respectively. Well responses for $L_D = 0.5$ and 1, computed by using the above values of x_D^*, are plotted as a function of time in Fig. 4.3.3 (the unbroken lines). Also shown in Fig. 4.3.3 are the responses of uniform-flux wells (the dashed lines). The values of r_{wDz} and z_{wD} used in this figure are 10^{-4} and 0.5, respectively. The line AA' denotes the times for the flow across the tips of the well to affect the well response and the line CC' denotes the times for the beginning of the steady flow period for uniform-flux wells (see Fig. 4.1.3). As discussed above, differences between the infinite-conductivity and uniform-flux solutions are evident only following the initial radial flow period. Fig. 4.3.3 indicates that the characteristics of the responses of infinite-conductivity wells are, not unexpectedly, similar to those of uniform-flux wells. The magnitude of the difference between the infinite-conductivity and uniform-flux solutions for the range of L_D investigated in this study is too small to be shown on a log-log plot of p_{wD} vs. t_D. Therefore, we will not present the infinite-conductivity counterparts of Figs. 4.1.3 and 4.1.4.

4.3 Well Performances Under Bottom Water Drive Conditions

Solutions presented in the previous sections should be useful in analyzing the well test data and determining the production capacities of the wells. In presence of contiguous water, however, the production capacity of a well, as defined by a rate-pressure relation, is not, by itself, a measure of the performance of the well. Mutual existence of oil and water in a reservoir may result in a producing mechanism commonly referred to as water drive. The term water drive is used to describe the situations where the production of oil is only by virtue of the drive provided by the advance of the water into the oil zone. When the direction of this motion is parallel to the planes of stratification, that is, the water moves largely from the lateral boundaries of the formation into the oil zone, the descriptive legend of the

production mechanism is edge water drive. Lateral edge water drive is mostly accompanied with the intrusion of the oil zone by the water rising from a bottom water table. Although it does not contribute significantly to the driving mechanism, it places severe restrictions on the production rates allowable to ensure water-free oil production. Another situation which is likely to encounter in oil fields occurs when the oil producing strata is underlain by a large body of water (an active aquifer) that supplies fluids into the oil zone without significant loss of its potential. The name bottom water drive is then assigned to the production mechanism in situations where the oil production results from the displacement of oil by the rising water-oil interface. An excellent classification of water drive reservoirs and the documentation of the geological and field conditions under which one of the aforementioned models (or a combination of them) can be used to investigate the production characteristics of water drive fields are available in Refs. 11 and 12. It appears, however, that the distinct characteristics of bottom water drive reservoirs are sometimes not given cognizance and models that are suitable for investigating the performance of lateral edge water drive systems are simply adopted for use in case of bottom water drive systems.

In this section, we first discuss the flow characteristics of bottom water drive and edge water drive reservoirs. This discussion is intended to provide the physical background for the model chosen here to investigate the horizontal well performance under bottom water drive conditions. As a suplement to the discussion presented here, in Appendix D, we obtain the solution for pressure distribution in edge water drive reservoirs produced via a horizontal wellbore and briefly discuss the theory of Muskat and Wyckoff[65] to investigate the performance of wells producing subject to edge water drive. For bottom water drive reservoirs, we use the displacement efficiencies as a measure of the productivity of wells. We also present the productivity comparison of vertical and horizontal wells producing under bottom water drive conditions.

I. Flow Characteristics of Bottom Water Drive and Edge Water Drive

Reservoirs Perhaps the most powerful tool in visualizing the differences between bottom water drive and edge water drive systems is a picture of flow lines showing the paths traveled by the fluid particles until they enter the wellbore. The mathematical analogue of these paths are the lines along which the stream function, ψ, does not change. Since the stream function, ψ, is related to the pressure function, p, the stream function, ψ, can be readily obtained from the knowledge of the pressure distribution, p. For simplicity, if we neglect flow in the x direction (long horizontal well assumption; see §§4.1 V and 4.2 III), the following relations should be satisfied by the stream function, ψ, and the dimensionless pressure function, p_D:

$$\frac{\partial \psi}{\partial z_D} = -\frac{141.2q}{L_h/2}\frac{\partial p_D}{\partial y_D}, \tag{4.4.1}$$

$$\frac{\partial \psi}{\partial y_D} = \frac{141.2qL_h}{2h^2}\frac{\partial p_D}{\partial z_D}. \tag{4.4.2}$$

Integration of Eq. 4.4.1 from z_D to $z_D = 1$ yields

$$\psi_D = -2\int_{z_D}^{z_D=1} \frac{\partial p_D}{\partial y_D} dz_D, \tag{4.4.3}$$

where we defined

$$\psi_D = \frac{L_h/2}{141.2q}\left[\psi\left(z_D = 1\right) - \psi\left(z_D\right)\right]. \tag{4.4.4}$$

A general expression for the steady state pressure distribution created by long horizontal wells under bottom water drive conditions is obtained in §4.3 II and is given by the following expression:

$$p_D = \frac{\beta}{8L_D}\left[\ln\frac{1+2\exp\left(-\pi L_D|y_D|/2\right)\cos\frac{\pi}{2}|z_D - z_{wD}| + \exp\left(-\pi L_D|y_D|\right)}{1-2\exp\left(-\pi L_D|y_D|/2\right)\cos\frac{\pi}{2}|z_D - z_{wD}| + \exp\left(-\pi L_D|y_D|\right)}\right.$$

$$\left. - \ln\frac{1+2\exp\left(-\pi L_D|y_D|/2\right)\cos\frac{\pi}{2}\left(z_D + z_{wD}\right) + \exp\left(-\pi L_D|y_D|\right)}{1-2\exp\left(-\pi L_D|y_D|/2\right)\cos\frac{\pi}{2}\left(z_D + z_{wD}\right) + \exp\left(-\pi L_D|y_D|\right)}\right], \tag{4.4.5}$$

where

$$\beta = \begin{cases} 2 & \text{for } |x_D| < 1, \\ 1 & \text{for } |x_D| = 1, \\ 0 & \text{for } |x_D| > 1. \end{cases} \tag{4.4.6}$$

The steady state pressure distribution due to production from a long horizontal well under edge water drive conditions is obtained in Appendix D and is given by

$$\begin{aligned} p_D = & \frac{\pi\beta}{4}(y_{eD} - |y_D|) \\ & - \frac{\beta}{8L_D}\{\ln[1 - 2\exp(-\pi L_D|y_D|)\cos\pi|z_{wD} - z_D| + \exp(-2\pi L_D|y_D|)] \\ & + \ln[1 - 2\exp(-\pi L_D|y_D|)\cos\pi(z_{wD} + z_D) + \exp(-2\pi L_D|y_D|)]\}, \end{aligned} \tag{4.4.7}$$

where β is given by Eq. 4.4.6. The dimensionless stream function, ψ_D, for bottom water drive and edge water drive conditions, is then obtained from Eqs. 4.4.3, 4.4.5, and 4.4.7 and for $|x_D| < 1$ is given, respectively, by

$$\begin{aligned} \psi_D = & \arctan\frac{2\exp\left(-\frac{\pi}{2}L_D|y_D|\right)\sin\frac{\pi}{2}(z_D + z_{wD})}{1 - \exp(-\pi L_D|y_D|)} \\ & - \arctan\frac{2\exp\left(-\frac{\pi}{2}L_D|y_D|\right)\sin\frac{\pi}{2}|z_D - z_{wD}|}{1 - \exp(-\pi L_D|y_D|)}, \end{aligned} \tag{4.4.8}$$

and

$$\begin{aligned} \psi_D = & \pi(1 - z_D) - \arctan\frac{\exp(-\pi L_D|y_D|)\sin\pi(z_{wD} + z_D)}{1 - \exp(-\pi L_D|y_D|)\cos\pi(z_{wD} + z_D)} \\ & + \arctan\frac{\exp(-\pi L_D|y_D|)\sin\pi|z_{wD} - z_D|}{1 - \exp(-\pi L_D|y_D|)\cos\pi(z_{wD} - z_D)}. \end{aligned} \tag{4.4.9}$$

Using the formulas given by Eqs. 4.4.8 and 4.4.9, we obtained the curves of constant ψ_D and plotted as a function of the dimensionless vertical distance z_D and the dimensionless horizontal distance $\pi L_D y_D/2$ in Figs. 4.4.1 and 4.4.2 for bottom water drive and $\pi L_D y_D$ in Figs. 4.4.3 and 4.4.4 for edge water drive systems. In Figs. 4.4.1 and 4.4.3, the well is assumed to be located midway between the horizontal boundaries of the reservoir ($z_{wD} = 0.5$). Figs. 4.4.2 and 4.4.4 display the case where the well is located immediately below the top boundary of the reservoir ($z_{wD} = 1$). Note that because of the long horizontal well assumption (flow in the x direction is negligible), Eqs. 4.4.8 and 4.4.9 are independent of the x coordinate. Therefore, Figs. 4.4.1 – 4.4.4 show the streamline distribution in any vertical plane ($y - z$) perpendicular to the well axis. Figs. 4.4.1 – 4.4.4 indicate that the oil flow is predominantly in the vertical direction in bottom water drive

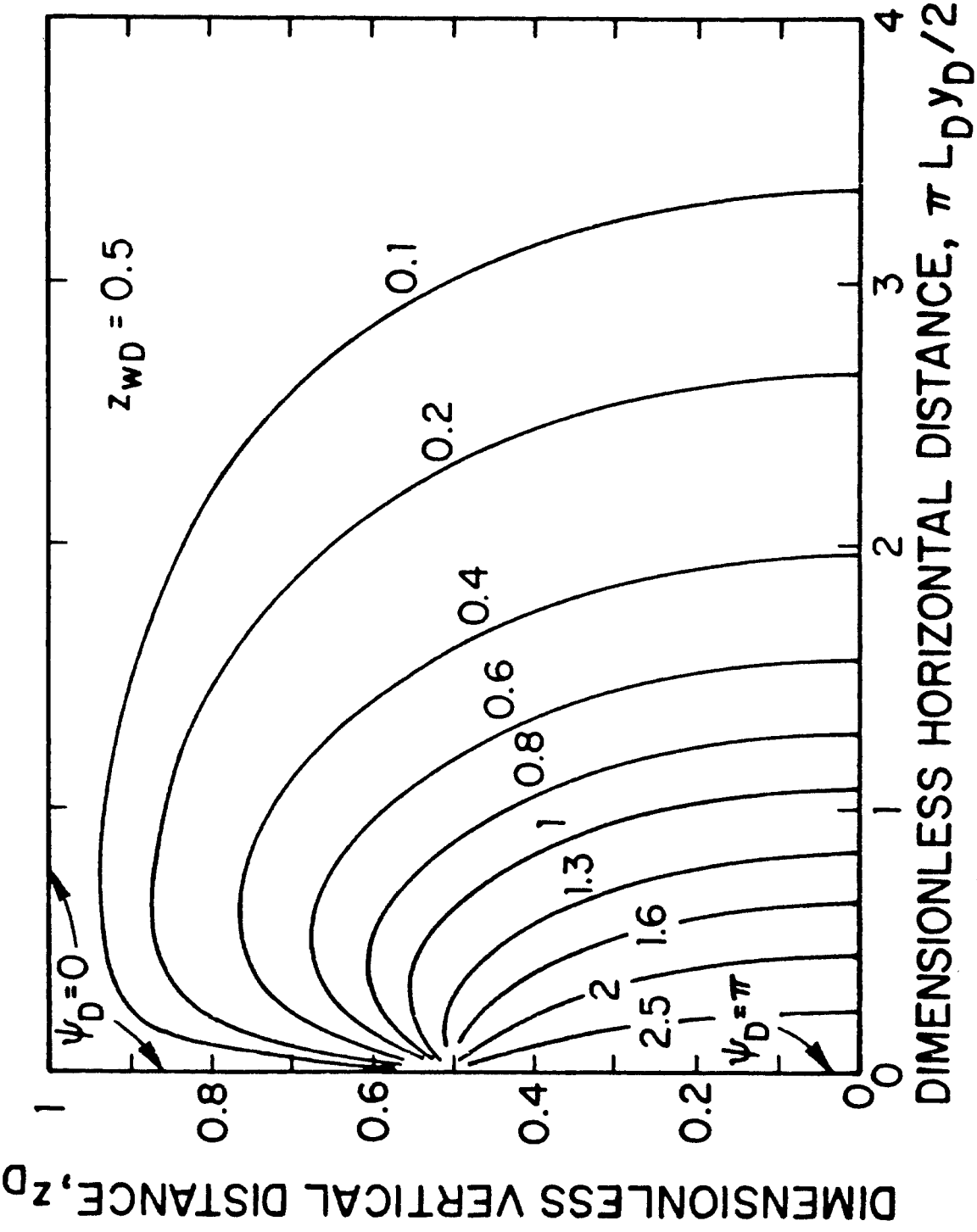

Fig. 4.4.1 - Streamline Distribution for a Long Horizontal Well ($z_{wD} = 0.5$) – Bottom Water Drive.

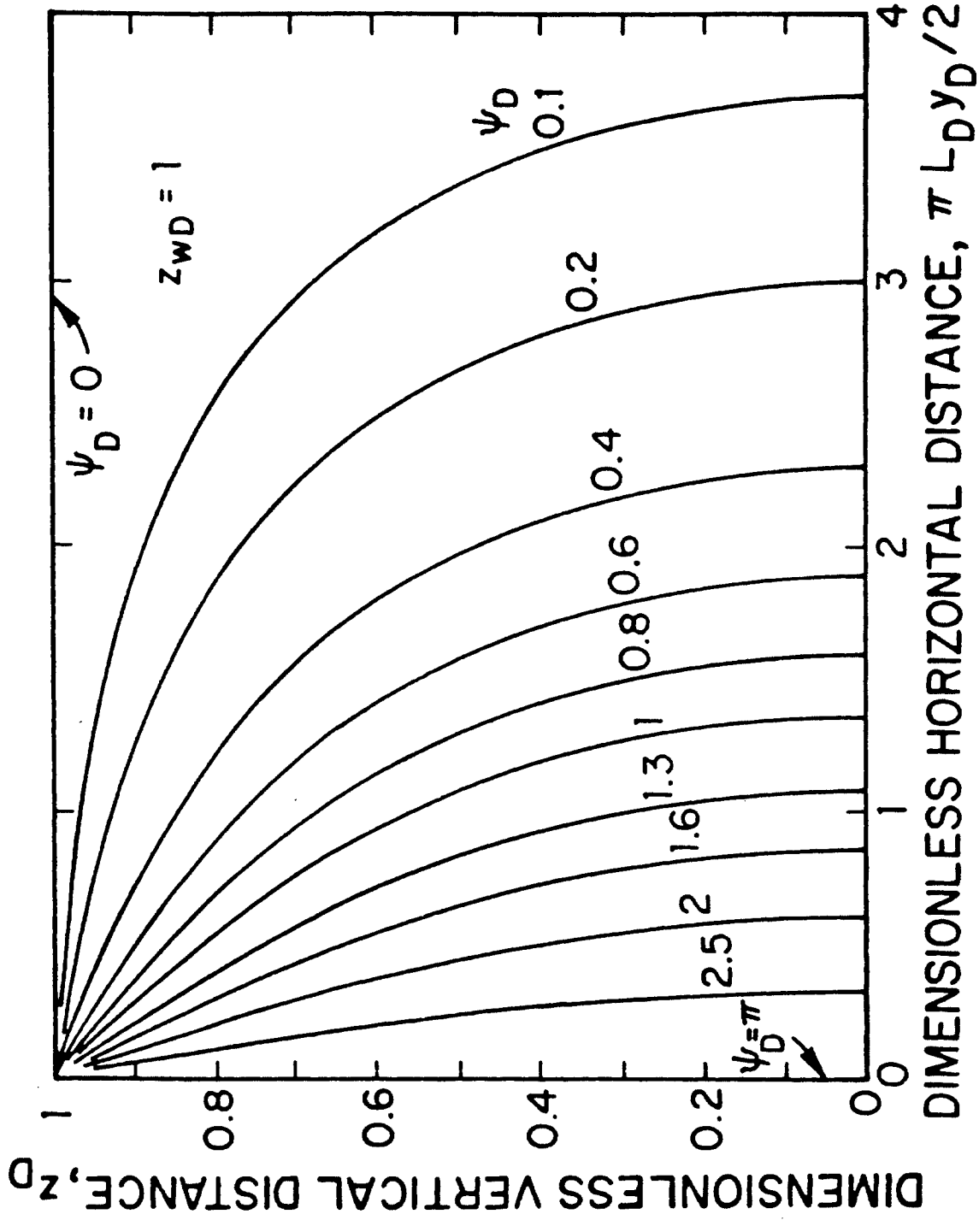

Fig. 4.4.2 - Streamline Distribution for a Long Horizontal Well ($z_{wD} = 1$) – Bottom Water Drive.

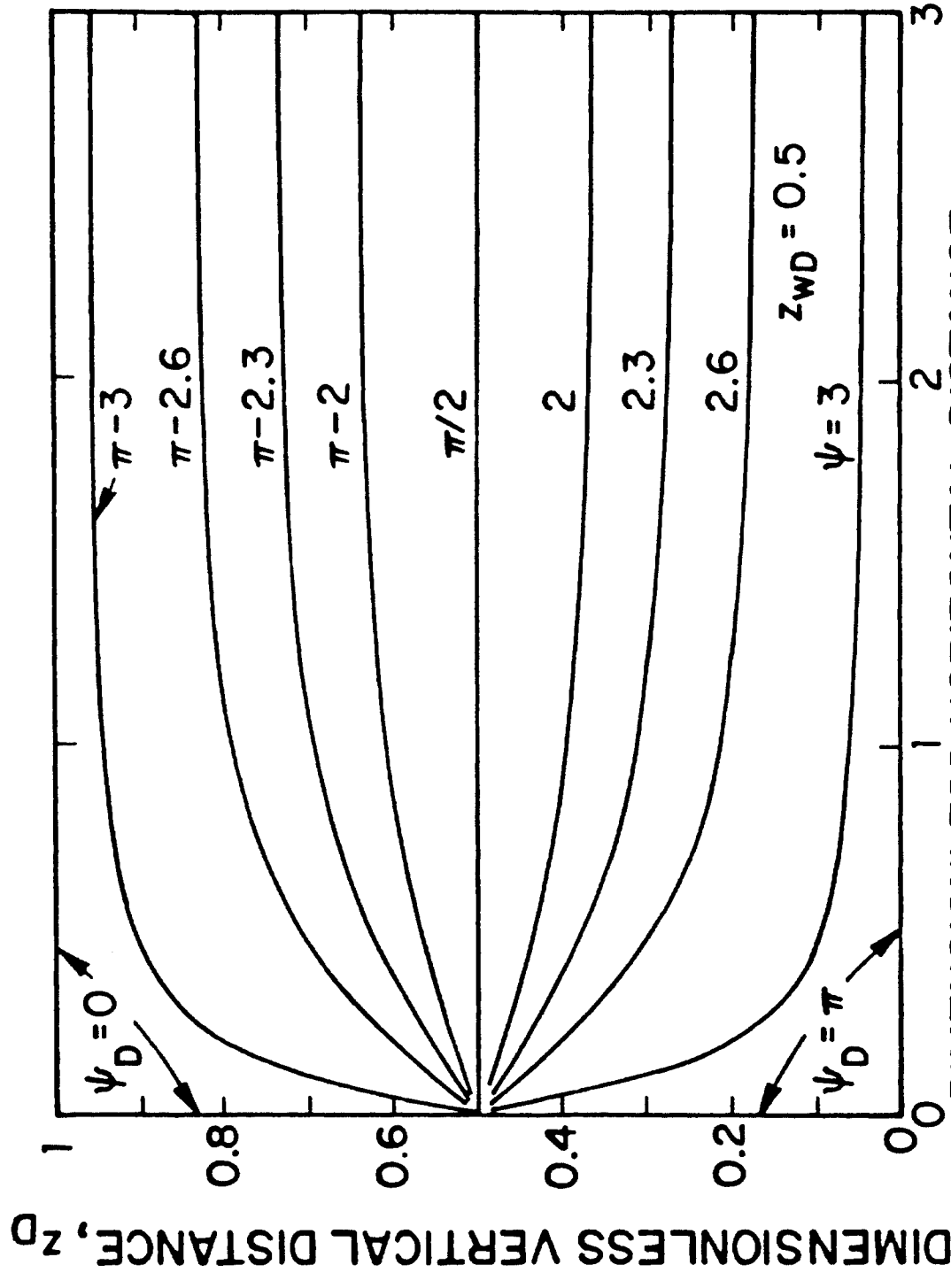

Fig. 4.4.3 - Streamline Distribution for a Long Horizontal Well ($z_{wD} = 0.5$) – Edge Water Drive.

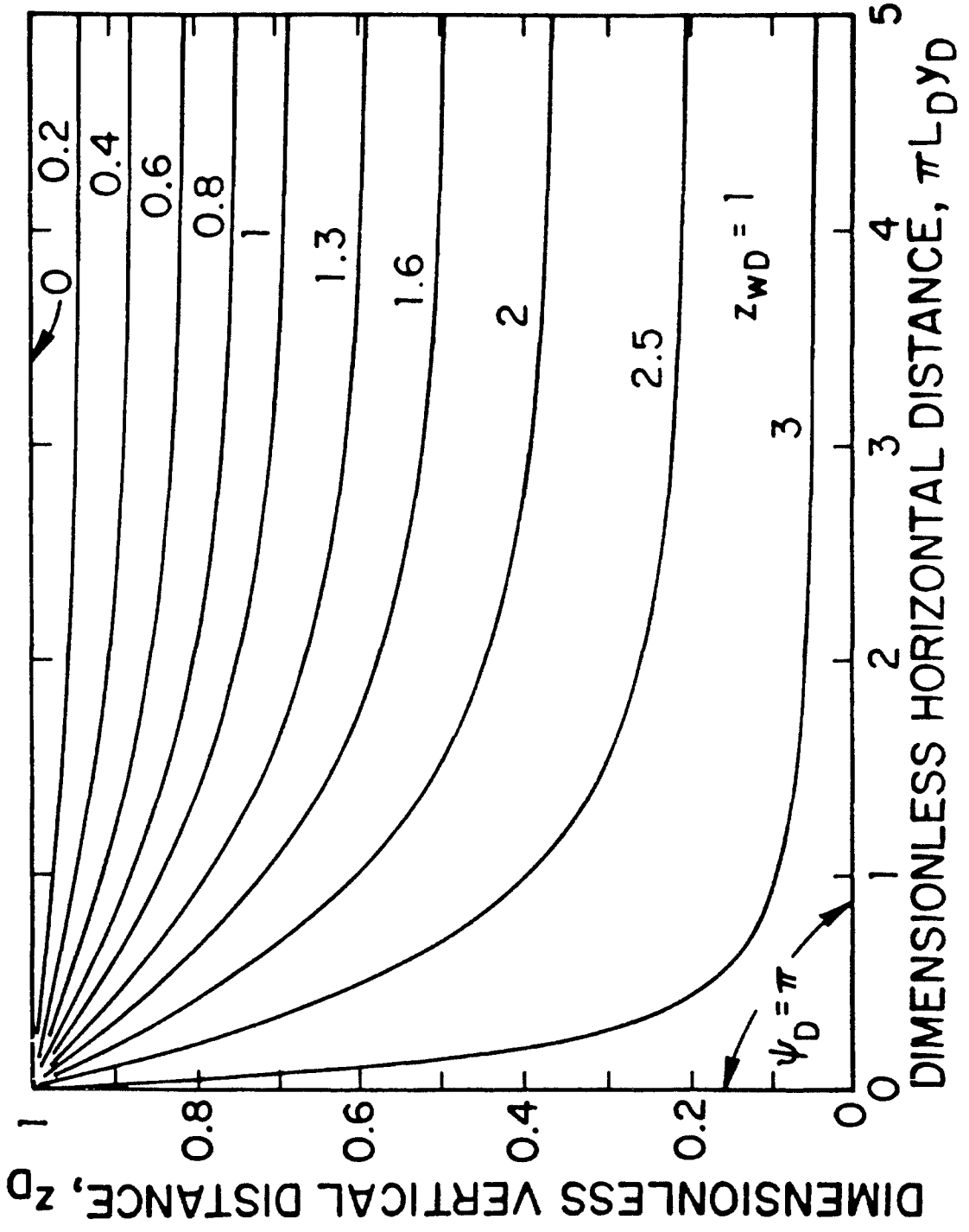

Fig. 4.4.4 - Streamline Distribution for a Long Horizontal Well ($z_{wD} = 1$) – Edge Water Drive.

systems whereas in edge water drive systems, convergence of flow toward the well is mainly in the horizontal direction. Clearly, the direction of flow coincides with the direction of displacement of oil by the water. Noting from Eq. 4.4.2 that $\partial\psi_D/\partial y_D$ is proportional to $\partial p_D/\partial z_D$, we may conclude from Figs. 4.4.1 – 4.4.4 that the maximum rate of advance of bottom water would be in the vertical plane passing through the well axis ($y_D = 0$). Therefore, as the water moves into the oil zone, the water-oil interface would resemble a crest with its apex at $y_D = 0$. Figs. 4.4.1 and 4.4.2 indicate that the vertical velocities in a bottom water drive system would not be negligible until an appreciable distance from the well axis in contrast to rapidly vanishing vertical velocities in an edge water drive system as indicated by Figs. 4.4.3 and 4.4.4. Therefore, in an edge water drive system, the bottom water crest would be more localized and steeper compared to the one in a bottom water drive system.

This detailed discussion is provided here to also investigate the validity of the claim made in Ref. 64 that the pattern of flow lines for the bottom water drive mechanism is the same as that for the lateral edge water drive mechanism in the vicinity of the well and hence the shape of the oil-water boundary obtained for the latter can be used for the former in the neighborhood of the well. Figs. 4.4.1 – 4.4.4 display patterns quite contrary to this claim. In addition to this crucial assumption in the neighborhood of the well, Ref. 64 also claims that, at some distance from the well, the use of Dupuit-Forchheimer approximation[69,70] would yield results that are accurate enough in bottom water drive systems. Realizing that the Dupuit-Forchheimer approximation is based on the premise that the streamlines would be approximately horizontal for small inclinations of free surfaces in gravity drainage systems[52], under most favorable conditions, this approximation could be considered to be more appropriate for lateral edge water drive systems (see Figs. 4.4.3 and 4.4.4). For bottom water drive systems however, even at great distances from the well, the streamlines are essentially vertical (see Figs. 4.4.1 and 4.4.2) and hence the use of Dupuit-Forchheimer approximation should be inadequate. With these underlying assumptions, the model used in Ref. 64 would, at best, represent the

behavior of an edge water drive system in which the height of the water-oil interface at the lateral boundaries of the reservoir would change with time.

In this work, we follow the approach taken by Muskat[53,66] to investigate the performance of vertical wells producing under bottom water drive conditions. Our primary goal is to derive general conclusions on the gross performance features of horizontal wells producing bottom water drive reservoirs. Provided that the assumptions and their influences discussed below are understood completely, the results obtained here can be used with confidence to determine the productivity improvements that can be expected from horizontal well completions.

II. Assumptions In order to restrict the discussion to complete bottom water drive systems, we assume that pressures throughout the system are above the bubble point. This ensures that the sole source of energy to drive the oil toward the well is the movement of the oil-water interface; that is, there is no aid of the internal dissolved gas. For simplicity, oil stripping is not taken into account; but stripping would not have a major impact on calculated displacement efficiencies. Since our objective is to develop general guidelines pertaining to the efficacy of horizontal well completions and compare them to vertical well completions, we also assume, as in other studies[53,66,63,64], that the mobility of water in the flooded portion of the oil zone is the same as the mobility of oil. The necessity for this assumption arises when two phase flow effects are neglected for the sake of analytical simplicity.

If we accept the above assumptions, the most critical assumption appears to be the neglect of the density difference between the oil and water. Intuitively, it can be expected that if the pressure gradients are comparable to the hydrostatic gradient, then the density difference would help flatten the oil-water interface and delay breakthrough. Such a control of pressure gradients, however, would be highly impractical for bottom water drive systems. Under reasonable production rates, it can be expected that the pressure gradients would be exceedingly higher than the hydrostatic gradient and the influence of the density difference would be negligible. The consequences of this assumption are discussed in more detail later. At

this stage, it should be noted that the assumption that the density differences are negligible results in conservative estimates of displacement efficiency for it represents the least favorable conditions for oil displacement. (In this respect, we fully recognize the attempt of Ref. 64 to take into account the density differences; but unfortunately, this attempt fails in properly modeling the behavior of bottom water drive reservoirs.)

III. Displacement Efficiencies Following Muskat[53,66], the displacement efficiency is defined as the fraction of the volume of oil pay that is swept out by the time the water first reaches the well. If V is the volume of the oil zone swept by the water until the water breaks into the well, h is the thickness of the oil pay, and a is the well spacing ($a = 2x_e$), the displacement efficiency, E, is defined by

$$E = \frac{V}{a^2 h}, \tag{4.4.10}$$

where

$$V = \frac{qt_b}{f}. \tag{4.4.11}$$

In Eq. 4.4.11, t_b is the breakthrough time, q is the constant production rate, and f is the microscopic displacement efficiency defined by

$$f = \phi\left(1 - S_{wc} - S_{oir}\right). \tag{4.4.12}$$

Here ϕ is the porosity of the oil zone, S_{wc} is the connate water saturation, and S_{oir} is the irreducible oil saturation.

For an oil particle originally at the oil-water interface ($z = 0$) travels to the well along a streamline (see Figs. 4.4.1 and 4.4.2), we can express this motion along the streamline by the relation

$$dS_\psi = v_\psi dt \tag{4.4.13}$$

where S_ψ is the distance traveled by the particle along a streamline, v_ψ is the velocity of the particle along this path, and t is the time of travel. By Darcy's law,

v_ψ is proportional to the actual velocity. This proportionality is expressed by the following relation:

$$v_\psi = 1.127\text{x}10^{-3}\frac{k_\psi}{f\mu}\frac{\partial p}{\partial S_\psi}. \tag{4.4.14}$$

Therefore, for a given streamline, the time, t, and the distance traveled S_ψ, are related by

$$t = \frac{f\mu}{1.127\text{x}10^{-3}k_\psi}\int_0^{S_\psi}\frac{dS_\psi}{\partial p/\partial S_\psi}. \tag{4.4.15}$$

As the water rises most rapidly at $x = y = 0$, the time t_b in Eq. 4.4.11 corresponds to the time for an oil particle originally located at $x = y = z = 0$ to travel to the well along the streamline that coincides with the vertical (z) direction (see Figs. 4.4.1 and 4.4.2). Then letting z_b denote the location of the bottom of the well, the breakthrough time t_b is obtained from Eq. 4.4.15 as

$$t_b = \frac{f\mu}{1.127\text{x}10^{-3}k_z}\int_0^{z_b}\frac{dz}{(\partial p/\partial z)_{y=0}}. \tag{4.4.16}$$

Combining Eqs. 4.4.10, 4.4.11, and 4.4.16 and using the definitions of dimensionless variables, the displacement efficiency, E, can be written as

$$E = \frac{F}{a_D^2}. \tag{4.4.17}$$

In Eq. 4.4.17, the dimensionless parameter a_D and the dimensionless function F, which we will name after Muskat as the effective well spacing and the sweep efficiency function respectively, are defined by

$$a_D = \frac{a}{h}\sqrt{\frac{k_z}{k}}, \tag{4.4.18}$$

and

$$F = 2\pi\int_0^{z_{bD}}\frac{dz_D}{(\partial p_D/\partial z_D)_{y_D=0}}. \tag{4.4.19}$$

Note that the sweep efficiency function, F, is also equal to

$$F = \frac{qt_b}{fh^3}\frac{k_z}{k}. \tag{4.4.20}$$

Thus, the right hand side of Eq. 4.4.20 indicates that F is a measure of clean oil produced prior to breakthrough. Also, if F is known, then the breakthrough time

for a specific value of flow rate can be estimated from Eq. 4.4.20. The steady state production rates to be used in these computations can be obtained from the relations presented in the previous section (Eq. 4.2.28 or 4.2.41). In the discussion that follows, information is provided to determine the function F.

We computed the displacement efficiencies of horizontal wells producing under bottom water drive conditions from Eq. 4.4.17 by using Eq. 4.2.41. For comparison purposes, we also reproduced the results of Refs. 53 and 66 for partially penetrating vertical wells. A summary of the equations used in the vertical well case is also presented in Appendix E.

Prior to presenting the central discussion of this section, we will comment on two points that are of secondary importance to the goals of this investigation. Although the results presented in this section were obtained by using the infinite-conductivity well condition, the results of our investigation indicated that the uniform-flux well idealization would not significantly affect the computed displacement efficiency. We observed a little discrepancy between the two cases for intermediate values of L_D ($0.1 < L_D < 2.3$). On the basis of our earlier discussion, the agreement between the infinite-conductivity and uniform-flux results for $L_D \geq 2.3$ should be expected. The explanation for the agreement between the two cases at small values of L_D is based on the expectation that the displacement efficiencies of short horizontal wells ($L_D \leq 0.1$) would approach that of a point source well. The results presented below justify this explanation. Similarly, we found that the influence of the wellbore radius on the displacement efficiencies of horizontal wells was not significant for practical purposes (in case of vertical wells, this variable appears to be slightly more important). Therefore, the following discussion can be generalized for both flux conditions and all wellbore radii.

<u>IV. Discussion of the Results</u> Fig. 4.4.5 presents the displacement efficiency, E, vs. the effective well spacing, a_D for horizontal and vertical wells. The unbroken lines in Fig. 4.4.5 denote the variation of the displacement efficiencies for horizontal wells as a function of effective well spacing. The dimensionless well half length, L_D,

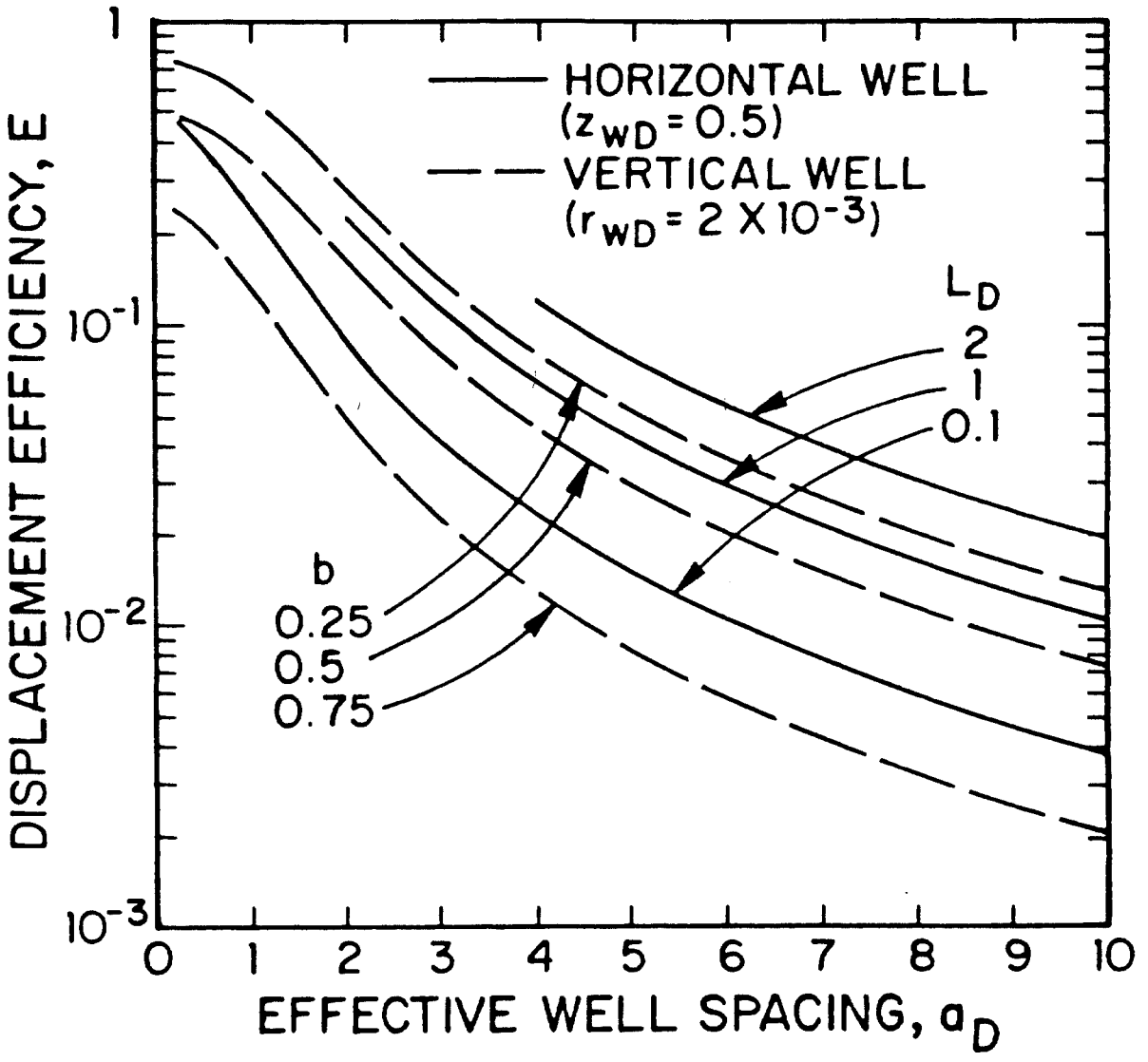

Fig. 4.4.5 - Displacement Efficiencies of Horizontal and Vertical Wells.

is the variable of interest. The horizontal well is assumed to be located midway between the top and the bottom boundaries of the reservoir ($z_{wD} = 0.5$). The dashed lines in Fig. 4.4.5 correspond to the displacement efficiencies of vertical wells ($r_{wD} = 2 \times 10^{-3}$, the influence of r_{wD} is, however, negligible; see Refs. 53 and 66). Here, the variable of interest is the penetration ratio, $b = h_w/h$, where h_w is the thickness of the penetrated interval and h is the total thickness of the oil pay. The maximum value of E for horizontal wells occurs at the minimum value of a_D correponding to $x_{eD} = 1$. Similarly, the maximum value of E for partially penetrating vertical wells occurs at $a_D = 0$ and is equal to $1-b$. Fig. 4.4.5 indicates that the displacement efficiency decreases with increasing effective well spacing for fixed values of L_D (horizontal well) and b (vertical well). For large values of a_D, the sweep efficiency function, F, becomes independent of the well spacing and therefore the displacement efficiency, E, becomes proportional to $1/a_D^2$. This result implies that the incremental oil recovery per additional well decreases as the well density increases.

The influence of anisotropy on displacement efficiency can also be determined from Fig. 4.4.5. As explained by Muskat[53,66], this variable is extremely important. For vertical wells, since a_D is proportional to $\sqrt{k_z/k}$, the displacement efficiency, E, decreases as k_z/k increases, assuming that the well penetration, h_w, and the formations thickness, h, are fixed. For horizontal wells, however, both a_D and L_D include the effect of anisotropy. Thus, determining the influence of anisotropy is more complicated for horizontal wells. For example, if the ratio of k_z/k increases by a factor of 4, then assuming that a, h, and L_h are fixed, both a_D and L_D increase by a factor of 2. From Fig. 4.4.5, we note that the displacement efficiency of the case corresponding to $a_D = 5$ and $L_D = 1$ is higher than the displacement efficiency of the case corresponding to $a_D = 10$ and $L_D = 2$. Similar observations can be made for other combinations of a_D and L_D. Thus, in general, as in the case of vertical wells, everything else being the same, the displacement efficiencies of horizontal wells decrease as the ratio of vertical to horizontal permeability, k_z/k, increases. On the other hand, if L_h is increased, everything else being fixed, the displacement

efficiencies of horizontal wells increse.

The fact that the displacement efficiency for a horizontal well depends on both a_D and L_D makes horizontal wells a better canditate than vertical wells in reservoirs with high k_z/k ratio. Consider for example a reservoir with a certain ratio of k_z/k and assume that corresponding to the given ratio of k_z/k, the dimensionless well spacing, $a_D = 5$. If we compare a horizontal well with $L_D = 1$ and a vertical well with $b = 0.25$ located in this reservoir, Fig. 4.4.5 indicates that the displacement efficiency of the vertical well would be higher than that of the horizontal well. If we now consider another reservoir where the ratio of k_z/k is higher by a factor of 4, then everything else being constant, $L_D = 2$ and $a_D = 10$ (the penetration ratio b of the vertical well would remain to be same). For this case, the displacement efficiency for the horizontal well would be higher than that of the vertical well.

Although Fig. 4.4.5 provides information on displacement efficiency, this information is incomplete for the purpose of evaluating the influence of water drive. For example, the time for breakthrough (which would also govern the amount of clean oil produced) is of interest. This information can be obtained by examining the behavior of the sweep efficiency function, F.

The sweep efficiency function, F, vs. the effective well spacing, a_D, for a network of vertical wells (with square drainage region) is shown in Fig. 4.4.6. In this figure, the dimensionless wellbore radius, r_{wD}, is assumed to be 2 x 10^{-3}. The variable of interest here is the penetration ratio, b. As can be expected, the sweep efficiency function is larger for smaller well penetrations. For a fixed value of b, F increases as a_D increases and if a_D is large enough, it becomes independent of a_D; that is, for fixed values of b, h, and k_z/k, the sweep efficiency increases as the distance between the wells increases (as a increases) and finally attains a constant value. Refs. 53 and 66 report that for $a_D \geq 3.5$, the sweep efficiency becomes independent of effective well spacing. If we assume that we are above this limit, then Eq. 4.4.20 indicates that breakthrough time, t_b, is inversely proportional to k_z/k, all other variables being constant.

In Fig. 4.4.7 we have plotted the sweep efficiency function, F, of an individual

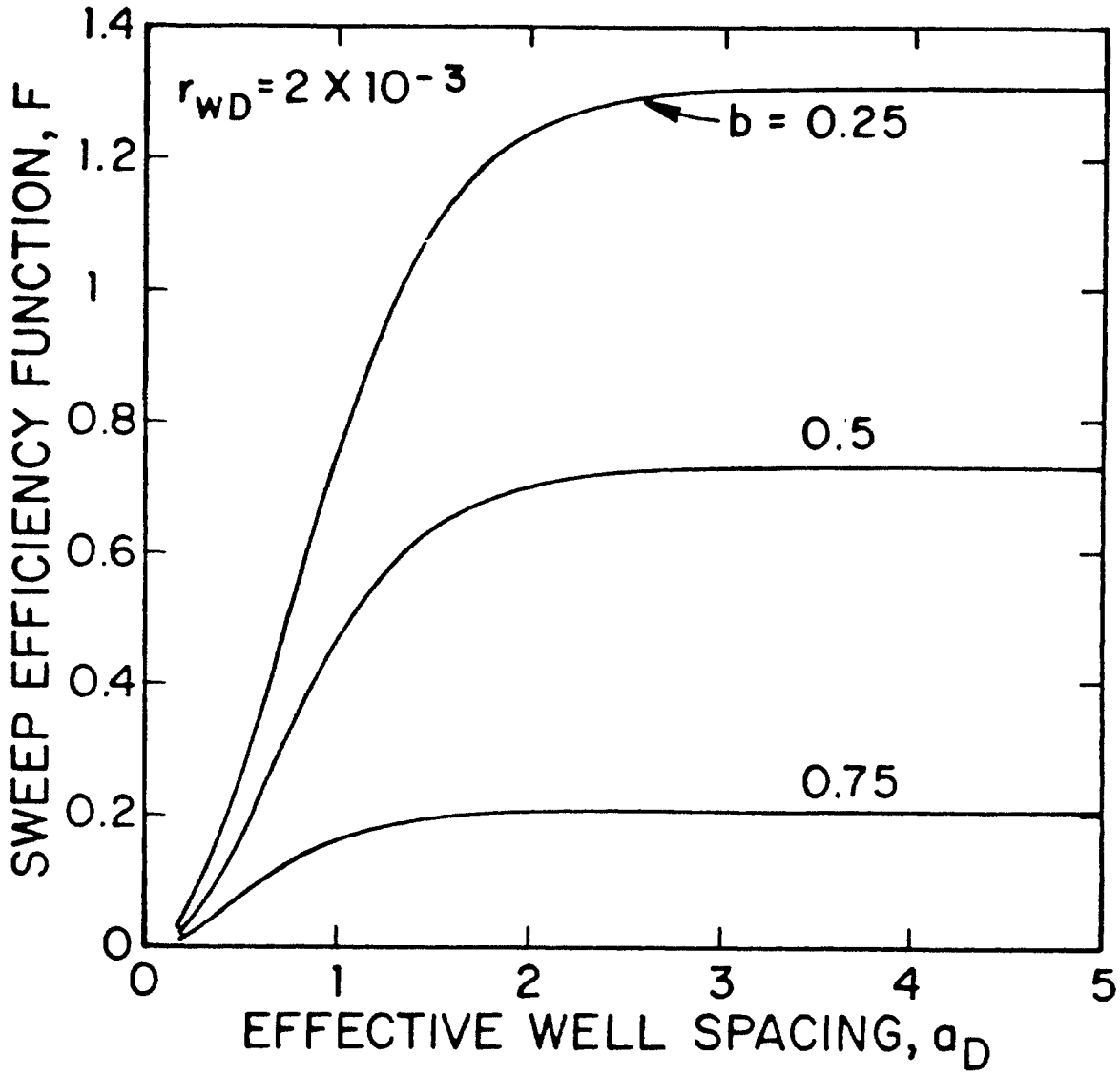

Fig. 4.4.6 - Sweep Efficiency Function F for Vertical Wells – Correlation for Breaktrough Time.

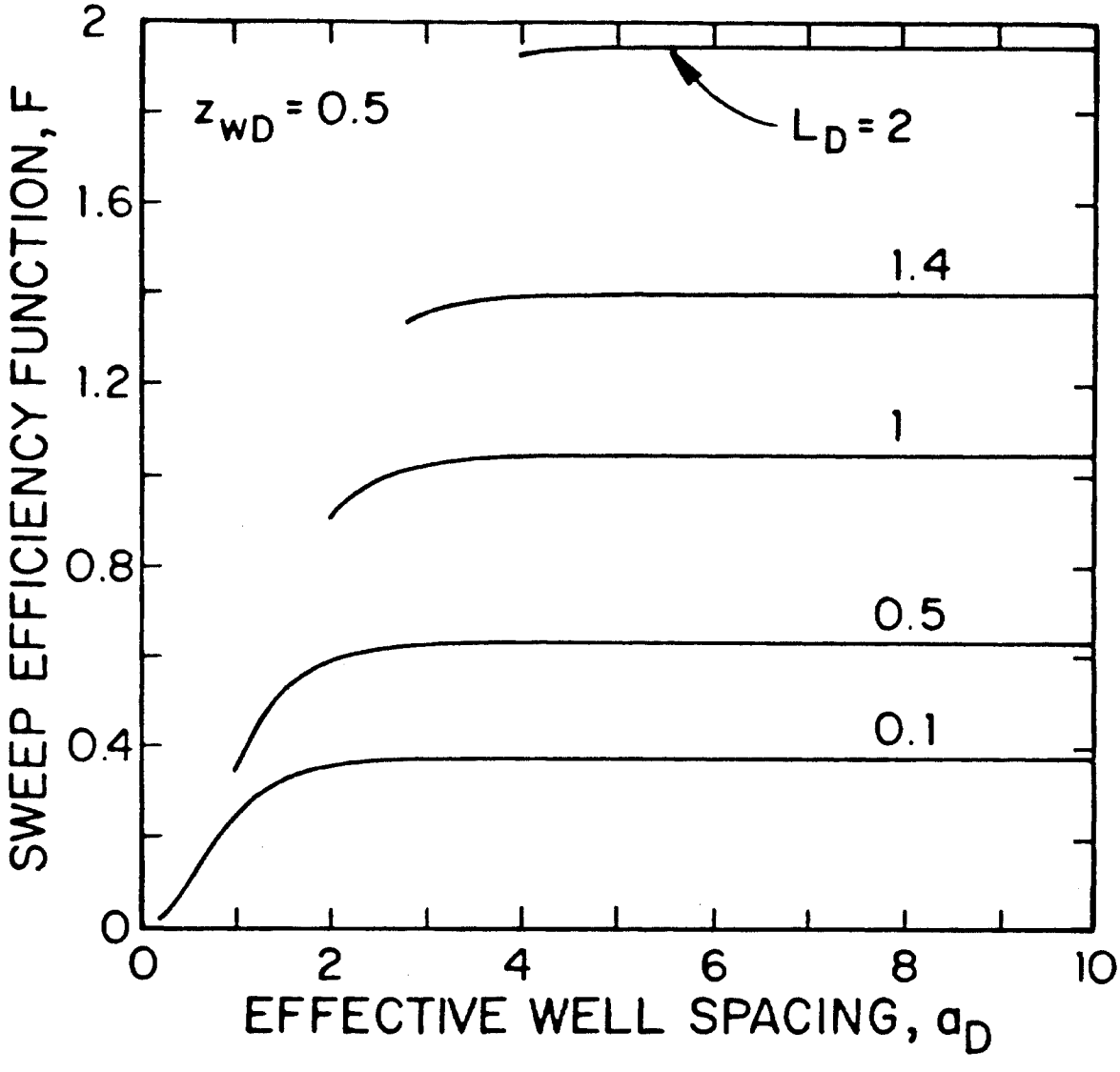

Fig. 4.4.7 - Sweep Efficiency Function F for Horizontal Wells – Correlation for Breakthrough Time.

well in a regular network of horizontal wells ($x_{eD} = y_{eD}$) as a function of effective well spacing. The well is assumed to be located at mid-height of the reservoir ($z_{wD} = 0.5$). The variable of interest is the dimensionless well half length, L_D. Fig. 4.4.7 indicates that for fixed values of a_D, the sweep efficiency function, F, increases as L_D increases; also for fixed L_D, F increases as a_D increases and it becomes independent of a_D at large values of a_D. This behavior is consistent with the observation made earlier that pressure gradients are negligible beyond the points defined by the relation $x_D L_D = 7.2/\pi$. Then Fig. 4.4.7 indicates that the water-free oil production obtained from an individual well in a regular network of horizontal wells increases until the effective drainage area dictated by the spacing between the wells becomes equal to the maximum drainage area defined by Eqs. 4.1.29 and 4.1.30. Thus, if a_D is large enough, breakthrough time is inversely proportional to k_z/k, all other parameters being fixed (see Eq. 4.4.20). Although the results shown in Fig. 4.4.7 are similar to that shown in Fig. 4.4.6, the role of anisotropy is more important in horizontal well case since L_D is a function of k_z/k.

One interesting point to note in Fig. 4.4.7 is that F is independent of a_D if L_D is large enough. This result is also true for other values of z_{wD}. The results shown in Fig. 4.4.8 may be used to determine the value of F for large values of L_D. The unbroken lines in Fig. 4.4.8 show the influence of the well length, L_h, and the well location, z_w, on the sweep efficiency function, F, for a horizontal well located in an infinite reservoir. For large values of L_D ($L_D \geq 2.3$), the sweep efficiency function, F, of horizontal wells becomes a linear function of L_D. This observation is consistent with that made from examination of Figs. 4.2.1 and 4.2.2. Using these values of F, the displacement efficiency, E, can be readily determined for large values of L_D (note that a_D only involves the physical dimensions of the reservoir). It is also possible to obtain the breakthrough times from Fig. 4.4.8 by using Eq. 4.4.20. Since for $L_D \geq 2.3$, F is proportional to L_D, we can decide from Eq. 4.4.20 that the breakthrough times for long horizontal wells are inversely proportional to $\sqrt{k_z/k}$ whereas the breakthrough times for vertical wells are inversely proportional to k_z/k.

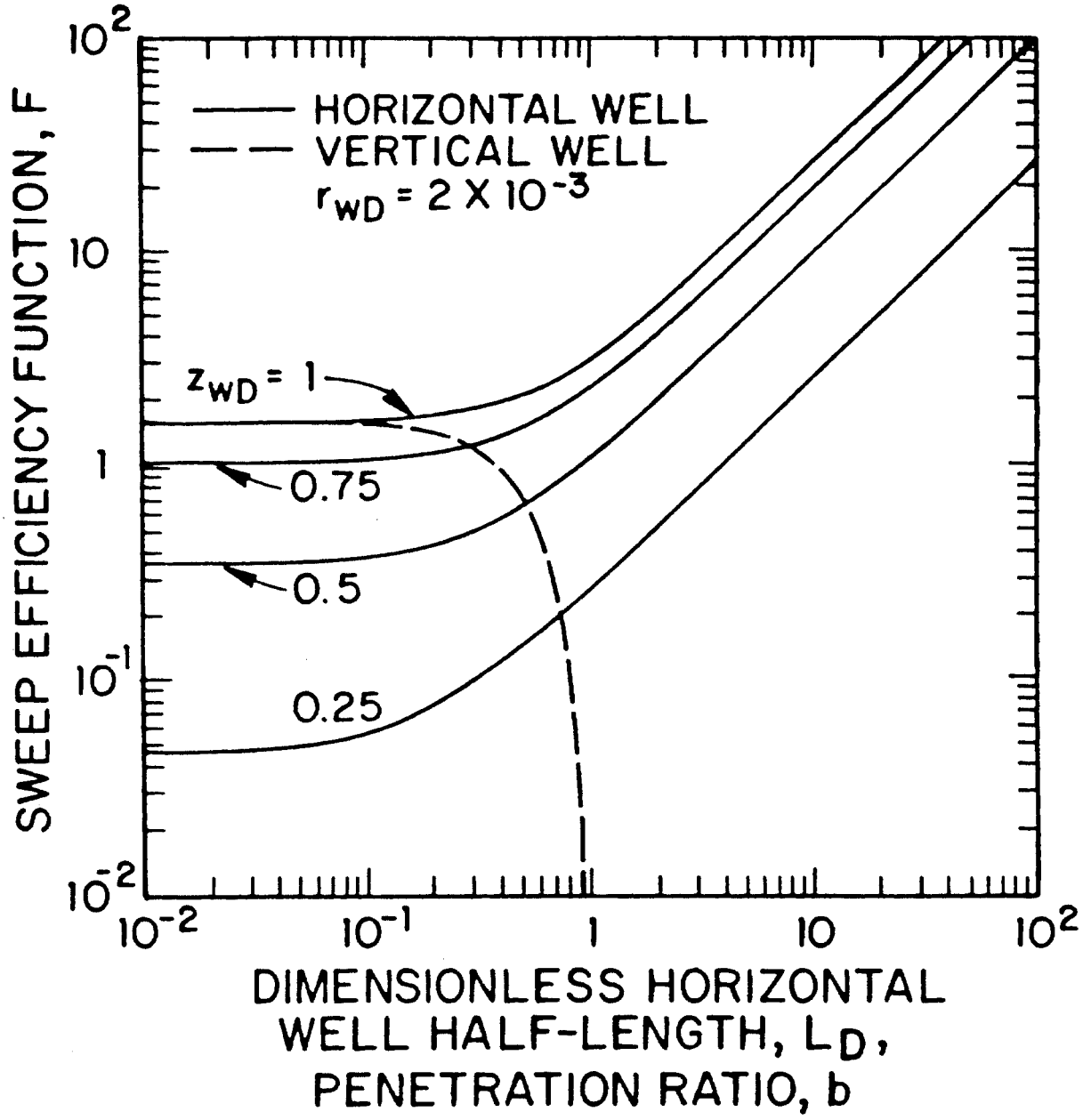

Fig. 4.4.8 - Sweep Efficiency Function F for Vertical and Horizontal Wells - Laterally Infinite Reservoir.

Fig. 4.4.8 may also be used to compare vertical and horizontal well productivities. The dashed line in Fig. 4.4.8 shows the variation of the sweep efficiency function, F, for a partially penetrating vertical well as a function of the penetration ratio b. Fig. 4.4.8 indicates that the sweep efficiency function, F, increases as the distance of the horizontal well from the original oil-water interface increases (as z_{wD} increases). Similarly, for vertical wells, the sweep efficiency increases as the distance of the bottom of the well from the original oil-water contact increases or as b decreases. The intersection points of the sweep efficiency curves for various elevations of horizontal wells (unbroken curves) and the curve representing the sweep efficiencies of vertical wells (dashed curve) mark the pairs of L_D and b for which the cumulative production until breakthrough from horizontal and vertical wells is the same. Similarly, corresponding to every vertical well penetration, b, it is possible to find a range of horizontal well elevations, z_{wD}, and horizontal well lengths, L_D, for which horizontal wells would perform better compared to vertical wells. The results shown in this figure also indicate that for small values of L_D ($L_D \leq 0.1$), the sweep efficiency function becomes independent of the well length. Our computations indicated that, the value of F obtained for $L_D \leq 0.1$ would approach to the sweep efficiency of a point source well located at the same elevation as the horizontal well. A summary of the equations used for the point source well calculations is presented in Appendix E. This result also applies to vertical wells with extremely small penetration ratios. In Fig. 4.4.8, we note that vertical well solutions for small values of b merge with the horizontal well solutions for $z_{wD} = 1$ and small values of L_D. Based on the observation that the point source idealization is applicable for small values of L_D or b, this result is not surprising.

<u>V. Influence of Gravity Effects</u> The analysis presented above is based on the fact that the water-free oil recovery is inversely proportional to the velocities of the oil-water interface. As already mentioned, one would expect density differences between the oil and water to reduce the velocity of the oil-water interface. On physical grounds, we can argue that the reduction in the interface velocities due to

density difference would be a maximum below the well axis at $x_D = y_D = 0$, where the elevation of the interface is at a maximum, and it would gradually decrease as the elevation of the interface decreases at distant points. Similarly, as a result of rapidly increasing pressure gradients in the vicinity of the well, the influence of the gravitational gradient would become smaller as the oil-water interface approaches the well. Thus, if we assumed that the reduction in the interface velocities were uniform everywhere at the oil-water interface and along the path from the original oil-water interface ($z = 0$) to the bottom of the well and it were equal to that at $x_D = y_D = z_D = 0$, we would be considering the situation where the influence of the gravity on the water-free oil production would be maximum. Therefore, it is possible to obtain an upper limit for the reduction in the interface velocities due to the influence of gravity by comparing the pressure gradients corresponding to the density difference with the pressure gradients at the original oil-water interface. Since the cumulative oil production before breakthrough is inversely proportional to the interface velocities, this would be equivalent to obtaining an upper limit for the increase in water-free oil recovery due to the influence of gravity.

Table 4.4.1 presents the upper limit estimates of the percent increases in water-free oil recoveries for an example case. For this example, the density difference between the oil and water is 18.73 lb_m/ft^3 and the equivalent pressure gradient is 0.13 psi/ft. For an original oil pay thickness of 25 ft and a wellbore pressure drop of 147 psi, pressure gradients at the original oil-water interface can be found from the following relation by using Eq. 4.2.30 (here we assumed an infinite reservoir).

$$\frac{\partial p}{\partial z}|_{z=0} = -\frac{p_i - p_{wf}}{hp_D}\frac{\partial p_D}{\partial z_D}|_{z_D=0}. \tag{4.4.21}$$

We computed the pressure gradients at the oil-water interface for three well locations, $z_{wD} = 1$, 0.5, and 0.25, and for two dimensionless well half lengths, $L_D = 5$ and 0.5. The results of these computations are shown in Cols. 2 and 4 of Table 4.4.1. The percent increases in water-free oil production given in Cols. 3 and 5 of Table 4.4.1 represent the ratios of the pressure gradient corresponding to the density difference between the water and oil to the pressure gradients at the origi-

TABLE 4.4.1

INFLUENCE OF GRAVITY ON WATER-FREE OIL RECOVERY

$$\rho_w - \rho_o = 18.73\ lb_m/ft^3$$
$$p_i - p_{wf} = 147\ psi$$
$$h = 25\ ft$$

Dimensionless Well Location z_{wD}	$L_D = 5$		$L_D = 0.5$	
	$\partial p/\partial z\|_{z=0}$	% Increase in Water-free Oil Recovery	$\partial p/\partial z\|_{z=0}$	% Increase in Water-free Oil Recovery
1.00	1.43	9.1	0.81	16.1
0.50	4.04	3.2	3.07	4.2
0.25	8.65	1.5	7.96	1.6

nal oil-water interface. (Note that if we assume that the pressure gradient is equal to the gravitational gradient, then this situation implies that the well is produced such that the pressure gradient is exactly equal to the gravitational gradient. This is analogus to the critical rate calculations done for the water coning problem in edge water drive systems.)

The results shown in Table 4.4.1 indicate that the influence of gravity on the water-free oil production becomes more important as the well length becomes shorter. Similarly, as the distance of the well from the original oil-water interface increases, the influence of the gravity becomes more significant. From Eq. 4.4.21, we can decide that for higher pressure drops than that assumed here (that is, at higher production rates), the influence of gravity on the water-free oil recovery would be less significant. For greater pay thicknesses, on the other hand, the percent increases in the water-free oil recoveries would be higher than those presented in Table 4.4.1. [For the same case considered here, Muskat computed (see author's reply in the end of Ref. 66) the improvements in the clean oil recoveries of vertical wells to be 20 and 3 percent for 50 and 90 percent well penetrations, respectively. He concluded that the effect of gravity would be greater for smaller well penetrations.]

At this stage, two points should be noted. First, we have assumed an infinite reservoir system. Had we assumed a finite reservoir system, then $\partial p/\partial z$ would be greater than or equal to the values noted here and thus percent increases in oil recovery would be less than those noted here. Second, had we assumed that $\partial p/\partial z$ was variable and compared increases in water-free oil recovery, then the increase in recovery would be less than that noted here. As a result of these observations, in actual circumstances, the influence of gravity would be much less than that noted here.

The quantitative example presented here, as well as the physical arguments provided, indicates that the assumption that the gravity would not have a major impact on the displacement efficiencies is not as important as it might have appeared initially. Therefore, the results presented in this work can be used with confidence to determine the productivities of horizontal wells and compare the horizontal and

vertical well productivities under bottom water drive conditions.

CHAPTER V

CONCLUSIONS

The primary subject of investigation in this work is the performance of horizontal wells. Preliminary results of our investigation indicate that the productivity of horizontal wells can be comparable to that of vertically fractured wells and hence horizontal well completions are an alternative option to conventional well completion techniques. In addition, this mode of completion should be effective in reservoirs wherin the invasion of the oil pay by water or gas precludes the efficient operation of vertical wells since horizontal wells provide a larger surface area for fluid withdrawal that results in reduced pressure gradients in the reservoir.

Several solutions are avaliable in the literature concerning the transient flow behavior of horizontal wells in homogeneous reservoirs. In this work, the transient flow solutions to horizontal well problem have been obtained through the use of the source function approach of Gringarten and Ramey[3]. The challenging problem, however, has been the extention of these solutions to more complex situations such as incorporating the influence of wellbore storage and skin, variable rate production, and production from naturally fractured reservoirs. The approach taken in this work to solve the aforementioned problems is a synthesis of two powerful methods in solving unsteady flow problems in reservoirs; the method of sources and the Laplace transformation technique. In essence, the procedure developed in this study covers a broad range of viable well-reservoir systems and many new solutions have been obtained as a result of the new source function approach.

The major contributions and the specific conclusions of this work are documented below following the outline of the text.

In Chapter II, a new source function approach has been developed to solve the problem of unsteady flow in reservoirs. The new approach is a culmination of attempts over a number of years to obtain the Laplace transformation to several important solutions in well test analysis, so that the utility of these solutions can be enhanced to other problems of considerable interest – solutions that incorporate the combined influence of wellbore storage and skin and solutions that can incorporate variable rate production. Initial efforts were not fruitful primarily because these attempts involved obtaining the appropriate Laplace transforms from the solutions given in Ref. 3. Our realization that many of the problems one encounters can be resolved, if one examines extensions of the Laplace transformation of Lord Kelvin's point source solution for a wide variety of outer boundary conditions removed the major obstacle in attaining the goal of this work. This aspect of our study is new for until now the use of Lord Kelvin's solution and its extensions in the petroleum engineering literature consider pressure distributions only in the time domain and not in terms of the Laplace variable. Solutions for various wellbore configurations (partially penetrating vertical wells, horizontal wells, and partially penetrating vertically fractured wells) are then obtained in the manner suggested by Carslaw and Jaeger[23]; sources are distributed along the appropriate space coordinate(s) and the pressure distribution is obtained by simple integration along the space coordinate(s). As an application of this procedure, an extensive library of solutions useful in well test analysis has been developed. Many of the solutions presented here are new and the fact that this library involves solutions in terms of the Laplace transform variable provides the analyst with the power to solve complex practical problems of interest.

Even if appropriate solutions are obtained with respect to the Laplace variable, myriad problems in the inversion of the solution by the Stehfest algorithm[9] must be overcome. The major problems are: *(i)* computations of integrals involving the modified Bessel function, $K_0(u)$ as $u \to 0$, *(ii)* recasting series that behave as if they are divergent series into convergent forms, and *(iii)* computations of series that involve double infinite Fourier series (limited entry wells in bounded reservoir systems).

These problems are also addressed in detail in Chapter II of this study; the results presented represent tangiable evidence of the claims regarding the computability of our solutions. Procedures to compute the horizontal well responses in bounded reservoir systems should be particularly useful since horizontal well lengths can be comparable to the dimensions of the drainage area. New expressions for shape factors for various well configurations in rectangular and cylindrical drainage areas are presented. These expressions can be used to predict long term well deliverability and also to compare well performance for various completion conditions. They serve the purpose of the pseudoskin factor for infinite-acting systems.

Although many specific results are presented, the central contribution of Chapter II is broad in scope. Briefly, the procedures developed in Chapter II permit the analyst to exploit the extraordinary advantages of the Laplace transformation technique to solve a wide variety of complex problems of interest in well test analysis.

In Chapter III, we have computed pressure responses of horizontal wells located between impermeable top and bottom boundaries of a laterally infinite reservoir and compared these responses to the responses of fully penetrating vertical fractures. Two classical boundary conditions, namely infinite-conductivity and uniform-flux, have been considered. Analytical expressions for the pseudoskin factor and the effective wellbore radius are presented. These expressions should be extremely useful for designing completions and comparing productivities. Physical explanations and interpretations provided in this chapter are not available in the literature. A new method to determine formation properties is also proposed. Pressure responses normalized by the derivative provide a novel procedure to analyze data.

Specific conclusions that result from the work presented in Chapter III are as follows:

1. For a single horizontal well or a drainhole, the infinite-conductivity idealization is the only viable boundary condition. For two drainholes drilled in diametrically opposite directions from a single vertical well, either the infinite-conductivity or the uniform-flux idealization is appropriate.

2. Horizontal well pressure responses are a function of the dimensionless well

length, L_D, and the dimensionless well radius, r_{wD}.

3. If the dimensionless well length, L_D, is greater than 25, then the long time ($t_D > 10$) pressure response of a horizontal well is essentially identical to that of a fully penetrating vertical fracture. If $L_D \geq 50$, the pressure response of horizontal well is indistinguishable from that of a vertically fractured well for $t_D > 10^{-2}$. This result implies that pseudoskin factors are negligible if $L_D \geq 5$.

4. The pressure response of horizontal wells and pseudoskin factors are, for all practical purposes, insensitive to the well location in the vertical plane of the reservoir.

In Chapter IV, we have presented analytical solutions together with approximating forms at short and long times for the pressure distribution created by horizontal wells producing under bottom water drive conditions. The influence of the reservoir boundaries on the pressure responses of horizontal wells is also investigated. The information provided on the flow characteristics enhances our understanding of the basic phenomena that underly the performance of horizontal wells subject to bottom water drive conditions. The productivity of horizontal wells is discussed in terms of the efficiency of the displacement mechanism provided by the water drive. Comparison of horizontal and vertical well performances under bottom water drive conditions can be easily obtained from the charts presented here. The results presented can also be used to determine the breakthrough times and the water-free oil recovery.

Based on the work presented in Chapter IV, the following conclusions regarding the performance of horizontal wells under bottom water drive conditions are estabilished:

1. Behavior of horizontal wells under bottom water drive conditions posseses unique characteristics. Performance predictions obtained under edge water drive assumption cannot be used for wells subject to bottom water drive.

2. The early time behavior of horizontal wells subject to bottom water drive is identical to that of horizontal wells located between impermeable top and bottom boundaries. For times $t_D \geq 20/\left(\pi L_D^2\right)$, the influence of the constant pressure

bottom boundary is estabilished and steady state flow prevails in the reservoir.

3. If bottom water drive is the major producing mechanism, then the pressure gradients in the reservoir beyond the points determined by the relations $x_D L_D \geq 2.3$ and $y_D L_D \geq 2.3$ are negligible. Similarly, if $L_D \geq 2.3$, then the pressure gradients beyond the tips of the well are negligible. This indicates that the maximum drainage area of a horizontal well under bottom water drive conditions is equal to $21.2h^2\,(k/k_z)$ if $L_D < 2.3$ and it is equal to L_h^2 if $L_D \geq 2.3$. Therefore, a small formation thickness or a large vertical to horizontal permeability contrast has a reducing effect on the maximum drainage area of the well. This result provides guidelines as to the number of wells required to develop a reservoir subject to bottom water drive.

4. The water-free oil production increases as the horizontal well length increases and for $L_D \geq 2.3$ it becomes proportional to L_D. As the dimensionless well-half length, L_D, becomes smaller than 0.1, the productivity of horizontal wells approaches the productivity of point source wells located at the same elevation as the horizontal well. Water-free oil production also increases as the distance of the well from the original oil-water interface increases.

5. Water-free oil production of an individual well in a network of horizontal wells increases as the spacing between the wells increases. Once the effective drainage area of the well becomes equal to a critical value, further increases in the well spacing do not influence the productivity of an individual well. Expressions to obtain this critical value are summarized in this study. Gains in the water-free oil production per additional well, however, continuously decrease with increasing number of wells.

6. The productivities of horizontal and vertical wells decrease as the ratio of vertical to horizontal permeability increases. The influence of anisotropy, however, is less on the productivity of horizontal wells compared to the influence on the vertical well productivities.

NOMENCLATURE

a = well spacing, ft, $[m]$

a_D = effective well spacing

b = penetration ratio

B = formation volume factor, RB/STB, $[res\ m^3/stock-tank\ m^3]$

C = shape factor

C_A = vertical well shape factor

C_{Af} = vertically fractured well shape factor

C_{Ah} = horizontal well shape factor

c_t = total compressibility, psi^{-1}, $[Pa^{-1}]$

E = displacement efficiency

F = sweep efficiency

F = horizontal well pseudoskin factor

f = microscopic displacement efficiency

$f(s)$ = defined in Eq. 2.1.23 or 2.1.42

$\overline{g}$ = Laplace transform of g

h = reservoir thickness, ft, $[m]$

h_D = dimensionless formation thickness

h_w = open interval of the pay in vertical direction, ft, $[m]$

k = permeability, md, $[m^2]$

k_l = permeability in the l-direction, $l = x$, y, or z, md, $[m^2]$

L = reference length in the system, ft, $[m]$

$\mathcal{L}$ = Laplace transform operator

l_D = dimensionless linear distance, $l = x$, y, or z

L_D = dimensionless horizontal well half length

L_h = horizontal well length, ft, $[m]$

L_{x_f} = fracture half length, ft, $[m]$

p = pressure, psi, $[Pa]$

p_D = dimensionless pressure

p_{Df} = vertical fracture dimensionless pressure

p_{Dh} = horizontal well dimensionless pressure

p_{Dv} = vertical well dimensionless pressure

p_i = initial pressure, psi, $[Pa]$

p_{wD} = dimensionless wellbore pressure

p_{wf} = wellbore pressure, psi, $[Pa]$

q = production rate, STB/D, $[m^3/s]$

$\tilde{q}$ = production rate from point source, STB/D, $[m^3/s]$

q^* = volumetric flow rate from the matrix system to the fracture system

r = radial distance, ft, $[m]$

r_D = dimensionless radial distance

r_{eD} = dimensionless drainage radius

r_w = wellbore radius, ft, $[m]$

r_{wD} = dimensionless wellbore radius (Eq. 3.3.3)

r_{wDz} = dimensionless wellbore radius (Eq. 3.3.4)

s = Laplace transform variable with respect to t_D

$\tilde{s}$ = Laplace transform variable with respect to t_{DA}

S = length, area, or volume of the source, ft, ft^2, or ft^3 $[m, m^2, \text{or } m^3]$

S = dimensionless skin factor

$\tilde{S}$ = unit storage factor, RB/psi, $[m^3/Pa]$

S_D = dimensionless storage constant

S_j = source function in the j-direction

S_ψ = distance traveled along a streamline, ft, $[m]$

t = time, $hours$, $[s]$

t_b = breakthrough time, $days$, $[s]$

t_D = dimensionless time

t_{DA} = dimensionless time based on drainage area

$u = sf(s)$

$\tilde{u} = \tilde{s}f(\tilde{s})$

V = relative volume with respect to the bulk volume

V = volume of oil pay swept by the water, ft^3, $[m^3]$

v_ψ = velocity along a streamline

x = distance in the x-direction, ft, $[m]$

x_D = dimensionless distance in the x-direction

x_D^* = dimensionless equivalent pressure point

$\tilde{x}_D$ = dimensionless distance in the x direction (Eq. 4.1.9)

$\widetilde{x}_{D1}$ = defined in Eq. 2.2.26

$\widetilde{x}_{D2}$ = defined in Eq. 2.2.27

x_e = reservoir length in x-direction, ft, $[m]$

x_{eD} = dimensionless reservoir length in the x-direction

$\tilde{x}_{eD}$ = dimensionless reservoir length

x_i = boundary of influence in the x direction, ft, $[m]$

x_{iD} = dimensionless boundary of influence in the x direction

x_w = well location in the x-direction, ft, $[m]$

x_{wD} = dimensionless well location in the x-direction

$\tilde{x}_{wD}$ = dimensionless well location in the x direction

y = distance in the y-direction, ft, $[m]$

y_D = dimensionless distance in the y-direction

$\tilde{y}_D$ = dimensionless distance in the y direction (Eq. 4.1.10)

$\widetilde{y}_{D1}$ = defined in Eq. 2.2.28

$\widetilde{y}_{D2}$ = defined in Eq. 2.2.29

y_e = reservoir length in the y-direction, ft, $[m]$

y_{eD} = dimensionless reservoir length in the y-direction

$\tilde{y}_{eD}$ = dimensionless reservoir width

y_i = boundary of influence in the y direction, ft, $[m]$

y_{iD} = dimensionless boundary of influence in the y direction

y_w = well location in the y-direction, ft, $[m]$

y_{wD} = dimensionless well location in the y-direction

$\tilde{y}_{wD}$ = dimensionless well location in the y direction

z = distance in the z-direction, ft, $[m]$

z_b = vertical location of the bottom of the well, ft, $[m]$

z_{bD} = dimensionless vertical location of the bottom of the well

z_D = dimensionless distance in the z-direction

$\tilde{z}_{D1}$ = defined in Eq. 2.2.30

$\tilde{z}_{D2}$ = defined in Eq. 2.2.31

z_w = well location in the z-direction, ft, $[m]$

z_{wD} = dimensionless well location in the z-direction

α = interporosity shape factor

γ = Euler's constant ($\gamma = 0.5772...$)

Δp = pressure difference from the initial pressure, psi, $[Pa]$

η_j = diffusivity constant, $j = x$, y, or z, $ft^2/hour$, $[m^2/s]$

σ = verticall fractured well pseudoskin factor

λ = dimensionless transfer coefficient (Warren and Root model)

λ' = dimensionless transfer coefficient (deSwaan-O model)

μ = fluid viscosity, cp, $[Pa.s]$

ρ_o = density of oil, lb_m/ft^3, $[kg.m^{-3}]$

ρ_w = density of water, lb_m/ft^3, $[kg.m^{-3}]$

ϕ = porosity, $fraction$

φ = defined in Eqs. 2.7.35 and 3.4.7

ψ = stream function

ψ_D = dimensionless stream function

ω = dimensionless matrix storativity (Warren and Root model)

ω' = dimensionless matrix storativity (deSwaan-O model)

Subscripts

f = fracture system

m = matrix system

REFERENCES

1. Vicanek, J.: "Oil Production with Horizontal Wells," *Erdoel - Erdgas*, Vol. 101, No. 3, March 1985, 85-90.
2. Giger, F. M., Reiss, L. H., and Jourdan, A.P.: "The Reservoir Engineering Aspects of Horizontal Drilling," paper SPE 13024 presented at the 59th Annual Technical Conference and Exhibition, Dallas, Texas, Sept. 16-19, 1984.
3. Gringarten, A. C. and Ramey, H. J., Jr.: "The Use of Source and Green's Functions in Solving Unsteady-Flow Problems in Reservoirs," *Soc. Pet. Eng. J.* (Oct. 1973) 285-296; *Trans.*, AIME, Vol. 255.
4. Chow, V. T.: "On the Determination of Transmissibility and Storage Coefficients From Pumping Test Data," *Trans.*, Am. Geophys. Un. (1952), Vol. 33, 397-404.
5. Ozkan, E., Raghavan, R., and Joshi, S. D.: "Horizontal Well Pressure Analysis," paper SPE 16378, presented at the 1987 California Regional Meeting, Ventura, CA, April 8-10, 1987.
6. Onur, M. and Reynolds, A. C.: "A New Approach for Constructing Derivative Type Curves for Well Test Analysis," *SPEFE* (March 1988) 197-206.
7. Onur, M., Yeh, N., and Reynolds, A. C.: "New Derivative Type Curves for Well Test Analysis," paper SPE 16810, presented at the 1987 Annual Technical Conference and Exhibition, Dallas, TX, Sept. 27-30, 1987.
8. Duong, A. N.: "A New Set of Type Curves for Well Test Interpretation Using the Pressure Derivative Ratio," paper SPE 16812, presented at the 1987 Annual Technical Conference and Exhibition, Dallas, TX, Sept. 27-30, 1987.
9. Stehfest, H.: "Algorithm 368, Numerical Inversion of Laplace Transforms," D-5, *Communications of the ACM* (Jan. 1970) 13, No. 1, 47.

10. Gringarten, A. C., Ramey, H. J., Jr., and Raghavan, R.: "Unsteady-State Pressure Distributions Created by a Well With a Single Infinite-Conductivity Vertical Fracture," *Soc. Pet. Eng. J.* (Aug. 1974) 347-360; *Trans.*, AIME, Vol. 257.

11. Kucuk, F.: "Generalized Transient Pressure Solutions with Wellbore Storage," paper SPE 15671, SPE, Richardson, TX, 1986.

12. Ramey, H. J., Jr. and Gringarten, A. C.: "Effect of High Volume Vertical Fractures on Geothermal Steam Well Behavior," *Proc. Second United Nations Symposium on the Use and Development of Geothermal Energy*, San Francisco, May 20-29, 1975.

13. Raghavan, R.: "Some Practical Considerations in the Analysis of Pressure Data," *J. Pet. Tech.* (Oct. 1976) 1256-1268; *Trans.*, AIME, Vol. 257.

14. Yeh, N., Davison, M. J., and Raghavan, R.: "Fractured Well Responses in Heterogeneous Systems – Application to Devonian Shale and Austin Chalk Resrvoirs," *J. Energy Resources Technology* (June 1986) 120-130; *Trans.*, ASME, Vol. 108.

15. Houze, O. P., Horne, R., and Ramey, H. J., Jr.: "Infinite Conductivity Vertical Fracture in a Reservoir With Double Porosity Behavior," paper SPE 12778, presented at the 1984 California Regional Meeting, Long Beach, CA, April 11-13, 1984.

16. van Everdingen A. F. and Hurst, W.: "The Application of the Laplace Transformation to Flow Problems in Reservoirs," *Trans.*, AIME (1949) Vol. 186, 305-324.

17. Ozkan, E. and Raghavan, R.: "Performance of Horizontal Wells Subject to Bottom Water Drive," paper SPE 18559, SPE, Richardson, TX, 1988.

18. Warren, J. E. and Root, P. J.: "The Behavior of Naturally Fractured Reservoirs," *Soc. Pet. Eng. J.* (Sept. 1963) 245-255.

19. Kazemi, H.: "Pressure Transient Analysis of Naturally Fractured Reservoirs," *Trans.* AIME, 1969, Vol. 246, 451-461.

20. deSwaan - O, A.:"Analytical Solutions for Determining Naturally Fractured

Reservoir Properties by Well Testing," *Soc. Pet. Eng. J.* (June 1976) 117-122.

21. Barenblatt, G. I. and Zeltov, Yu. P.: "Fundamental Equations of Homogeneous Liquids in Fissured Rocks," *Dokl. Akad. Nauk SSR* (June 1960) 132, No. 3, 545-548.
22. Cinco-Ley, H., Kuchuk, F., Ayoub, J., Samaniego-V, F., and Ayesteran, L.: "Analysis of Pressure Tests Through the Use of Instantaneous Source Response Concepts," paper SPE 15476 presented at the 1986 Annual Technical Conference and Exhibition, New Orleans, LA, Oct. 5-8.
23. Carslaw, H. S. and Jaeger, J. C.: *Conduction of Heat in Solids*, Oxford University Press, Oxford (1986) 42, 255-277, 490.
24. Serra, K., Reynolds, A. C., and Raghavan, R.: "New Pressure Transient Analysis Procedures for Naturally Fractured Reservoirs," *J. Pet. Tech.* (Dec. 1983) 2271-2284.
25. Wijesinghe, A. M.: "Green's Functions for Solving Unsteady Flow Problems in Naturally Fractured Reservoirs With Arbitrary Fracture Connectivity: Part I – Theory," paper SPE 13626, presented at the 1985 California Regional Meeting, Bakersfield, CA, March 27-29, 1985.
26. Wijesinghe, A. M. and Kececioglu, I.: "Green's Functions for Solving Unsteady Flow Problems in Naturally Fractured Reservoirs With Arbitrary Fracture Connectivity: Part II – Applications," paper SPE 15113, presented at the 1986 California Regional Meeting, Oakland, CA, April 2-4, 1986.
27. Abramowitz, M. and Stegun, I. A.: *Handbook of Mathematical Functions*, Dover Publications, Inc., New York (1972) 1019-1030, 480.
28. Kuchuk, F. J.: "New Methods for Estimating Parameters of Low Permeability Reservoirs," paper SPE/DOE 16394, presented at the SPE/DOE Low Permeability Reservoir Symposium, Denver, CO, May 18-19, 1987.
29. Kuchuk, F. J. and Kirwan, P. A.: "New Skin and Wellbore Storage Type Curves for Partially Penetrating Wells," *SPEFE* (Dec. 1987) 546-554.
30. Muskat, M.: *The Flow of Homogeneous Fluids through Porous Media*, reprinted by I. H. R. D. C., Boston (1982) 263-277.

31. Dougherty, D. E. and Babu, D. K.: "Flow to a Partially Penetrating Well in a Double-Porosity Medium," *Water Resources Research* (Aug. 1984) Vol. 20, No. 8, 1116-1122.

32. Fraim, M. L. and Lee, W. J.: "Determination of Formation Properties From Long-Term Gas Well Production Affected by Non-Darcy Flow," paper SPE 16934, presented at the 62nd Annual Technical Conference, Dallas, TX, Sept. 27-30, 1987.

33. Yeh, N., Davison, M. J., and Raghavan, R.: "Fractured Well Responses in Heterogeneous Systems – Application to Devonian Shale and Austin Chalk Resrvoirs," *J. Energy Resources Technology* (June 1986) 120-130; *Trans.*, ASME, Vol. 108.

34. Davison, M. J.: *Pressure Behavior of Fractured Wells in Naturally Fractured Reservoirs Subject to the Warren and Root Idealization*, MS thesis, The University of Tulsa, Tulsa, OK, 1984.

35. Spainer, J. and Oldham, K. B.: *An Atlas of Functions*, Hemisphere Publishing Corporation, Washington (1987) 506.

36. Gradshteyn, I. S. and Ryzhik, I. M.: *Table of Integrals, Series, and Products*, Academic Press, Inc., Orlando (1980) 40.

37. Daviau, F., Mouronval, G., Bourdarot, G. and Curutchet, P.: "Pressure Analysis for Horizontal Wells," paper SPE 14251 presented at the 60th Annual Technical Conference and Exhibition, Las Vegas, Sept. 22-25, 1985.

38. Clonts, M. D. and Ramey, H. J., Jr.: "Pressure Transient Analysis for Wells with Horizontal Drainholes," paper SPE 15116, presented at the 56th California Regional Meeting, Oakland, CA, April. 2-4, 1986.

39. Prats, M.: "Effect of Vertical Fractures on Reservoir Behavior – Incompressible Fluid Case," *Soc. Pet. Eng. J.* (June 1961) 105-118.

40. Prats, M., Hazebroek, P., and Strickler, W. R.: "Effect of Vertical Fractures on Reservoir Behavior – Compressible Fluid Case," *Soc. Pet. Eng. J.* (June 1962) 87-94.

41. Dietz, D. N.: "Determination of Average Reservoir Pressure From Buildup

Surveys," *J. Pet. Tech.* (Aug. 1965) 955-959; *Trans.*, AIME, Vol. 234.

42. Russell, D. G. and Truitt, N. E.: "Transient Pressure Behavior in Vertically Fractured Reservoirs," *J. Pet. Tech.* (Oct. 1964) 1159-1170; *Trans.*, AIME, Vol. 231.
43. Gringarten, A. C.: "Reservoir Limit Testing For Fractured Wells," paper SPE 7452, presented at the 53rd Annual Technical Conference and Exhibition, Dallas, TX, Oct. 1-3, 1978.
44. Earlougher R. C., Jr.: *Advances in Well Test Analysis*, Monograph Series, SPE, Dallas (1977) Vol. 5.
45. Bennett, C. O.: *Analysis of Fractured Wells*, Ph.D. Dissertation, The University of Tulsa, Tulsa, OK, 1982.
46. Suresh, P. K. and Tiab, D.: "Application of p'_D Function to Vertically Fractured Wells – Field Cases," paper SPE 11028, presented at the 57th Annual Technical Conference and Exhibition, New Orleans, LA, Sept. 26-29, 1982.
47. Algoa, A., Bourdet, D., and Ayoub, J. A.: "How to Simplify the Analysis of Fractured Well Tests," *World Oil* (Oct. 1985) 97-102.
48. Ramey, H. J. and Agarwal, R. G.: "Annulus Unloading Rates as Influenced by Wellbore Storage and Skin Effects," *Soc. Pet. Eng. J.* (Oct. 1972) 453-462; *Trans.*, AIME, Vol. 253.
49. Joshi, S. D.: "A Review of Horizontal Well and Drainhole Technology," paper SPE 16868 presented at the 1987 Annual Technical Conference, Dallas, TX, Sept. 27 – 30.
50. Goode, P. A. and Thambynayagam, R. K. M.: "Pressure Drawdown and Buildup Analysis of Horizontal Wells in Anisotropic Media," *SPEFE* (Dec. 1987) 683 – 697.
51. Reiss, L. H.: "'Horizontal Wells' Production After Five Years," paper SPE 14338 presented at the 1985 Annual Technical Conference, Las Vegas, Nevada, Sept. 22-25.
52. Muskat, M.: *The Flow of Homogeneous Fluids Through Porous Media*, reprinted by I.H.R.D.C., Boston (1982).

53. Muskat, M.: *Physical Principles of Oil Production*, reprinted by I.H.R.D.C., Boston (1981).

54. Van Der Vlis, A. C., Duns, H., and Luque, R. F.: "Increasing Well Productivity in Tight Chalk Reservoirs," *Proc.* 10th World Petroleum Congress, Vol. 3, Buchaiest, Hungary (1979), 71-78.

55. Giger, F., Combe, J., and Reiss, L. H.: "L'Intérêt Du Forage Horizontal Pour L'Explotation De Gisements D'Hydracarbures," *Revue De L'Institut Français Du Pétrole*, Vol. 38, No. 3, May-June 1983, 329-350.

56. Rosa, A. J. and Carvalho, R. S.: "A Mathematical Model for Pressure Evaluation in an Infinite Conductivity Horizontal Well," paper SPE 15967, SPE, Richardson, TX.

57. Giger, F.M.: "Horizontal Wells Production Techniques in Heterogeneous Reservoirs," paper SPE 13710, presented at the 1985 Middle East Oil Technical Conference and Exhibition, Bahrain, March 11-14, 1985.

58. Joshi, S.D.: "Augmentation of Well Productivity Using Slant and Horizontal Wells," paper SPE 15375, presented at the 61st Annual Technical Conference and Exhibition, New Orleans, Oct. 5-8, 1986.

59. Rodriguez, F., Horne, R.N., and Cinco-Ley, H.: "Partially Penetrating Fractured Well: Pressure Transient Analysis of an Infinite-Conductivity Vertical Fracture," paper SPE 12743, presented at the 54th California Regional Meeting, Long Beach, April 11-13, 1984.

60. Horner, D.R.: "Pressure Build-up in Wells," *Proc.*, Third World Pet. Cong., The Hague (1951) II, 503-521.

61. Raghavan, R.: "The Effect of Producing Time on Type Curve Analysis," *J. Pet. Tech.* (Oct. 1980) 1053-64.

62. Chaperon, I.: "Theoretical Study of Coning Toward Horizontal and Vertical Wells in Anisotropic Formations: Subcritical and Critical Rates," paper SPE 15377 presented at the 1986 Annual Technical Conference, New Orleans, LA, Oct. 5-8.

63. Giger, F.: "Évaluation Théorique De L'Effet D'Arête D'Eau Sur La Production

Par Puits Horizontaux," *Revue De L'Institut Français Du Pétrole*, Vol. 38, No. 3, May-June 1983, 361-370.

64. Giger, F.: "Analytic 2D Models of Water Cresting Before Breakthrough for Horizontal Wells," paper SPE 15378 presented at the 1986 Annual Technical Conference, New Orleans, LA, Oct. 5-8.
65. Muskat, M. and Wyckoff, R. D.: "An Approximate Theory of Water-coning in Oil Production," *Trans.* AIME (1935) 114, 144-163.
66. Muskat, M.: "The Performance of Bottom Water-drive Reservoirs," *Trans.* AIME (1947) 170, 81-111.
67. Kuchuk, F. J., Goode, P. A., Wilkinson, D. J., and Thambynayagam, R. K. M.: "Pressure Transient Behavior of Horizontal Wells With and Without Gas Cap or Aquifer," paper SPE 17413 presented at the 1988 California Regional Meeting, Long Beach, CA, March 23-25.
68. Hansen. E. R.: *A Table of Series and Products*, Prentice-Hall, Inc., Englewood Cliffs, N. J. (1975).
69. Dupuit, J.: *Etudes Théorique Et Pratiques Sur Le Mouvement Des Eaux*, 2nd Ed., Dunod, Paris (1863).
70. Forchheimer, P.: *Hydraulik Encyklopädie Der Mathematishen Wissenschaften*, 4.20. B. G. Teubner, Leipzig (1901-1908).
71. Giger, F.: "Réduction Du Nombre De Puits Par L'utilisation De Forages Horizontaux," *Revue De L'Institut Français Du Pétrole*, Vol. 38, No. 3, May-June 1983, 351-360.
72. Buhidma, I. M and Raghavan, R.: "Transient Pressure Behavior of Partially Penetrating Wells Subject to Bottomwater Drive," *JPT* (July 1980) 1251-1261.
73. Nisle, R. G.: "The Effect of Partial Penetration on Pressure Buildup in Oil Wells," *Trans.* AIME (1958) 213, 85-90.

APPENDIX A

SOME SOLUTIONS USEFUL IN WELL TESTING

In this appendix, we present a library of Laplace domain solutions useful in well test analysis. The procedure to obtain these solutions is discussed in §§2.1 and 2.2 of this work. Table 1 presents the solutions for laterally infinite reservoirs. Table 2 lists the solutions for cylindrical reservoirs. In Table 3, continuous point source solutions for rectangular drainage regions are presented. The procedure to obtain the solutions for different well configurations by using the point source solutions given in Table 3 is discussed in §§2.2 III and 2.3.

In Tables 1 – 3, h_w denotes the length of the penetrated interval in case of limited entry wells and fractures, L_{x_f} is the half length of a vertical fracture in the lateral direction, and L_h is the length of a horizontal well. For each type of well considered in Tables 1 – 3, the appropriate relation between the withdrawal rate from the well, q, and the withdrawal rate from the point source, $\tilde{q}$, is also noted. The location of the well is determined by x_{wD}, y_{wD}, and z_{wD}, except in Table 2 where the well is assumed to be located at the center of the circular drainage area ($x_{wD} = y_{wD} = 0$). In Table 2, r_{eD} is the dimensionless drainage area where $r_D = \sqrt{x_D^2 + y_D^2}$ defines the dimensionless radial distance and $\tilde{r}_D = \sqrt{\left(x_D - \alpha\sqrt{k/k_x}\right)^2 + y_D^2}$. The coordinate system for the solutions given in Table 3 is chosen to be at the bottom left hand corner of the reservoir, and the dimensions of the reservoir are defined by x_{eD}, y_{eD}, and h_D. To the left of each solution given in Table 3 is the areal view of the rectangular drainage region for the particular solution. The well is assumed to be located at some arbitrary point x_{wD}, y_{wD}, z_{wD}. $ch(x)$ and $sh(x)$ used in these solutions denote the hyperbolic cosine and hyperbolic sine functions respectively.

TABLE 1-A
SOLUTIONS FOR WELLS IN INFINITE RESERVOIRS
IMPERMEABLE BOUNDARIES AT $z_D = 0$ AND $z_D = h_D$

WELL TYPE	PRESSURE DISTRIBUTION IN LAPLACE SPACE, $\overline{\Delta p}$
POINT SOURCE $q = \tilde{q}$	$\frac{\tilde{q}\mu}{2\pi k L h_D s}\left[K_0\left(r_D\sqrt{u}\right) + 2\sum_{n=1}^{\infty} K_0\left(r_D\sqrt{u+\frac{n^2\pi^2}{h_D^2}}\right)\cos n\pi\frac{z}{h}\cos n\pi\frac{z_w}{h}\right]$
FULLY PENETRATING VERTICAL WELL $q = \tilde{q}h$	$\frac{\tilde{q}\mu h}{2\pi k L h_D s} K_0\left(r_D\sqrt{u}\right)$
PARTIALLY PENETRATING VERTICAL WELL $q = \tilde{q}h_w$	$\frac{\tilde{q}\mu h_w}{2\pi k L h_D s} K_0\left(r_D\sqrt{u}\right) + \frac{2\tilde{q}\mu h}{\pi^2 k L h_D s}\sum_{n=1}^{\infty}\left[\frac{1}{n}K_0\left(r_D\sqrt{u+\frac{n^2\pi^2}{h_D^2}}\right)\sin n\pi\frac{h_w}{2h}\cos n\pi\frac{z_w}{h}\cos n\pi\frac{z}{h}\right]$
FULLY PENETRATING VERTICAL FRACTURE $q = 2\tilde{q}hL_{x_f}$	$\frac{\tilde{q}\mu h}{2\pi k h_D s}\int_{-L_{x_f}/L}^{+L_{x_f}/L} K_0\left[\sqrt{u}\sqrt{(x_D - x_{wD} - \alpha\sqrt{k/k_x})^2 + (y_D - y_{wD})^2}\right] d\alpha$
PARTIALLY PENETRATING VERTICAL FRACTURE $q = 2\tilde{q}h_w L_{x_f}$	$\frac{\tilde{q}\mu h_w}{2\pi k h_D s}\int_{-L_{x_f}/L}^{+L_{x_f}/L} K_0\left[\sqrt{u}\sqrt{(x_D - x_{wD} - \alpha\sqrt{k/k_x})^2 + (y_D - y_{wD})^2}\right] d\alpha + \frac{2\tilde{q}\mu h}{\pi^2 k h_D s}\sum_{n=1}^{\infty}\frac{1}{n}\sin n\pi\frac{h_w}{2h}\cos n\pi\frac{z_w}{h}\cos n\pi\frac{z}{h}\int_{-L_{x_f}/L}^{+L_{x_f}/L} K_0\left[\sqrt{u+\frac{n^2\pi^2}{h_D^2}}\sqrt{(x_D - x_{wD} - \alpha\sqrt{k/k_x})^2 + (y_D - y_{wD})^2}\right] d\alpha$
HORIZONTAL WELL $q = \tilde{q}L_h$	$\frac{\tilde{q}\mu}{2\pi k h_D s}\left\{\int_{-L_h/(2L)}^{+L_h/(2L)} K_0\left[\sqrt{u}\sqrt{(x_D - x_{wD} - \alpha\sqrt{k/k_x})^2 + (y_D - y_{wD})^2}\right] d\alpha + 2\sum_{n=1}^{\infty}\cos n\pi\frac{z}{h}\cos n\pi\frac{z_w}{h}\int_{-L_h/(2L)}^{+L_h/(2L)} K_0\left[\sqrt{u+\frac{n^2\pi^2}{h_D^2}}\sqrt{(x_D - x_{wD} - \alpha\sqrt{k/k_x})^2 + (y_D - y_{wD})^2}\right] d\alpha\right\}$

TABLE 1-B
SOLUTIONS FOR WELLS IN INFINITE RESERVOIRS
CONSTANT PRESSURE BOUNDARIES AT $z_D = 0$ AND $z_D = h_D$

WELL TYPE	PRESSURE DISTRIBUTION IN LAPLACE SPACE, $\overline{\Delta p}$
POINT SOURCE $q = \tilde{q}$	$\frac{\tilde{q}\mu}{\pi k L h_D s} \sum_{n=1}^{\infty} K_0 \left(r_D \sqrt{u + \frac{n^2\pi^2}{h_D^2}} \right) \sin n\pi \frac{z}{h} \sin n\pi \frac{z_w}{h}$
PARTIALLY PENETRATING VERTICAL WELL $q = \tilde{q} h_w$	$\frac{2\tilde{q}\mu h}{\pi^2 k L h_D s} \sum_{n=1}^{\infty} \frac{1}{n} K_0 \left(r_D \sqrt{u + \frac{n^2\pi^2}{h_D^2}} \right) \sin n\pi \frac{h_w}{2h} \sin n\pi \frac{z_w}{h} \sin n\pi \frac{z}{h}$
PARTIALLY PENETRATING VERTICAL FRACTURE $q = 2\tilde{q} h_w L_{x_f}$	$\frac{2\tilde{q}\mu h}{\pi^2 k h_D s} \sum_{n=1}^{\infty} \frac{1}{n} \sin n\pi \frac{h_w}{2h} \sin n\pi \frac{z_w}{h} \sin n\pi \frac{z}{h}$ $\int_{-L_{s_f}/L}^{+L_{s_f}/L} K_0 \left[\sqrt{u + \frac{n^2\pi^2}{h_D^2}} \sqrt{(x_D - x_{wD} - \alpha\sqrt{k/k_x})^2 + (y_D - y_{wD})^2} \right] d\alpha$
HORIZONTAL WELL $q = \tilde{q} L_h$	$\frac{\tilde{q}\mu}{\pi k h_D s} \sum_{n=1}^{\infty} \sin n\pi \frac{z}{h} \sin n\pi \frac{z_w}{h}$ $\int_{-L_h/(2L)}^{+L_h/(2L)} K_0 \left[\sqrt{u + \frac{n^2\pi^2}{h_D^2}} \sqrt{(x_D - x_{wD} - \alpha\sqrt{k/k_x})^2 + (y_D - y_{wD})^2} \right] d\alpha$

TABLE 1-C

SOLUTIONS FOR WELLS IN INFINITE RESERVOIRS

IMPERMEABLE BOUNDARY AT $z_D = 0$, CONSTANT PRESSURE BOUNDARY AT $z_D = h_D$

WELL TYPE	PRESSURE DISTRIBUTION IN LAPLACE SPACE, $\overline{\Delta p}$
POINT SOURCE $q = \tilde{q}$	$\frac{\tilde{q}\mu}{\pi k L h_D s} \sum_{n=1}^{\infty} K_0 \left[r_D \sqrt{u + \frac{(2n-1)^2\pi^2}{4h_D^2}} \right] \cos(2n-1)\frac{\pi}{2}\frac{z}{h} \cos(2n-1)\frac{\pi}{2}\frac{z_w}{h}$
PARTIALLY PENETRATING VERTICAL WELL $q = \tilde{q} h_w$	$\frac{4\tilde{q}\mu h}{\pi^2 k L h_D s} \sum_{n=1}^{\infty} \frac{1}{(2n-1)} K_0 \left[r_D \sqrt{u + \frac{(2n-1)^2\pi^2}{4h_D^2}} \right]$ $\sin(2n-1)\frac{\pi}{2}\frac{h_w}{2h} \sin(2n-1)\frac{\pi}{2}\frac{z_w}{h} \cos(2n-1)\frac{\pi}{2}\frac{z}{h}$
PARTIALLY PENETRATING VERTICAL FRACTURE $q = 2\tilde{q} h_w L_{x_f}$	$\frac{4\tilde{q}\mu h}{\pi^2 k h_D s} \sum_{n=1}^{\infty} \frac{1}{(2n-1)} \sin(2n-1)\frac{\pi}{2}\frac{h_w}{2h} \sin(2n-1)\frac{\pi}{2}\frac{z_w}{h} \cos(2n-1)\frac{\pi}{2}\frac{z}{h}$ $\int_{-L_{x_f}/L}^{+L_{x_f}/L} K_0 \left[\sqrt{u + \frac{(2n-1)^2\pi^2}{4h_D^2}} \sqrt{(x_D - x_{wD} - \alpha\sqrt{k/k_x})^2 + (y_D - y_{wD})^2} \right] d\alpha$
HORIZONTAL WELL $q = \tilde{q} L_h$	$\frac{\tilde{q}\mu}{\pi k h_D s} \sum_{n=1}^{\infty} \cos(2n-1)\frac{\pi}{2}\frac{z}{h} \cos(2n-1)\frac{\pi}{2}\frac{z_w}{h}$ $\int_{-L_h/(2L)}^{+L_h/(2L)} K_0 \left[\sqrt{u + \frac{(2n-1)^2\pi^2}{4h_D^2}} \sqrt{(x_D - x_{wD} - \alpha\sqrt{k/k_x})^2 + (y_D - y_{wD})^2} \right] d\alpha$

TABLE 2-A
POINT SOURCE WELLS
BOUNDED RESERVOIRS - CYLINDRICAL COORDINATES

BOUNDARY CONDITION AT $z_D = 0$ AND h_D	BOUNDARY CONDITION AT $r_D = r_{cD}$	PRESSURE DISTRIBUTION IN LAPLACE SPACE, $\overline{\Delta p}$
$\frac{\partial \overline{\Delta p}}{\partial z_D}\|_{z_D=0,h_D} = 0$	$\frac{\partial \overline{\Delta p}}{\partial r_D}\|_{r_D=r_{cD}} = 0$	$\frac{\tilde{q}\mu}{2\pi k L h_D s}\left\{K_0\left(r_D\sqrt{u}\right) + \frac{I_0\left(r_D\sqrt{u}\right)K_1\left(r_{cD}\sqrt{u}\right)}{I_1\left(r_{cD}\sqrt{u}\right)} + 2\sum_{n=1}^{\infty}\cos n\pi\frac{z}{h}\cos n\pi\frac{z_w}{h}\left[K_0\left(r_D\sqrt{u+\frac{n^2\pi^2}{h_D^2}}\right) + \frac{I_0\left(r_D\sqrt{u+\frac{n^2\pi^2}{h_D^2}}\right)K_1\left(r_{cD}\sqrt{u+\frac{n^2\pi^2}{h_D^2}}\right)}{I_1\left(r_{cD}\sqrt{u+\frac{n^2\pi^2}{h_D^2}}\right)}\right]\right\}$
	$\overline{\Delta p}\|_{r_D=r_{cD}} = 0$	$\frac{\tilde{q}\mu}{2\pi k L h_D s}\left\{K_0\left(r_D\sqrt{u}\right) - \frac{I_0\left(r_D\sqrt{u}\right)K_0\left(r_{cD}\sqrt{u}\right)}{I_0\left(r_{cD}\sqrt{u}\right)} + 2\sum_{n=1}^{\infty}\cos n\pi\frac{z}{h}\cos n\pi\frac{z_w}{h}\left[K_0\left(r_D\sqrt{u+\frac{n^2\pi^2}{h_D^2}}\right) - \frac{I_0\left(r_D\sqrt{u+\frac{n^2\pi^2}{h_D^2}}\right)K_0\left(r_{cD}\sqrt{u+\frac{n^2\pi^2}{h_D^2}}\right)}{I_0\left(r_{cD}\sqrt{u+\frac{n^2\pi^2}{h_D^2}}\right)}\right]\right\}$
$\overline{\Delta p}\|_{z_D=0,h_D} = 0$	$\frac{\partial \overline{\Delta p}}{\partial r_D}\|_{r_D=r_{cD}} = 0$	$\frac{\tilde{q}\mu}{\pi k L h_D s}\sum_{n=1}^{\infty}\sin n\pi\frac{z}{h}\sin n\pi\frac{z_w}{h}\left[K_0\left(r_D\sqrt{u+\frac{n^2\pi^2}{h_D^2}}\right) + \frac{I_0\left(r_D\sqrt{u+\frac{n^2\pi^2}{h_D^2}}\right)K_1\left(r_{cD}\sqrt{u+\frac{n^2\pi^2}{h_D^2}}\right)}{I_1\left(r_{cD}\sqrt{u+\frac{n^2\pi^2}{h_D^2}}\right)}\right]$
	$\overline{\Delta p}\|_{r_D=r_{cD}} = 0$	$\frac{\tilde{q}\mu}{\pi k L h_D s}\sum_{n=1}^{\infty}\sin n\pi\frac{z}{h}\sin n\pi\frac{z_w}{h}\left[K_0\left(r_D\sqrt{u+\frac{n^2\pi^2}{h_D^2}}\right) - \frac{I_0\left(r_D\sqrt{u+\frac{n^2\pi^2}{h_D^2}}\right)K_0\left(r_{cD}\sqrt{u+\frac{n^2\pi^2}{h_D^2}}\right)}{I_0\left(r_{cD}\sqrt{u+\frac{n^2\pi^2}{h_D^2}}\right)}\right]$

TABLE 2-A (Cont.)
POINT SOURCE WELLS
BOUNDED RESERVOIRS - CYLINDRICAL COORDINATES

BOUNDARY CONDITION AT $z_D = 0$ AND h_D	BOUNDARY CONDITION AT $r_D = r_{eD}$	PRESSURE DISTRIBUTION IN LAPLACE SPACE, $\overline{\Delta p}$
$\frac{\partial \overline{\Delta p}}{\partial z_D}\|_{z_D=0} = 0$	$\frac{\partial \overline{\Delta p}}{\partial r_D}\|_{r_D=r_{eD}} = 0$	$\frac{\tilde{q}\mu}{\pi k L h_D s} \sum_{n=1}^{\infty} \cos(2n-1)\frac{\pi}{2}\frac{z}{h} \cos(2n-1)\frac{\pi}{2}\frac{z_w}{h} \left\{ K_0\left[r_D\sqrt{u+\frac{(2n-1)^2\pi^2}{4h_D^2}}\right] + \frac{I_0\left[r_D\sqrt{u+\frac{(2n-1)^2\pi^2}{4h_D^2}}\right] K_1\left[r_{eD}\sqrt{u+\frac{(2n-1)^2\pi^2}{4h_D^2}}\right]}{I_1\left[r_{eD}\sqrt{u+\frac{(2n-1)^2\pi^2}{4h_D^2}}\right]} \right\}$
$\overline{\Delta p}\|_{z_D=h_D} = 0$	$\overline{\Delta p}\|_{r_D=r_{eD}} = 0$	$\frac{\tilde{q}\mu}{\pi k L h_D s} \sum_{n=1}^{\infty} \cos(2n-1)\frac{\pi}{2}\frac{z}{h} \cos(2n-1)\frac{\pi}{2}\frac{z_w}{h} \left\{ K_0\left[r_D\sqrt{u+\frac{(2n-1)^2\pi^2}{4h_D^2}}\right] - \frac{I_0\left(r_D\sqrt{u+\frac{(2n-1)^2\pi^2}{4h_D^2}}\right) K_0\left(r_{eD}\sqrt{u+\frac{(2n-1)^2\pi^2}{4h_D^2}}\right)}{I_0\left(r_{eD}\sqrt{u+\frac{(2n-1)^2\pi^2}{4h_D^2}}\right)} \right\}$

TABLE 2-B
FULLY PENETRATING WELLS
BOUNDED RESERVOIRS - CYLINDRICAL COORDINATES
IMPERMEABLE BOUNDARIES AT $z_D = 0$ AND $z_D = h_D$

$$\tilde{r}_D = \sqrt{(x_D - \alpha\sqrt{k/k_z})^2 + y_D^2}$$

WELL TYPE	BOUNDARY CONDITION AT $r_D = r_{eD}$	PRESSURE DISTRIBUTION IN LAPLACE SPACE, $\overline{\Delta p}$
VERTICAL LINE SOURCE WELL $q = \tilde{q}h$	$\left.\frac{\partial \overline{\Delta p}}{\partial r_D}\right\|_{r_D = r_{eD}} = 0$	$\frac{\tilde{q}\mu h}{2\pi k L h_D s}\left[K_0\left(r_D\sqrt{u}\right) + \frac{I_0\left(r_D\sqrt{u}\right)K_1\left(r_{eD}\sqrt{u}\right)}{I_1\left(r_{eD}\sqrt{u}\right)}\right]$
	$\left.\overline{\Delta p}\right\|_{r_D = r_{eD}} = 0$	$\frac{\tilde{q}\mu h}{2\pi k L h_D s}\left[K_0\left(r_D\sqrt{u}\right) - \frac{I_0\left(r_D\sqrt{u}\right)K_0\left(r_{eD}\sqrt{u}\right)}{I_0\left(r_{eD}\sqrt{u}\right)}\right]$
PLANE VERTICAL FRACTURE $q = 2\tilde{q}hL_{x_f}$	$\left.\frac{\partial \overline{\Delta p}}{\partial r_D}\right\|_{r_D = r_{eD}} = 0$	$\frac{\tilde{q}\mu h}{2\pi k h_D s}\int_{-L_{x_f}/L}^{+L_{x_f}/L}\left[K_0\left(\tilde{r}_D\sqrt{u}\right) + \frac{I_0\left(\tilde{r}_D\sqrt{u}\right)K_1\left(r_{eD}\sqrt{u}\right)}{I_1\left(r_{eD}\sqrt{u}\right)}\right]d\alpha$
	$\left.\overline{\Delta p}\right\|_{r_D = r_{eD}} = 0$	$\frac{\tilde{q}\mu h}{2\pi k h_D s}\int_{-L_{x_f}/L}^{+L_{x_f}/L}\left[K_0\left(\tilde{r}_D\sqrt{u}\right) - \frac{I_0\left(\tilde{r}_D\sqrt{u}\right)K_0\left(r_{eD}\sqrt{u}\right)}{I_0\left(r_{eD}\sqrt{u}\right)}\right]d\alpha$

TABLE 2-C
PARTIALLY PENETRATING VERTICAL LINE SOURCE WELL
BOUNDED RESERVOIRS - CYLINDRICAL COORDINATES
$q = \tilde{q} h_w$

BOUNDARY CONDITION AT $z_D = 0$ AND h_D	BOUNDARY CONDITION AT $r_D = r_{eD}$	PRESSURE DISTRIBUTION IN LAPLACE SPACE, $\overline{\Delta p}$
$\frac{\partial \overline{\Delta p}}{\partial z_D}\|_{z_D=0,h_D} = 0$	$\frac{\partial \overline{\Delta p}}{\partial r_D}\|_{r_D=r_{eD}} = 0$	$\frac{\tilde{q}\mu h_w}{2\pi k L h_D s}\left[K_0(r_D\sqrt{u}) + \frac{I_0(r_D\sqrt{u})\,K_1(r_{eD}\sqrt{u})}{I_1(r_{eD}\sqrt{u})}\right] + \frac{2\tilde{q}\mu h}{\pi^2 k L h_D s}\sum_{n=1}^{\infty}\frac{1}{n}\sin n\pi\frac{h_w}{2h}\cos n\pi\frac{z_w}{h}\cos n\pi\frac{z}{h}\left[K_0\left(r_D\sqrt{u+\frac{n^2\pi^2}{h_D^2}}\right) + \frac{I_0\left(r_D\sqrt{u+\frac{n^2\pi^2}{h_D^2}}\right)K_1\left(r_{eD}\sqrt{u+\frac{n^2\pi^2}{h_D^2}}\right)}{I_1\left(r_{eD}\sqrt{u+\frac{n^2\pi^2}{h_D^2}}\right)}\right]$
	$\overline{\Delta p}\|_{r_D=r_{eD}} = 0$	$\frac{\tilde{q}\mu h_w}{2\pi k L h_D s}\left[K_0(r_D\sqrt{u}) - \frac{I_0(r_D\sqrt{u})\,K_0(r_{eD}\sqrt{u})}{I_0(r_{eD}\sqrt{u})}\right] + \frac{2\tilde{q}\mu h}{\pi^2 k L h_D s}\sum_{n=1}^{\infty}\frac{1}{n}\sin n\pi\frac{h_w}{2h}\cos n\pi\frac{z_w}{h}\cos n\pi\frac{z}{h}\left[K_0\left(r_D\sqrt{u+\frac{n^2\pi^2}{h_D^2}}\right) - \frac{I_0\left(r_D\sqrt{u+\frac{n^2\pi^2}{h_D^2}}\right)K_0\left(r_{eD}\sqrt{u+\frac{n^2\pi^2}{h_D^2}}\right)}{I_0\left(r_{eD}\sqrt{u+\frac{n^2\pi^2}{h_D^2}}\right)}\right]$
$\overline{\Delta p}\|_{z_D=0,h_D} = 0$	$\frac{\partial \overline{\Delta p}}{\partial r_D}\|_{r_D=r_{eD}} = 0$	$\frac{2\tilde{q}\mu h}{\pi^2 k L h_D s}\sum_{n=1}^{\infty}\frac{1}{n}\sin n\pi\frac{h_w}{2h}\sin n\pi\frac{z_w}{h}\sin n\pi\frac{z}{h}\left[K_0\left(r_D\sqrt{u+\frac{n^2\pi^2}{h_D^2}}\right) + \frac{I_0\left(r_D\sqrt{u+\frac{n^2\pi^2}{h_D^2}}\right)K_1\left(r_{eD}\sqrt{u+\frac{n^2\pi^2}{h_D^2}}\right)}{I_1\left(r_{eD}\sqrt{u+\frac{n^2\pi^2}{h_D^2}}\right)}\right]$
	$\overline{\Delta p}\|_{r_D=r_{eD}} = 0$	$\frac{2\tilde{q}\mu h}{\pi^2 k L h_D s}\sum_{n=1}^{\infty}\frac{1}{n}\sin n\pi\frac{h_w}{2h}\sin n\pi\frac{z_w}{h}\sin n\pi\frac{z}{h}\left[K_0\left(r_D\sqrt{u+\frac{n^2\pi^2}{h_D^2}}\right) - \frac{I_0\left(r_D\sqrt{u+\frac{n^2\pi^2}{h_D^2}}\right)K_0\left(r_{eD}\sqrt{u+\frac{n^2\pi^2}{h_D^2}}\right)}{I_0\left(r_{eD}\sqrt{u+\frac{n^2\pi^2}{h_D^2}}\right)}\right]$

TABLE 2-C (Cont.)
PARTIALLY PENETRATING VERTICAL LINE SOURCE WELL
BOUNDED RESERVOIRS - CYLINDRICAL COORDINATES
$q = \tilde{q} h_w$

BOUNDARY CONDITION AT $z_D = 0$ AND h_D	BOUNDARY CONDITION AT $r_D = r_{eD}$	PRESSURE DISTRIBUTION IN LAPLACE SPACE, $\overline{\Delta p}$
$\frac{\partial \overline{\Delta p}}{\partial z_D}\|_{z_D=0} = 0$	$\frac{\partial \overline{\Delta p}}{\partial r_D}\|_{r_D=r_{eD}} = 0$	$\frac{4\tilde{q}\mu h}{\pi^2 k L h_D s} \sum_{n=1}^{\infty} \frac{1}{(2n-1)} \sin(2n-1)\frac{\pi}{2}\frac{h_w}{2h} \cos(2n-1)\frac{\pi}{2}\frac{z_w}{h} \cos(2n-1)\frac{\pi}{2}\frac{z}{h}$ $\left\{ K_0\left[r_D\sqrt{u+\frac{(2n-1)^2\pi^2}{4h_D^2}}\right] + \frac{I_0\left[r_D\sqrt{u+\frac{(2n-1)^2\pi^2}{4h_D^2}}\right] K_1\left[r_{eD}\sqrt{u+\frac{(2n-1)^2\pi^2}{4h_D^2}}\right]}{I_1\left[r_{eD}\sqrt{u+\frac{(2n-1)^2\pi^2}{4h_D^2}}\right]} \right\}$
$\overline{\Delta p}\|_{z_D=h_D} = 0$	$\overline{\Delta p}\|_{r_D=r_{eD}} = 0$	$\frac{4\tilde{q}\mu h}{\pi^2 k L h_D s} \sum_{n=1}^{\infty} \frac{1}{(2n-1)} \sin(2n-1)\frac{\pi}{2}\frac{h_w}{2h} \cos(2n-1)\frac{\pi}{2}\frac{z_w}{h} \cos(2n-1)\frac{\pi}{2}\frac{z}{h}$ $\left\{ K_0\left[r_D\sqrt{u+\frac{(2n-1)^2\pi^2}{4h_D^2}}\right] - \frac{I_0\left(r_D\sqrt{u+\frac{(2n-1)^2\pi^2}{4h_D^2}}\right) K_0\left(r_{eD}\sqrt{u+\frac{(2n-1)^2\pi^2}{4h_D^2}}\right)}{I_0\left(r_{eD}\sqrt{u+\frac{(2n-1)^2\pi^2}{4h_D^2}}\right)} \right\}$

TABLE 2-D
PARTIALLY PENETRATING VERTICAL FRACTURE
BOUNDED RESERVOIRS - CYLINDRICAL COORDINATES

$$q = \tilde{q} h_w L_{x_f}, \tilde{r}_D = \sqrt{(x_D - \alpha\sqrt{k/kx})^2 + y_D^2}$$

BOUNDARY CONDITION AT $z_D = 0$ AND h_D	BOUNDARY CONDITION AT $r_D = r_{eD}$	PRESSURE DISTRIBUTION IN LAPLACE SPACE, $\overline{\Delta p}$
$\frac{\partial \overline{\Delta p}}{\partial z_D}\|_{z_D=0,h_D} = 0$	$\frac{\partial \overline{\Delta p}}{\partial r_D}\|_{r_D=r_{eD}} = 0$	$\frac{\tilde{q}\mu h_w}{2\pi k h_D s}\int_{-L_{sf}/L}^{+L_{sf}/L}\left[K_0(\tilde{r}_D\sqrt{u}) + \frac{I_0(\tilde{r}_D\sqrt{u})\,K_1(r_{eD}\sqrt{u})}{I_1(r_{eD}\sqrt{u})}\right]d\alpha + \frac{2\tilde{q}\mu h}{\pi^2 k h_D s}\sum_{n=1}^{\infty}\frac{1}{n}\sin n\pi\frac{h_w}{2h}\cos n\pi\frac{z_w}{h}\cos n\pi\frac{z}{h}\int_{-L_{sf}/L}^{+L_{sf}/L}\left[K_0\left(\tilde{r}_D\sqrt{u+\frac{n^2\pi^2}{h_D^2}}\right) + \frac{I_0\left(\tilde{r}_D\sqrt{u+\frac{n^2\pi^2}{h_D^2}}\right)K_1\left(r_{eD}\sqrt{u+\frac{n^2\pi^2}{h_D^2}}\right)}{I_1\left(r_{eD}\sqrt{u+\frac{n^2\pi^2}{h_D^2}}\right)}\right]d\alpha$
	$\overline{\Delta p}\|_{r_D=r_{eD}} = 0$	$\frac{\tilde{q}\mu h_w}{2\pi k h_D s}\int_{-L_{sf}/L}^{+L_{sf}/L}\left[K_0(\tilde{r}_D\sqrt{u}) - \frac{I_0(\tilde{r}_D\sqrt{u})\,K_0(r_{eD}\sqrt{u})}{I_0(r_{eD}\sqrt{u})}\right]d\alpha + \frac{2\tilde{q}\mu h}{\pi^2 k h_D s}\sum_{n=1}^{\infty}\frac{1}{n}\sin n\pi\frac{h_w}{2h}\cos n\pi\frac{z_w}{h}\cos n\pi\frac{z}{h}\int_{-L_{sf}/L}^{+L_{sf}/L}\left[K_0\left(\tilde{r}_D\sqrt{u+\frac{n^2\pi^2}{h_D^2}}\right) - \frac{I_0\left(\tilde{r}_D\sqrt{u+\frac{n^2\pi^2}{h_D^2}}\right)K_0\left(r_{eD}\sqrt{u+\frac{n^2\pi^2}{h_D^2}}\right)}{I_0\left(r_{eD}\sqrt{u+\frac{n^2\pi^2}{h_D^2}}\right)}\right]d\alpha$
$\overline{\Delta p}\|_{z_D=0,h_D} = 0$	$\frac{\partial \overline{\Delta p}}{\partial r_D}\|_{r_D=r_{eD}} = 0$	$\frac{2\tilde{q}\mu h}{\pi^2 k h_D s}\sum_{n=1}^{\infty}\frac{1}{n}\sin n\pi\frac{h_w}{2h}\sin n\pi\frac{z_w}{h}\sin n\pi\frac{z}{h}\int_{-L_{sf}/L}^{+L_{sf}/L}\left[K_0\left(\tilde{r}_D\sqrt{u+\frac{n^2\pi^2}{h_D^2}}\right) + \frac{I_0\left(\tilde{r}_D\sqrt{u+\frac{n^2\pi^2}{h_D^2}}\right)K_1\left(r_{eD}\sqrt{u+\frac{n^2\pi^2}{h_D^2}}\right)}{I_1\left(r_{eD}\sqrt{u+\frac{n^2\pi^2}{h_D^2}}\right)}\right]d\alpha$
	$\overline{\Delta p}\|_{r_D=r_{eD}} = 0$	$\frac{2\tilde{q}\mu h}{\pi^2 k h_D s}\sum_{n=1}^{\infty}\frac{1}{n}\sin n\pi\frac{h_w}{2h}\sin n\pi\frac{z_w}{h}\sin n\pi\frac{z}{h}\int_{-L_{sf}/L}^{+L_{sf}/L}\left[K_0\left(\tilde{r}_D\sqrt{u+\frac{n^2\pi^2}{h_D^2}}\right) - \frac{I_0\left(\tilde{r}_D\sqrt{u+\frac{n^2\pi^2}{h_D^2}}\right)K_0\left(r_{eD}\sqrt{u+\frac{n^2\pi^2}{h_D^2}}\right)}{I_0\left(r_{eD}\sqrt{u+\frac{n^2\pi^2}{h_D^2}}\right)}\right]d\alpha$

TABLE 2-D (Cont.)
PARTIALLY PENETRATING VERTICAL FRACTURE
BOUNDED RESERVOIRS - CYLINDRICAL COORDINATES

$$q = \tilde{q} h_w L_{x_f}, \tilde{r}_D = \sqrt{(x_D - \alpha\sqrt{k/kx})^2 + y_D^2}$$

BOUNDARY CONDITION AT $z_D = 0$ AND h_D	BOUNDARY CONDITION AT $r_D = r_{eD}$	PRESSURE DISTRIBUTION IN LAPLACE SPACE, $\overline{\Delta p}$
$\frac{\partial \overline{\Delta p}}{\partial z_D}\|_{z_D=0} = 0$	$\frac{\partial \overline{\Delta p}}{\partial r_D}\|_{r_D=r_{eD}} = 0$	$\frac{4\tilde{q}\mu h}{\pi^2 k h_D s} \sum_{n=1}^{\infty} \frac{1}{(2n-1)} \sin(2n-1)\frac{\pi}{2}\frac{h_w}{2h} \sin(2n-1)\frac{\pi}{2}\frac{z_w}{h} \cos(2n-1)\frac{\pi}{2}\frac{z}{h}$ $\int_{-L_{x_f}/L}^{+L_{x_f}/L} \left\{ K_0\left[\tilde{r}_D\sqrt{u + \frac{(2n-1)^2\pi^2}{4h_D^2}}\right] + \frac{I_0\left[\tilde{r}_D\sqrt{u + \frac{(2n-1)^2\pi^2}{4h_D^2}}\right] K_1\left[r_{eD}\sqrt{u + \frac{(2n-1)^2\pi^2}{4h_D^2}}\right]}{I_1\left[r_{eD}\sqrt{u + \frac{(2n-1)^2\pi^2}{4h_D^2}}\right]} \right\} d\alpha$
$\overline{\Delta p}\|_{z_D=h_D} = 0$	$\overline{\Delta p}\|_{r_D=r_{eD}} = 0$	$\frac{4\tilde{q}\mu h}{\pi^2 k h_D s} \sum_{n=1}^{\infty} \frac{1}{(2n-1)} \sin(2n-1)\frac{\pi}{2}\frac{h_w}{2h} \sin(2n-1)\frac{\pi}{2}\frac{z_w}{h} \cos(2n-1)\frac{\pi}{2}\frac{z}{h}$ $\int_{-L_{x_f}/L}^{+L_{x_f}/L} \left\{ K_0\left[\tilde{r}_D\sqrt{u + \frac{(2n-1)^2\pi^2}{4h_D^2}}\right] - \frac{I_0\left[\tilde{r}_D\sqrt{u + \frac{(2n-1)^2\pi^2}{4h_D^2}}\right] K_0\left[r_{eD}\sqrt{u + \frac{(2n-1)^2\pi^2}{4h_D^2}}\right]}{I_0\left[r_{eD}\sqrt{u + \frac{(2n-1)^2\pi^2}{4h_D^2}}\right]} \right\} d\alpha$

TABLE 2-E
HORIZONTAL WELL
BOUNDED RESERVOIRS - CYLINDRICAL COORDINATES
$q = \tilde{q}L_h, \tilde{r}_D = \sqrt{(x_D - \alpha\sqrt{k/k_x})^2 + y_D^2}$

BOUNDARY CONDITION AT $z_D = 0$ AND h_D	BOUNDARY CONDITION AT $r_D = r_{eD}$	PRESSURE DISTRIBUTION IN LAPLACE SPACE, $\overline{\Delta p}$
$\frac{\partial \overline{\Delta p}}{\partial z_D}\|_{z_D=0,h_D} = 0$	$\frac{\partial \overline{\Delta p}}{\partial r_D}\|_{r_D=r_{eD}} = 0$	$\frac{\tilde{q}\mu}{2\pi k h_D s}\left\{\int_{-L_h/(2L)}^{+L_h/(2L)}\left[K_0\left(\tilde{r}_D\sqrt{u}\right) + \frac{I_0\left(\tilde{r}_D\sqrt{u}\right)K_1\left(r_{eD}\sqrt{u}\right)}{I_1\left(r_{eD}\sqrt{u}\right)}\right]d\alpha\right.$ $+2\sum_{n=1}^{\infty}\cos n\pi\frac{z}{h}\cos n\pi\frac{z_w}{h}\int_{-L_h/(2L)}^{+L_h/(2L)}\left[K_0\left(\tilde{r}_D\sqrt{u+\frac{n^2\pi^2}{h_D^2}}\right)\right.$ $\left.\left.+\frac{I_0\left(\tilde{r}_D\sqrt{u+\frac{n^2\pi^2}{h_D^2}}\right)K_1\left(r_{eD}\sqrt{u+\frac{n^2\pi^2}{h_D^2}}\right)}{I_1\left(r_{eD}\sqrt{u+\frac{n^2\pi^2}{h_D^2}}\right)}\right]d\alpha\right\}$
	$\overline{\Delta p}\|_{r_D=r_{eD}} = 0$	$\frac{\tilde{q}\mu}{2\pi k h_D s}\left\{\int_{-L_h/(2L)}^{+L_h/(2L)}\left[K_0\left(\tilde{r}_D\sqrt{u}\right) - \frac{I_0\left(\tilde{r}_D\sqrt{u}\right)K_0\left(r_{eD}\sqrt{u}\right)}{I_0\left(r_{eD}\sqrt{u}\right)}\right]d\alpha\right.$ $+2\sum_{n=1}^{\infty}\cos n\pi\frac{z}{h}\cos n\pi\frac{z_w}{h}\int_{-L_h/(2L)}^{+L_h/(2L)}\left[K_0\left(\tilde{r}_D\sqrt{u+\frac{n^2\pi^2}{h_D^2}}\right)\right.$ $\left.\left.-\frac{I_0\left(\tilde{r}_D\sqrt{u+\frac{n^2\pi^2}{h_D^2}}\right)K_0\left(r_{eD}\sqrt{u+\frac{n^2\pi^2}{h_D^2}}\right)}{I_0\left(r_{eD}\sqrt{u+\frac{n^2\pi^2}{h_D^2}}\right)}\right]d\alpha\right\}$
$\overline{\Delta p}\|_{z_D=0,h_D} = 0$	$\frac{\partial \overline{\Delta p}}{\partial r_D}\|_{r_D=r_{eD}} = 0$	$\frac{\tilde{q}\mu}{\pi k h_D s}\sum_{n=1}^{\infty}\sin n\pi\frac{z}{h}\sin n\pi\frac{z_w}{h}$ $\int_{-L_h/(2L)}^{+L_h/(2L)}\left[K_0\left(\tilde{r}_D\sqrt{u+\frac{n^2\pi^2}{h_D^2}}\right)\right.$ $\left.+\frac{I_0\left(\tilde{r}_D\sqrt{u+\frac{n^2\pi^2}{h_D^2}}\right)K_1\left(r_{eD}\sqrt{u+\frac{n^2\pi^2}{h_D^2}}\right)}{I_1\left(r_{eD}\sqrt{u+\frac{n^2\pi^2}{h_D^2}}\right)}\right]d\alpha$
	$\overline{\Delta p}\|_{r_D=r_{eD}} = 0$	$\frac{\tilde{q}\mu}{\pi k h_D s}\sum_{n=1}^{\infty}\sin n\pi\frac{z}{h}\sin n\pi\frac{z_w}{h}$ $\int_{-L_h/(2L)}^{+L_h/(2L)}\left[K_0\left(\tilde{r}_D\sqrt{u+\frac{n^2\pi^2}{h_D^2}}\right)\right.$ $\left.-\frac{I_0\left(\tilde{r}_D\sqrt{u+\frac{n^2\pi^2}{h_D^2}}\right)K_0\left(r_{eD}\sqrt{u+\frac{n^2\pi^2}{h_D^2}}\right)}{I_0\left(r_{eD}\sqrt{u+\frac{n^2\pi^2}{h_D^2}}\right)}\right]$

TABLE 2-E (Cont.)
HORIZONTAL WELL
BOUNDED RESERVOIRS - CYLINDRICAL COORDINATES
$q = \tilde{q}L_h, \tilde{r}_D = \sqrt{(x_D - \alpha\sqrt{k/k_x})^2 + y_D^2}$

BOUNDARY CONDITION AT $z_D = 0$ AND h_D	BOUNDARY CONDITION AT $r_D = r_{eD}$	PRESSURE DISTRIBUTION IN LAPLACE SPACE, $\overline{\Delta p}$
$\frac{\partial \overline{\Delta p}}{\partial z_D}\|_{z_D=0} = 0$	$\frac{\partial \overline{\Delta p}}{\partial r_D}\|_{r_D=r_{eD}} = 0$	$\frac{\tilde{q}\mu}{\pi k h_D s}\sum_{n=1}^{\infty}\cos(2n-1)\frac{\pi}{2}\frac{z}{h}\cos(2n-1)\frac{\pi}{2}\frac{z_w}{h}$ $\int_{-L_h/(2L)}^{+L_h/(2L)}\left\{K_0\left[\tilde{r}_D\sqrt{u+\frac{(2n-1)^2\pi^2}{4h_D^2}}\right] + \frac{I_0\left[\tilde{r}_D\sqrt{u+\frac{(2n-1)^2\pi^2}{4h_D^2}}\right]K_1\left[r_{eD}\sqrt{u+\frac{(2n-1)^2\pi^2}{4h_D^2}}\right]}{I_1\left[r_{eD}\sqrt{u+\frac{(2n-1)^2\pi^2}{4h_D^2}}\right]}\right\}d\alpha$
$\overline{\Delta p}\|_{z_D=h_D} = 0$	$\overline{\Delta p}\|_{r_D=r_{eD}} = 0$	$\frac{\tilde{q}\mu}{\pi k h_D s}\sum_{n=1}^{\infty}\cos(2n-1)\frac{\pi}{2}\frac{z}{h}\cos(2n-1)\frac{\pi}{2}\frac{z_w}{h}$ $\int_{-L_h/(2L)}^{+L_h/(2L)}\left\{K_0\left[\tilde{r}_D\sqrt{u+\frac{(2n-1)^2\pi^2}{4h_D^2}}\right] - \frac{I_0\left[\tilde{r}_D\sqrt{u+\frac{(2n-1)^2\pi^2}{4h_D^2}}\right]K_0\left[r_{eD}\sqrt{u+\frac{(2n-1)^2\pi^2}{4h_D^2}}\right]}{I_0\left[r_{eD}\sqrt{u+\frac{(2n-1)^2\pi^2}{4h_D^2}}\right]}\right\}d\alpha$

TABLE 3-A

POINT SOURCE WELLS

RECTANGULAR RESERVOIRS

IMPERMEABLE BOUNDARIES AT $z_D = 0$ AND $z_D = h_D$

$\tilde{y}_{D1} = y_{eD} - |y_D - y_{wD}|, \quad \tilde{y}_{D2} = y_{eD} - (y_D + y_{wD})$

AREAL VIEW	PRESSURE DISTRIBUTION IN LAPLACE SPACE, $\overline{\Delta p}$
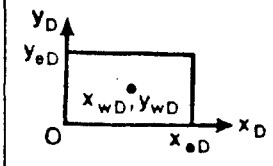 $s_{111}+s_{211}+s_{121}+s_{221}+s_{112}+s_{212}+s_{122}+s_{222}$	$\frac{\tilde{q}\mu}{2kLx_{eD}s}\left\{\frac{ch\sqrt{u}\,(\tilde{y}_{D1})+ch\sqrt{u}\,(\tilde{y}_{D2})}{\sqrt{u}\,sh\sqrt{u}\,y_{eD}}\right.$ $+2\sum_{k=1}^{\infty}\cos k\pi\frac{x_D}{x_{eD}}\cos k\pi\frac{x_{wD}}{x_{eD}}\frac{ch\sqrt{u+\frac{k^2\pi^2}{x_{eD}^2}}(\tilde{y}_{D1})+ch\sqrt{u+\frac{k^2\pi^2}{x_{eD}^2}}(\tilde{y}_{D2})}{\sqrt{u+\frac{k^2\pi^2}{x_{eD}^2}}sh\sqrt{u+\frac{k^2\pi^2}{x_{eD}^2}}y_{eD}}$ $+2\sum_{n=1}^{\infty}\cos n\pi\frac{z_D}{h_D}\cos n\pi\frac{z_{wD}}{h_D}\left[\frac{ch\sqrt{u+\frac{n^2\pi^2}{h_D^2}}(\tilde{y}_{D1})+ch\sqrt{u+\frac{n^2\pi^2}{h_D^2}}(\tilde{y}_{D2})}{\sqrt{u+\frac{n^2\pi^2}{h_D^2}}sh\sqrt{u+\frac{n^2\pi^2}{h_D^2}}y_{eD}}\right.$ $+2\sum_{k=1}^{\infty}\cos k\pi\frac{x_D}{x_{eD}}\cos k\pi\frac{x_{wD}}{x_{eD}}$ $\left.\left.\frac{ch\sqrt{u+\frac{n^2\pi^2}{h_D^2}+\frac{k^2\pi^2}{x_{eD}^2}}(\tilde{y}_{D1})+ch\sqrt{u+\frac{n^2\pi^2}{h_D^2}+\frac{k^2\pi^2}{x_{eD}^2}}(\tilde{y}_{D2})}{\sqrt{u+\frac{n^2\pi^2}{h_D^2}+\frac{k^2\pi^2}{x_{eD}^2}}sh\sqrt{u+\frac{n^2\pi^2}{h_D^2}+\frac{k^2\pi^2}{x_{eD}^2}}y_{eD}}\right]\right\}$
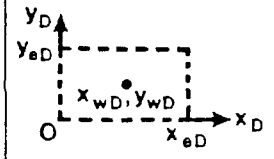 $s_{111}-s_{211}-s_{121}+s_{221}+s_{112}-s_{212}-s_{122}+s_{222}$	$\frac{\tilde{q}\mu}{kLx_{eD}h_Ds}\left\{\sum_{k=1}^{\infty}\sin k\pi\frac{x_D}{x_{eD}}\sin k\pi\frac{x_{wD}}{x_{eD}}\right.$ $\frac{ch\sqrt{u+\frac{k^2\pi^2}{x_{eD}^2}}(\tilde{y}_{D1})-ch\sqrt{u+\frac{k^2\pi^2}{x_{eD}^2}}(\tilde{y}_{D2})}{\sqrt{u+\frac{k^2\pi^2}{x_{eD}^2}}sh\sqrt{u+\frac{k^2\pi^2}{x_{eD}^2}}y_{eD}}$ $+2\sum_{n=1}^{\infty}\cos n\pi\frac{z_D}{h_D}\cos n\pi\frac{z_{wD}}{h_D}\sum_{k=1}^{\infty}\sin k\pi\frac{x_D}{x_{eD}}\sin k\pi\frac{x_{wD}}{x_{eD}}$ $\left.\left.\frac{ch\sqrt{u+\frac{n^2\pi^2}{h_D^2}+\frac{k^2\pi^2}{x_{eD}^2}}(\tilde{y}_{D1})-ch\sqrt{u+\frac{n^2\pi^2}{h_D^2}+\frac{k^2\pi^2}{x_{eD}^2}}(\tilde{y}_{D2})}{\sqrt{u+\frac{n^2\pi^2}{h_D^2}+\frac{k^2\pi^2}{x_{eD}^2}}sh\sqrt{u+\frac{n^2\pi^2}{h_D^2}+\frac{k^2\pi^2}{x_{eD}^2}}y_{eD}}\right]\right\}$

TABLE 3-A (Cont.)
POINT SOURCE WELLS
RECTANGULAR RESERVOIRS
IMPERMEABLE BOUNDARIES AT $z_D = 0$ AND $z_D = h_D$
$\tilde{y}_{D1} = y_{eD} - |y_D - y_{wD}|, \quad \tilde{y}_{D2} = y_{eD} - (y_D + y_{wD})$

AREAL VIEW	PRESSURE DISTRIBUTION IN LAPLACE SPACE, $\overline{\Delta p}$
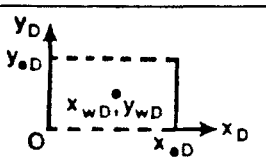 $s_{111}+s_{211}-s_{121}-s_{221}+s_{112}+s_{212}-s_{122}+s_{222}$	$\frac{\tilde{q}\mu}{2kLx_{eD}h_D s}\left\{\frac{ch\sqrt{u}\,(\tilde{y}_{D1})-ch\sqrt{u}\,(\tilde{y}_{D2})}{\sqrt{u}\,sh\sqrt{u}\,y_{eD}}\right.$ $+2\sum_{k=1}^{\infty}\cos k\pi\frac{x_D}{x_{eD}}\cos k\pi\frac{x_{wD}}{x_{eD}}$ $\frac{ch\sqrt{u+\frac{k^2\pi^2}{x_{eD}^2}}\,(\tilde{y}_{D1})-ch\sqrt{u+\frac{k^2\pi^2}{x_{eD}^2}}\,(\tilde{y}_{D2})}{\sqrt{u+\frac{k^2\pi^2}{x_{eD}^2}}\,sh\sqrt{u+\frac{k^2\pi^2}{x_{eD}^2}}\,y_{eD}}$ $+2\sum_{n=1}^{\infty}\cos n\pi\frac{z_D}{h_D}\cos n\pi\frac{z_{wD}}{h_D}$ $\left[\frac{ch\sqrt{u+\frac{n^2\pi^2}{h_D^2}}\,(\tilde{y}_{D1})-ch\sqrt{u+\frac{n^2\pi^2}{h_D^2}}\,(\tilde{y}_{D2})}{\sqrt{u+\frac{n^2\pi^2}{h_D^2}}\,sh\sqrt{u+\frac{n^2\pi^2}{h_D^2}}\,y_{eD}}\right.$ $+2\sum_{k=1}^{\infty}\cos k\pi\frac{x_D}{x_{eD}}\cos k\pi\frac{x_{wD}}{x_{eD}}$ $\left.\left.\frac{ch\sqrt{u+\frac{n^2\pi^2}{h_D^2}+\frac{k^2\pi^2}{x_{eD}^2}}\,(\tilde{y}_{D1})-ch\sqrt{u+\frac{n^2\pi^2}{h_D^2}+\frac{k^2\pi^2}{x_{eD}^2}}\,(\tilde{y}_{D2})}{\sqrt{u+\frac{n^2\pi^2}{h_D^2}+\frac{k^2\pi^2}{x_{eD}^2}}\,sh\sqrt{u+\frac{n^2\pi^2}{h_D^2}+\frac{k^2\pi^2}{x_{eD}^2}}\,y_{eD}}\right]\right\}$
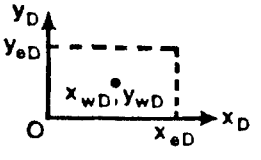 $(-1)^k(-1)^m(s_{111}+s_{211}+s_{121}+s_{221}+s_{112}+s_{212}+s_{122}+s_{222})$	$\frac{\tilde{q}\mu}{kLx_{eD}h_D s}\left\{\sum_{k=1}^{\infty}\cos(2k-1)\frac{\pi}{2}\frac{x_D}{x_{eD}}\cos(2k-1)\frac{\pi}{2}\frac{x_{wD}}{x_{eD}}\right.$ $\left[\frac{sh\sqrt{u+\frac{(2k-1)^2\pi^2}{4x_{eD}^2}}\,(\tilde{y}_{D1})+sh\sqrt{u+\frac{(2k-1)^2\pi^2}{4x_{eD}^2}}\,(\tilde{y}_{D2})}{\sqrt{u+\frac{(2k-1)^2\pi^2}{4x_{eD}^2}}\,ch\sqrt{u+\frac{(2k-1)^2\pi^2}{4x_{eD}^2}}\,y_{eD}}\right.$ $+2\sum_{n=1}^{\infty}\cos n\pi\frac{z_D}{h_D}\cos n\pi\frac{z_{wD}}{h_D}$ $\left.\left.\frac{sh\sqrt{u+\frac{n^2\pi^2}{h_D^2}+\frac{(2k-1)^2\pi^2}{4x_{eD}^2}}\,(\tilde{y}_{D1})+sh\sqrt{u+\frac{n^2\pi^2}{h_D^2}+\frac{(2k-1)^2\pi^2}{4x_{eD}^2}}\,(\tilde{y}_{D2})}{\sqrt{u+\frac{n^2\pi^2}{h_D^2}+\frac{(2k-1)^2\pi^2}{4x_{eD}^2}}\,ch\sqrt{u+\frac{n^2\pi^2}{h_D^2}+\frac{(2k-1)^2\pi^2}{4x_{eD}^2}}\,y_{eD}}\right]\right\}$

TABLE 3-A (Cont.)
POINT SOURCE WELLS
RECTANGULAR RESERVOIRS
IMPERMEABLE BOUNDARIES AT $z_D = 0$ AND $z_D = h_D$
$\tilde{y}_{D1} = y_{eD} - |y_D - y_{wD}|, \quad \tilde{y}_{D2} = y_{eD} - (y_D + y_{wD})$

AREAL VIEW	PRESSURE DISTRIBUTION IN LAPLACE SPACE, $\overline{\Delta p}$
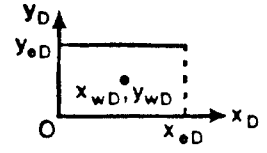 $(-1)^k(s_{111}+s_{211}+s_{121}+s_{221}+s_{112}+s_{212}+s_{122}+s_{222})$	$\frac{\tilde{q}\mu}{kLx_{eD}h_D s}\left\{\sum_{k=1}^{\infty}\cos(2k-1)\frac{\pi}{2}\frac{x_D}{x_{eD}}\cos(2k-1)\frac{\pi}{2}\frac{x_{wD}}{x_{eD}}\right.$ $\left[\frac{ch\sqrt{u+\frac{(2k-1)^2\pi^2}{4x_{eD}^2}}(\tilde{y}_{D1})+ch\sqrt{u+\frac{(2k-1)^2\pi^2}{4x_{eD}^2}}(\tilde{y}_{D2})}{\sqrt{u+\frac{(2k-1)^2\pi^2}{4x_{eD}^2}}sh\sqrt{u+\frac{(2k-1)^2\pi^2}{4x_{eD}^2}}y_{eD}}\right.$ $+2\sum_{n=1}^{\infty}\cos n\pi\frac{z_D}{h_D}\cos n\pi\frac{z_{wD}}{h_D}$ $\left.\left.\frac{ch\sqrt{u+\frac{n^2\pi^2}{h_D^2}+\frac{(2k-1)^2\pi^2}{4x_{eD}^2}}(\tilde{y}_{D1})+ch\sqrt{u+\frac{n^2\pi^2}{h_D^2}+\frac{(2k-1)^2\pi^2}{4x_{eD}^2}}(\tilde{y}_{D2})}{\sqrt{u+\frac{n^2\pi^2}{h_D^2}+\frac{(2k-1)^2\pi^2}{4x_{eD}^2}}sh\sqrt{u+\frac{n^2\pi^2}{h_D^2}+\frac{(2k-1)^2\pi^2}{4x_{eD}^2}}y_{eD}}\right]\right\}$
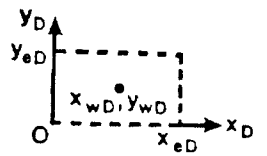 $(-1)^k(s_{111}+s_{211}-s_{121}-s_{221}+s_{112}+s_{212}-s_{122}-s_{222})$	$\frac{\tilde{q}\mu}{kLx_{eD}h_D s}\left\{\sum_{k=1}^{\infty}\cos(2k-1)\frac{\pi}{2}\frac{x_D}{x_{eD}}\cos(2k-1)\frac{\pi}{2}\frac{x_{wD}}{x_{eD}}\right.$ $\left[\frac{ch\sqrt{u+\frac{(2k-1)^2\pi^2}{4x_{eD}^2}}(\tilde{y}_{D1})-ch\sqrt{u+\frac{(2k-1)^2\pi^2}{4x_{eD}^2}}(\tilde{y}_{D2})}{\sqrt{u+\frac{(2k-1)^2\pi^2}{4x_{eD}^2}}sh\sqrt{u+\frac{(2k-1)^2\pi^2}{4x_{eD}^2}}y_{eD}}\right.$ $+2\sum_{n=1}^{\infty}\cos n\pi\frac{z_D}{h_D}\cos n\pi\frac{z_{wD}}{h_D}$ $\left.\left.\frac{ch\sqrt{u+\frac{n^2\pi^2}{h_D^2}+\frac{(2k-1)^2\pi^2}{4x_{eD}^2}}(\tilde{y}_{D1})-ch\sqrt{u+\frac{n^2\pi^2}{h_D^2}+\frac{(2k-1)^2\pi^2}{4x_{eD}^2}}(\tilde{y}_{D2})}{\sqrt{u+\frac{n^2\pi^2}{h_D^2}+\frac{(2k-1)^2\pi^2}{4x_{eD}^2}}sh\sqrt{u+\frac{n^2\pi^2}{h_D^2}+\frac{(2k-1)^2\pi^2}{4x_{eD}^2}}y_{eD}}\right]\right\}$

TABLE 3-B

POINT SOURCE WELLS

RECTANGULAR RESERVOIRS

CONSTANT PRESSURE BOUNDARIES AT $z_D = 0$ AND h_D

$\tilde{y}_{D1} = y_{eD} - |y_D - y_{wD}|, \quad \tilde{y}_{D2} = y_{eD} - (y_D + y_{wD})$

$\tilde{z}_{D1} = h_D - |z_D - z_{wD}|, \quad \tilde{z}_{D2} = h_D - (z_D + z_{wD})$

AREAL VIEW	PRESSURE DISTRIBUTION IN LAPLACE SPACE, $\overline{\Delta p}$
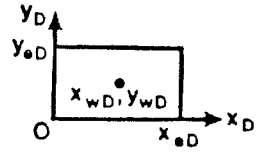 $s_{111}+s_{211}+s_{121}+s_{221}-s_{112}-s_{212}-s_{122}-s_{222}$	$\frac{\tilde{q}\mu}{2kLx_{eD}y_{eD}s}\left\{\frac{ch\sqrt{u}\,(\tilde{z}_{D1})-ch\sqrt{u}\,(\tilde{z}_{D2})}{\sqrt{u}\,sh\sqrt{u}\,h_D}\right.$ $+2\sum_{k=1}^{\infty}\cos k\pi\frac{x_D}{x_{eD}}\cos k\pi\frac{x_{wD}}{x_{eD}}\frac{ch\sqrt{u+\frac{k^2\pi^2}{x_{eD}^2}}\,(\tilde{z}_{D1})-ch\sqrt{u+\frac{k^2\pi^2}{x_{eD}^2}}\,(\tilde{z}_{D2})}{\sqrt{u+\frac{k^2\pi^2}{x_{eD}^2}}\,sh\sqrt{u+\frac{k^2\pi^2}{x_{eD}^2}}\,h_D}$ $+2\sum_{m=1}^{\infty}\cos m\pi\frac{y_D}{y_{eD}}\cos m\pi\frac{y_{wD}}{y_{eD}}\left[\frac{ch\sqrt{u+\frac{m^2\pi^2}{y_{eD}^2}}\,(\tilde{z}_{D1})-ch\sqrt{u+\frac{m^2\pi^2}{y_{eD}^2}}\,(\tilde{z}_{D2})}{\sqrt{u+\frac{m^2\pi^2}{y_{eD}^2}}\,sh\sqrt{u+\frac{m^2\pi^2}{y_{eD}^2}}\,h_D}\right.$ $+2\sum_{k=1}^{\infty}\cos k\pi\frac{x_D}{x_{eD}}\cos k\pi\frac{x_{wD}}{x_{eD}}$ $\left.\left.\frac{ch\sqrt{u+\frac{m^2\pi^2}{y_{eD}^2}+\frac{k^2\pi^2}{x_{eD}^2}}\,(\tilde{z}_{D1})-ch\sqrt{u+\frac{m^2\pi^2}{y_{eD}^2}+\frac{k^2\pi^2}{x_{eD}^2}}\,(\tilde{z}_{D2})}{\sqrt{u+\frac{m^2\pi^2}{y_{eD}^2}+\frac{k^2\pi^2}{x_{eD}^2}}\,sh\sqrt{u+\frac{m^2\pi^2}{y_{eD}^2}+\frac{k^2\pi^2}{x_{eD}^2}}\,h_D}\right]\right\}$
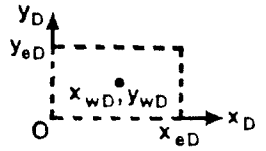 $s_{111}-s_{211}-s_{121}+s_{221}-s_{112}+s_{212}-s_{122}+s_{222}$	$\frac{2\tilde{q}\mu}{kLx_{eD}h_Ds}\left\{\sum_{n=1}^{\infty}\sin n\pi\frac{z_D}{h_D}\sin n\pi\frac{z_{wD}}{h_D}\right.$ $\sum_{k=1}^{\infty}\sin k\pi\frac{x_D}{x_{eD}}\sin k\pi\frac{x_{wD}}{x_{eD}}$ $\left.\frac{ch\sqrt{u+\frac{n^2\pi^2}{h_D^2}+\frac{k^2\pi^2}{x_{eD}^2}}\,(\tilde{y}_{D1})-ch\sqrt{u+\frac{n^2\pi^2}{h_D^2}+\frac{k^2\pi^2}{x_{eD}^2}}\,(\tilde{y}_{D2})}{\sqrt{u+\frac{n^2\pi^2}{h_D^2}+\frac{k^2\pi^2}{x_{eD}^2}}\,sh\sqrt{u+\frac{n^2\pi^2}{h_D^2}+\frac{k^2\pi^2}{x_{eD}^2}}\,y_{eD}}\right\}$
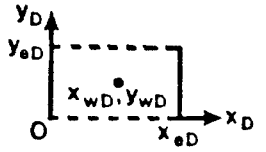 $s_{111}+s_{211}-s_{121}-s_{221}-s_{112}-s_{212}+s_{122}+s_{222}$	$\frac{\tilde{q}\mu}{kLx_{eD}h_Ds}\left\{\sum_{n=1}^{\infty}\sin n\pi\frac{z_D}{h_D}\sin n\pi\frac{z_{wD}}{h_D}\right.$ $\left[\frac{ch\sqrt{u+\frac{n^2\pi^2}{h_D^2}}\,(\tilde{y}_{D1})-ch\sqrt{u+\frac{n^2\pi^2}{h_D^2}}\,(\tilde{y}_{D2})}{\sqrt{u+\frac{n^2\pi^2}{h_D^2}}\,sh\sqrt{u+\frac{n^2\pi^2}{h_D^2}}\,y_{eD}}\right.$ $+2\sum_{k=1}^{\infty}\cos k\pi\frac{x_D}{x_{eD}}\cos k\pi\frac{x_{wD}}{x_{eD}}$ $\left.\left.\frac{ch\sqrt{u+\frac{k^2\pi^2}{x_{eD}^2}+\frac{n^2\pi^2}{h_D^2}}\,(\tilde{y}_{D1})-ch\sqrt{u+\frac{k^2\pi^2}{x_{eD}^2}+\frac{n^2\pi^2}{h_D^2}}\,(\tilde{y}_{D2})}{\sqrt{u+\frac{k^2\pi^2}{x_{eD}^2}+\frac{n^2\pi^2}{h_D^2}}\,sh\sqrt{u+\frac{k^2\pi^2}{x_{eD}^2}+\frac{n^2\pi^2}{h_D^2}}\,y_{eD}}\right]\right\}$

TABLE 3-B (Cont.)

POINT SOURCE WELLS

RECTANGULAR RESERVOIRS

CONSTANT PRESSURE BOUNDARIES AT $z_D = 0$ AND h_D

$\tilde{y}_{D1} = y_{eD} - |y_D - y_{wD}|, \quad \tilde{y}_{D2} = y_{eD} - (y_D + y_{wD})$

$\tilde{z}_{D1} = h_D - |z_D - z_{wD}|, \quad \tilde{z}_{D2} = h_D - (z_D + z_{wD})$

AREAL VIEW	PRESSURE DISTRIBUTION IN LAPLACE SPACE, $\overline{\Delta p}$
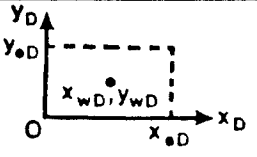 $(-1)^k (-1)^m (s_{111} + s_{211} + s_{121} + s_{221} - s_{112} - s_{212} - s_{122} - s_{222})$	$\frac{2\tilde{q}\mu}{kLx_{eD}h_D s}\left\{\sum_{n=1}^{\infty}\sin n\pi\frac{z_D}{h_D}\sin n\pi\frac{z_{wD}}{h_D}\right.$ $\sum_{k=1}^{\infty}\cos(2k-1)\frac{\pi}{2}\frac{x_D}{x_{eD}}\cos(2k-1)\frac{\pi}{2}\frac{x_{wD}}{x_{eD}}$ $\left.\frac{sh\sqrt{u+\frac{n^2\pi^2}{h_D^2}+\frac{(2k-1)^2\pi^2}{4x_{eD}^2}}(\tilde{y}_{D1})+sh\sqrt{u+\frac{n^2\pi^2}{h_D^2}+\frac{(2k-1)^2\pi^2}{4x_{eD}^2}}(\tilde{y}_{D2})}{\sqrt{u+\frac{n^2\pi^2}{h_D^2}+\frac{(2k-1)^2\pi^2}{4x_{eD}^2}}ch\sqrt{u+\frac{n^2\pi^2}{h_D^2}+\frac{(2k-1)^2\pi^2}{4x_{eD}^2}}y_{eD}}\right\}$
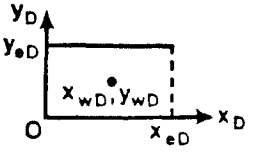 $(-1)^k (s_{111} + s_{211} + s_{121} + s_{221} - s_{112} - s_{212} - s_{122} - s_{222})$	$\frac{\tilde{q}\mu}{kLx_{eD}y_{eD}s}\left\{\sum_{k=1}^{\infty}\cos(2k-1)\frac{\pi}{2}\frac{x_D}{x_{eD}}\cos(2k-1)\frac{\pi}{2}\frac{x_{wD}}{x_{eD}}\right.$ $\left[\frac{ch\sqrt{u+\frac{(2k-1)^2\pi^2}{4x_{eD}^2}}(\tilde{z}_{D1})-ch\sqrt{u+\frac{(2k-1)^2\pi^2}{4x_{eD}^2}}(\tilde{z}_{D2})}{\sqrt{u+\frac{(2k-1)^2\pi^2}{4x_{eD}^2}}sh\sqrt{u+\frac{(2k-1)^2\pi^2}{4x_{eD}^2}}h_D}\right.$ $+2\sum_{m=1}^{\infty}\cos m\pi\frac{y_D}{y_{eD}}\cos m\pi\frac{y_{wD}}{y_{eD}}$ $\left.\left.\frac{ch\sqrt{u+\frac{m^2\pi^2}{y_{eD}^2}+\frac{(2k-1)^2\pi^2}{4x_{eD}^2}}(\tilde{z}_{D1})-ch\sqrt{u+\frac{m^2\pi^2}{y_{eD}^2}+\frac{(2k-1)^2\pi^2}{4x_{eD}^2}}(\tilde{z}_{D2})}{\sqrt{u+\frac{m^2\pi^2}{y_{eD}^2}+\frac{(2k-1)^2\pi^2}{4x_{eD}^2}}sh\sqrt{u+\frac{m^2\pi^2}{y_{eD}^2}+\frac{(2k-1)^2\pi^2}{4x_{eD}^2}}h_D}\right]\right\}$
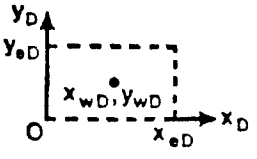 $(-1)^k (s_{111} + s_{211} - s_{121} - s_{221} - s_{112} - s_{212} + s_{122} + s_{222})$	$\frac{\tilde{q}\mu}{kLx_{eD}h_D s}\left\{\sum_{k=1}^{\infty}\cos(2k-1)\frac{\pi}{2}\frac{x_D}{x_{eD}}\cos(2k-1)\frac{\pi}{2}\frac{x_{wD}}{x_{eD}}\right.$ $\left[\frac{ch\sqrt{u+\frac{(2k-1)^2\pi^2}{4x_{eD}^2}}(\tilde{y}_{D1})-ch\sqrt{u+\frac{(2k-1)^2\pi^2}{4x_{eD}^2}}(\tilde{y}_{D2})}{\sqrt{u+\frac{(2k-1)^2\pi^2}{4x_{eD}^2}}sh\sqrt{u+\frac{(2k-1)^2\pi^2}{4x_{eD}^2}}y_{eD}}\right.$ $+2\sum_{n=1}^{\infty}\sin n\pi\frac{z_D}{h_D}\sin n\pi\frac{z_{wD}}{h_D}$ $\left.\left.\frac{ch\sqrt{u+\frac{n^2\pi^2}{h_D^2}+\frac{(2k-1)^2\pi^2}{4x_{eD}^2}}(\tilde{y}_{D1})-ch\sqrt{u+\frac{n^2\pi^2}{h_D^2}+\frac{(2k-1)^2\pi^2}{4x_{eD}^2}}(\tilde{y}_{D2})}{\sqrt{u+\frac{n^2\pi^2}{h_D^2}+\frac{(2k-1)^2\pi^2}{4x_{eD}^2}}sh\sqrt{u+\frac{n^2\pi^2}{h_D^2}+\frac{(2k-1)^2\pi^2}{4x_{eD}^2}}y_{eD}}\right]\right\}$

TABLE 3-C

POINT SOURCE WELLS

RECTANGULAR RESERVOIRS

IMPERMEABLE BOUNDARY AT $z_D = 0$, CONSTANT PRESSURE BOUNDARY AT $z_D = h_D$

$$\tilde{y}_{D1} = y_{eD} - |y_D - y_{wD}|, \quad \tilde{y}_{D2} = y_{eD} - (y_D + y_{wD})$$

$$\tilde{z}_{D1} = h_D - |z_D - z_{wD}|, \quad \tilde{z}_{D2} = h_D - (z_D + z_{wD})$$

AREAL VIEW	PRESSURE DISTRIBUTION IN LAPLACE SPACE, $\overline{\Delta p}$
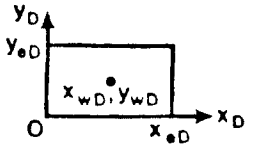 $(-1)^n(s_{111}+s_{211}+s_{121}+s_{221}+s_{112}+s_{212}+s_{122}+s_{222})$	$$\frac{\tilde{q}\mu}{kLx_{eD}h_D s}\left\{\sum_{n=1}^{\infty}\cos(2n-1)\frac{\pi}{2}\frac{z_D}{h_D}\cos(2n-1)\frac{\pi}{2}\frac{z_{wD}}{h_D}\right.$$ $$\left[\frac{ch\sqrt{u+\frac{(2n-1)^2\pi^2}{4h_D^2}}(\tilde{y}_{D1})+ch\sqrt{u+\frac{(2n-1)^2\pi^2}{4h_D^2}}(\tilde{y}_{D2})}{\sqrt{u+\frac{(2n-1)^2\pi^2}{4h_D^2}}\,sh\sqrt{u+\frac{(2n-1)^2\pi^2}{4h_D^2}}y_{eD}}\right.$$ $$+2\sum_{k=1}^{\infty}\cos k\pi\frac{x_D}{x_{eD}}\cos k\pi\frac{x_{wD}}{x_{eD}}$$ $$\left.\left.\frac{ch\sqrt{u+\frac{k^2\pi^2}{x_{eD}^2}+\frac{(2n-1)^2\pi^2}{4h_D^2}}(\tilde{y}_{D1})+ch\sqrt{u+\frac{k^2\pi^2}{x_{eD}^2}+\frac{(2n-1)^2\pi^2}{4h_D^2}}(\tilde{y}_{D2})}{\sqrt{u+\frac{k^2\pi^2}{x_{eD}^2}+\frac{(2n-1)^2\pi^2}{4h_D^2}}\,sh\sqrt{u+\frac{k^2\pi^2}{x_{eD}^2}+\frac{(2n-1)^2\pi^2}{4h_D^2}}y_{eD}}\right]\right\}$$
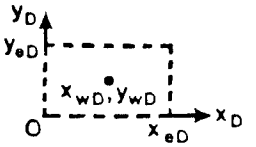 $(-1)^n(s_{111}-s_{211}-s_{121}+s_{221}+s_{112}-s_{212}-s_{122}+s_{222})$	$$\frac{\tilde{q}\mu}{kLx_{eD}h_D s}\left\{\sum_{n=1}^{\infty}\cos(2n-1)\frac{\pi}{2}\frac{z_D}{h_D}\cos(2n-1)\frac{\pi}{2}\frac{z_{wD}}{h_D}\right.$$ $$\left[\frac{ch\sqrt{u+\frac{(2n-1)^2\pi^2}{4h_D^2}}(\tilde{y}_{D1})-ch\sqrt{u+\frac{(2n-1)^2\pi^2}{4h_D^2}}(\tilde{y}_{D2})}{\sqrt{u+\frac{(2n-1)^2\pi^2}{4h_D^2}}\,sh\sqrt{u+\frac{(2n-1)^2\pi^2}{4h_D^2}}y_{eD}}\right.$$ $$+2\sum_{k=1}^{\infty}\sin k\pi\frac{x_D}{x_{eD}}\sin k\pi\frac{x_{wD}}{x_{eD}}$$ $$\left.\left.\frac{ch\sqrt{u+\frac{k^2\pi^2}{x_{eD}^2}+\frac{(2n-1)^2\pi^2}{4h_D^2}}(\tilde{y}_{D1})-ch\sqrt{u+\frac{k^2\pi^2}{x_{eD}^2}+\frac{(2n-1)^2\pi^2}{4h_D^2}}(\tilde{y}_{D2})}{\sqrt{u+\frac{k^2\pi^2}{x_{eD}^2}+\frac{(2n-1)^2\pi^2}{4h_D^2}}\,sh\sqrt{u+\frac{k^2\pi^2}{x_{eD}^2}+\frac{(2n-1)^2\pi^2}{4h_D^2}}y_{eD}}\right]\right\}$$
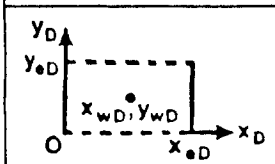 $(-1)^n(s_{111}+s_{211}-s_{121}-s_{221}+s_{112}+s_{212}-s_{122}-s_{222})$	$$\frac{\tilde{q}\mu}{kLx_{eD}h_D s}\left\{\sum_{n=1}^{\infty}\cos(2n-1)\frac{\pi}{2}\frac{z_D}{h_D}\cos(2n-1)\frac{\pi}{2}\frac{z_{wD}}{h_D}\right.$$ $$\left[\frac{ch\sqrt{u+\frac{(2n-1)^2\pi^2}{4h_D^2}}(\tilde{y}_{D1})-ch\sqrt{u+\frac{(2n-1)^2\pi^2}{4h_D^2}}(\tilde{y}_{D2})}{\sqrt{u+\frac{(2n-1)^2\pi^2}{4h_D^2}}\,sh\sqrt{u+\frac{(2n-1)^2\pi^2}{4h_D^2}}y_{eD}}\right.$$ $$+2\sum_{k=1}^{\infty}\cos k\pi\frac{x_D}{x_{eD}}\cos k\pi\frac{x_{wD}}{x_{eD}}$$ $$\left.\left.\frac{ch\sqrt{u+\frac{k^2\pi^2}{x_{eD}^2}+\frac{(2n-1)^2\pi^2}{4h_D^2}}(\tilde{y}_{D1})-ch\sqrt{u+\frac{k^2\pi^2}{x_{eD}^2}+\frac{(2n-1)^2\pi^2}{4h_D^2}}(\tilde{y}_{D2})}{\sqrt{u+\frac{k^2\pi^2}{x_{eD}^2}+\frac{(2n-1)^2\pi^2}{4h_D^2}}\,sh\sqrt{u+\frac{k^2\pi^2}{x_{eD}^2}+\frac{(2n-1)^2\pi^2}{4h_D^2}}y_{eD}}\right]\right\}$$

TABLE 3-C (Cont.)

POINT SOURCE WELLS

RECTANGULAR RESERVOIRS

IMPERMEABLE BOUNDARY AT $z_D = 0$, CONSTANT PRESSURE BOUNDARY AT $z_D = h_D$

$$\tilde{y}_{D1} = y_{eD} - |y_D - y_{wD}|, \quad \tilde{y}_{D2} = y_{eD} - (y_D + y_{wD})$$

$$\tilde{z}_{D1} = h_D - |z_D - z_{wD}|, \quad \tilde{z}_{D2} = h_D - (z_D + z_{wD})$$

AREAL VIEW	PRESSURE DISTRIBUTION IN LAPLACE SPACE, $\overline{\Delta p}$
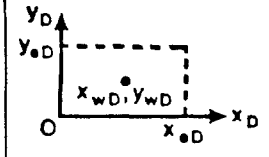 $(-1)^k(-1)^m(-1)^n(s_{111}+s_{211}+s_{121}+s_{221}+s_{112}+s_{212}+s_{122}+s_{222})$	$$\frac{2\tilde{q}\mu}{kLx_{eD}h_D s}\left\{\sum_{n=1}^{\infty}\cos(2n-1)\frac{\pi}{2}\frac{x_D}{h_D}\cos(2n-1)\frac{\pi}{2}\frac{x_{wD}}{h_D}\sum_{k=1}^{\infty}\cos(2k-1)\frac{\pi}{2}\frac{x_D}{x_{eD}}\cos(2k-1)\frac{\pi}{2}\frac{x_{wD}}{x_{eD}}\right.$$ $$\left.\frac{sh\sqrt{u+\frac{(2k-1)^2\pi^2}{4x_{eD}^2}+\frac{(2n-1)^2\pi^2}{4h_D^2}}(\tilde{y}_{D1})+sh\sqrt{u+\frac{(2k-1)^2\pi^2}{4x_{eD}^2}+\frac{(2n-1)^2\pi^2}{4h_D^2}}(\tilde{y}_{D2})}{\sqrt{u+\frac{(2k-1)^2\pi^2}{4x_{eD}^2}+\frac{(2n-1)^2\pi^2}{4h_D^2}}\,ch\sqrt{u+\frac{(2k-1)^2\pi^2}{4x_{eD}^2}+\frac{(2n-1)^2\pi^2}{4h_D^2}}y_{eD}}\right\}$$
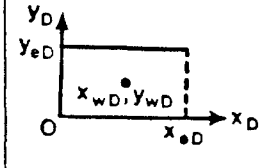 $(-1)^k(-1)^n(s_{111}+s_{211}+s_{121}+s_{221}+s_{112}+s_{212}+s_{122}+s_{222})$	$$\frac{\tilde{q}\mu}{kLx_{eD}y_{eD}s}\left\{\sum_{k=1}^{\infty}\cos(2k-1)\frac{\pi}{2}\frac{x_D}{x_{eD}}\cos(2k-1)\frac{\pi}{2}\frac{x_{wD}}{x_{eD}}\right.$$ $$\left[\frac{sh\sqrt{u+\frac{(2k-1)^2\pi^2}{4x_{eD}^2}}(\tilde{z}_{D1})+sh\sqrt{u+\frac{(2k-1)^2\pi^2}{4x_{eD}^2}}(\tilde{z}_{D2})}{\sqrt{u+\frac{(2k-1)^2\pi^2}{4x_{eD}^2}}\,ch\sqrt{u+\frac{(2k-1)^2\pi^2}{4x_{eD}^2}}h_D}\right.$$ $$+2\sum_{m=1}^{\infty}\cos m\pi\frac{y_D}{y_{eD}}\cos m\pi\frac{y_{wD}}{y_{eD}}$$ $$\left.\left.\frac{sh\sqrt{u+\frac{m^2\pi^2}{y_{eD}^2}+\frac{(2k-1)^2\pi^2}{4x_{eD}^2}}(\tilde{z}_{D1})+sh\sqrt{u+\frac{m^2\pi^2}{y_{eD}^2}+\frac{(2k-1)^2\pi^2}{4x_{eD}^2}}(\tilde{z}_{D2})}{\sqrt{u+\frac{m^2\pi^2}{y_{eD}^2}+\frac{(2k-1)^2\pi^2}{4x_{eD}^2}}\,ch\sqrt{u+\frac{m^2\pi^2}{y_{eD}^2}+\frac{(2k-1)^2\pi^2}{4x_{eD}^2}}h_D}\right]\right\}$$
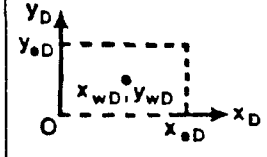 $(-1)^k(-1)^n(s_{111}+s_{211}-s_{121}-s_{221}+s_{112}+s_{212}-s_{122}-s_{222})$	$$\frac{2\tilde{q}\mu}{kLx_{eD}y_{eD}s}\left\{\sum_{k=1}^{\infty}\cos(2k-1)\frac{\pi}{2}\frac{x_D}{x_{eD}}\cos(2k-1)\frac{\pi}{2}\frac{x_{wD}}{x_{eD}}\sum_{m=1}^{\infty}\sin m\pi\frac{y_D}{y_{eD}}\sin m\pi\frac{y_{wD}}{y_{eD}}\right.$$ $$\left.\frac{sh\sqrt{u+\frac{m^2\pi^2}{y_{eD}^2}+\frac{(2k-1)^2\pi^2}{4x_{eD}^2}}(\tilde{z}_{D1})+sh\sqrt{u+\frac{m^2\pi^2}{y_{eD}^2}+\frac{(2k-1)^2\pi^2}{4x_{eD}^2}}(\tilde{z}_{D2})}{\sqrt{u+\frac{m^2\pi^2}{y_{eD}^2}+\frac{(2k-1)^2\pi^2}{4x_{eD}^2}}\,ch\sqrt{u+\frac{m^2\pi^2}{y_{eD}^2}+\frac{(2k-1)^2\pi^2}{4x_{eD}^2}}h_D}\right\}$$

APPENDIX B

REDUCTION OF TRIPLE INFINITE FOURIER SERIES

In applying the method of images in x, y, and z directions to obtain the point source solutions in rectangular reservoirs (solutions given in Table 3 of Appendix A) we encounter triple infinite series of Eq. 2.1.40. Here we present summation formulas to be used in generating the solutions given in Table 3 of Appendix A.

First we consider the triple summation given by

$$TS = \sum_{k=-\infty}^{+\infty} \sum_{m=-\infty}^{+\infty} \sum_{n=-\infty}^{+\infty} S, \qquad (B-1)$$

where

$$S = \frac{\exp\left[-\sqrt{u}\sqrt{(\tilde{x}_D - 2kx_{eD})^2 + (\tilde{y}_D - 2my_{eD})^2 + (\tilde{z}_D - 2nh_D)^2}\right]}{\sqrt{(\tilde{x}_D - 2kx_{eD})^2 + (\tilde{y}_D - 2my_{eD})^2 + (\tilde{z}_D - 2nh_D)^2}}. \qquad (B-2)$$

By using the summation formula given by Eq. 2.2.5 in §2.2 and[23]

$$K_0(z) = \frac{1}{2}\int_0^{\infty} \exp\left(-\xi - \frac{z^2}{4\xi}\right)\frac{d\xi}{\xi};\ R(z^2) > 0, \qquad (B-3)$$

Eq. $B-1$ can be written as

$$TS = \frac{1}{2h_D}\left\{\int_0^{\infty} \exp(-\xi) \sum_{k=-\infty}^{+\infty} \exp\left[-\frac{u(\tilde{x}_D - 2kx_{eD})^2}{4\xi}\right]\right.$$

$$\left.\sum_{m-\infty}^{+\infty} \exp\left[-\frac{u(\tilde{y}_D - 2my_{eD})^2}{4\xi}\right]\frac{d\xi}{\xi}\right.$$

$$+2\sum_{n=1}^{+\infty}\cos n\pi\frac{\tilde{z}_D}{h_D}\int_0^{\infty}\exp(-\xi)\sum_{k=-\infty}^{+\infty}\exp\left[-\frac{\left(u+\frac{n^2\pi^2}{h_D^2}\right)(\tilde{x}_D-2kx_{eD})^2}{4\xi}\right]$$

$$\sum_{m=-\infty}^{+\infty}\exp\left[-\frac{\left(u+\frac{n^2\pi^2}{h_D^2}\right)(\tilde{y}_D-2my_{eD})^2}{4\xi}\right]\frac{d\xi}{\xi}\Bigg\}. \qquad (B-4)$$

Using Poisson's summation formula given by Eq. 2.2.4 in §2.2 to evaluate the summation terms in Eq. $B-4$, performing the integrations, and then using[36]

$$\sum_{k=1}^{\infty}\frac{\cos k\pi x}{k^2+a^2}=\frac{\pi}{2a}\frac{ch\left[a\pi(1-x)\right]}{sh\,(a\pi)}-\frac{1}{2a^2};\ [0\le x\le 2]\,, \qquad (B-5)$$

Eq. $B-4$ becomes

$$\begin{aligned}\sum_{k=-\infty}^{+\infty}\sum_{m=-\infty}^{+\infty}\sum_{n=-\infty}^{+\infty}S=\frac{\pi}{2x_{eD}h_D}\Bigg\{&\frac{ch\sqrt{u}(y_{eD}-|\tilde{y}_D|)}{\sqrt{u}sh\sqrt{u}y_{eD}}\\&+2\sum_{k=1}^{\infty}\cos k\pi\frac{\tilde{x}_D}{x_{eD}}\frac{ch\sqrt{u+\frac{\pi^2k^2}{x_{eD}^2}}(y_{eD}-|\tilde{y}_D|)}{\sqrt{u+\frac{\pi^2k^2}{x_{eD}^2}}sh\sqrt{u+\frac{\pi^2k^2}{x_{eD}^2}}y_{eD}}\\&+2\sum_{n=1}^{\infty}\cos n\pi\frac{\tilde{z}_D}{h_D}\Bigg[\frac{ch\sqrt{u+\frac{n^2\pi^2}{h_D^2}}(y_{eD}-|\tilde{y}_D|)}{\sqrt{u+\frac{n^2\pi^2}{h_D^2}}sh\sqrt{u+\frac{n^2\pi^2}{h_D^2}}y_{eD}}\\&+2\sum_{k=1}^{\infty}\cos k\pi\frac{\tilde{x}_D}{x_{eD}}\frac{ch\sqrt{u+\frac{n^2\pi^2}{h_D^2}+\frac{k^2\pi^2}{x_{eD}^2}}(y_{eD}-|\tilde{y}_D|)}{\sqrt{u+\frac{n^2\pi^2}{h_D^2}+\frac{k^2\pi^2}{x_{eD}^2}}sh\sqrt{u+\frac{n^2\pi^2}{h_D^2}+\frac{k^2\pi^2}{x_{eD}^2}}y_{eD}}\Bigg]\Bigg\}.\end{aligned} \qquad (B-6)$$

Here we have reduced the triple infinite series to expressions involving double infinite series. In a similar fashion, we can obtain the following triple summation formulas:

$$\begin{aligned}&\sum_{k=-\infty}^{+\infty}\sum_{m=-\infty}^{+\infty}\sum_{n=-\infty}^{+\infty}(-1)^k S=\\&\frac{\pi}{h_D x_{eD}}\Bigg\{\sum_{k=1}^{\infty}\cos(2k-1)\frac{\pi}{2}\frac{\tilde{x}_D}{x_{eD}}\Bigg[\frac{ch\sqrt{u+\frac{(2k-1)^2\pi^2}{4x_{eD}^2}}(y_{eD}-|\tilde{y}_D|)}{\sqrt{u+\frac{(2k-1)^2\pi^2}{4x_{eD}^2}}sh\sqrt{u+\frac{(2k-1)^2\pi^2}{4x_{eD}^2}}y_{eD}}\\&+2\sum_{n=1}^{\infty}\cos n\pi\frac{\tilde{z}_D}{h_D}\frac{ch\sqrt{u+\frac{n^2\pi^2}{h_D^2}+\frac{(2k-1)^2\pi^2}{4x_{eD}^2}}(y_{eD}-|\tilde{y}_D|)}{\sqrt{u+\frac{n^2\pi^2}{h_D^2}+\frac{(2k-1)^2\pi^2}{4x_{eD}^2}}sh\sqrt{u+\frac{n^2\pi^2}{h_D^2}+\frac{(2k-1)^2\pi^2}{4x_{eD}^2}}y_{eD}}\Bigg]\Bigg\},\end{aligned} \qquad (B-7)$$

$$\sum_{k=-\infty}^{+\infty}\sum_{m=-\infty}^{+\infty}\sum_{n=-\infty}^{+\infty}(-1)^k(-1)^m S =$$

$$\frac{\pi}{h_D x_{eD}}\left\{\sum_{k=1}^{\infty}\cos(2k-1)\frac{\pi}{2}\frac{\tilde{x}_D}{x_{eD}}\left[\frac{sh\sqrt{u+\frac{(2k-1)^2\pi^2}{4x_{eD}^2}}(y_{eD}-|\tilde{y}_D|)}{\sqrt{u+\frac{(2k-1)^2\pi^2}{4x_{eD}^2}}ch\sqrt{u+\frac{(2k-1)^2\pi^2}{4x_{eD}^2}}y_{eD}}\right.\right.$$

$$\left.\left.+2\sum_{n=1}^{\infty}\cos n\pi\frac{\tilde{z}_D}{h_D}\frac{sh\sqrt{u+\frac{n^2\pi^2}{h_D^2}+\frac{(2k-1)^2\pi^2}{4x_{eD}^2}}(y_{eD}-|\tilde{y}_D|)}{\sqrt{u+\frac{n^2\pi^2}{h_D^2}+\frac{(2k-1)^2\pi^2}{4x_{eD}^2}}ch\sqrt{u+\frac{n^2\pi^2}{h_D^2}+\frac{(2k-1)^2\pi^2}{4x_{eD}^2}}y_{eD}}\right]\right\}, \tag{B-8}$$

and

$$\sum_{k=-\infty}^{+\infty}\sum_{m=-\infty}^{+\infty}\sum_{n=-\infty}^{+\infty}(-1)^m(-1)^k(-1)^n S =$$

$$\frac{2\pi}{x_{eD}h_D}\left[\sum_{n=1}^{\infty}\cos(2n-1)\frac{\pi}{2}\frac{\tilde{z}_D}{h_D}\sum_{k=1}^{\infty}\cos(2k-1)\frac{\pi}{2}\frac{\tilde{x}_D}{x_{eD}}\right.$$

$$\left.\frac{sh\sqrt{u+\frac{(2n-1)^2\pi^2}{4h_D^2}+\frac{(2k-1)^2\pi^2}{4x_{eD}^2}}(y_{eD}-|\tilde{y}_D|)}{\sqrt{u+\frac{(2n-1)^2\pi^2}{4h_D^2}+\frac{(2k-1)^2\pi^2}{4x_{eD}^2}}ch\sqrt{u+\frac{(2n-1)^2\pi^2}{4h_D^2}+\frac{(2k-1)^2\pi^2}{4x_{eD}^2}}y_{eD}}\right]. \tag{B-9}$$

Eqs. $B-6$ - $B-9$ can be used to derive all expressions given in Table 3 of Appendix A.

APPENDIX C

SHORT TIME APPROXIMATIONS RECTANGULAR RESERVOIRS

In §2.7 we outline a procedure to obtain the short time approximations of the solutions that describe the pressure distribution in bounded reservoirs. Here we present an alternate approach that can be used to derive the short time approximations of the solutions for rectangular reservoirs. This approach involves first replacing the ratios of hyperbolic functions in the solution by their short time approximations and then using the standart procedures to find a short approximation of the resulting form of the solution. In the following, we first derive the short time approximations for the ratios of hyperbolic functions appearing in the solutions given in Table 3 of Appendix A. We then consider the solution for a vertically fractured well in a rectangular drainage area to demonstrate the procedure to obtain the short time approximations of the solutions for wells in rectangular drainage areas.

I. Short Time Approximations for the Ratios of Hyperbolic Functions

In order to obtain a short time approximation, we first express the ratios of hyperbolic functions in terms of the exponential function and then evaluate the resulting expression as $s \to \infty$ (or $u = sf(s) \to \infty$). Consider first

$$\lim_{s \to \infty} \left\{ \frac{ch\sqrt{u}\left[y_{eD} - (y_D + y_{wD})\right] + ch\sqrt{u}\left(y_{eD} - |y_D - y_{wD}|\right)}{2\sqrt{u}sh\sqrt{u}y_{eD}} \right\} =$$

$$\lim_{s \to \infty} \left\{ \frac{1}{2\sqrt{u}\left[1 - e^{-2\sqrt{u}y_{eD}}\right]} \left[e^{-\sqrt{u}|y_D - y_{wD}|} + e^{-\sqrt{u}(y_D + y_{wD})} \right. \right.$$

$$+e^{-\sqrt{u}(2y_{eD}-|y_D-y_{wD}|)}+e^{-\sqrt{u}|2y_{eD}-(y_D+y_{wD})|}\Big]\Big\}. \qquad (C-1)$$

If we assume that

$$\lim_{s\to\infty}\exp\left(-2\sqrt{u}y_{eD}\right)=0, \qquad (C-2)$$

then Eq. $C-1$ can be written as

$$\lim_{s\to\infty}\left\{\frac{ch\sqrt{u}\left[y_{eD}-(y_D+y_{wD})\right]+ch\sqrt{u}\left(y_{eD}-|y_D-y_{wD}|\right)}{2\sqrt{u}sh\sqrt{u}y_{eD}}\right\}=$$

$$\frac{1}{2\sqrt{u}}\Big\{e^{-\sqrt{u}|y_D-y_{wD}|}+e^{-\sqrt{u}(y_D+y_{wD})} \qquad (C-3)$$

$$+e^{-\sqrt{u}(2y_{eD}-|y_D-y_{wD}|)}+e^{-\sqrt{u}|2y_{eD}-(y_D+y_{wD})|}\Big\}.$$

Similarly, assuming that the condition given by Eq. $C-2$ holds, we can write

$$\lim_{s\to\infty}\left\{\frac{ch\sqrt{u}\left[y_{eD}-(y_D+y_{wD})\right]-ch\sqrt{u}\left(y_{eD}-|y_D-y_{wD}|\right)}{2\sqrt{u}sh\sqrt{u}y_{eD}}\right\}=$$

$$\frac{1}{2\sqrt{u}}\Big\{e^{-\sqrt{u}|y_D-y_{wD}|}-e^{-\sqrt{u}(y_D+y_{wD})} \qquad (C-4)$$

$$+e^{-\sqrt{u}(2y_{eD}-|y_D-y_{wD}|)}-e^{-\sqrt{u}|2y_{eD}-(y_D+y_{wD})|}\Big\},$$

and

$$\lim_{s\to\infty}\left\{\frac{sh\sqrt{u}\left[y_{eD}-(y_D+y_{wD})\right]+sh\sqrt{u}\left(y_{eD}-|y_D-y_{wD}|\right)}{2\sqrt{u}sh\sqrt{u}y_{eD}}\right\}=$$

$$\frac{1}{2\sqrt{u}}\Big\{e^{-\sqrt{u}|y_D-y_{wD}|}+e^{-\sqrt{u}(y_D+y_{wD})} \qquad (C-5)$$

$$-e^{-\sqrt{u}(2y_{eD}-|y_D-y_{wD}|)}-e^{-\sqrt{u}|2y_{eD}-(y_D+y_{wD})|}\Big\}.$$

If we also assume that the following conditions hold

$$\exp\left[-\sqrt{u}\left(y_D+y_{wD}\right)\right]\approx 0, \qquad (C-6)$$

$$\exp\left\{-\sqrt{u}\left(2y_{eD}-|y_D-y_{wD}|\right)\right\}\approx 0, \qquad (C-7)$$

and

$$\exp\left\{-\sqrt{u}\,[2y_{eD}-(y_D+y_{wD})]\right\}\approx 0, \qquad (C-8)$$

then letting HF denote the ratios of the hyperbolic functions on the left hand sides of Eqs. $C-4$, $C-5$ and $C-6$, we can write

$$\lim_{s\to\infty}\left\{HF\right\}=\frac{1}{2\sqrt{u}}\exp\left(-\sqrt{u}|y_D-y_{wD}|\right). \qquad (C-9)$$

Eq. $C-9$ can be used to replace the ratios of hyperbolic functions in the solutions given in Table 3 of Appendix A when s is large (small times).

<u>II. Vertically Fractured Well</u> Consider the solution given by Eq. 2.3.4 in §2.3 for a vertically fractured well in a closed rectangular reservoir:

$$\begin{aligned}\overline{p}_D(x_D,y_D)=\frac{\pi}{x_{eD}s}\Bigg[&\frac{ch\sqrt{u}\,(y_{eD}-|y_D-y_{wD}|)+ch\sqrt{u}[y_{eD}-(y_D+y_{wD})]}{\sqrt{u}\;sh\;\sqrt{u}y_{eD}}\\&+\frac{2x_{eD}}{\pi}\sum_{k=1}^{\infty}\frac{1}{k}\sin\;k\pi\frac{1}{x_{eD}}\cos\;k\pi\frac{x_{wD}}{x_{eD}}\cos\;k\pi\frac{x_D}{x_{eD}}\\&\frac{ch\sqrt{u+\frac{k^2\pi^2}{x_{eD}^2}}(y_{eD}-|y_D-y_{wD}|)+ch\sqrt{u+\frac{k^2\pi^2}{x_{eD}^2}}[y_{eD}-(y_D+y_{wD})]}{\sqrt{u+\frac{k^2\pi^2}{x_{eD}^2}}\,sh\sqrt{u+\frac{k^2\pi^2}{x_{eD}^2}}\,y_{eD}}\Bigg].\end{aligned} \qquad (C-10)$$

Using Eq. $C-9$ and substituting sw for u as suggested by Eq. 2.7.1 as $s\to\infty$, we can write the following approximation for Eq. $C-10$:

$$\begin{aligned}\lim_{s\to\infty}\left\{\frac{sx_{eD}}{2\pi}\overline{p}_D\right\}&=\frac{1}{2\sqrt{sw}}\exp\left(-\sqrt{sw}|y_D-y_{wD}|\right)\\&+\frac{2x_{eD}}{\pi}\sum_{k=1}^{\infty}\frac{1}{k}\sin k\pi\frac{1}{x_{eD}}\cos k\pi\frac{x_{wD}}{x_{eD}}\cos k\pi\frac{x_D}{x_{eD}}\\&\frac{1}{2\sqrt{sw+\frac{k^2\pi^2}{x_{eD}}}}\exp\left(-\sqrt{sw+\frac{k^2\pi^2}{x_{eD}}}|y_D-y_{wD}|\right).\end{aligned} \qquad (C-11)$$

We can now follow the standart procedures to obtain an approximation for the right hand side of Eq. $C-11$ as $s\to\infty$. If we let sw denote the Laplace transform variable with respect to ξ and $\mathcal{L}$ denote the Laplace transform operator, then taking

the inverse Laplace transform of the right hand side of Eq. $C-11$ with respect to sw, we can write

$$\lim_{s\to\infty}\left\{\frac{sx_{eD}}{2\pi}\overline{p}_D\right\}=\mathcal{L}\left\{\frac{1}{2\sqrt{\pi\xi}}\exp\left[-\frac{(y_D-y_{wD})^2}{4\xi}\right]\right.$$
$$\left[1+\frac{2x_{eD}}{\pi}\sum_{k=1}^{\infty}\frac{1}{k}\sin k\pi\frac{1}{x_{eD}}\cos k\pi\frac{x_{wD}}{x_{eD}}\cos k\pi\frac{x_D}{x_{eD}}\right. \qquad (C-12)$$
$$\left.\left.\exp\left(-\frac{k^2\pi^2\xi}{x_{eD}}\right)\right]\right\}.$$

Since the right hand side of Eq. $C-11$ is to be evaluated as $s\to\infty$, the right hand side of Eq. $C-12$ should be evaluated as $\xi\to 0$. One can evaluate the function inside curly braces on the right hand side of Eq. $C-12$ for small values of ξ; however, if we recognize that the bracketed term on the right hand side of Eq. $C-12$ is the Function $X(x)$ given in Table $2-b$ of Ref. 3 then its approximation for small values of ξ can be found in Table 3 of Ref. 3. Therefore, using Table 3 of Ref. 3, we can write Eq. $C-12$ as

$$\lim_{s\to\infty}\left\{\frac{sx_{eD}}{2\pi}\overline{p}_D\right\}=\mathcal{L}\left\{\frac{\beta x_{eD}}{8\sqrt{\pi\xi}}\exp\left[-\frac{(y_{eD}-y_{wD})^2}{4\xi}\right]\right\}, \qquad (C-13)$$

where

$$\beta=\begin{cases}2 & \text{for } |x_D-x_{wD}|<1,\\ 1 & \text{for } |x_D-x_{wD}|=1,\\ 0 & \text{for } |x_D-x_{wD}|>1.\end{cases} \qquad (C-14)$$

Evaluating the Laplace transform of the function inside curly braces on the right hand side of Eq. $C-13$ with respect to ξ and simplifying, we obtain the following expression:

$$\lim_{s\to\infty}\overline{p}_D=\frac{\pi\beta}{4s\sqrt{sw}}\exp\left(-\sqrt{sw}|y_D-y_{wD}|\right). \qquad (C-15)$$

Evaluating the Laplace inversion of Eq. $C-15$ with respect to s, we finally obtain the following short time approximation for the vertically fractured well solution:

$$\overline{p}_D=\frac{\beta}{2}\left\{\sqrt{\pi t_D/w}\exp\left[-\frac{(y_D-y_{wD})^2}{4t_D/w}\right]\right.$$
$$\left.-\frac{\pi}{2\sqrt{w}}|y_D-y_{wD}|\operatorname{erfc}\left(\frac{|y_D-y_{wD}|}{2\sqrt{t_D/w}}\right)\right\}. \qquad (C-16)$$

Not unexpectedly, Eq. $C-16$ is identical to the short time approximation given by Eq. 2.7.12 in §2.7.

APPENDIX D

HORIZONTAL WELL PERFORMANCE SUBJECT TO BOTTOM WATER DRIVE

Here we present a brief discussion of the long term performance of horizontal wells producing under edge water drive conditions. This appendix is intended merely as a supplement to the discussion presented in Chapter IV regarding the distinct flow characteristics of bottom water drive and edge water drive mechanisms and not to discuss in detail the performance of horizontal wells under edge water drive conditions.

The word steady state is generally used in well testing literature to describe the long time flow behavior of wells located in reservoirs surrounded by constant pressure boundaries in the lateral extent. Geologically, constant pressure boundaries in the lateral extent of the reservoir may develop as a result of an adjacent aquifer which is large enough to maintain the pressure at the water-oil contact (reservoir boundary) at its original level without significant loss of its potential. Reservoirs that are surrounded by a large aquifer in the lateral extent are mostly underlain by a water table of finite volume. Due to its finite volume, the influence of the water table on the production mechanism is negligible compared to the influence of the edge water and therefore the water-oil interface at the bottom of the oil pay can be idealized as an impermeable boundary. As production continues, however, because of the pressure gradients developing at the water-oil boundary below the oil pay, the bottom water tends to advance into the oil zone and this places severe restrictions on the maximum allowable production rates (critical rate) to guarantee water-free oil production. If the well is produced at or under the critical rate, then

it can be expected that the bottom water would rise to the point where the pressure gradients are balanced by the gravitational gradient and remain stable at this point.

In light of the physical view of the system described above, here we will derive expressions that describe the long term (steady state) flow behavior of horizontal wells operating under edge water drive conditions. The transient flow solution for the system considered here can be found in Ref. 37. Approximate steady state solutions for long horizontal wells have been extensively used in the literature (see for example Refs. 58, and 71). Here we first derive a general steady state solution for a point source well subject to edge water drive; then by appropriate integration as described in Chapter II and Ref. 3, we obtain the solution for a horizontal well. This solution does not involve the assumption used in the literature that the horizontal well length is long. The point source solution derived here can also be used to obtain solutions for other well configurations. We also derive an approximate solution for long horizontal wells. This solution has not been reported in the literature and is used in Chapter IV to derive conclusions on the flow characteristics of horizontal wells producing under edge water drive conditions.

The maximum allowable production rates (critical rates) have been investigated in Refs. 62, 63, and 64. For completeness, here we present a summary of the approximate procedure to determine critical rates suggested by Muskat and Wyckoff[65] and applied to horizontal wells by Chaperon[62]. Discussion of critical rates is outside the scope of this appendix.

I. Steady State Solutions Consider a point source in a reservoir that extends to infinity in x and y directions and is bounded by impermeable boundaries at $z = 0$ and h. Following the lines suggested in Ref. 3, the source functions that are used to construct the solution are given by

$$S_x(x,t) = \frac{1}{2\sqrt{\pi\eta_x t}} \exp\left[-\frac{(x-x_w)^2}{4\eta_x t}\right], \qquad (D-1)$$

$$S_y(y,t) = \frac{1}{2\sqrt{\pi\eta_y t}} \exp\left[-\frac{(y-y_w)^2}{4\eta_y t}\right], \qquad (D-2)$$

and

$$S_z(z,t) = \frac{1}{h}\left[1 + 2\sum_{n=1}^{\infty} \exp\left(-\frac{n^2\pi^2\eta_z t}{h^2}\right) \cos n\pi\frac{z_w}{h} \cos n\pi\frac{z}{h}\right], \qquad (D-3)$$

where η_x, η_y, and η_z are given by

$$\eta_j = \frac{k_j}{\phi c_t \mu}, \quad j = x,\ y,\ \text{or } z. \qquad (D-4)$$

Assuming that the flux distribution is uniform in time, the pressure distribution in the reservoir is given by[3]

$$\Delta p = \frac{\tilde{q}}{\phi c_t}\int_0^t S_x(x,\tau)\, S_y(y,\tau)\, S_z(z,\tau)\, d\tau. \qquad (D-5)$$

Here $\tilde{q}$ is the withdrawal rate from a point source. Note that if we assume $\eta = \eta_x = \eta_y$, then we can write

$$\Delta p = (I_1 + I_2) \qquad (D-6)$$

where

$$I_1 = \int_0^t \frac{\tilde{q}}{4\pi h\eta\tau\phi c_t} \exp\left(-\frac{r^2}{4\eta\tau}\right) d\tau, \qquad (D-7)$$

and

$$I_2 = \int_0^t \frac{\tilde{q}}{2\pi h\eta\tau\phi c_t} \sum_{n=1}^{\infty} \exp\left(-\frac{n^2\pi^2\eta_z\tau}{h^2} - \frac{r^2}{4\eta\tau}\right) \cos n\pi\frac{z_w}{h} \cos n\pi\frac{z}{h} d\tau. \qquad (D-8)$$

In Eqs. $D-7$ and $D-8$, r is the radial distance defined by

$$r = \sqrt{(x-x_w)^2 + (y-y_w)^2}. \qquad (D-9)$$

We can recognize the function I_1 given by Eq. $D-7$ as the line source solution for a vertical well in an infinite reservoir (see for example Ref. 3). If we let Δp_l denote the line source solution, then we can write the point source solution in a laterally infinite reservoir, Δp, as

$$\Delta p = \Delta p_l + I_2. \qquad (D-10)$$

The Laplace transform of Eq. $D-10$ is given by

$$\overline{\Delta p} = \overline{\Delta p_l} + \overline{I_2}, \qquad (D-11)$$

where

$$\overline{\Delta p_l} = \frac{\tilde{q}}{2\pi h\eta\phi c_t s} K_0\left(r\sqrt{s/\eta}\right), \qquad (D-12)$$

and

$$\overline{I_2} = \frac{\tilde{q}}{\pi h\eta\phi c_t s}\sum_{n=1}^{\infty}\cos n\pi\frac{z_w}{h}\cos n\pi\frac{z}{h}K_0\left(\frac{r}{\sqrt{\eta}}\sqrt{s+\frac{n^2\pi^2\eta_z}{h^2}}\right). \qquad (D-13)$$

The influence of the constant pressure boundary located at $r = r_e$ can be incorporated by the procedure described in §2.2 of this work and the resulting expression is given by (see Eq. 2.2.4)

$$\overline{\Delta p_b} = \overline{\Delta p_{lb}} + \overline{I_{2b}} \qquad (D-14)$$

where the subscript b refers to the bounded system solution and $\overline{\Delta p_{lb}}$ and $\overline{I_{2b}}$ are given by

$$\overline{\Delta p_{lb}} = \frac{\tilde{q}}{2\pi h\eta\phi c_t s}\left\{K_0\left(r\sqrt{s/\eta}\right) - \frac{I_0\left(r\sqrt{s/\eta}\right)K_0\left(r_e\sqrt{s/\eta}\right)}{I_0\left(r_e\sqrt{s/\eta}\right)}\right\}, \qquad (D-15)$$

and

$$\overline{I_{2b}} = \frac{\tilde{q}}{\pi h\eta\phi c_t s}\sum_{n=1}^{\infty}\cos n\pi\frac{z_w}{h}\cos n\pi\frac{z}{h}$$
$$\left\{K_0\left(\frac{r}{\sqrt{\eta}}\sqrt{s+\frac{n^2\pi^2\eta_z}{h^2}}\right) - \frac{I_0\left(\frac{r}{\sqrt{\eta}}\sqrt{s+\frac{n^2\pi^2\eta_z}{h^2}}\right)K_0\left(\frac{r_e}{\sqrt{\eta}}\sqrt{s+\frac{n^2\pi^2\eta_z}{h^2}}\right)}{I_0\left(\frac{r_e}{\sqrt{\eta}}\sqrt{s+\frac{n^2\pi^2\eta_z}{h^2}}\right)}\right\}. \qquad (D-16)$$

The long time approximation of the solution given by Eq. $D-15$ can be obtained following the lines suggested by Ref. 16 for a line source well in a bounded reservoir and is given by the following well-known expression:

$$\Delta p_{lb} = \frac{\tilde{q}\mu}{2\pi kh}\ln\frac{r_e}{r}. \qquad (D-17)$$

The long time approximation of the function I_{2b} is obtained by assuming that s is small enough that $s + n^2\pi^2\eta_z/h^2 \approx n^2\pi^2\eta_z/h^2$ in Eq. $D-16$ and then taking the

inverse Laplace transform of Eq. D-16. This procedure yields

$$I_{2b} = \frac{\tilde{q}\mu}{\pi kh} \sum_{n=1}^{\infty} \cos n\pi \frac{z_w}{h} \cos n\pi \frac{z}{h}$$
$$\left\{ K_0 \left(\frac{n\pi}{h} \sqrt{\frac{\eta_z}{\eta}} r \right) - \frac{I_0 \left(\frac{n\pi}{h} \sqrt{\frac{\eta_z}{\eta}} r \right) K_0 \left(\frac{n\pi}{h} \sqrt{\frac{\eta_z}{\eta}} r_e \right)}{I_0 \left(\frac{n\pi}{h} \sqrt{\frac{\eta_z}{\eta}} r_e \right)} \right\}. \qquad (D-18)$$

Therefore, the steady state pressure behavior of a point source well producing under edge water drive conditions is described by

$$\Delta p = \frac{\tilde{q}\mu}{2\pi kh} \left\{ \ln \frac{r_e}{r} + 2 \sum_{n=1}^{\infty} \cos n\pi \frac{z_w}{h} \cos n\pi \frac{z}{h} \right.$$
$$\left. \left[K_0 \left(\frac{n\pi}{h} \sqrt{\frac{\eta_z}{\eta}} r \right) - \frac{I_0 \left(\frac{n\pi}{h} \sqrt{\frac{\eta_z}{\eta}} r \right) K_0 \left(\frac{n\pi}{h} \sqrt{\frac{\eta_z}{\eta}} r_e \right)}{I_0 \left(\frac{n\pi}{h} \sqrt{\frac{\eta_z}{\eta}} r_e \right)} \right] \right\}. \qquad (D-19)$$

To obtain the steady state solution for a horizontal line source well producing under edge water drive conditions, we integrate the right hand side of Eq. $D-19$ from $-L_h/2$ to $L_h/2$ with respect to x_w where L_h is the length of the horizontal well. The result is given by

$$p_D = \ln r_{eD} + \sigma(x_D, y_D) + 1 + \sum_{n=1}^{\infty} \cos n\pi z_D \cos n\pi z_{wD}$$
$$\int_{-1}^{+1} \left[K_0 (n\pi L_D \tilde{r}_D) - \frac{I_1 (n\pi L_D \tilde{r}_D) K_0 (n\pi L_D r_{eD})}{I_1 (n\pi L_D r_{eD})} \right] d\alpha \qquad (D-20)$$

where

$$p_D = \frac{2\pi kh}{q\mu} \Delta p, \qquad (D-21)$$

$$z_D = \frac{z}{h}, \qquad (D-22)$$

$$L_D = \frac{L_h}{2h}, \qquad (D-23)$$

$$\tilde{r}_D = \frac{2\sqrt{(x-\alpha)^2 + (y-y_w)^2}}{L_h}, \qquad (D-24)$$

and

$$r_{eD} = \frac{2\sqrt{x_e^2 + y_e^2}}{L_h}. \qquad (D-25)$$

The function $\sigma(x_D, y_D)$ in Eq. $D-20$ is given by

$$\sigma(x_D, y_D) = 0.25\Bigg\{(x_D-1)\ln\left[(x_D-1)^2+y_D^2\right]$$

$$-(x_D+1)\ln\left[(x_D+1)^2+y_D^2\right] - 2y_D \operatorname{arctg}\frac{2y_D}{x_D^2+y_D^2-1}\Bigg\}. \qquad (D-26)$$

II. Steady State Solution for Long Horizontal Wells We consider a long horizontal well located at some elevation z_w between the impermeable bottom ($z=0$) and top ($z=h$) boundaries of the reservoir. The well is assumed to be parallel to the constant pressure boundaries located at $y=0$ and $2y_e$. Using the source function approach of Ref. 3, the source functions in x, y and z directions are given by

$$S_x(x,t) = 0.5\left[\operatorname{erf}\frac{L_h/2+(x-x_w)}{2\sqrt{\eta_x t}} + \operatorname{erf}\frac{L_h/2-(x-x_w)}{2\sqrt{\eta_x t}}\right], \qquad (D-27)$$

$$S_y(y,t) = \frac{1}{y_e}\sum_{n=1}^{\infty}\exp\left(-\frac{n^2\pi^2\eta_y t}{4y_e^2}\right)\sin n\pi\frac{y_w}{2y_e}\sin n\pi\frac{y+y_w}{2y_e}, \qquad (D-28)$$

and

$$S_z(z,t) = \frac{1}{h}\left[1+2\sum_{n=1}^{\infty}\exp\left(-\frac{n^2\pi^2\eta_z t}{h^2}\right)\cos n\pi\frac{z_w}{h}\cos n\pi\frac{z}{h}\right]. \qquad (D-29)$$

Note that in Eq. $D-28$, y is the distance measured from the center of the well. The pressure distribution in the reservoir is given by[3]

$$\Delta p = \frac{\tilde{q}}{\phi c_t}\int_0^t S_x(x,\tau)S_y(y,\tau)S_z(z,\tau)\,d\tau. \qquad (D-30)$$

Note that, when the influence of the constant pressure boundaries at $y=0$ and $2y_e$ is established, the source function $S_y \approx 0$ [from Table 3 of Ref. 3, the time for S_y to be negligible is found as $t \le 20y_e^2/(\pi^2\eta_y)$]. This indicates that the upper limit of the integral in the right hand side of Eq. $D-30$ can be replaced by the time for the onset of steady flow period. It is also clear that the conditions established in the reservoir prior to steady state are preserved during the steady state flow period.

Here we will assume that the horizontal well is long so that the influence of the constant pressure boundaries become dominant prior to the start of flow across the tips of the well. When the flow across the tips of the well is negligible, then we can replace the source function S_x by its short time approximation given by[3]

$$S_x(x,t) = \frac{\beta}{2} \qquad (D-31)$$

where

$$\beta = \begin{cases} 2 & \text{for} |x - x_w| < L_h/2, \\ 1 & \text{for} |x - x_w| = L_h/2, \\ 0 & \text{for} |x - x_w| > L_h/2. \end{cases} \qquad (D-32)$$

Therefore, using the source functions S_x, S_y and S_z given by Eqs. $D-31$, $D-28$ and $D-29$, we can write Eq. $D-30$ as

$$\Delta p = I_1 + I_2 \qquad (D-33)$$

where

$$I_1 = \frac{\tilde{q}\beta}{2\phi c_t h\ y_e} \int_0^t \sum_{n=1}^{\infty} \exp\left(-\frac{n^2\pi^2\eta_y\tau}{4y_e^2}\right) \sin n\pi\frac{y_w}{2y_e} \sin n\pi\frac{y+y_w}{2y_e} d\tau, \qquad (D-34)$$

and

$$I_2 = \frac{\tilde{q}\beta}{\phi c_t h y_e} \int_0^t \left[\sum_{n=1}^{\infty} \exp\left(-\frac{n^2\pi^2\eta_y\tau}{4y_e^2}\right) \sin n\pi\frac{y_w}{2y_e} \sin n\pi\frac{y+y_w}{2y_e}\right] \left[\sum_{k=1}^{\infty} \exp\left(-\frac{k^2\pi^2\eta_z\tau}{h^2}\right) \cos n\pi\frac{z_w}{h} \cos n\pi\frac{z}{h}\right] d\tau. \qquad (D-35)$$

Let us first consider the long time approximation of the function I_1. The Laplace transform of the function I_1 is given by

$$\overline{I_1} = \frac{2\tilde{q}\beta}{\phi c_t h y_e s} \sum_{n=1}^{\infty} \frac{\sin n\pi\frac{y_w}{2y_e} \sin n\pi\frac{y+y_w}{2y_e}}{s + \frac{n^2\pi^2\eta_y}{4y_e^2}}. \qquad (D-36)$$

If we assume that s becomes small so that $s + n^2\pi^2\eta_y/\left(4y_e^2\right) \approx n^2\pi^2\eta_y/\left(4y_e^2\right)$ and evaluate the inverse Laplace transform of Eq. $D-36$, we obtain the following long time approximation:

$$I_1 = \frac{2\tilde{q}\beta y_e}{\phi c_t h \pi^2 \eta_y} \sum_{n=1}^{\infty} \frac{\sin n\pi\frac{y_w}{2y_e} \sin n\pi\frac{y+y_w}{2y_e}}{n^2}. \qquad (D-37)$$

If we also note that[68]

$$\sum_{k=1}^{\infty} \frac{\sin kx \sin ky}{k^2} = (\pi - y)\frac{x}{2}, \quad [0 \le |x| \le |y| \le \pi], \qquad (D-38)$$

then we can write

$$I_1 = \begin{cases} \frac{\tilde{q}\mu\beta}{2k_y h}\left(y_e - \frac{y}{2} - \frac{y_w}{2}\right)\frac{y_w}{y_e}, & \text{for } y \ge 0, \\ \frac{\tilde{q}\mu\beta}{2k_y h}\left(y_e - \frac{y_w}{2}\right)\frac{y+y_w}{y_e}, & \text{for } y \le 0. \end{cases} \qquad (D-39)$$

The Laplace transform of the function I_2 (Eq. $D-35$) is given by

$$\overline{I_2} = \frac{\tilde{q}\beta}{\phi c_t h y_e s}\sum_{n=1}^{\infty}\cos n\pi\frac{z}{h}\cos n\pi\frac{z_w}{h} \sum_{n=1}^{\infty}\frac{\sin k\pi\frac{y_w}{2y_e}\sin k\pi\frac{y+y_w}{2y_e}}{s + \frac{k^2\pi^2\eta_x}{4y_e^2} + \frac{n^2\pi^2\eta_z}{h^2}}. \qquad (D-40)$$

As in Eq. $D-36$, if we assume that s becomes small enough so that $s+k^2\pi^2\eta_y/\left(4y_e^2\right) \approx k^2\pi^2\eta_y/\left(4y_e^2\right)$, then the inverse Laplace transform of Eq. $D-40$ yields the following expression for large values of time:

$$I_2 = \frac{4\tilde{q}\beta y_e}{\phi c_t h\pi^2\eta_y}\sum_{n=1}^{\infty}\cos n\pi\frac{z}{h}\cos n\pi\frac{z_w}{h}\ I_3, \qquad (D-41)$$

where

$$I_3 = \sum_{k=1}^{\infty}\frac{\sin k\pi\frac{y_w}{2y_e}\sin k\pi\frac{y+y_w}{2y_e}}{k^2 + \frac{4n^2y_e^2\eta_z}{h^2\eta_y}}. \qquad (D-42)$$

Noting that

$$\sin k\pi\frac{y_w}{2y_e}\sin k\pi\frac{y+y_w}{2y_e} = 0.5\left[\cos k\pi\frac{y}{2y_e} - \cos k\pi\frac{y+2y_w}{2y_e}\right], \qquad (D-43)$$

and using[36]

$$\sum_{k=1}^{\infty}\frac{\cos kx}{k^2+a^2} = \frac{\pi}{2a}\frac{ch\ a(\pi-x)}{sh\ a\pi} - \frac{1}{2a^2}, \quad [0 \le x \le 2\pi], \qquad (D-44)$$

we can write the function I_3 as

$$I_3 = \frac{\pi h}{8ny_e}\sqrt{\frac{\eta_y}{\eta_z}} \frac{ch\frac{n\pi}{h}\sqrt{\frac{\eta_z}{\eta_y}}(2y_e - |y|) - ch\frac{n\pi}{h}\sqrt{\frac{\eta_z}{\eta_y}}[2y_e - (y+2y_w)]}{sh\frac{n\pi}{h}\sqrt{\frac{\eta_z}{\eta_y}}2y_e}. \qquad (D-45)$$

By a similar procedure to that outlined in Appendix C, if we assume that

$$\exp\left(-\frac{n\pi}{h}\sqrt{\frac{\eta_z}{\eta_y}}2y_e\right) \approx 0, \tag{$D-46$}$$

then Eq. $D-45$ yields

$$\begin{aligned} I_3 = \frac{\pi h}{8ny_e}\sqrt{\frac{\eta_y}{\eta_z}}\Bigg\{ & \exp\left(-\frac{n\pi}{h}\sqrt{\frac{\eta_z}{\eta_y}}|y|\right) \\ & + \exp\left[-\frac{n\pi}{h}\sqrt{\frac{\eta_z}{\eta_y}}\,(y+2y_w)\right] \\ & - \exp\left[-\frac{n\pi}{h}\sqrt{\frac{\eta_z}{\eta_y}}\,(4y_e-|y|)\right] - \exp\left[-\frac{n\pi}{h}\sqrt{\frac{\eta_z}{\eta_y}}\,(4y_e-y-2y_w)\right]\Bigg\}. \end{aligned} \tag{$D-47$}$$

Therefore, the function I_2 (Eq. $D-41$) can be written as

$$\begin{aligned} I_2 = {} & \frac{\tilde{q}\beta}{2\phi c_t \pi\sqrt{\eta_y\eta_z}}\sum_{n=1}^{\infty}\frac{\cos n\pi\frac{z}{h}\cos n\pi\frac{z_w}{h}}{n} \\ & \Bigg\{\exp\left(-\frac{n\pi}{h}\sqrt{\frac{\eta_z}{\eta_y}}|y|\right) + \exp\left[-\frac{n\pi}{h}\sqrt{\frac{\eta_z}{\eta_y}}\,(y+2y_w)\right] \\ & \exp\left[-\frac{n\pi}{h}\sqrt{\frac{\eta_z}{\eta_y}}\,(4y_e-|y|)\right] - \exp\left[-\frac{n\pi}{h}\sqrt{\frac{\eta_z}{\eta_y}}\,(4y_e-y-2y_w)\right]\Bigg\}. \end{aligned} \tag{$D-48$}$$

If we consider the case where the well is located midway between the constant pressure boundaries at $y=0$ and $2y_e$ $(y_w = y_e)$, then from Eqs. $D-33$, $D-39$ and $D-48$, we can write

$$\begin{aligned} \Delta p = {} & \frac{\tilde{q}\mu\beta}{2k_y h}(y_e-y) + \frac{\tilde{q}\mu\beta}{2\pi\sqrt{k_y k_z}}\sum_{n=1}^{\infty}\frac{\cos n\pi\frac{z}{h}\cos n\pi\frac{z_w}{h}}{n} \\ & \Bigg\{\exp\left(-\frac{n\pi}{h}\sqrt{\frac{\eta_z}{\eta_y}}|y|\right) + \exp\left[-\frac{n\pi}{h}\sqrt{\frac{\eta_z}{\eta_y}}\,(2y_e+y)\right] \\ & - \exp\left[-\frac{n\pi}{h}\sqrt{\frac{\eta_z}{\eta_y}}\,(4y_e-y)\right] - \exp\left[-\frac{n\pi}{h}\sqrt{\frac{\eta_z}{\eta_y}}\,(2y_e-y)\right]\Bigg\}. \end{aligned} \tag{$D-49$}$$

If we further assume that

$$\exp\left[-\frac{n\pi}{h}\sqrt{\frac{\eta_z}{\eta_y}}\,(2y_e+y)\right] \approx 0, \tag{$D-50$}$$

$$\exp\left[-\frac{n\pi}{h}\sqrt{\frac{\eta_z}{\eta_y}}\,(4y_e - y)\right] \approx 0, \qquad (D-51)$$

$$\exp\left[-\frac{n\pi}{h}\sqrt{\frac{\eta_z}{\eta_y}}\,(2y_e - y)\right] \approx 0, \qquad (D-52)$$

then Eq. $D-49$ can be written as

$$p_D = \frac{\pi\beta}{4}\,(y_{eD} - |y_D|) + \frac{\beta}{2L_D}\sum_{n=1}^{\infty}\frac{\cos n\pi z_{wD}\cos n\pi z_D}{n}\exp\left(-n\pi L_D|y_D|\right). \qquad (D-53)$$

In Eq. $D-53$, p_D, z_D and L_D are defined by Eqs. $D-21$ - $D-23$ (with $k=k_y$ and $q=\tilde{q}L_h$) and y_D is defined by

$$y_D = \frac{2y}{L_h}. \qquad (D-54)$$

Note that, in physical terms, the assumptions stated by Eqs. $D-46$ and $D-50$ - $D-52$ are to ensure that the influence of the impermeable boundaries at $z=0$ and h is fully established at every point in the reservoir prior to the influence of the constant pressure boundaries at $y=0$ and $2y_e$.

The following summation formula is given in Ref. 36:

$$\sum_{k=1}^{\infty}\frac{p^k\cos kx}{k} = -0.5\ln\left(1-2p\cos x+p^2\right), \quad \left[0<x<2\pi, p^2\le 1\right]. \qquad (D-55)$$

Using Eq. $D-55$ with $p=\exp\left(-\pi L_D|y_D|\right)$, we can write Eq. $D-53$ as

$$p_D = \frac{\pi\beta}{4}\,(y_{eD} - |y_D|) - \frac{\beta}{8L_D}\ln\left[1-2\exp\left(-\pi L_D|y_D|\right)\cos\pi|z_D - z_{wD}| + \exp\left(-2\pi L_D|y_D|\right)\right] - \frac{\beta}{8L_D}\ln\left[1-2\exp\left(-\pi L_D|y_D|\right)\cos\pi\left(z_{wD}+z_D\right) + \exp\left(-2\pi L_D|y_D|\right)\right]. \qquad (D-56)$$

Note that in Eq. $D-56$, we cannot have $y_D=0$ and $z_D=z_{wD}$ at the same time. If $z_D\neq z_{wD}$, then at $y_D=0$ Eq. $D-56$ yields

$$p_D = \frac{\beta}{2}\left\{\pi y_{eD} - \frac{1}{L_D}\ln 2 - \frac{1}{2L_D}\ln\left[\sin\frac{\pi}{2}|z_D - z_{wD}|\sin\frac{\pi}{2}\left(z_D+z_{wD}\right)\right]\right\}. \qquad (D-57)$$

III. Critical Production Rate Here we consider a system where there exists a finite volume aquifer beneath the oil bearing formation. We assume that the bottom water does not contribute to the production mechanism. Since the water is of greater density than the oil, under static conditions, it would remain at the bottom of the formation and the water-oil interface would be flat. Once the production starts from the oil zone, due to the dynamical effect of the motion of the oil, the bottom water would rise into the oil zone and the water-oil interface would resemble a cone (or a crest in case of horizontal wells). It is reasonable to expect that if there exists an elevation below the well at which the pressure gradients are balanced by the differential hydrostatic head, then the bottom water would rise to that point and remain at dynamic equilibrium with the oil. Therefore, although it does not contribute to the drive of oil into the well, the movement of the bottom water is determinant on the maximum allowable production rates to ensure water-free oil production (critical rate).

The water cresting phenomena and the critical production rate for the case of production via a horizontal wellbore have been investigated in Refs. 62 and 64. Here, we briefly discuss the procedure used in Ref. 62 which is an extension of the approximate theory of Muskat and Wyckoff[65] to horizontal wells. We note that Ref. 62 makes the assumption that the horizontal well extends to infinity in both directions and uses a solution similar to that given by Eq. $D-56$. In this appendix, we derived a solution that can be used for all horizontal well lengths (Eq. $D-20$). Our intent here is to develop the framework in which the solution given by Eq. $D-20$ can be simply inserted to improve the procedure used in Ref. 62 for all horizontal well lengths.

The condition of static equilibrium as stated by Muskat and Wyckoff[65] assumes that the water initially at pressure p_i lying statically beneath the oil zone ($z=0$) will rise to an elevation z and be in static equilibrium with oil if the drop in oil pressure at this point from its initial level is balanced by the differential hydrostatic

head. Therefore, the condition of static equilibrium is given by

$$p_i - p(x,y,z) = (\rho_o - \rho_w)\, gz. \qquad (D-58)$$

It is also conceivable that beyond the height at which the pressure gradient in the oil zone is just equal to the opposing differential gravitational force, $(\rho_o - \rho_w)g$, acting upon the water, no water crest (or cone) will be stable, and that any slight increase in the height of the water crest above this point will result in flow of water into the well. From this discussion, the condition of dynamic equilibrium is stated as

$$-\frac{\partial p}{\partial z} = (\rho_o - \rho_w)\, g. \qquad (D-59)$$

In terms of the dimensionless variables, we can write Eqs. $D-58$ and $D-59$ as

$$p_D = \frac{2\pi kh^2}{q\mu}(\rho_o - \rho_w)\, gz_D \qquad (D-60)$$

and

$$\frac{\partial p_D}{\partial z_D} = \frac{2\pi kh^2}{q\mu}(\rho_o - \rho_w)\, g. \qquad (D-61)$$

According to our discussion above, Eqs. $D-60$ and $D-61$ are mutually satisfied at $z_D = z_{cD}$ where z_{cD} is the critical crest height. Then combining Eqs. $D-60$ and $D-61$, we obtain the implicit equation to be solved for the critical crest height, z_{cD}, as

$$z_{cD} = \left(\frac{p_D}{\frac{\partial p_D}{\partial z_D}}\right)_{z_D = z_{cD}} \qquad (D-62)$$

If we define a dimensionless rate as in Ref. 62 by

$$q_D = \frac{q\mu}{2\pi kh^2(\rho_o - \rho_w)\, g}, \qquad (D-63)$$

then substituting Eq. $D-61$ (or $D-60$) into Eq. $D-63$ at $z_D = z_{cD}$, we obtain an expression for the dimensionless critical rate, q_{cD}, given by

$$q_{cD} = \frac{1}{\left(\frac{\partial p_D}{\partial z_D}\right)_{z_D = z_{cD}}} = \left(\frac{z_D}{p_D}\right)_{z_D = z_{cD}} \qquad (D-64)$$

To solve Eqs. $D-62$ and $D-64$ for the critical crest height, the pressure distribution, p_D, must be known. Muskat-Wyckoff[65] theory of water coning assumes that the pressure distribution solution for the case where the water-oil interface is flat (Eq. $D-20$ or $D-56$) can be used to represent the pressure distribution in case of the existence of a water cone (or crest). In addition, since the critical crest height is the maximum crest height which will be in the vertical plane passing through the well axis (the plane at $y_D = 0$), we only need to know the pressure distribution, p_D, at $y_D = 0$.

Detailed discussion of the water cresting phenomena for horizontal wells is outside the scope of this work. The discussion presented above is merely intended to demonstrate the use of the solutions given by Eqs. $D-20$ and $D-56$ to determine the critical production rates along the lines suggested by Muskat and Wyckoff and extended to horizontal wells by Ref. 62.

APPENDIX E

PARTIALLY PENETRATING VERTICAL WELL AND POINT SOURCE WELL SUBJECT TO BOTTOM WATER DRIVE

Here we derive the solutions for pressure distribution due to production from a partially penetrating vertical well and a point source well subject to bottom water drive. We also obtain the steady state solutions for both well completions. These solutions can be used in the manner discussed in Chapter IV to determine the productivities of partially penetrating vertical wells and point source wells under bottom water drive conditions.

I. Partially Penetrating Vertical Well The solution for a partially penetrating vertical well in a bounded reservoir subject to bottom water drive is given in Ref. 72. Here we present the solution for a laterally infinite system. The solution for this system is obtained in the same fashion as described in §4.1 I for a horizontal well. The source functions in the x and y directions are infinite plane sources in an infinite reservoir and are given by[3]

$$S_x(x,t) = \frac{1}{2\sqrt{\pi\eta_x t}} \exp\left[-\frac{(x-x_w)^2}{4\eta_x t}\right], \qquad (E-1)$$

and

$$S_y(y,t) = \frac{1}{2\sqrt{\pi\eta_y t}} \exp\left[-\frac{(y-y_w)^2}{4\eta_y t}\right]. \qquad (E-2)$$

The source function in the z direction is an infinite slab source in an infinite slab reservoir and, for our problem, is given by[3]

$$S_z(z,t) = \frac{8}{\pi}\sum_{n=1}^{\infty} \frac{1}{(2n-1)} \exp\left[-\frac{(2n-1)^2\pi^2\eta_z t}{4h^2}\right]$$

$$\sin(2n-1)\frac{\pi}{2}\frac{z_w}{h}\sin(2n-1)\frac{\pi}{2}\frac{h_w}{2h}\sin(2n-1)\frac{\pi}{2}\frac{z}{h}, \qquad (E-3)$$

where h_w is the height of the penetrated interval of the oil pay. In Eqs. $E-1$ - $E-3$, $\eta_j = k_j t/(\phi c_t \mu)$ with $j = x$, y, or z. The pressure distribution in the reservoir is then obtained by using the following relation:

$$\Delta p = \frac{\tilde{q}}{\phi c_t}\int_0^t S_x(x,\tau)S_y(y,\tau)S_z(z,\tau)d\tau, \qquad (E-4)$$

where we assumed $\tilde{q}(t) = \tilde{q} =$ constant. If we assume that the flux distribution along the well length is uniform, then $\tilde{q}$ is related to the total production rate from the well length, q, by $q(t) = q/h_w$. Using Eqs. $E-1$ - $E-4$, the solution for dimensionless pressure distribution in the reservoir is obtained to be

$$p_D = \frac{4}{\pi b}\int_0^{t_D}\exp\left(-\frac{x_D^2+y_D^2}{4\tau}\right)\sum_{n=1}^{\infty}\frac{1}{(2n-1)}\exp\left[-(2n-1)^2\pi^2\frac{\tau}{4h_D^2}\right]$$

$$\sin(2n-1)\frac{\pi}{2}z_D\sin(2n-1)\frac{\pi}{2}z_{wD}\sin(2n-1)\frac{\pi}{4}b\frac{d\tau}{\tau}. \qquad (E-5)$$

In Eq. $E-5$, the dimensionless variables are defined by

$$p_D = \frac{2\pi\sqrt{k_x k_y}h\Delta p}{q\mu}, \qquad (E-6)$$

$$t_D = \frac{kt}{\phi c_t \mu r_w^2} \qquad (E-7)$$

$$x_D = \frac{x-x_w}{r_w}\sqrt{\frac{k}{k_x}}, \qquad (E-8)$$

$$y_D = \frac{y-y_w}{r_w}\sqrt{\frac{k}{k_y}}, \qquad (E-9)$$

$$z_D = \frac{z}{h}, \qquad (E-10)$$

$$h_D = \frac{h}{r_w}\sqrt{\frac{k}{k_z}}, \qquad (E-11)$$

and

$$b = h_w/h. \qquad (E-12)$$

In these definitions, k is the equivalent horizontal permeability for an isotropic system and is qiven by $k = \sqrt{k_x k_y}$.

The short time approximation of Eq. $E-5$ is given by[73]

$$p_D = -\frac{1}{2b}\mathrm{Ei}\left(-\frac{r_D^2}{4t_D}\right), \qquad (E-13)$$

where

$$r_D^2 = x_D^2 + y_D^2 \qquad (E-14)$$

Eq. $E-14$ is applicable when

$$t_D \leq \delta_D^2/20 \qquad (E-15)$$

where δ_D is the dimensionless distance between the point at which the pressure is measured and the top or the bottom of the wellbore opening whichever is the nearest.

The Laplace transform of Eq. $E-5$ is given by

$$\overline{p}_D = \frac{4}{\pi b s}\sum_{n=1}^{\infty}\frac{\sin(2n-1)\frac{\pi}{2}z_D \sin(2n-1)\frac{\pi}{2}z_{wD}\sin(2n-1)\frac{\pi}{4}b}{(2n-1)}\mathrm{K}_0\left(r_D\sqrt{s+a}\right), \qquad (E-16)$$

where

$$a = \frac{(2n-1)^2\pi^2}{4h_D^2}. \qquad (E-17)$$

If we evaluate the inverse Laplace transform of Eq. $E-16$ subject to the condition that $s+a \approx a$ $(s \to 0)$, then we obtain the following long time solution in real time domain:

$$p_D = \frac{4}{\pi b}\sum_{n=1}^{\infty}\frac{\sin(2n-1)\frac{\pi}{2}z_D \sin(2n-1)\frac{\pi}{2}z_{wD}\sin(2n-1)\frac{\pi}{4}b}{(2n-1)}$$

$$\mathrm{K}_0\left[(2n-1)\frac{\pi}{2h_D}r_D\right], \qquad (E-18)$$

when

$$t_D \geq 20\,(h_D/\pi)^2. \qquad (E-19)$$

The solution given by Eq. $E-18$ is expressed in terms of the flow potential in Ref. 66. An alternate form of this expression to be used for small values of r_D can also be found in Ref. 66 in terms of the flow potential.

II. Point Source Well (Single Perforation) Solution for this case can be simply obtained by evaluating the partially penetrating vertical well solution given by Eq. $E-5$ at the limit as the penetration ratio, b, approaches zero. This procedure yields the following expression:

$$p_D = \int_0^{t_D} \exp\left(-\frac{x_D^2+y_D^2}{4\tau}\right) \sum_{n=1}^{\infty} \exp\left[-(2n-1)^2\pi^2\frac{\tau}{4h_D^2}\right] \sin(2n-1)\frac{\pi}{2}z_D \sin(2n-1)\frac{\pi}{2}z_{wD}\frac{d\tau}{\tau}. \qquad (E-20)$$

The short time approximation of Eq. $E-20$ is given by

$$p_D = \frac{h_D}{4\pi}\int_0^{t_D} \exp\left[-\frac{x_D^2+y_D^2+(z_D-z_{wD})^2 h_D^2}{4\tau}\right]\frac{d\tau}{\tau^{3/2}} \qquad (E-21)$$

when

$$t_D \le \min\begin{cases}(z_D+z_{wD})^2 h_D^2/20, \\ [(z_D+z_{wD})+2]^2 h_D^2/20.\end{cases} \qquad (E-22)$$

The long time approximation is obtained similarly by evaluating Eq. $E-18$ at the limit as $b \to 0$ and is given by

$$p_D = \sum_{n=1}^{\infty} \sin(2n-1)\frac{\pi}{2}z_D \sin(2n-1)\frac{\pi}{2}z_{wD} \mathrm{K}_0\left[(2n-1)\frac{\pi}{2h_D}r_D\right] \qquad (E-23)$$

when

$$t_D \ge 20\,(h_D/\pi)^2. \qquad (E-24)$$